DETECTION OF CAVITIES BY A CONTINUOUS-WAVE SEISMIC METHOD

Thesis

Submitted by

GEOFFREY A. CARRINGTON, B.Sc

for the

degree of Doctor of Philosophy

of the University of London

May, 1985

Department of Geophysics
Imperial College of Science
and Technology
London S.W.7.

"Tunnel construction is one of the most costly and, at the same time, one of the most hazardous of all engineering undertakings.....".

Wahlstrom, 1974

Dedicated to Lori
and to my Mother

DETECTION OF CAVITIES BY A CONTINUOUS-WAVE SEISMIC METHOD

ABSTRACT

The aim of this research was to determine whether tunnelling machine noise could be used to predict ground conditions ahead of an advancing tunnel face and also, if other types of machine noise could be used to detect subterranean cavities using the techniques of spectral analysis.

The initial study was a feasibility trial of a tunnelling machine at a site in Warrington, Cheshire. The data was recorded using a single -channel and then a four-channel F.M. system, allowing simultaneous recording of the output from three geophones. Subsequent spectral analysis of this data showed that the frequency spectrum of energy imparted to the ground by the tunnelling machine was not stationary, thus, precluding the use of quantitative analysis to determine ground conditions.

The next field experiment, at a site near Cocking Village, West Sussex, was a study of the effects of a large cavity on the characteristic spectra of a continuous-wave source operated at the surface of the ground. The source used was a petrol-driven soil-compaction tool, operated near a disused railway tunnel which acted as the cavity. Spectral analysis showed anomalous attenuation caused by the disturbed ground around the tunnel. Cavity resonance was not observed and correlation and phase differencing techniques failed to provide information about seismic velocities in the near-surface.

A final experiment was conducted over a near-surface cavity, at a site near Creswell Crags, in Derbyshire. A comprehensive receiver grid was laid over the cavity utilizing both vertical and three-component geophones and an electrically-driven soil compaction tool was used as the source. Cavity resonance was not observed, although some delay in arrival times was seen in the vicinity of the cavity during a conventional refraction survey. It was not possible to calculate attenuation or divergence factors for the simultaneously recorded lines of vertical geophones as the amplitudes were distorted by resonant air-wave coupling.

It was concluded that machine noise is unsuitable for the detection of cavities as, the inherent lack of stationarity of this type of source makes quantitative analysis unreliable.

CONTENTS

LIST OF FIGURES

LIST OF FIGURES Cont'd.....

LIST OF FIGURES Cont'd.....

LIST OF FIGURES Cont'd.....

LIST OF FIGURES Cont'd.....

LIST OF TABLES

ACKNOWLEDGEMENTS

I would like to extend my thanks to all those who have contributed towards the investigation described herein.

I am especially grateful to my supervisor, Dr. A. Thomas-Betts, for her guidance, encouragement and criticism of this manuscript.

Special thanks are due to the Engineering Geology Unit of the Institute of Geological Sciences for the provision of data for the Warrington work, the loan of much of the field equipment and the use of their microcomputer. Mr. R. Baria and Dr. D. M. McCann deserve a special mention for their advice and great willingness to help.

I am indebted to the Natural Environment Research Council for providing the grant to enable me to pursue this research, and for meeting the fieldwork expenses.

Thanks are also due to, Dr. A. Thenuwara for help during the initial stages of the work, Dr. D. Bloxham for help with the digitizing and to all those members of the department whose encouragement helped me along the way.

Finally, thanks are due to my wife, Lori, who put up with me during the writing of the thesis and to Sue Bridge my appreciation of her skills in the superb typing of the manuscript.

CHAPTER I

INTRODUCTION

1.1 INTRODUCTION

In recent years the use of shields and excavating machines has become more popular for constructing tunnels in both hard and soft rock environments (Peck et. al., 1972). However, the investment in a tunnelling machine is so great that rapid progress becomes essential for the recovery of profit. Unfortunately, tunnelling machines are overly sensitive to changes in the nature of the ground. These two factors combine to make an accurate knowledge of ground conditions along the proposed route of the tunnel absolutely essential.

1.2 EXPLORATION IN A TUNNELLING ENVIRONMENT

The tunnelling environment is unique for several reasons; the excavation is also the construction, the work can take place along a route that is several miles long and access to the site of excavation is usually severely restricted.

At present, unless horizontal probe drilling is carried out during construction of the tunnel (see Section 2.9), the tunneller relies exclusively on geologic predictions based on the original site investigations. The typical site investigation is reasonably comprehensive and requires regional and local geologic mapping using aerial photography and may also include, diamond drilling (for core samples),

water pressure testing, seismic studies, borehole photography and general observation of the material in situ (Merritt, 1972). But, a recent survey of seven tunnels in Colorado, U.S.A. (Dowding, 1976) showed that a comparison of predicted and encountered geology noted little success in the locational prediction of geologic phenomena. However, Brekke and Howard (1972) had previously suggested that an examination of case histories revealed that it was most often the behaviour of unstable zones (particularly in terms of their time-dependent behaviour) that was not predicted rather than their existence.

For shallow tunnels, often constructed in alluvial deposits or soft rock and often located in an urban environment, the dynamic behaviour of the soil becomes especially important because of the likelihood of ground subsidence caused by soil compaction (New, 1978) and movement of soil into the work-face. This can cause severe damage to property (Newbury and Davenport, 1975) and is a serious problem, especially in urban areas.

The decision to carry out exploration for tunnelling is one that can be taken under very uncertain conditions. A solution is achieved by use of decision analysis (Labreche et. al., 1976) applied to a probabilistic model such as the Tunnel Cost Model (Lindner et. al., 1975). This method makes use of existing geologic knowledge, the possible construction strategies and their costs, and the cost of possible exploration methods. An exploration method is assigned a value, characterized by its costs and reliability and this is weighed against the possible benefits of the exploration (also

assigned a value), to decide if the information is worth the cost of gathering it. It has been recognized for some time that an effective geophysical method of exploration for tunnels does not exist. However, it is likely that geophysical methods of probing ahead for tunnels offer more hope of cost and risk effectiveness than direct contact methods.

In 1973 a working party was set up under the aegis of the Building Research Establishment (BRE) and the Transport and Road Research Laboratory (TRRL) specifically to examine the problem of probing ahead for tunnels. One of their recommendations for future research (TRRL, 1975) was a study of the potential of the tunnelling machine as a seismic source and the use of such a source for detecting potential hazards a few tens of metres ahead of the tunnel face. An investigation of this problem was begun in 1976.

1.3 METHOD OF INVESTIGATION

Since no work of this nature had been previously reported in the literature it was expected that this work, reported herein, would be part of a long-term study.

The first step was a study of the feasibility of using a tunnelling machine, which was boring a 2 m diameter tunnel for an outfall sewer at Warrington in Cheshire, as a seismic source. The proposed length of the tunnel was over 1 km and it was possible to follow the progress of the tunnelling machine for several hundred metres. The data were gathered

during several visits to the site by the Engineering Geology Unit of the Institute of Geological Sciences. For the initial stages only one geophone output could be recorded at a time, but this was later increased to three.

Portions of the data were then selected for analysis and digitized. Limitations in the amount of data which could be handled meant that only frequencies up to 100 Hz could be analyzed. However, prior examination of the data on an analogue spectrum analyzer had revealed most of the power to be in the region of 10 to 50 Hz. Subsequent spectral analysis confirmed this and a predominant frequency of 12 Hz was revealed which was thought to be due to the main motors of the tunnelling machine which operated at approximately 720 r.p.m. Comparing spectra of records from separate visits showed that the tunnelling machine did not have a consistent spectrum which could be used for quantitative measurements such as attenuation. Unfortunately, due to problems on the site no further work was possible at Warrington.

An experiment was conducted over a disused railway tunnel near Cocking Village, W. Sussex to see whether the presence of a large cavity (5 m in diameter, at a depth of about 8 m) would affect the characterisitc spectra of a "continuous-wave" source, which imparted a succession of impulses into the ground for the duration of the recording time. The source used was a petrol-driven earth tamper known as a Warsop. Although it was obviously not as powerful as a tunnelling machine, useful signals could be detected up to 70 m away. Numerous geophone lines were laid over and away from the

cavity in an attempt to detect any cavity resonance which might occur and to look for relative changes in the spectra.

A final experiment was conducted over a 2 m diameter cylindrical cavity at Creswell Crags, near Sheffield. The source used was similar to the Warsop but was electrically driven. Much better geophone coverage was made possible by the use of a seven-channel tape recorder. A regular grid of geophone lines at 2 m spacing was laid over the area of the cavity. A three-component geophone was also used in conjunction with a four-channel tape recorder to provide simultaneous recordings of three mutually perpendicular directions of vibration. The data were spectrally analyzed and presented in a novel way to aid interpretation. Analysis was possible up to 167 Hz for the three-component geophone and up to 256 Hz for the vertical geophones.

1.4 SCOPE OF THE THESIS

A brief introduction to the objectives of this study and to exploration in a tunnelling environment has been presented.

In Chapter II the problem of detection of cavities in a tunnelling environment is presented. The various geophysical methods are reviewed and compared and contrasted with non-geophysical methods.

Chapter III deals with the theoretical and practical aspects of spectral analysis, including the inherent uncertainties introduced by digital sampling and smoothing of the spectra.

Several methods of spectral estimation are presented and the accuracy and speed of Fourier, Walsh and Maximum Entropy methods are compared using a 2048-bit sample of a real seismic time series.

Chapter IV presents the first part of the experimental work, the feasibility trial of the tunnelling machine at Warrington. Brief accounts are given of the problems of scattering, attenuation, geometrical spreading and interference. The recording, preparation and analysis of the data are described, including the instrumentation and computer programs used.

Chapter V is the first part of the study of detection of cavities. The source used and the new method of preparation and analysis of the data are described in detail. Several methods of finding anomalies due to the cavity are presented, but these achieved only partial success.

Chapter VI is the final experimental chapter and details two surveys carried out over a known cylindrical cavity. A novel way of presenting the results is shown and how this could be an aid to interpreting spectra.

Chapter VII, the final chapter, includes a summary of the conclusions and recommendations for further work.

CHAPTER II

METHODS OF EXPLORATION IN A TUNNELLING ENVIRONMENT

2.1 INTRODUCTION

This chapter is a review of the many geophysical techniques available to the tunnelling engineer for exploration ahead of an advancing tunnel face and includes a discussion of each of the commonly used geophysical techniques, each one under its "classical" title. Two methods which have only recently been introduced to geophysics, acoustic holography and interborehole acoustic scanning, are also included, as is a section on remote sensing. In order to provide a comparison with non-geophysical methods of exploration, a section on exploration by drilling and coring, and by the construction of pilot tunnels is included.

Other summaries may be found in the literature (Baria et al., 1978; B.R.E./T.R.R.L., 1975; Majtenyi, 1976; Maxwell, 1976; Mossman, 1972; Sturgeon, 1975; Symposium, 1977; Wahlstrom, 1974).

2.2 THE MAGNETIC METHOD

In this method the value of either the vertical component of the magnetic field, or the total magnetic field at a point is measured, depending upon the nature of the instrumentation

used. After correcting for normal spatial and temporal variations in the earth's magnetic field, this method will reveal changes in the magnetic susceptibility or remanent magnetism of the underlying rock. No physical contact with the ground is required. However, for the detection of cavities the magnetic method has limited use in that a large contrast is required between the magnetic susceptibility of the void and the surrounding rock. In addition, rocks that have a high magnetic susceptibility also tend to have variable magnetic characteristics which may produce anomalies larger than those produced by voids. An exception to this might be for clay-filled cavities or sink holes in limestone and dolomites (clay gives a magnetic high), and possibly for locating tunnels or mines in hard rock (igneous or metamorphic).

The method has been used with some success by Lange (1965), who used it to locate and delineate lava tubes. However, he did not find it possible to use his data to obtain the depths or dimensions of these tubes. Magnetic methods have found greatest use in regional reconnaissance studies, as a magnetometer can easily be adapted for towing behind an aircraft. In their land-based mode, magnetometers have found useful application in the detection of old mine workings (Maxwell, 1976).

The principal advantages of magnetic methods are their speed of operation, low cost, and ease of use in inaccessible areas.

Unfortunately they cannot be used in urban areas because of the large amount of interference from metal structures, cars etc.

2.3 THE GRAVITY METHOD

The gravity method is used to detect gross contrasts in density. In order to find a subsurface inhomogeneity, the amplitude of its associated anomaly must be distinct from small local variations as well as the larger regional variation. The anomalies associated with subsurface cavities are generally quite small, e.g., a horizontal cylindrical cavity of radius 5 m, depth of burial 10 m, and density contrast of 2.7 gm/cm^3 (an air-filled cavity in limestone), will produce an anomaly of approximately 0.3 mgal. Often, the anomaly is less than that given by theory, due to joints, dissolution collapses and such like, which all serve to decrease the bulk density and thus decrease the magnitude of the gravity anomaly due to the cavity. Theoretical studies (Colley, 1963) have shown that the half-width of the anomaly varies with the depth of burial, but the half-width is generally difficult to measure accurately.

Gravity methods are usually successful when the cavity radius and depth of burial are comparable. But, for significant results, microgravity requires a laborious technique both in the field and during interpretation. Neumann (1973) has studied field techniques and claims a repeatable accuracy of

better than 0.005 mgal after reductions. Speed (1973) examined errors in data reduction and concluded that the major errors are, elevation and topographic corrections, and density estimation.

The gravity method has been used with some success in a variety of situations; detecting mine shafts (Maxwell, 1976), voids created by mining (Snowdowne, 1968), and caves (Neumann, 1967, 1973; Goelen, 1973). It has the advantage of being operable in an urban environment, but suffers badly from the effects of vibrations.

2.4 ELECTRICAL METHODS

Electrical methods include resistivity, induced polarization (I.P.), and self potential (S.P.). I.P. and S.P. are not usually used for the detection of cavities, except in areas of extant mining activities, and the resistivity method is the only electrical method in regular use for detecting cavities.

There are three standard resistivity techniques for detecting large cavities, fractures and fault zones, called depth sounding, profiling and single electrode. Some commonly used electrode spreads are shown in Figure 2.1.

2.4.1 Resistivity Depth Sounding

This method measures the vertical variation of resistivity of the subsurace layers and enables estimation of depths to

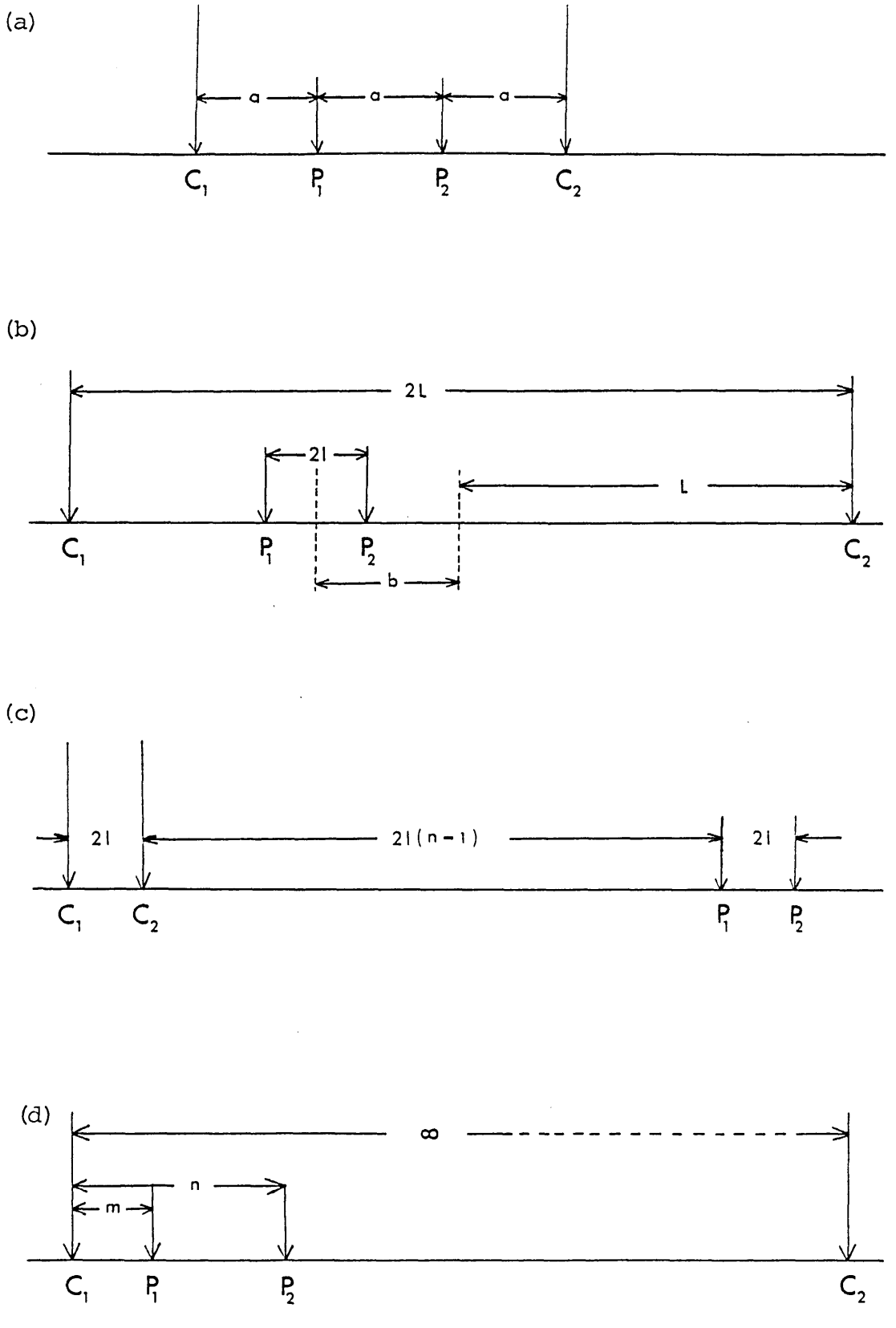

Figure 2.1 Commonly used electrode spreads. (Resistivity method)
(a) Wenner spread.
(b) Schlumberger spread (often used with b = o).
(c) double dipole spread (N > 1).
(d) single electrode spread (also known as three-point spread).

discontinuity horizons. The current and potential electrodes are placed in a straight line and expanded about a fixed central point, so sampling progressively larger depths. The interpretation technique used depends upon the electrode configuration and the thickness and resistivity of the subsurface layers. One of the first people to use this method for the location of cavities was Palmer (1954), and it has also been used with great success to locate the entrance to a large cavity near Bristol (Tratman, 1963). In recent years this technique has fallen out of favour as being time-consuming and inaccurate.

The sounding technique is generally able to quantify the depth to a cavity provided the ratio r/h (where, r is the radius of the cavity, and h is the depth below surface to the top of the cavity) is large, and if the location of the cavity is known. However, the resolution of this method is not good, especially if r/h is small.

2.4.2. Resistivity Profiling

This method determines the lateral variation of apparent resistivity of the ground along a traverse (to a depth depending on the electrode separation). The electrodes are maintained in a straight line and at a constant separation, the distance of which depends on the depth of interest. The whole configuration is moved along the line of the traverse

and the resistivity calculated for each central position. This technique has met with limited success, but has been used in Britain for detecting old mine workings (Maxwell, 1976).

2.4.3 The Single Electrode Technique

The single electrode technique, as detailed in a paper by Bristow, (1966), was designed to increase the resolving power of the resistivity method and to permit a simple and graphical method of data interpretation. It relies on the assumption that equipotential surfaces due to an isolated current electrode are practically hemispherical. The configuration of the electrode spread is shown in Figure 2.1 (d).

More recently, Bates (1973) has used a modified Bristow method with great success. He claims to have located a cavity with a depth-to-size ratio of 15:1, which is considerably better than that achieved by any other method. The advantages of this method are, that prior knowledge of the position of the cavity is not required, and that the interpretation will give its approximate dimensions. Although several workers have claimed success for this method, a survey conducted recently over a shallow cave in limestone (Samson, 1979) failed to locate it, even with rigorous attention to field and interpretation procedures.

2.5 REMOTE SENSING TECHNIQUES

These include aerial photography, and radar and thermal imagery. There are three systems in common use in addition to the conventional photography from aircraft, and are known as; side-looking radar imagery (SLAR), thermal radiometric imagery, and colour- infrared photography.

Side-looking radar emits a narrow beam of radio frequency pulses from a scanning directional antenna. Any energy re-radiated back to the antenna is recorded on a continuous film strip. This technique is particularly useful in interpreting the configuration of ground and bedrock exposures in regions of very heavy forest cover.

Thermal imagery makes use of the infra-red radiation emitted from the earth's surface, usually in the 8-13 micron wavelength band. This is picked up by a sensitive radiometric scanning system which translates differences in incoming radiation to a moving film. This method has found great use in identifying subsurface features, such as fault zones saturated with ground water.

Colour infra-red photography uses film with high sensitivity in the near infra-red waveband, and used with special filters can show geologic features that may not be apparent using conventional film.

These methods have been used in Vietnam (Symposium, 1977) in an attempt to detect tunnel systems used by the Vietcong.

Unfortunately, they were unsuccessful in detecting these subterranean features and so these methods, when used by the military, must remain as tools for surface reconnaissance only.

2.6 ELECTROMAGNETIC METHODS

These include radiometrics, low frequency and ground-probing radar. Claims have been made for the success of microwave techniques, for locating cavities by the detection of their associated radiometric temperature anomaly (Kennedy, 1968). But, theoretical and laboratory studies (Richer, 1970) have shown that the depths of penetration of microwaves claimed by Kennedy are impossible, and that his interpretation of the results is suspect. Low frequency methods (Slingram and Turam systems) used in a high resolution mode provide information on ground conductivity and magnetic susceptibility without electrical contact. Their application is mainly in the mapping of near-surface conductivities and in the search for ore-bodies.

Ground probing radar has become a very popular technique in recent years, and much work has been done to find an optimum system. The use of radar techniques for probing the ground was first proposed and demonstrated in 1956 (Cook, 1960) and has since been used for measurement of ice thickness, coal seams, pipe location, tunnel detection, archaeological survey work, and many others (Watts et al., 1974; Cooper et al., 1974; Cook, 1970, 1974, 1975; Anderson, 1973; Peters, 1976;

Lyons, 1976). However, the range of possible applications is limited due to the need for high frequencies to resolve small targets, which severely restricts the penetration depth. So, in any field situation, careful attention must be paid to finding the best compromise between penetration and resolution. It is possible to achieve high penetration depths in dry rock environments (see Fig. 2.2). In hard, reasonably dry rock, long wave radar can (theoretically) penetrate to about 75 m (Cook, 1972), although radar probing in a salt mine has detected a water layer with an accuracy better than 1% over a range of 335 m (Unterberger, 1978). But, rock salt is an almost ideal medium for the transmission of VHF electromagnetic waves and, depending on the size of the target, radar ranges in salt can vary from a few metres up to 9 km (for a high power system), (Tarantolo Jr., 1978).

The pulse type of radar, with field applications including the detection of seams, voids, and faults has been described by Moffat and Puskar (1976). A block diagram of their system and a response record, which illustrates the general principle of ground-probing radar is given in Figure 2.3. The antennas are orthogonally arrayed dipoles lying flush with the earth's surface. The generator provides very sharp, (45 nsec typical) pulses with repetition rates from 10^1 to 10^6 pulses/second. The antennas transmit these pulses into the ground and also detect the reflections produced by buried targets. The detected signal is displayed on the oscilloscope from which, using the directly coupled signal as reference, the delay time, and hence the range, can be calculated.

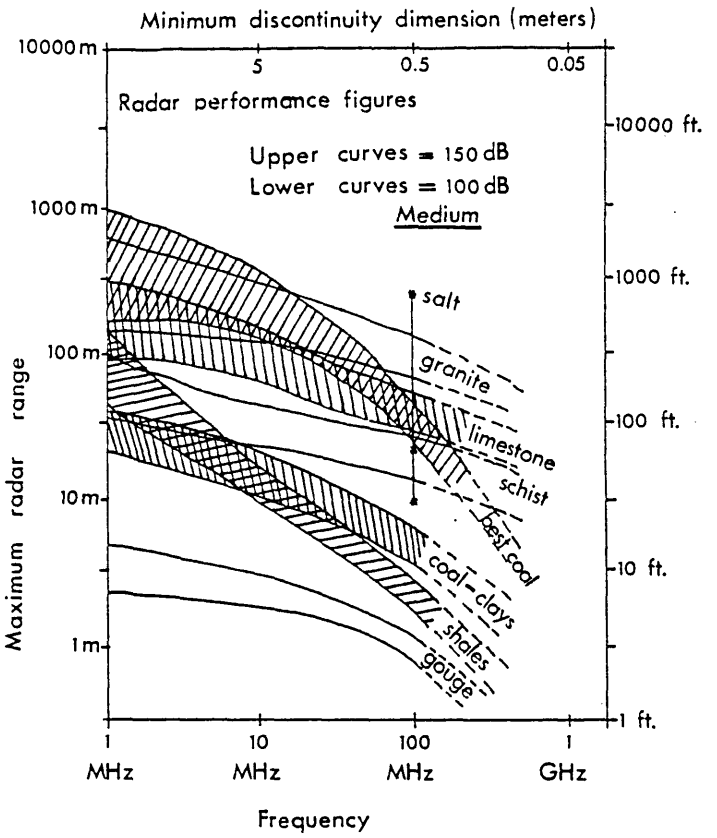

Figure 2.2 Radar probing distances through some typical geologic media. (modified from Moffat & Puskar, 1976)

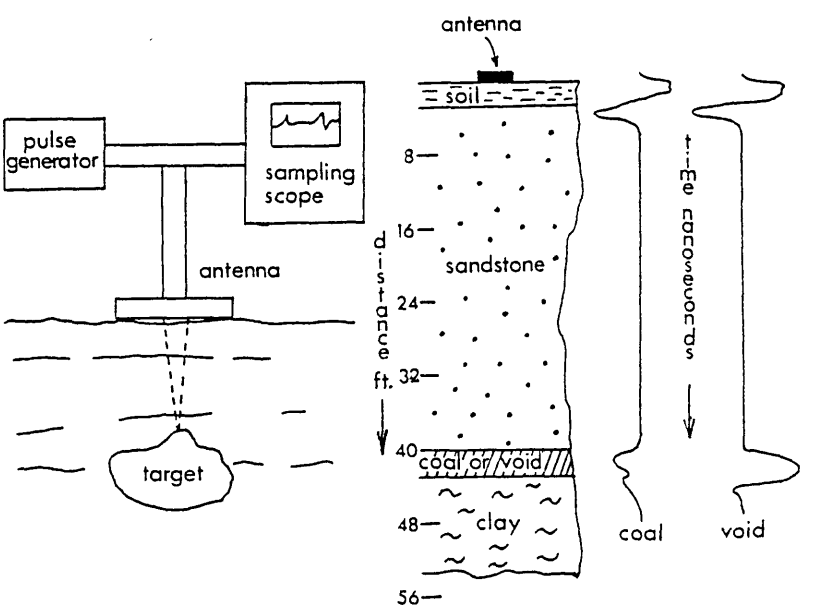

Figure 2.3 Basic underground radar system and simplified response examples. (after Moffat & Puskar, 1976)

Early work with pulsed radar systems (Moffat, 1972) using a series of metal and plastic pipes of various lengths and buried at different depths, indicated the feasibility of an electromagnetic pulse sounding system. Recent field trials of ground probing radar systems have now shown their suitability in real situations (Dolphin, 1978). Increased sophistication of instrumentation and better understanding of the mechanisms of propagation of electromagnetic waves in geologic media, have enabled a more accurate interpretation of results and the use of radar in a greater variety of applications.

Radar has several advantages over the more conventional geophysical exploration methods. It can provide accurate information on the distance to a reflector and can often give the direction, with a detection range greater than that of other methods. There is hope that the character of the reflector will be found by observing changes in the polarization, amplitude, and shape of the signal. Radar exploration is very quick, operated either from the surface or in tunnels. It can even give data on a continuous basis if the complete radar array is slowly moved (Unterberger, 1978). There is a strong possibility that radar and seismic techniques will be mutually helpful, as they detect different physical properties of the ground and have different limitations.

Radar methods are easily adapted for use in boreholes, and radar logging equipment has been developed which can fit into a 2 inch diameter hole. It can be used either to log single holes or to explore large volumes of rock between boreholes (Lytle et al., 1979).

2.7 OTHER METHODS

In this section, two techniques that have only recently entered the field of geophysics and are still very much in the development stage are described briefly. These are, Acoustic Holography and Interborehole Acoustic Scanning. The potential of a holographic approach to seismic exploration was first recognized about seventeen years ago (Farr, 1968). This method used the principles of optical holography i.e., an interferogram (hologram) is constructed from the direct and reflected or diffracted acoustic signals. An "image" of the reflecting or diffracting object can then be reconstructed from the hologram using lasers or by computer (Hoover, 1972). Much work has been done to develop this into a practical method (Booer, 1976; Kalra, 1976), and recent advances in image enhancement for seismic frequency holograms (Fitzpatrick, 1977), hold great promise for the future.

Interborehole Acoustic Scanning is a technique which has been developed and used by the Institute of Geological Sciences. The source used is a high power sparker (up to 1kJ) which is operated in a water-filled borehole (McCann et al., 1975).

The hydrophone receiver array is in another water-filled borehole, the water providing good coupling between the instrumentation and the rock. This method has been tested in field situations for detection of cavities and the results have been encouraging (Baria, 1977; Baria, 1978).

This method suffers from the need for at least two boreholes capable of being filled with water, and probably several more, to cover a reasonable area adequately. But, in the shallow tunnelling environment, the area to cover is usually not large and it may be possible to incorporate boreholes drilled for a previous site investigation. So, this method promises to be quick, and with relatively simple interpretation, economical.

2.8 SEISMIC METHODS

2.8.1 Introduction

Since the birth of geophysics, the seismic method has had an enormous amount of attention focussed upon it. This is due to its use, almost to the exclusion of all other methods, by the petroleum industry. This means that attention has been concentrated on discovering what lies at great depth, while the near-surface regions (less than 500 metres depth) has been neglected. In recent years, due to the search for ever smaller structures, more accurate determinations of near-surface structure have been made in order to improve the

quality of seismic records. Even so, it has been recognized for some considerable time that the standard seismic techniques are inadequate for shallow exploration (Evison, 1952). The limitations of these techniques for shallow work are both practical and fundamental, and are due mainly to the fact that explosives are inherently unsuitable for this kind of exploration.

2.8.2 Sources

The seismic technique offers a bewildering array of methods of imparting energy into the earth, but this energy is usually in the form of an impulse, or a linear vibrator sweep lasting several seconds and having a prescribed frequency content. Whilst dynamite is the most versatile of the available sources (Wardell, 1970), it is unsuitable for shallow work. Many other types of source have been tried for near-surface exploration, with varying degrees of success.

The VIBROSEIS method has received considerable attention in recent years as it has the advantage of a controlled input waveform (Goupillaud, 1976; Rietsch, 1977) and the facility to use multiple source arrays as well as multiple receiver arrays to optimize the signal-to-noise ratio (Edelmann, 1966; Krey, 1969). This method has been used very successfully on an extensive tunnelling project in Chicago, U.S.A. (Mossman, 1972).

Developments of the standard techniques, in field and/or in interpretation procedures have produced some successes. Cook (1964; 1965) mapped large brine filled cavities in salt mines using SH- and P-waves generated by horizontally directed explosives. The National Coal Board has been carrying out research into the use of SH Channel waves, generated by in-seam explosions or hammer blows, to detect discontinuities by reflection. This method is most useful for detecting faults with a high angle of dip (>40°) (Buchanan, 1978; Freystatter, 1978).

Another type of source that was first used to investigate soils as long ago as 1936 (Terzaghi, 1943) is the eccentric machine. This can produce monofrequency waves, the frequency of which depends upon the speed of the machine. Yet another type of source is the electro-mechanical shaker, which can produce short pulses, a continuous monofrequency wave, or a sweep of frequencies as in Vibroseis (Evison, 1956; Evison, 1957; Horton, 1959; Howell, 1940).

2.8.3 Standard Techniques

There have been many attempts to use standard seismic techniques for shallow exploration. Some complex interpretation methods have been developed to find subtle anomalies which could be ascribed to cavities and similar features (Dieterich, 1975; Meissner, 1961; Rockwell, 1967; WIllmore, 1960). Development of seismic hardware has benefitted

enormously from the advent of solid state circuitry and the microprocessor. Systems now exist which can stack reflected or refracted signals with repeated use of a hammer or dropped weight source, which will enhance the signal and tend to cancel random noise (Mooney, 1976). However, the problem of noise on seismic records is one which, although well known (Olhovich, 1964), can only be partially solved by means of such techniques as stacking, filtering and receiver or source arrays.

Records taken in the vicinity of cavities, using standard refraction techniques, frequently exhibit constant frequency oscillations for up to four seconds after the shot instant. Several field investigations by Watkins et al (1967) led them to believe that this was due to radial oscillations of the cavity. They based their interpretation on the theoretical work of Biot (1952), who calculated the frequency of oscillation and its dependence upon the radius of the cavity and the shear-wave velocity. Cundall (1971) interprets these oscillations as asymmetric excitation of the cavity about its axis. He assumes that Rayleigh waves are propagated around the free surface of the cavity. Godson and Watkins (1968) looked at the resonances induced by charges of several different sizes buried at various depths. It was found that resonances were more often induced by small, shallow charges, indicating that Rayleigh waves may be the triggering mechanism.

Watkins et al. (1967) also looked at amplitude attenuation and arrival times observed on seismic records obtained over a known cavity. They observed an increase in attenuation for first arrivals in the vicinity of the cavity, but there was no delay in arrival times, except for later arrivals interpreted to be Rayleigh waves. However, their results were inconclusive. Waller (1972) used a concentric array of geophones to produce a contour map of delay times. This work was not followed up, and so the success of this method remains unconfirmed.

2.8.4 Borehole Seismic Methods

There are several configurations of receiver and shot that can be used, utilizing one or more boreholes (Fig. 2.4). The best one to use in any given situation will, of course, depend upon the nature of the problem to be solved. Boreholes, drilled for previous site investigations, adapt well to the determination of seismic velocities by using one of the following; by recording down-hole velocities (Riggs, 1955) using in-hole detectors and near-surface shots; using continuous velocity logs; and by using cross-hole methods (see section 2.7), (McCann et al., 1975).

2.9 DIRECT CONTACT METHODS

These include vertical drilling, horizontal drilling (from the tunnel face), and pilot tunnels.

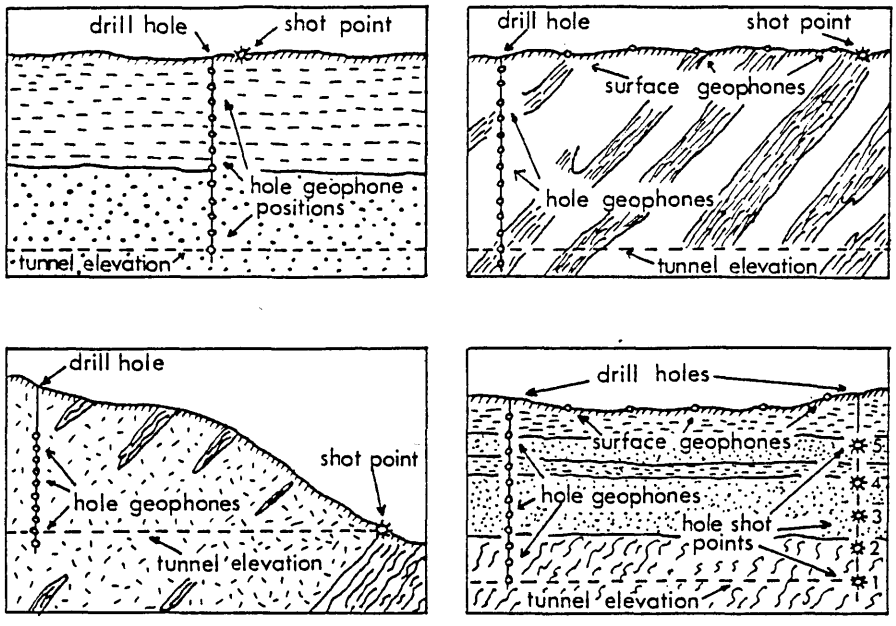

Figure 2.4 Some possible configurations for seismic investigation of bedrock utilizing drill holes. (Adapted from Bath, 1974)

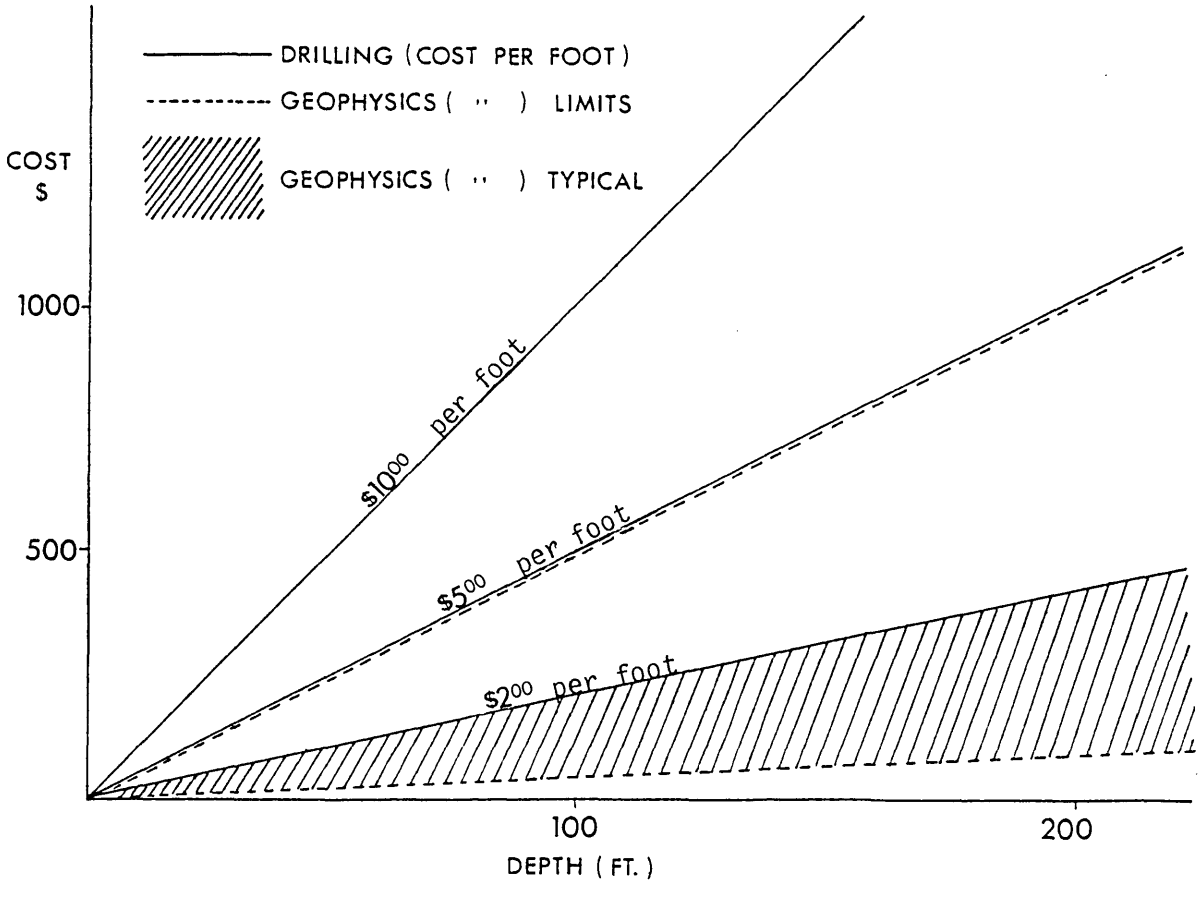

Figure 2.5 Geophysics versus drilling costs.

Vertical coring using a diamond bit (wireline) produces a sample which can be analyzed by a geologist. The core so produced may give a false impression of ground conditions due to its small size, but an experienced geologist and good drilling team should overcome this problem (ref. BRE/TRRL Report, 1975). However, using this method the information gained is at only a few points along the line of the tunnel, and it can be misleading to interpolate between them. The information gleaned from cores can be supplemented by lowering geophysical probes into the boreholes (as described in previous sections of this chapter), but, even so, this is an expensive method of exploration, as shown in Figure 2.5 which compares the typical cost of geophysical methods versus drilling costs. Also, when used in narrow boreholes, acoustical and electromagnetic techniques lose some of their direction-sensing capabilities due to the reduction in aperture (Majtenyi, 1976).

Horizontal boring, either between access shafts or from the tunnel face, is a method of exploration that has become more popular in recent years (BRE/TRRL, 1975; Majtenyi, 1976: Symposium, 1977; Williamson, 1972). This is due in part to the great increase in the cost of pilot tunnels (see Fig. 2.6), and the raising of safety standards. The cost of horizontal drilling is about one magnitude lower than that of a pilot tunnel, and this cost difference is expected to increase in the future. However, horizontal boreholes have all the problems associated with vertical boreholes, except

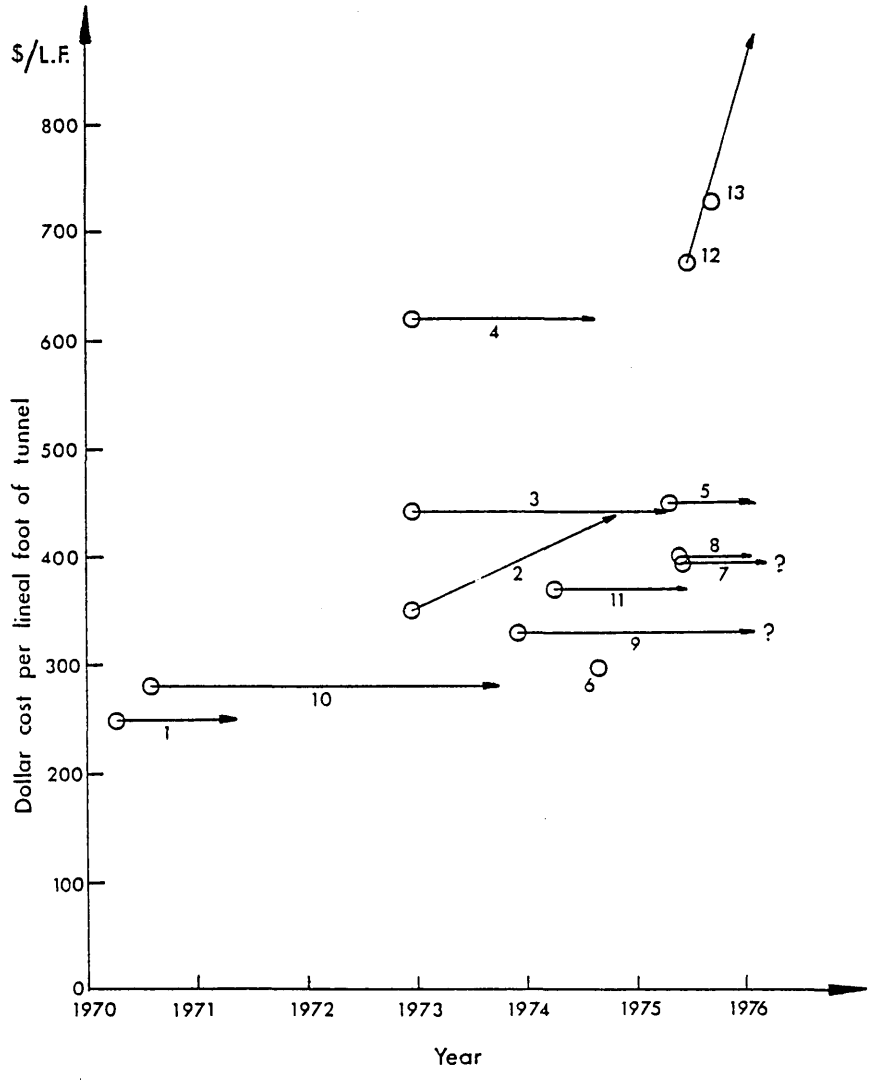

Figure 2.6 Pilot tunnel cost data.

that the coverage is better. But, when drilling long distance horizontal holes (4000 to 5000 feet is now possible) an additional problem is that of steering and surveying errors, which can be as much as 200 feet in the horizontal plane, and 100 feet in the vertical plane at the end of a 5000 feet hole (Harding et al., 1975). Surveying of a horizontal borehole may be required every 20-30 feet, and, including the procedures necessary to correct the line of the hole, can become the most important single cost item of the drilling (Tables 2.1 and 2.2).

Pilot tunnels are only used in the construction of very large tunnels and range in diameter from 6 to 12 feet. They are very expensive to construct (Table 2.3 and Fig. 2.6), but some of this cost can be offset against the secondary purposes which a pilot tunnel may serve. These include safety, grouting, placement of reinforcing, and multiple drift penetration. There are additional advantages in that a physical inspection of the rock in situ is allowed and that utilizing geophysical methods such as resistivity and ground penetrating radar, the orientation of fault zones and joint patterns, as well as the location of soil-rock interfaces and water-filled cavities, can be determined to a reasonable accuracy within a range of 25 to 100 feet from the pilot tunnel.

Name & Location	Owner or Contractor	Diameter (inches)	Length (feet)	Year	Cost ($/L.F.)
South Africa	Boart D. Ltd.	2.36	4,000	1975	-
ERDA, Mercury Site	Fenix & Sci.	3.00	3,690	1972	36.94
ERDA, Mercury Site	Fenix & Sci.	3.00	1,544	1972	25.20
ERDA, Mercury Site	Fenix & Sci.	3.00	2,002	1973	33.36
ERDA, Mercury Site	Fenix & Sci.	3.00	1,378	1972	38.35
ERDA, Mercury Site	Fenix & Sci.	3.00	2,653	1973	34.94
Cerritos Channel	Titan	3.50	1,126	1974	174.00
Wheeler Junction	C. S. Robinson	3.00	1,180	1970	15.00
Gorman, California	Soil. Samp. Serv.	4.75	940	1970	3.00
Drains in mines	Anaconda Min.	4.75	700	1976	8.00
Seikan Tunnel	Japan	6.75	5,300	1972	-

Table 2.1 Horizontal Drilling Data

Length of hole (feet)	Cost ($/L.F.)
1,000	32.16
2,000	37.45
3,000	45.10
4,000	52.90
5,000	60.59

Table 2.2 Average costs of wireline core drilling

No.	Name & Location	Owner	Date of Estimate	$/L.F.
1	Dupont Circle, Washington, D.C.	WMATA	03/03/70	250
2	Zoological Park, "	WMATA	12/19/72	350
3	Cleveland Park, "	WMATA	12/19/72	442
4	Van Ness, "	WMATA	12/19/72	620
5	Tenley Circle "	WMATA	03/26/75	450
6	Friendship Heights, "	WMATA	08/07/74	300
7	Bethesda, "	WMATA	04/23/75	400
8	Medical Center, "	WMATA	04/23/75	400
9	Cunningham, Colorado	Bu. of Reclamation	11/08/73	330
10	Hunter Tunnel, Colorado	Bu. of Reclamation	07/28/70	280
11	Yellowtail, Dam, Montana	Bu. of Reclamation	02/28/74	371
12	Bonneville, Washington	Corps. of Engineers	06/03/75	672
13	Drift, Eisenhower, Colorado	State of Colorado	08/08/75	773

Table 2.3 Pilot tunnel data

CHAPTER III

DATA ANALYSIS

3.1 AN INTRODUCTION TO POWER SPECTRAL ANALYSIS

This chapter discusses the techniques which are in general use for the analysis of time series, concentrating on spectral calculations by what is usually called the indirect or correlation-transform method (Bath, 1974). Most of the data used for this thesis has been analyzed using this method. It is the method favoured by Jenkins and Watts (1969), on whose book much of the analysis has been based. Other useful texts include, Blackman and Tukey (1958); Bendat and Piersol (1971); Bath (1974); and Chatfield (1975).

This chapter also includes a section on the direct, or periodogram, method of spectral calculation using the fast Fourier transform (FFT). Other methods, including the maximum entropy method (MEM) and the Walsh sequential spectrum method are briefly described. The final section is a comparison of spectral calculations using MEM, Walsh and Fourier methods on a 2048-bit sample of real data.

Unless otherwise acknowledged, the equations found in this chapter were obtained from Spectral Analysis and its Applications by Jenkins and Watts (1969), to which the reader is referred for derivations and background material.

3.1.1 Signal Types

In geophysics we meet three basic types of signal. These three types are known as periodic, transient, and random. The periodic type are also known as deterministic, i.e., their future behaviour can be predicted from a knowledge of their past behaviour. The two other types are non-deterministic and their future behaviour cannot be predicted. Due to their lack of periodicity, random and transient signals must be dealt with using statistical methods. Signals can be further classified as stationary or non-stationary, depending upon whether their statistical properties are time-independent or not. Periodic signals are stationary and transient signals are non-stationary, whereas random signals can be either.

A time series is either a deterministic or non-deterministic function x, of an independent variable t. The time series we are analyzing are non-deterministic and so we must adopt a statistical approach. Therefore, it is the average behaviour of the time series which is important.

3.1.2 Stochastic Process

A stochastic process is a collection of random variables which are ordered in time according to probabilistic laws. Any observed time series can be regarded as one example of the infinite set of time series which might have been observed. This doubly infinite set of time series is called the ensemble.

Thus, associated with each time series there is a probability model, and so, time series analysis is essentially concerned with evaluating the properties of this model. An important class of stochastic processes are those which are termed stationary, and it is these that we shall be concerned with.

3.1.3 Stationarity

In order to simplify the analysis of time series we must make certain important assumptions about them. The most important of these is that the associated stochastic process is stationary. In practice, stationarity of a stochastic process is taken to mean its second-order stationarity. This means that the process may be described by the lower moments of its probability distribution. These lower moments include the mean, variance and autocorrelation function. This assumption is strictly true for a Normal (Gaussian) process, but is usually true for most de-trended (see section 3.3.1) time series met in geophysics. In other words the time series may be said to be stationary if the statistical parameters describing it are time-independent.

3.1.4 Autocorrelation and the Power Spectrum

Consider the time series $x(t)$, existing $(-T/2, T/2)$ which we shall assume is stationary i.e., unaffected by translation of the origin in time. The autocovariance function (ACVF) is defined as:

$$C(u) = \lim_{T\to\infty} \frac{1}{T} \int_{-T/2}^{T/2} (x(t)-\bar{x})(x(t+u)-\bar{x})dt \qquad (3.1)$$

where u, and $\bar{x}$ are the lag and mean value of the variable x respectively. We shall assume that the mean value $\bar{x}$ is zero, and hence the autocovariance becomes;

$$C(u) = \underset{T\to\infty}{\text{Lt.}} \frac{1}{T} \int_{-T/2}^{T/2} x(t)x(t+u)dt \qquad (3.2)$$

This is related to the power spectrum by the Fourier transform relationship (Bracewell, 1965), that is, the autocovariance function and the power spectrum form a Fourier transform pair. The symmetry of the transform and inverse transform is evident from equations 3.3 and 3.4 below. The transform relationship between the autocovariance function and power spectrum holds irrespective of whether x(t) possesses a Fourier transform, so that the result covers stationary random functions as well as periodic ones (Champeney, 1973).

$$P_e(f) = \int_{-\infty}^{\infty} C(u).e^{-i2\pi fu}du \qquad (3.3)$$

and consequently,

$$C(u) = \int_{-\infty}^{\infty} P_e(f).e^{i2\pi fu}df \qquad (3.4)$$

Setting u = 0 in (3.2) and (3.4) gives,

$$C(o) = \int_{-\infty}^{\infty} P_e(f)df = \frac{1}{T} \int_{-T/2}^{T/2} x^2(t)dt = \sigma^2 \qquad (3.5)$$

and is the variance or total power in the signal. Thus, $P_e(f)$ shows how the signal power is distributed over frequency. $P_e(f)$ can be normalized by dividing by the variance σ^2. The function $P_e(f)/\sigma^2$ is called the spectral density function. This provides a useful method of comparing time series with different scales of measurement. From (3.3) it follows that,

$$P_e(f)/\sigma^2 = \int_{-\infty}^{\infty} \frac{C(u)}{C(o)} . e^{-i2\pi fu} du \qquad (3.6)$$

so that the spectral density function is the Fourier transform of the autocorrelation function (ACF).

These equations must be modified for a finite length of continuous record. The autocovariance function is now given by,

$$C(u) = \frac{1}{T} \int_{-(T-|u|)/2}^{(T-|u|)/2} x(t)\, x(t+u)\, dt \qquad (3.7)$$

and the power spectrum is given by

$$P_e(f) = \int_{-T}^{T} C(u) . e^{-i2\pi fu} du \qquad (3.8)$$

The power spectrum obtained using this method will have large variance. This can be seen in the following example (after Jenkins and Watts, 1969) of applying Fourier analysis to a

stochastic process consisting of a series of 400 random Normal deviates, known as Gaussian white noise. The spectrum for the first 50 and first 100 terms of the series is shown in Figure 3.1 for the frequencies f = 0.02, 0.04 ...., 0.5 Hz with the sampling interval, Δt = 1 sec. The theoretical spectrum is also shown and is constant in the range -1/2 <f<1/2. Note that the fluctuations for N=100 are as large as for N=50, indicating a lack of statistical convergence. Table 3.1 summarizes the results obtained from calculating the spectrum for N=50, 100, 200 and the full 400 terms of the series. The variances do not decrease as N increases.

N	50	100	200	400
mean	0.85	1.07	1.00	0.95
variance	0.630	0.777	0.886	0.826
mean square error	0.652	0.782	0.886	0.828

Table 3.1 Behaviour of sample spectra of white noise as the record length is increased.

The mean square error for spectral estimators is the expected or mean value of the square of the smoothed spectral estimator minus the theoretical spectrum; i.e., m.s.e. = $E\left[(\bar{P}_e(f) - P_t(f))^2\right]$. Time series are characterized by random changes of frequency, amplitude and phase and so the Fourier method must be modifed (Jenkins and Watts, 1969).

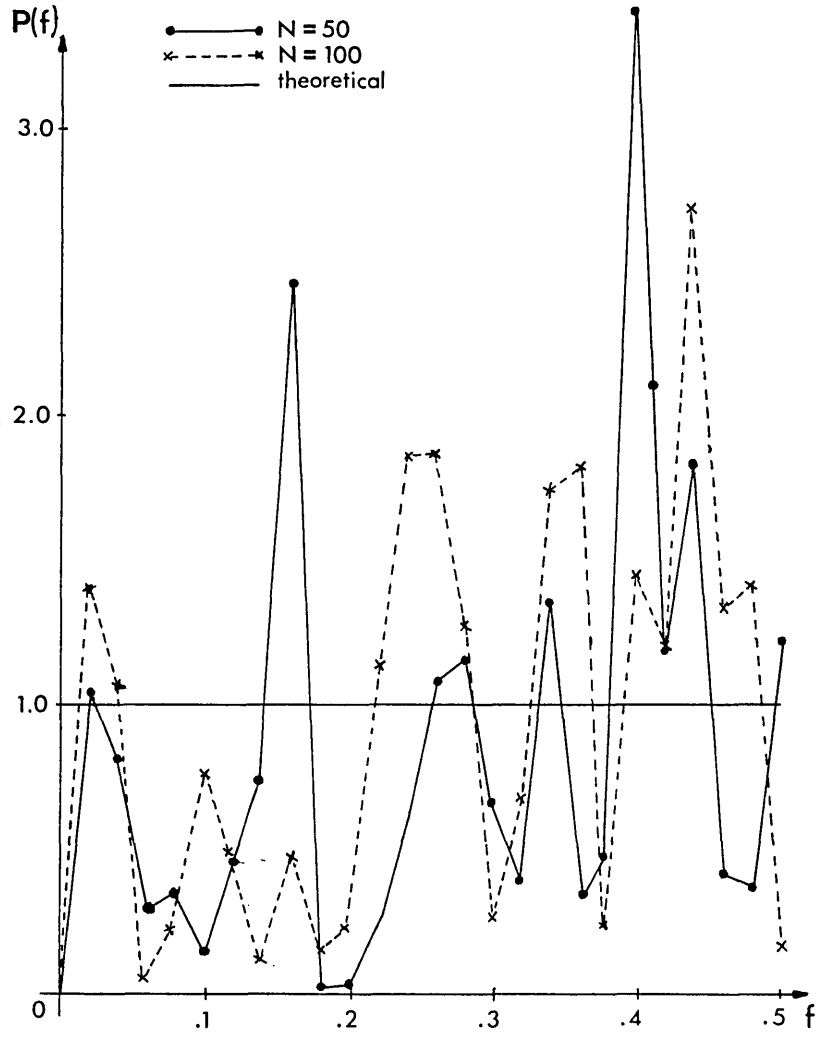

Figure 3.1 Sample spectra for 50 and 100 terms of a realization of discrete Normal white noise. (after Jenkins and Watts, 1969)

A method of reducing the variance associated with the Fourier method is by smoothing or windowing. This smoothing can be achieved by using a lag window (Blackman and Tukey, 1958), which is equivalent to segmental averaging (Bartlett, 1953). Bartlett showed the reduction in variance that was possible by averaging the sample spectra of eight subseries, formed by splitting the original time series into eight equal parts (Table 3.2). $P(f)$ is the spectral estimate of the original time series and $\bar{P}(f)$ is the smoothed spectral estimate formed by averaging the spectral estimates from the eight subseries.

	Mean	Variance	Mean sqr. error
$P(f)$	0.95	0.826	0.828
$\bar{P}(f)$	0.95	0.139	0.143

Table 3.2 Lower moments of smoothed and unsmoothed spectral estimates.

3.2 PREANALYSIS CONSIDERATIONS FOR DISCRETE DATA

Prior to estimating power spectra, it is necessary to consider the effect of using finite data records and representing the analogue signal by a succession of discrete points. Discretization of the data will introduce the special problem of aliasing, whilst using a finite data set will introduce problems such as the Gibbs phenomenon. The Gibbs phenomenon is the error caused by approximating a discontinuity using smoothly varying functions, as in the Fourier method.

3.2.1 Data Windows

In practice it is only possible to obtain finite lengths of record. Associated with this truncation there will be an error, or bias, even if x(t) is a deterministic function. The operation of taking a finite length of record is equivalent to multiplying the actual signal x(t) by the data window w(t), defined by,

$$w(t) = \begin{cases} 1, & |t| \leq T/2 \\ 0, & |t| > T/2 \end{cases} \qquad (3.9)$$

It follows that the transform X(f) is the convolution of the transforms of x(t) and w(t).

$$X(f) = \int_{-\infty}^{\infty} x(g)\, W(f-g)\, dg \qquad (3.10)$$

where, the spectral window W(f) is the Fourier transform of the data window and hence

$$W(f) = T\, \frac{\sin \pi ft}{\pi ft} \qquad (3.11)$$

Figure 3.2(a) and (b) illustrate the effect of two data windows of different width. The input signal is three unit delta functions and the frequency spacing f_2-f_1 is 1/T Hz. For the rectangular data windows T must be of the order $T \geq 1/(f_2-f_1)$ in order to resolve the two peaks.

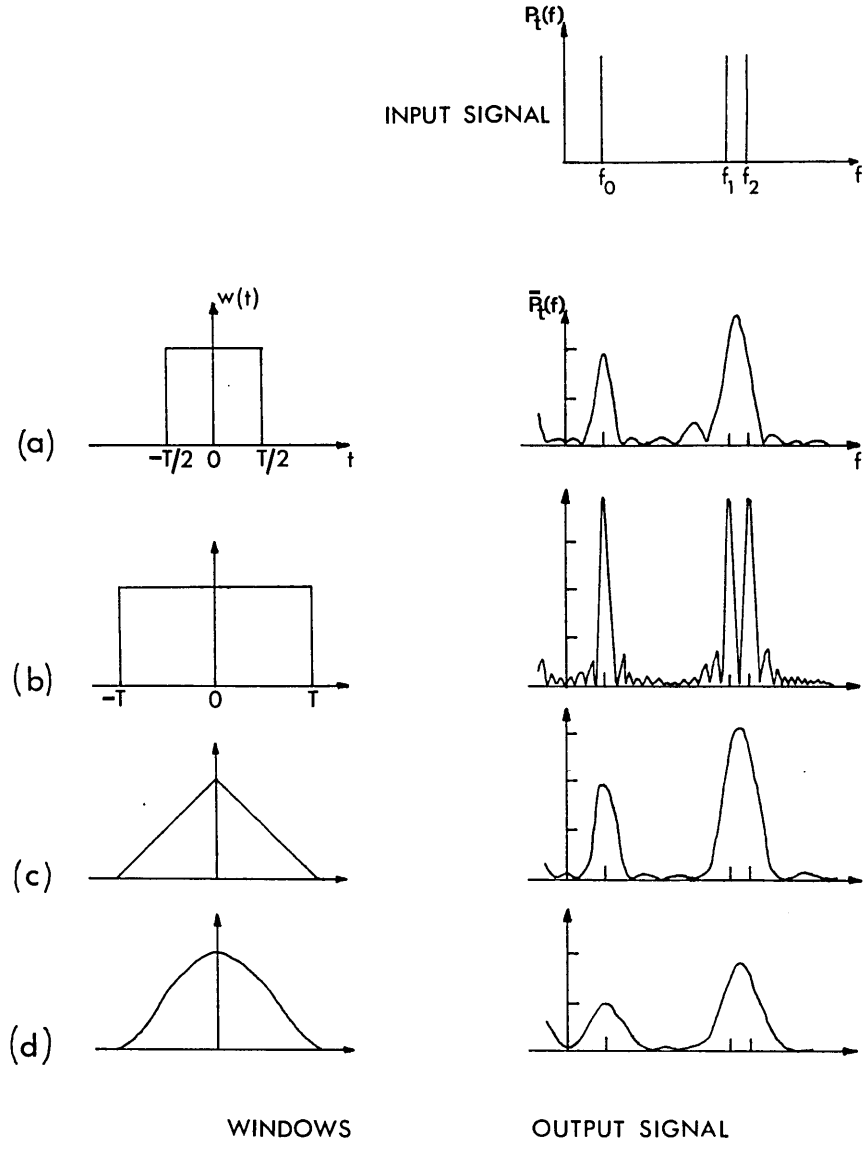

Figure 3.2 The effects of window shape and duration on signal spectra.

3.2.2 Smoothing of Spectra

It is not necessary to restrict the window to the form of Equation (3.9). It is possible to choose any reasonable shape and impose this upon the data set. Two such windows, of width 2T, are illustrated in Figure 3.2 (c) and (d). For non-rectangular windows such as these, their width must be greater than $2/(f_2-f_1)$ in order to resolve two peaks at frequency spacing (f_2-f_1). These chosen windows are normally called lag windows in the time domain, since they are given as a function of lag (Table 3.3), and spectral windows in the frequency domain, the spectral window being the Fourier transform of the lag window.

A general smoothed estimator of the form

$$\bar{P}_e(f) = \int_{-\infty}^{\infty} w(u)C(u).e^{-i2\pi fu}du \qquad (3.12)$$

will have a smaller variance than the unsmoothed estimator $P_e(f)$. The lag window $w(u)$ in (3.12) is a function satisfying the conditions:

(1) $w(o) = 1$

(2) $w(u) = w(-u)$

(3) $w(u) = 0, \quad |u| > T$

Description	Lag Window	Spectral Window ($-\infty < f < +\infty$)
Rectangular or Box-Car	$w_R(u) = \begin{cases} 1, & \lvert u\rvert \leq T_M \\ 0, & \lvert u\rvert > T_M \end{cases}$	$W_R(f) = 2T_M\left(\frac{\text{Sin } \omega T_M}{\omega T_M}\right)$
Bartlett	$w_B(u) = \begin{cases} 1 - \frac{\lvert u\rvert}{T_M}, & \lvert u\rvert \leq T_M \\ 0, & \lvert u\rvert > T_M \end{cases}$	$W_B(f) = T_M\left(\frac{\text{Sin } \omega/2T_M}{\omega/2\ T_M}\right)^2$
Tukey	$w_T(u) = \begin{cases} \frac{1}{2}\left(1 + \cos \frac{\pi\lvert u\rvert}{T_M}\right), & \lvert u\rvert \leq T_M \\ 0, & \lvert u\rvert > T_M \end{cases}$	$W_T(f) = T_M\left(\frac{\text{Sin } \omega T_M}{\omega T_M}\right)\left(\frac{1}{1-(\omega T_M/\pi)^2}\right)$
Parzen	$w_p(u) = \begin{cases} 1 - 6\left(\frac{\lvert u\rvert}{T_M}\right)^2 + 6\left(\frac{\lvert u\rvert}{T_M}\right)^3, & \lvert u\rvert \leq \frac{T_M}{2} \\ 2\left(1 - \frac{\lvert u\rvert}{T_M}\right)^3, & T_{M/2} < \lvert u\rvert \leq T_M \\ 0, & \lvert u\rvert > T_M \end{cases}$	$W_p(f) = \frac{3}{4}\ T_M\left(\frac{\text{Sin } \omega T_M/4}{\omega T_M/4}\right)^4$

Table 3.3 Lag and spectral windows

Description	Lag Window	Spectral Window ($-\infty < f < +\infty$)
Rectangular or Box-Car	$w_R(u) = \begin{cases} 1, & \lvert u\rvert \leq T_M \\ 0, & \lvert u\rvert > T_M \end{cases}$	$W_R(f) = 2T_M\left(\frac{\text{Sin } \omega T_M}{\omega T_M}\right)$
Bartlett	$w_B(u) = \begin{cases} 1 - \frac{\lvert u\rvert}{T_M}, & \lvert u\rvert \leq T_M \\ 0, & \lvert u\rvert > T_M \end{cases}$	$W_B(f) = T_M\left(\frac{\text{Sin } \omega/2T_M}{\omega/2\ T_M}\right)^2$
Tukey	$w_T(u) = \begin{cases} \frac{1}{2}(1 + \cos\frac{\pi\lvert u\rvert}{T_M}), & \lvert u\rvert \leq T_M \\ 0, & \lvert u\rvert > T_M \end{cases}$	$W_T(f) = T_M\left(\frac{\text{Sin } \omega T_M}{\omega T_M}\right)\left(\frac{1}{1-(\omega T_M/\pi)^2}\right)$
Parzen	$w_p(u) = \begin{cases} 1 - 6(\frac{\lvert u\rvert}{T_M})^2 + 6(\frac{\lvert u\rvert}{T_M})^3, & \lvert u\rvert \leq \frac{T_M}{2} \\ 2(1 - \frac{\lvert u\rvert}{T_M})^3, & T_{M/2} < \lvert u\rvert \leq T_M \\ 0, & \lvert u\rvert > T_M \end{cases}$	$W_p(f) = \frac{3}{4}\ T_M\left(\frac{\text{Sin } \omega T_M/4}{\omega T_M/4}\right)^4$

Table 3.3 Lag and spectral windows

In practice condition (3) is replaced by,

$$(4)\ w(u) = 0, \quad u \geqslant T_M,\ T_M < T$$

since covariances need then only be computed to lag T_M. Examples of lag windows are given in Table 3.3 and plotted in Figure 3.3. The corresponding spectral windows are also given, and plotted in Figure 3.4.

The general objective in any spectral analysis is to estimate the theoretical or true spectrum as accurately as possible. For this there are two requirements; (1) that the mean smoothed spectrum $\bar{P}_t(f)$ be as close to the true spectrum $P_t(f)$ as possible; and (2) that the variance of the smoothed spectral estimator $\bar{P}_e(f)$ be small, where,

$$\text{Var}\left[\bar{P}_e(f)\right] \simeq \frac{P_t^2(f)}{T}\,\frac{T_M}{b_1} \qquad (3.13)$$

For the first condition to be satisfied the bias, given by,

$$B(f) = \bar{P}_t(f) - P_t(f) \qquad (3.14)$$

must be as small as possible. The mean smoothed spectrum is the expected or average value of the spectral estimator, ($\bar{P}_t(f) = E\left[P_e(f)\right]$) and b_1 is the standarized bandwidth of the particular window used. The bandwidth b of a spectral window is defined as the width of a rectangular window which gives the same variance, and b_1 is equal to bT_M.

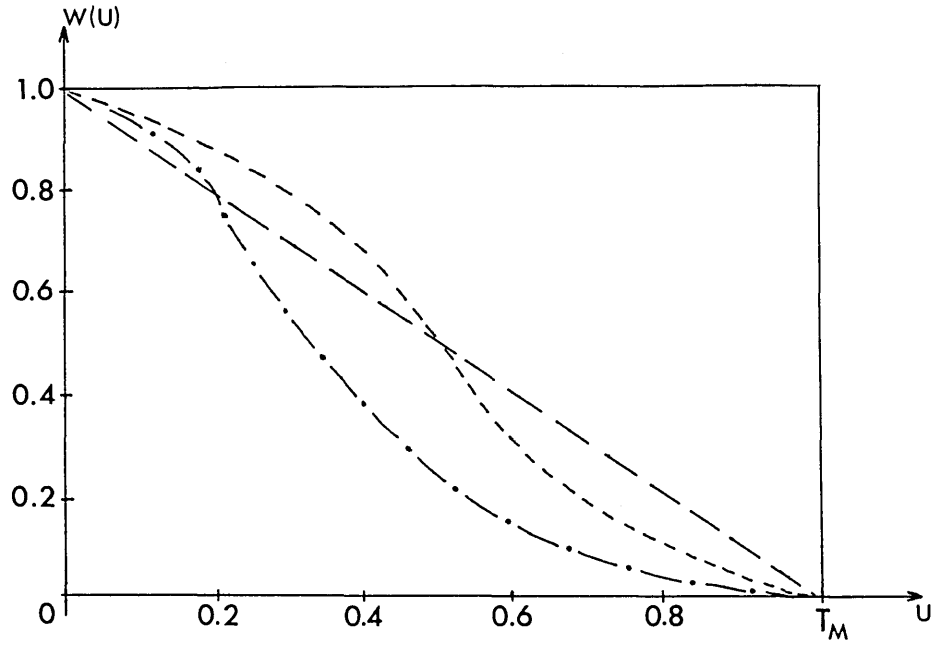

Figure 3.3 Some common lag windows.

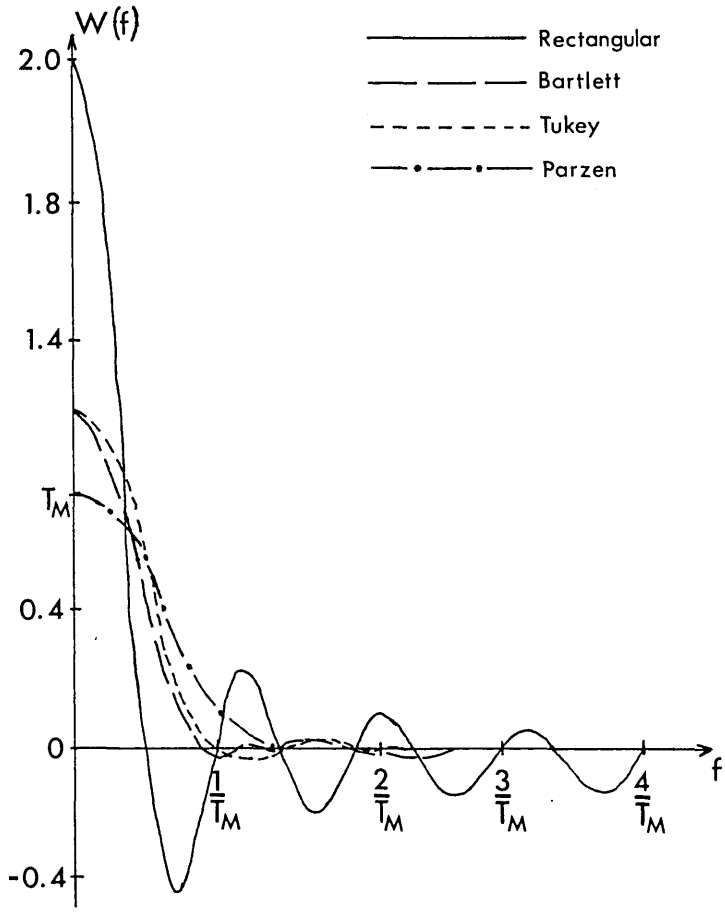

Figure 3.4 Spectral windows corresponding to the lag windows above.

In Figure 3.2 (a) and (b), if lag windows w(u) correspond to the data windows w(t) it is seen that as the base width ($\equiv T_M$) of the window decreases, so the bias will increase. Hence, in order to keep the bias small T_M must be large, typically greater than 10% of the record length. However, from the equation (3.13) for variance above, it is seen that T_M must be small for small variance. Thus, it is necessary to find a compromise in the size of T_M.

The need to compromise between bias and variance, and only having arbitrary optimality criteria, indicate an empirical approach to smoothing. The technique, called window closing by Jenkins and Watts (1969), suggests first to find a window of acceptable shape, then to compute smoothed spectral estimates. Initially, a wide bandwidth is used, and then progressively smaller bandwidths, exposing more and more detail in the spectrum. This process should continue until the bandwidth is less than the smallest significant detail in the spectrum. (This procedure was followed in the analysis of data used in this thesis; see Section 4.5).

3.2.3 Data Sampling

In geophysics one is normally dealing with the sampled form of a signal, which makes up a discrete time series. Any signal can be sampled, provided that the Nyquist frequency (see Section 3.2.4) is greater than the highest frequency of interest. A sampled signal can be thought of as the result of multiplying the original continuous signal x(t) with a Shah function:

$$s(t) = \sum_{n=-\infty}^{\infty} \delta (t - n \Delta t) \qquad (3.15)$$

This produces a sampled signal in the time domain $x_i(t)$, where

$$x_i(t) = x(t) . s(t) \tag{3.16}$$

Hence, using the convolution theorem, the Fourier transform of the sampled signal is given by,

$$X_i(f) = \int_{-\infty}^{\infty} X(f-g)\, S(g)\, dg \tag{3.17}$$

where S(g) is the Fourier transform of the Shah function (Lighthill), 1959) given by,

$$S(g) = \frac{1}{\Delta t} \sum_{n=-\infty}^{\infty} \delta \left(g-\frac{n}{\Delta t}\right) \tag{3.18}$$

Therefore, substituting the expression (3.18) for S(g), equation (3.17) becomes,

$$X_i(f) = \int_{-\infty}^{\infty} X(f-g) \frac{1}{\Delta t} \cdot \sum_{n=-\infty}^{\infty} \delta \left(g-\frac{n}{\Delta t}\right) dg$$

$$= \frac{1}{\Delta t} \sum_{n=-\infty}^{\infty} X \left(f-\frac{n}{\Delta t}\right) \tag{3.19}$$

The sampled signal $x_i(t)$ has a Fourier transform with period $1/\Delta t$, and if $X(f)$, the transform of the continuous signal, is zero when $|f| \geq 1/2\,\Delta t$, then $X_i(f)$ is simply a periodic version of $X(f)$. Therefore, it is possible to recover $X(f)$ from $X_i(f)$ by multiplying $X_i(f)$ by $H(f)$

$$X(f) = H(f)\, X_i(f) \tag{3.20}$$

where, $H(f)$ is given by,

$$H(f) = \begin{cases} \Delta t, & |f| \leq \dfrac{1}{2\Delta t} \\ 0, & |f| > \dfrac{1}{2\Delta t} \end{cases} \tag{3.21}$$

3.2.4 Aliasing

Since any time series $x(t)$ is pure real, the real part of its Fourier transform $X(f)$ is finite and even. From Section 3.2.3 it was seen that the sampled signal has a Fourier transform with a period $1/\Delta t$. Therefore, in the frequency domain the transform is centred on frequencies $n/\Delta t$ where $n = 0, 1, 2....$ etc., and Δt is the sampling interval. If only the harmonics up to $N/2$ ($= 1/2\,\Delta t$) exist in the signal then it is possible to recover $x(t)$ from $x_i(t)$ (Fig. 3.5a). But, if higher harmonics than $N/2$ exist in the signal then the situation as in Figure 3.5b will occur. For example, if $\Delta t = 0.1$ sec then $1/2\,\Delta t = 5$ Hz and the discrete transform $X_i(f)$ at 4 Hz will be made up of contributions from $X(f)$ at 4 Hz, 10+ 4 = 14 Hz, -10 + 4 = -6 Hz, 20 + 4 = 24 Hz, - 20 + 4 = -16 Hz, etc. (Fig. 3.5c). These additional frequencies are

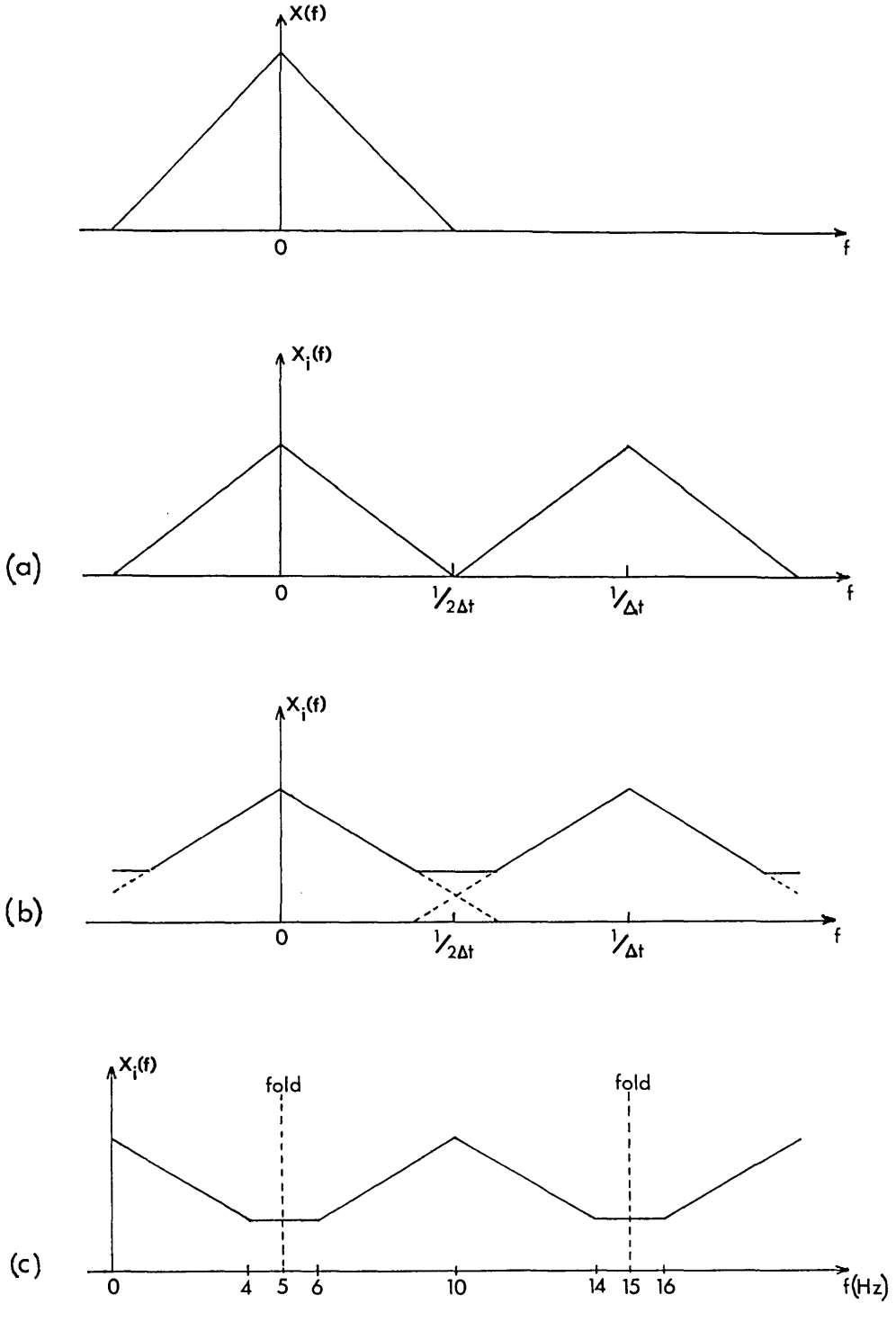

Figure 3.5 Transforms of a signal X (f) and sampled signals X_i (f).

called aliases of the 4 Hz. An illustration of how aliasing can occur from an insufficient sampling rate is found in Figure 3.6. The frequency $1/2\,\Delta t$ is called the Nyquist or folding frequency (Blackman and Tukey, 1958).

Thus, in any observed time series, any noise present at frequencies greater than the Nyquist frequency will be aliased to appear at lower frequency. The only ways to avoid aliasing are, either to sample the data at a high enough rate that $f_N > f_{MAX}$ of the signal (where f_N is the Nyquist and f_{MAX} the highest frequency contained in the signal), or to subject the signal to a low-pass filter before sampling. No filtering process after sampling can remove the effects of aliasing.

3.3 POWER SPECTRAL ESTIMATION OF DISCRETE TIME SERIES

In practical power spectral estimation we are almost invariably dealing with discrete values derived from the analogue signal at some chosen time interval. The formulae corresponding to those of the analogue case are obtained by replacing the integrals by summations.

Suppose that the discrete signal x_t, $t = 1, 2, \ldots N$, corresponds to values of the signal $x(t)$ at intervals of Δt. The autocovariance is then given by,

$$C(m) = \frac{1}{(N-m)} \sum_{t=o}^{N-m} x_t x_{t+m} \quad , \; m=0,1,2\ldots.L \tag{3.22}$$

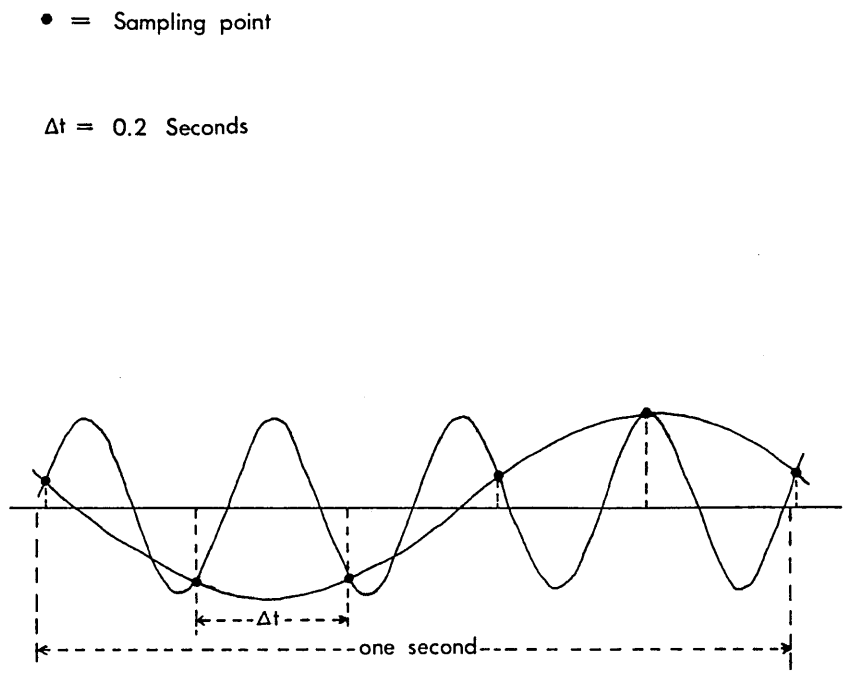

Figure 3.6 An example of aliasing. The 1 Hz signal is resolved but the 4 Hz is not.

where $L = T_M/\Delta t$ and T_M is the truncation point expressed in seconds; L is therefore the truncation point expressed in terms of the lag. Hence, the smoothed spectral estimate $\bar{P}(f)$ is given by,

$$\bar{P}(f) = \Delta t \sum_{m=-(L-1)}^{L-1} w(m)C(m).e^{-i2\pi f\Delta tm} \quad , \quad \left[\frac{-1}{2\Delta t} \leqslant f < \frac{1}{2\Delta t}\right] \tag{3.23}$$

where, w(m) is the lag window of width T_M. However, since $\bar{P}(f)$ is an even function of frequency (C(u) is an even function of time), only half of it need be calculated and the ACVF can be written as a cosine Fourier series with zero phase shift. But, in order to preserve the FT relationship between the sample spectrum and ACVF, it becomes necessary to double the power associated with each frequency in the range. Hence, the formula used for calculation of the smoothed power spectral estimates is

$$\bar{P}(f) = \Delta t\,(p(0)+2 \sum_{m=1}^{M} w(m)C(m)\ \cos 2\pi fm\Delta t) \tag{3.24}$$

$$\left[0 \leqslant f \leqslant \frac{1}{2\Delta t}\right]$$

where p(0) is the phase term.

3.3.1 De-Trending

In general, time series in geophysics are non-stationary. However, they can normally be made stationary, or nearly so, by the removal of the non-stationary component of the signal. This component is generally termed "drift", and can be of natural or instrumental origin, or introduced during analysis. De-trending means eliminating this drift, and must be complete

to avoid contamination of the spectrum (c.f. prewhitening, section 3.3.2). Detrending is usually achieved by either least squares removal of a trend curve obtained from an examination of the observations, or by low-cut/high pass filtering.

For observations of earth tides, gravity and magnetics, the major cause of drift is of instrumental or natural origin. In the case of continuous-wave seismics we are interested in time intervals which are short enough that only drift introduced during analysis need be considered.

3.3.2 Prewhitening

Prewhitening is the performing of a filtering operation on the data using a filter with carefully chosen frequency response function, the spectral analysis being carried out on the output from this filter. There are two reasons for this filtering operation.

(a) Errors will be incurred during the recording of the data and this "error spectrum" will probably be white. If the output from the filter is nearly white, then the effect of the error spectrum will be distributed evenly for all frequencies. This will work providing the prewhitening is done before sampling the data (Jenkins, 1961).

(b) The much more important reason is that if the spectrum to be estimated is not white, then there will be considerable distortion in a region where P(f) changes

> rapidly over the bandwidth of the window. In particular, a large contribution to the estimate corresponding to a given peak frequency might arise from leakage from a frequency at some distance away from this if P(f) had a peak at this point and simultaneously the spectral window had a side lobe. This means that by prewhitening, to make spectra as uniform and as smooth as possible, we may apply standard spectral windows and be sure that the reliability of the estimate will depend only upon the particular window used and not upon the spectral shape.

The prewhitened spectrum is obtained by applying a filter to the data which will result in as flat a spectrum as possible, the form of the filter obviously depending upon the frequency characteristics of the data. The spectrum is then calculated in the normal way. To obtain the true estimates an inverse prewhitening filter must be applied which will be the inverse of the amplitude function of the filter used. This operation is known as "post-colouring".

If a time-series has a non-zero average (biased), then a zero frequency peak will be introduced into $\bar{P}(f)$, whose side lobes will distort the low frequency end of the spectrum. Removal of the mean, or high-pass filtering to remove the whole of the near-zero frequency part of the spectrum is a special case of the application of prewhitening. Bolt and Marussi (1962) used a difference filter (high-pass) to prewhiten tidal spectra and found a signifcant improvement in the resulting spectra. (This approach was used on the data analyzed for this thesis; see section 4.5).

3.3.3 Reliability of Spectral Estimates

The variance of the smoothed spectral estimator, $\bar{P}_e(f)$ has an approximately chi-squared distribution with v degrees of freedom, where (Jenkins and Watts, 1969)

$$v = \frac{2T}{\int_{-\infty}^{\infty} w^2(u)\, du} \qquad (3.25)$$

where, T is the length of the record and w(u) is the lag window used. This is approximately equal to twice the width of the spectral window measured in units of T^{-1}. Chi-square is defined as a quantity distributed as $x_1^2 + x_2^2 + x_3^2 + ... + x_v^2$, where x_1, x_2, ..., x_v are independent random variables having a Gaussian distribution and having average zero and variance unity. Chi-squared can also be said to be the probability density function of the variance of Normal (or Gaussian) random variables. Thus, for any fixed number of degrees of freedom there is a probability that the true value lies between limits about an estimated value which are determined by the chi-square distribution and can be found from tables.

Now,

$$v = \frac{2T}{T_M} b_1 \qquad (3.26)$$

(Jenkins and Watts, 1969), where b_1 is the standardized bandwidth of the window. This gives a relative measure of the bandwidths of different spectral windows. Table 3.4 shows the standard windows with their associated standardized bandwidth and number of degrees of freedom. As can be seen from Table 3.4, a wide window such as the Parzen window Wp(f) will have the larger number of degrees of freedom and hence the smaller variance for a given truncation point T_M. However, this means that this window will have the larger bias.

Description	Degrees of Freedom ν	Standardized Bandwidth b_1
Rectangular	T/T_M	0.5
Bartlett	$3T/T_M$	1.5
Tukey	$2.667T/T_M$	1.333
Parzen	$3.71T/T_M$	1.86

Table 3.4 Properties of spectral windows.

Assuming a chi-square distribution, each $\bar{P}(f)$ will have an associated confidence interval depending upon the number of degrees of freedom (Table 3.5). For a smoothed spectral estimate the $(100 - \frac{a}{2})\%$ confidence interval is given by,

$$\frac{\nu\bar{P}(f)}{\chi_\nu(1-\frac{a}{2})} \quad , \quad \frac{\nu\bar{P}(f)}{\chi_\nu(\frac{a}{2})} \tag{3.27}$$

(Jenkins and Watts, 1969). From these equations it is seen that the confidence interval must be computed separately for each frequency. If, however, we take the logarithm of the power spectrum and plot this against frequency we have, from (3.27) the confidence interval for Log $\bar{P}(f)$ as,

Degrees of Freedom (v)	Confidence Limits (95%)
1	0.20 - 1000
2	0.21 - 40
3	0.32 - 14
4	0.36 - 8.3
5	0.39 - 6.0
6	0.42 - 4.8
8	0.46 - 3.8
10	0.49 - 3.1
15	0.55 - 2.4
20	0.59 - 2.1
50	0.69 - 1.55
100	0.78 - 1.35
150	0.81 - 1.27
200	0.83 - 1.23
300	0.86 - 1.18

Table 3.5 Confidence limits of power spectra assuming chi-squared distribution (After Munk et al., 1959).

$$\text{Log}\bar{P}(f) + \text{Log}\frac{v}{\chi_v(1-\frac{a}{2})} \quad , \quad \text{Log}\bar{P}(f) + \text{Log}\frac{v}{\chi_v(\frac{a}{2})} \qquad (3.28)$$

Therefore, the confidence interval can be given as a single value, independent of frequency.

It may not be necessary to calculate confidence intervals if it is only required to identify maxima and minima of the spectrum. Also, when the peaks are very pronounced as in Figure 3.7, any type of confidence test is made rather superfluous.

3.3.4 The Fast Fourier Transform

The fast Fourier transform (FFT) was first reported by Cooley and Tukey (1965), although it was not then known by this name. The FFT has a long and interesting history which has been summarized by Cooley, Lewis and Welch (1967). These papers are found in a special journal issue which was devoted entirely to the FFT (I.E.E.E.)

The FFT is an algorithm for the fast computation of discrete Fourier transforms but at the same time retaining accuracy. It takes advantage of the fact that the calculation of the coefficients of the discrete Fourier transform (DFT) can be carried out iteratively which results in a considerable saving of computation time. Specifically, if the time series consists of $N = 2^n$ samples then about $2N \log_2 N$ arithmetic

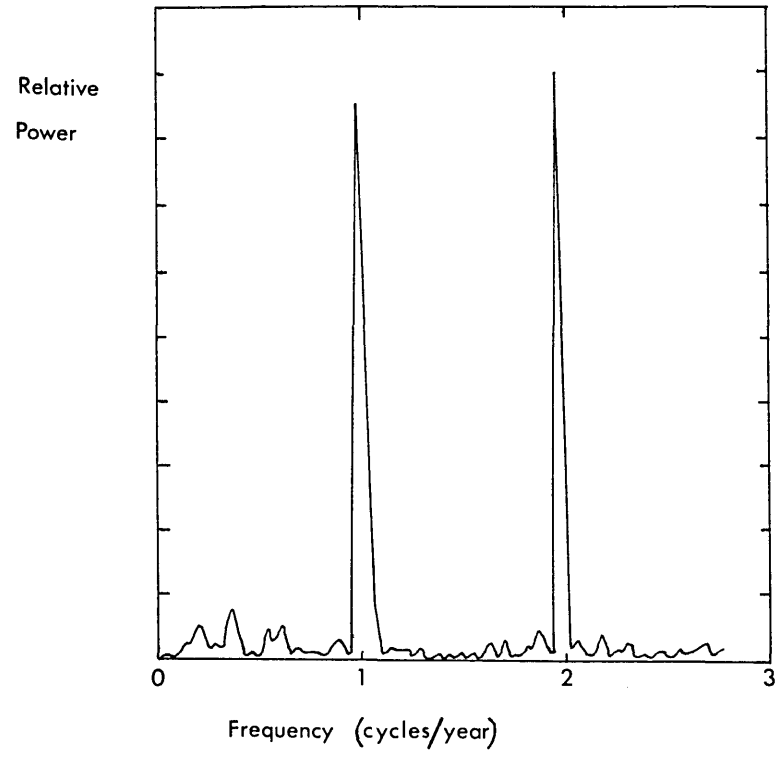

Figure 3.7 Exceptionally pronounced peaks in the power spectrum of a river runoff. After Reed (1971).

operations will be required to evaluate all N associated DFT coefficients using the FFT, whereas N^2 operations would be required using the straightforward Fourier transform procedures (Cochran et al., 1967).

However, Jenkins and Watts (1969) maintain that fast computers are adequate for the needs of spectral analysis, without use of the FFT. Also that the autocorrelation function is a very valuable intermediate stage in spectral analysis, especially for the choice of a suitable range of truncation points. But, it is possible to form the autocorrelation function using the FFT by performing an inverse transform on the power spectrum (Bingham et al., 1967).

Only a small amount of data used for this thesis has been analyzed using the FFT. This is because; (a) although the FFT method preserves the phase information, this was not useful in our case since for any frequency the phase will be random due to contributions from different paths (multiples) and different wavelengths (P-, S-, and surface-waves) at the same frequency; (b) the computer programs for calculating the power spectrum via the ACF already existed and only needed modification; (c) the time series used were not very long; (d) although much slower in calculation time the computing cost was not very different from that using the FFT (see Section 3.3.6); and (e) the autocorrelation was required and could be obtained at an intermediate stage in the spectral calculation. The autocorrelation is useful in deciding whether to difference (high-pass filter) the series or not and to help choose a suitable range of truncation points for the lag window.

3.3.5 Other Methods for Estimating Spectra

The two methods most used for the estimation of power spectra, the periodogram (Jones, 1965) and the autocorrelation method, both make unrealistic assumptions concerning the extension of the finite duration sample signal. The periodogram method assumes a periodic extension, whereas the autocorrelation method assumes zero extension.

The most efficient method to use will depend, to a certain extent, on the nature of the time series to be analyzed. For example, for transient phenomena it is more efficient to expand them in a series of functions with properties similar to the transients themselves. There is a class of such functions called Laguerre functions (Dean, 1964). For special purposes, expansion in other functions may be more appropriate. However, two methods that are gaining in popularity are the maximum entropy method (MEM), and the Walsh sequential spectral method.

The maximum entropy method was first suggested by Burg in 1967 (Burg, 1967), and a detailed description of the method can be found in a paper by Ulrych and Bishop (1975). The maximum entropy method uses Wiener optimum filter theory to design a prediction-error filter which will whiten the input time series. From the whitened output power spectrum and the response of the prediction filter, it is possible to compute the input power spectrum. This leads to an estimate with a very high resolution since the method uses the availble lags in the sample autocorrelation function without smoothing and

makes a non-zero prediction of the lags in the ACF beyond those which can be calculated directly from the available data.

The Walsh sequential spectrum is a method to analyze any given curve into a summation of square waves (Gubbins et al., 1971). Using square functions is analogous to Fourier methods, but two advantages of the Walsh transform are; (a) the Walsh transform is quicker and easier to calculate, because only additions and subtractions are involved; and (b) Walsh transforms have no Gibbs phenomenon and do not require any special windowing in the time domain.

3.3.6 A Comparison of Spectral Estimation Methods

This section compares the performance of four methods of estimating power spectra. These are; (a) power spectra via the ACF; (b) power spectra using the FFT: (c) the Walsh transform method; and (d) the maximum entropy method. The computer programs for the Fourier methods were based on Jenkins and Watts (1969) and the subroutine N log N (Robinson, 1967), respectively. The program for the Walsh spectral analysis came from the book by Beauchamp (1975), and that for the MEM, from two papers by Borrodale and Erickson (1980). All the calculations were performed on the same piece of field data, taken from the records obtained at Cocking (See Chapter V), which consisted of a 2048-bit sampled time series digitized at a rate of 333 Hz, thus giving a Nyquist frequency of 166.5 Hz. The computer used was a CDC 6500 belonging to the Imperial College Computer Centre.

(a) Fourier transform method via the autocorrelation function.

For this method a Parzen window was used with a truncation point of approximately 1/10th the data length. Thus, a bandwidth of about 3 Hz was achieved. The power spectrum obtained is shown in Figure 3.8 and peaks at 32 Hz, 54 Hz, 66 Hz, 75 Hz, 98 Hz and 133 Hz are clearly discernible. The execution time on the computer was 23.208 central processor (CPU) seconds which was slow, but the resolution and accuracy were good. The small peak just below the Nyquist frequency was due to aliasing and caused by an insufficiently sharp cut-off filter.

(b) Power spectrum via the FFT.

The spectrum obtained using this method is shown in Figure 3.9. Fewer points are plotted in this case but the peaks are again resolved as in case (a). The reduction in amplitude of the peaks is not significant since they still lie within the confidence interval (95%) of method (a). The execution time was 4.037 (CPU) seconds, about 5.5 times as fast as the autocorrelation method. However, the FFT method is only 0.5 times as expensive in total computer time since compilation, input/output and memory used must also be taken into consideration as well as the execution time. The accuracy is not quite as good as the previous method possibly due to the plotted points not exactly coinciding with the peaks.

(c) Walsh power spectrum.

The computer program is based on a fast Walsh transform (FWT) subroutine which gives the coefficients in sequency order. The Walsh coefficients are analogous to the Fourier coefficients and thus sequency is directly comparable with frequency. The sequency spectrum below (Fig. 3.10) shows a large amount of variance, but the spectrum has been smoothed and so the variance is probably due to the unsuitability of the Walsh transform for this kind of time series (cosinusoidal). The program is very fast (2.732 (CPU) secs execution time) but, the large variance precludes any degree of confidence in the estimates of amplitude.

(d) The maximum entropy method

The program of Barrodale and Erickson (1980) has been slightly modified but remains essentially theirs and is fully described in their paper. The program enables the use of forward prediction, backward prediction or both. The prediction filter coefficients are calculated by one of two subroutines (user-selected) and calculations continue until the Akaike final prediction error (FPE) is met, i.e., until a local minimum in the FPE is met. The FPE is given by,

$$FPE_m = \frac{n+m+1}{n-m-1} P_m \qquad (3.29)$$

Where, P_m is the mean square residual for the least squares solution to the system of normal equations (see Barrodale and Erikson, 1980) and m is the number of coefficients (or optimal order for the autoregressive process used for the prediction); n is the number of points in the time series.

Using forward and backward prediction the optimal solution was reached using 13 coefficients which took 7.333 (CPU) seconds execution time. As can be seen from the spectrum (Fig. 3.11) the optimality criterion must be used with caution since it is obvious that the spectrum is too smooth, i.e., m is too low. Recalculating with 20 coefficients (Fig. 3.12) gave a spectrum with well resolved peaks and took 10.336 (CPU) seconds. Comparing Figures 3.11 and 3.12 the calculated values of the spectral estimates are highly dependent upon m and some a priori knowledge of the amplitudes would facilitate the use of this method.

In summary, it appears that the best method to use for any particular data set is dependent upon the nature of that data. The FFT is best for smoothly varying data, whilst the FWT is best for discontinuous data. However, when only very few or less than one cycle is available the MEM will give best results. In all cases caution should be observed in the choice of window or filter length and the inherent inaccuracies of spectral analysis should be kept in mind.

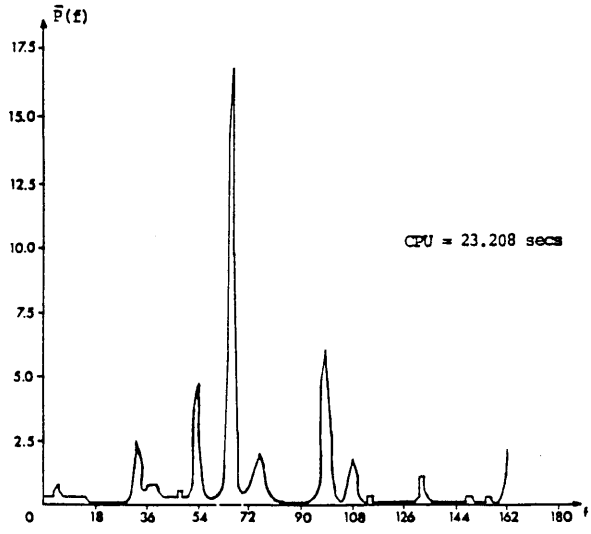

Figure 3.8 Power spectrum via the autocorrelation function.

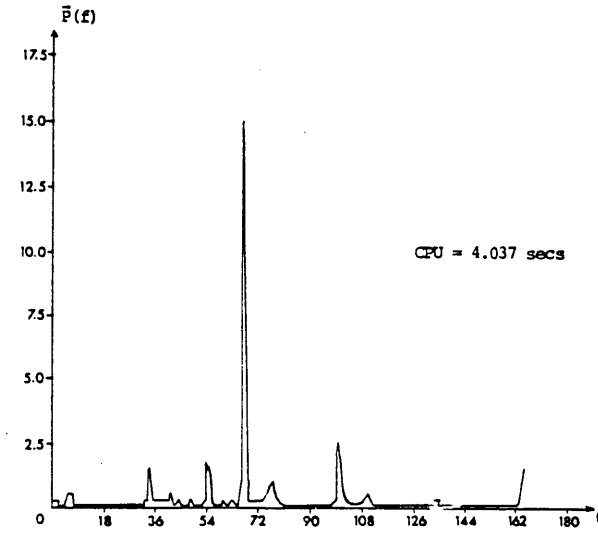

Figure 3.9 Power spectrum via the fast Fourier transform.

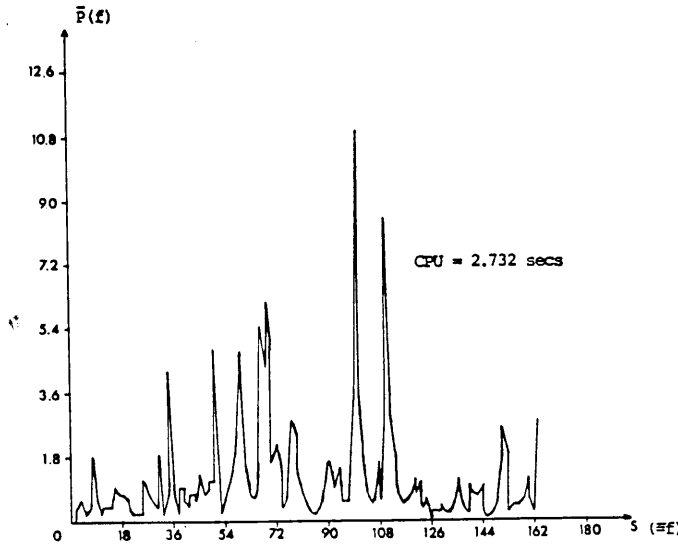

Figure 3.10 Power spectrum via the fast Walsh transform.

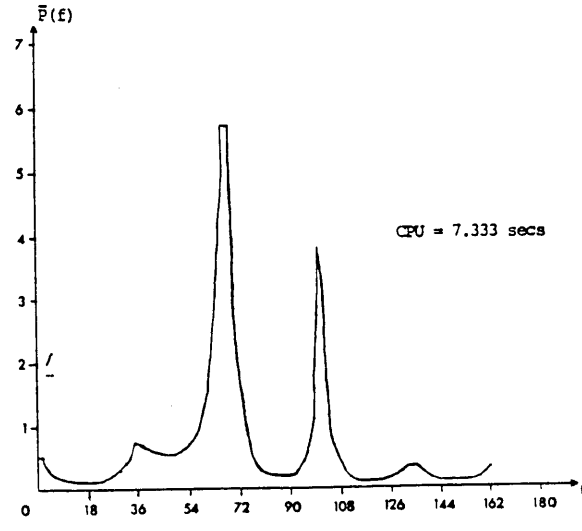

Figure 3.11 Power spectrum by the maximum entropy method (13 coefficients)

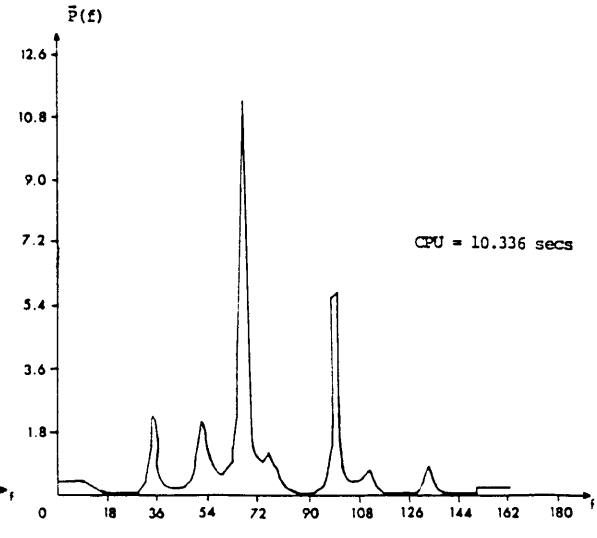

Figure 3.12 Power spectrum by the maximum entropy method (20 coefficients)

3.4 A GLOSSARY OF SOME NOTATION USED IN CHAPTER III

$\bar{x}$	mean value of the function, observation
$x(t)$	time series
$x_i(t)$, $x_t(t)$	discrete time series
$X(f)$	Fourier transform of $x(t)$
u	lag
$C(u)$	autocovariance function (ACVF)
$\frac{C(u)}{C(o)}$	autocorrelation function (ACF)
$w(t)$	data window
$w(u)$	lag window
$W(f)$	spectral window
E	expected or average value
$P(f)$	spectral estimate
$\bar{P}(f)$	smoothed spectral estimate
$P_e(f)$	spectral estimator
$\bar{P}_e(f)$	smoothed spectral estimator
$P_t(f)$	power spectrum (true or theoretical)
$\bar{P}_t(f)$	smoothed (mean) power spectrum ($\equiv E\left[\bar{P}_e(f)\right]$)

CHAPTER IV

WARRINGTON - A FEASIBILITY TRIAL

4.1 INTRODUCTION

The purpose of this first piece of experimental work was to establish whether a tunnelling machine could act as a seismic source suitable for probing ahead of the tunnel face using geophones on the ground surface as detectors. The major requirement for this was that the spectrum of the tunnelling machine should be stationary, i.e., the lower moments of its output signal should be constant for a given geological medium and model of operation. Also, the spectrum should possess some discrete peaks in order to carry out quantitative measurements, such as attenuation. It was also proposed to investigate whether changes in the characteristic power or amplitude spectrum of the tunnelling machine and changes in the attenuation constant would reflect changes in the local geology.

A feasibility study was carried out on a tunnelling machine in operation at Warrington New Town, Cheshire. The machine was a Mole type, with a rotary, full-face cutting action and weighed about 45 tons (Walsh and Biggart, 1976). The tunnel was for the construction of a relief outfall sewer and ran beneath a densely populated urban area. The tunnel was about 2.5 m in diameter and was to extend for 1.350 km.

The data on which this analysis is based was obtained by the Engineering Geology Unit of the Institute of Geological Sciences under a research contract with the Transport and Road Research Laboratories.

4.2 GEOLOGY

The route of the tunnel runs approximately parallel to the Manchester Ship Canal and only about 20 m from it. (Fig. 4.1) It has a minimum depth beneath the road of 3.2 m and passes through superficial deposits of alluvial sands and clays, fluvioglacial sands and gravels, blown sands, and boulder clay, which overlie Bunter Sandstone (Triassic).

When tunnelling began the face consisted wholly of the Bunter Sandstone. However, about 240 m along the route, the overlying alluvial deposits dip down to form a mixed face. The sandstone remained above the invert though, and over the next 100 m accounted for 50% to 75% of the face area, depending upon location. About 280 m along the route, and associated with the interface, a large number of dolerite and granite boulders up to 500 mm in diameter were encountered which were not revealed in the original site investigation (Bishop, 1977). The interface between the superficial deposits and the bedrock was sometimes difficult to delineate especially towards the eastern end of the route where the dense fluvioglacial sands overlie badly weathered sandstone. The eastern section of the drive (from about 340 m on) was mainly in alluvial deposits of loose to medium density sands (Walsh, 1976).

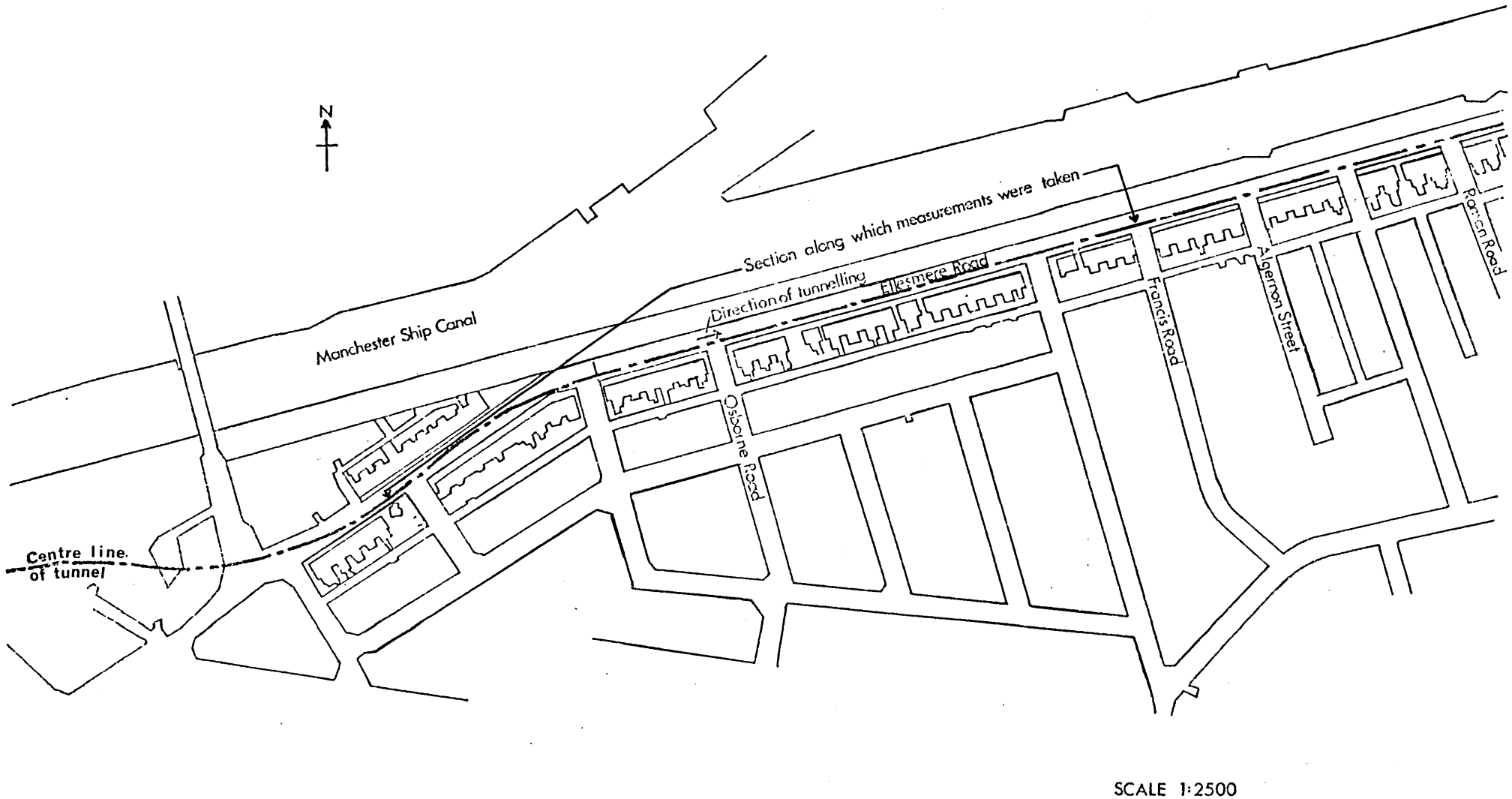

Figure 4.1 Route of the tunnel showing the section along which measurements used in this chapter were obtained.

A large number of boreholes were drilled for the site investigation. They were completed in two phases because of the failure of the first phase. The first phase, examples of which can be found in Figures 4.2 and 4.3 (nos. 378 to 381), were drilled in 1971 and subsequently the borehole logs were found to be in error. The second phase (Nos. 4905 and 4906) was completed in 1976 after a collapse of the tunnel face necessitated expensive remedial action, grouting, etc., to be undertaken.

The data that this chapter is based upon was collected from a section of tunnel about 340 m in length and commenced at about 185 m from the start of tunnelling.

4.3 DATA COLLECTION

This part of the work, carried out by the Engineering Geology Unit of the Institute of Geological Sciences, has been fully described elsewhere (Baria et al., 1978) and so only the main points will be given here.

A preliminary analysis, using an analogue spectrum analyzer, showed that the majority of the signals from the tunnelling machine was in the frequency range of 10 to 60 Hz. A system for recording this range of frequencies was designed accordingly.

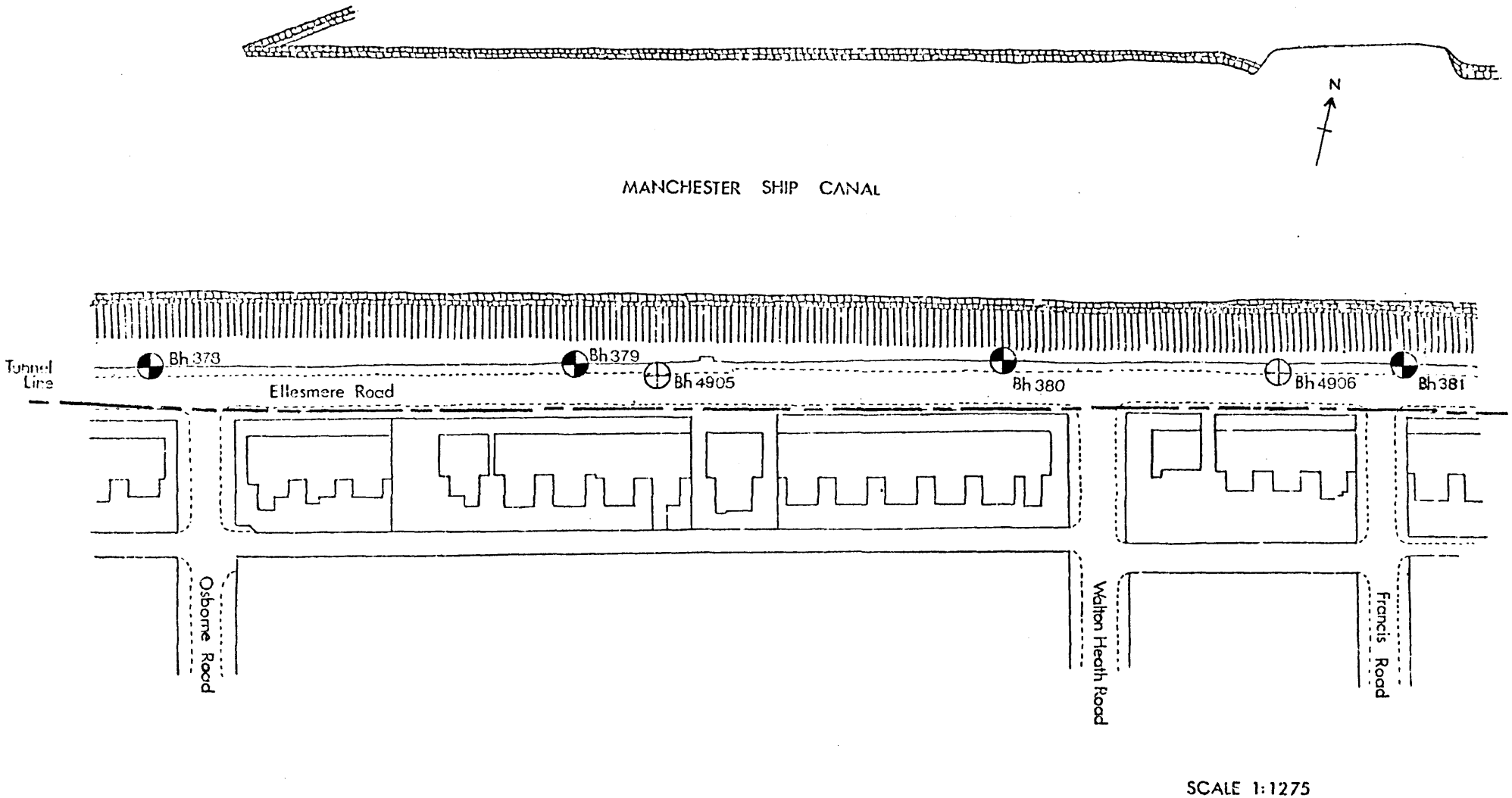

Figure 4.2 Section of tunnel showing the positions of the boreholes mentioned in the text. (After Baria et al., 1978)

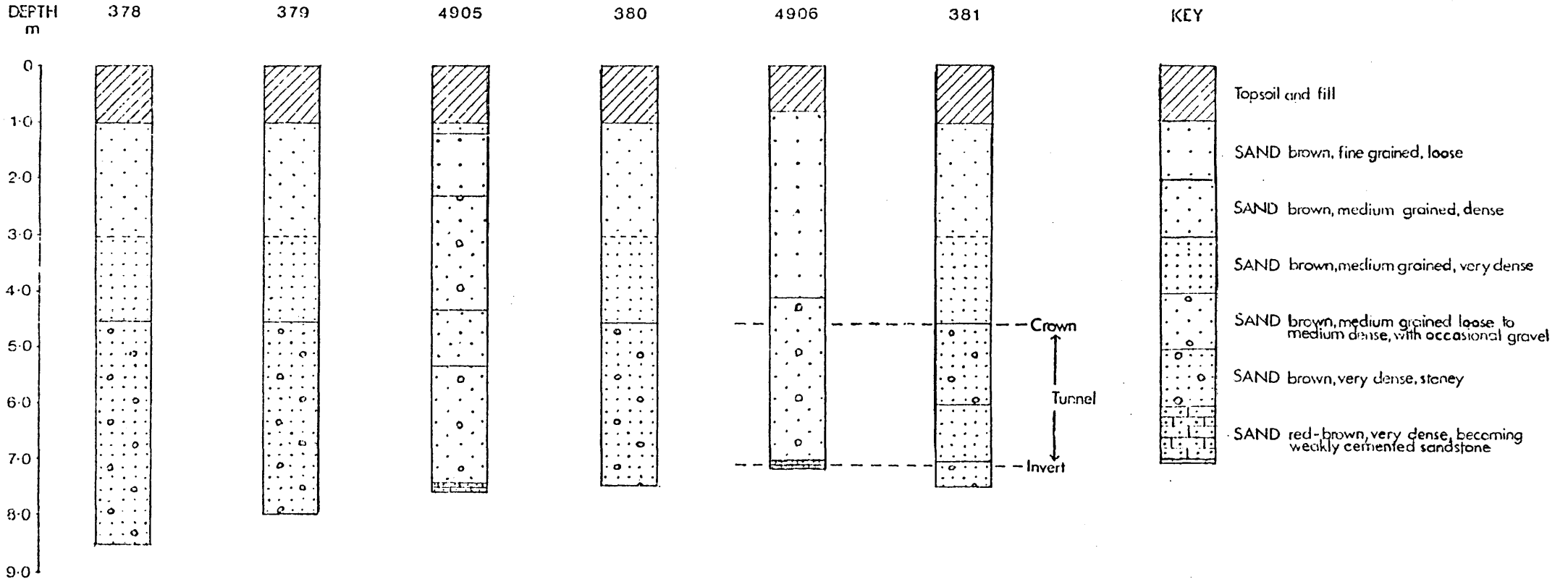

Figure 4.3 Borehole logs corresponding to the boreholes shown in Fig. 4.2. (After Baria et al., 1978)

The very early recording was done using only a single geophone placed on the surface, either directly above the tunnelling machine or a few metres ahead of it along the tunnel line. However, for most of the drive a four-channel amplifier was available which allowed the simultaneous recording of the outputs from three geophones, the fourth channel being used for a 1 kHz reference signal. Of the three geophones used, one was usually placed directly above the machine and the other two at various distances up to 60 m ahead of it. The geophones used were usually vertical type of 10 Hz natural frequency with a flat response up to 600 Hz, achieved by using a 1 k Ω shunt resistance which gave 68.5% damping. The whole signal acquisition system (Fig. 4.4) was designed to have a flat response over the frequencies of interest, and upon calibration and testing this was found to be so. The analogue data was recorded on 1/4 inch magnetic tape using a four-channel Fenlow FM tape recorder having a flat response from D.C. up to 1.5 kHz and a S/N ratio of 40 dB.

Some difficulty was experienced during recording in differentiating between times when the tunnelling machine was idling and when it was cutting. The monitor oscilloscope was not very helpful for this, but using headphones to monitor at the tape recorder was reasonably effective.

4.4 DATA PREPARATION

The first step was a visual inspection of the recorded data using the same Fenlow FM tape recorder to playback the tapes as was used for recording. At the same time the fourth

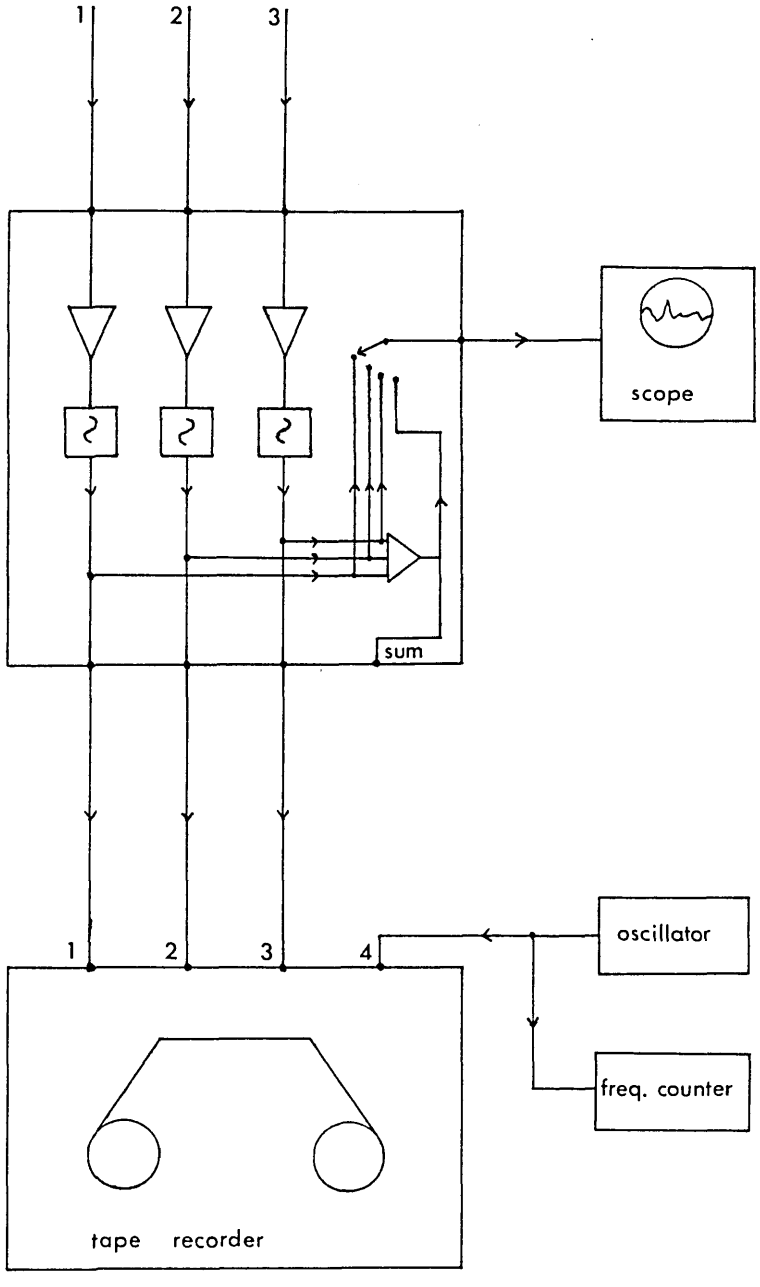

Key

▷ variable gain amp.

~ low pass filter

Figure 4.4 The signal acquisition system

channel was monitored using a digital frequency meter to reveal any fluctuations in the 1 kHz reference signal. It was also necessary to check the tape revolution counter against the field note book to take into account any variation and match the two exactly. Once suitable sections were chosen they were then digitized prior to analysis on the computer.

4.4.1 Analogue-to-Digital Conversion

The analogue-to-digital (A/D) converter used was that belonging to the Mechanical Engineering Department of Imperial College. It consisted of two basic parts; the timer unit and the converter unit. The timer unit was needed since it was required to digitize four channels simultaneously. This specially developed unit (Matthews, 1976) produced four, 2 microsecond pulses of 4 V amplitude with a separation frequency of 6.4 kHz. Therefore, the four analogue traces could be sampled sequentially with a time lag consistent with the 6.4 kHz frequency.

The A/D converter was an asynchronous, multiplexed 10-bit converter. It had a core store of 8 K and was designed for an input voltage of 0 to 10 V. The converter operated in conjunction with a PDP-15 computer which has a 16 K core store, 256 K word disc and 18 bit word length. To digitize the chosen records a systems program, called GE08 was used, written by Dr. R. Wing of the Mechanical Engineering Dept. The digitized data was first stored in the converter in 10-bit

words and then buffered into the PDP-15 where two 10-bit words were repacked into a new 18-bit word. The digitized signals were then dumped on to 8-track paper tape in two separate 4 K sections. The digitization system is shown in Figure. 4.5.

Additional facilities for checking the digitization were incorporated in the system and in GE08. The extra hardware was a Tektronix terminal and a line printer. Before producing any paper tape the four digitized channels could be displayed in turn on the Tektronix screen. If any of them were found to be unsatisfactory the record could be rejected and redigitized. The line printer produced hard copy of the first 200 values, in decimal, in each 4 K block of data. If all was found to be satisfactory the digitized values were dumped on to the paper tape in a binary-coded octal format. Each digitized value in millivolts (x 10) was in the form of a three-digit number which represented its location on the 0-10 V converter range.

The sections chosen for digitizing were played back using the Fenlow FM tape recorder and fed to the A/D converter via a specially constructed four-channel amplifier. The amplifier had a fixed gain on each channel of x 5 to use as much of 10 V range of the converter as possible without overloading it. Since the tape recorder gave an output of -1 V to +1 V, the amplifier also provided a bias of +5 V. Each channel of the amplifier was carefully checked and calibrated so that its response was known to be flat over the frequency range used and that any differences between the channels could be compensated for in later analysis.

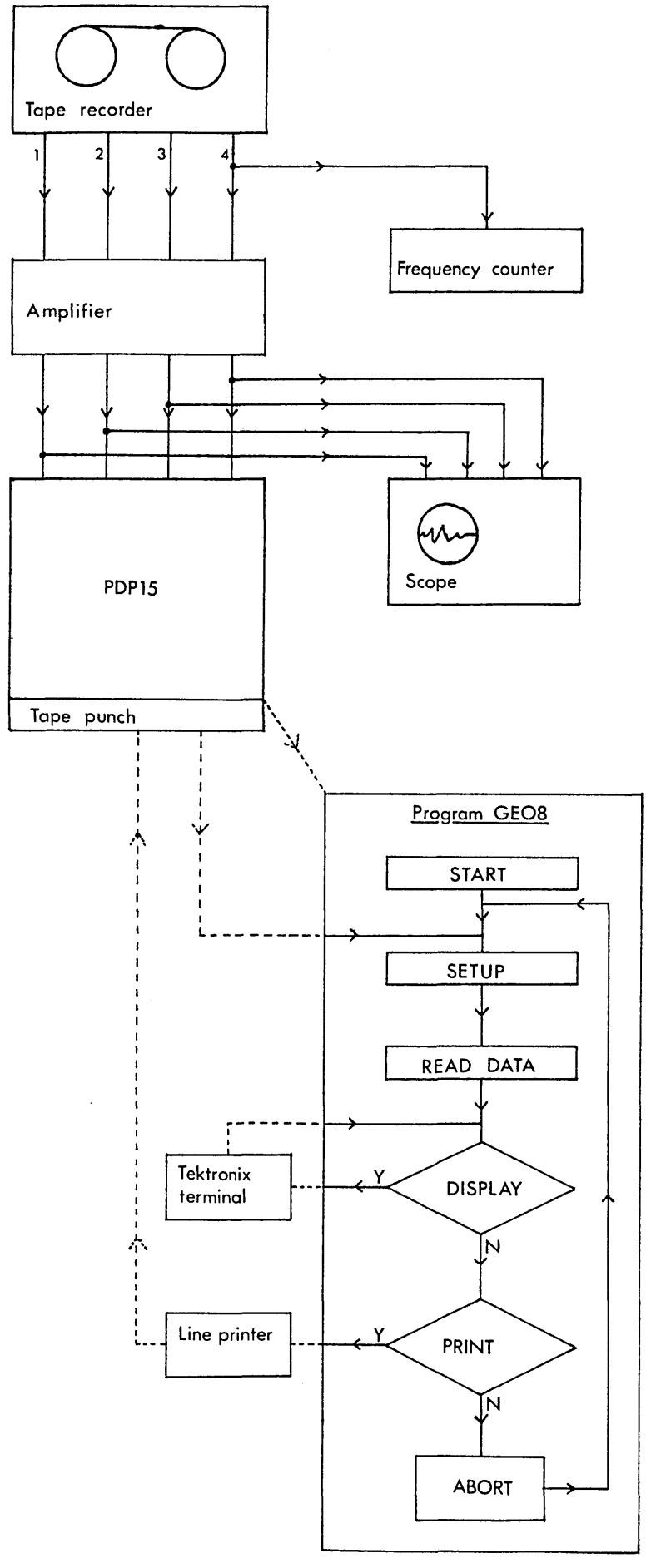

Figure 4.5 Schematic of the digitisation system and program GEO8

4.4.2 Conversion of Paper Tape

The paper tape containing the multiplexed, binary-coded octal values had to be converted to a form suitable for analysis and storage on the main computer system. The program used (CONVERT) first converted each frame of three binary values to an octal value, and then four octal values to the corresponding three-digit decimal number. These decimal numbers were then stored on disc from which they could be printed in order to check against the 400 decimal values for each record produced previously by the PDP-15. As a final check, each record could be plotted from the stored decimal values using programs SPLIT and REHASH (see Fig. 4.6).

4.5 DATA ANALYSIS

The data analysis by computer was done in two stages, calculation and plotting of the autocorrelation function, followed by calculation and plotting of the power spectrum. Each multiplexed record, containing four channels, were first demultiplexed so that each channel could be analyzed separately. But, before analysis began, the parameters for the analysis had to be chosen according to certain empirical criteria (see Chapter III). Since the A/D converter had a storage limit of only 2000 values per channel and the Nyquist frequency was chosen to be 100 Hz, the length of record was fixed at 10 seconds and the sampling interval (Δ t) at 0.005

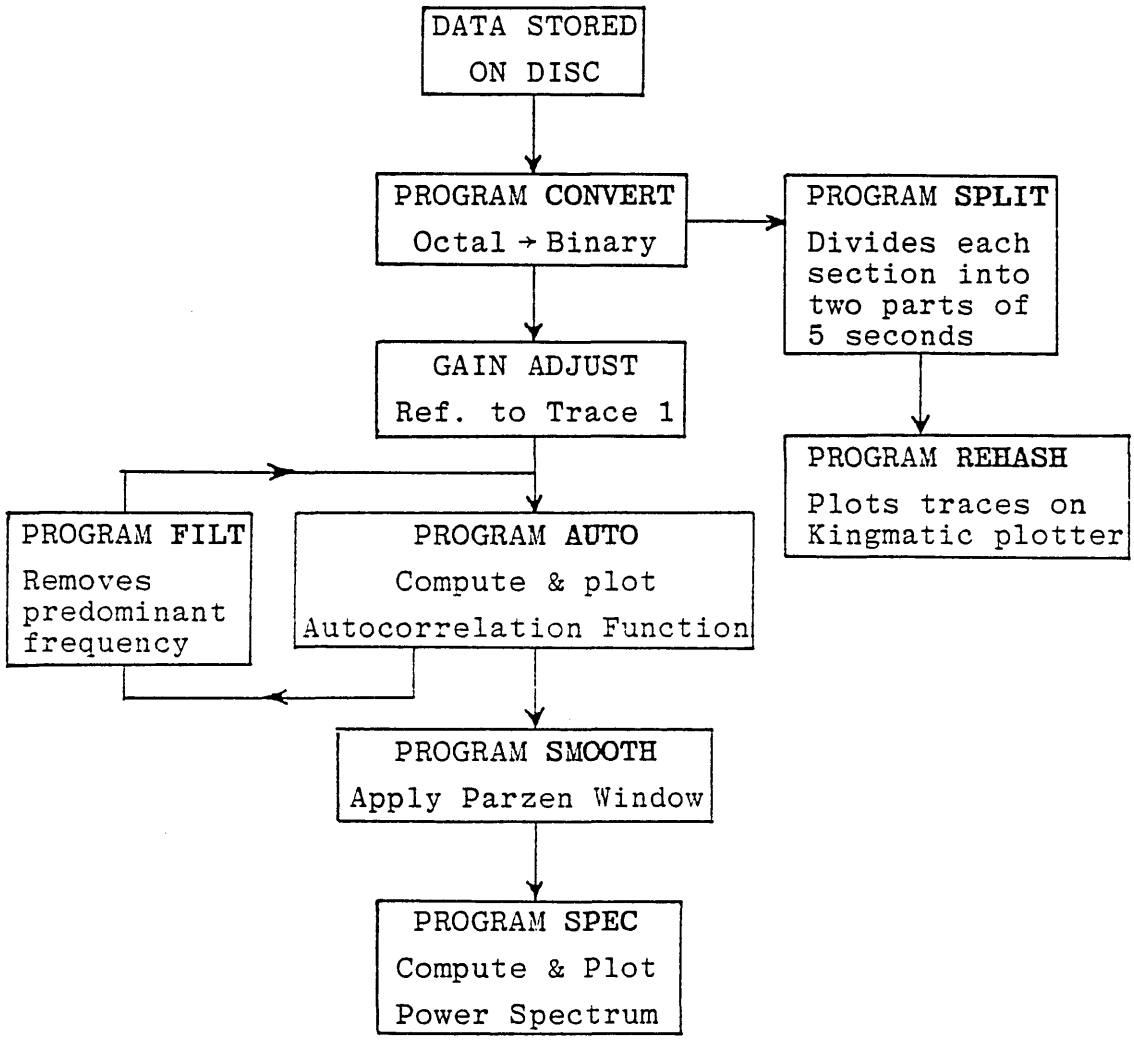

Figure 4.6 Programs and scheme for data analysis

seconds. Therefore, the choices remaining were the type and length of window to use. Jenkins and Watts (1969) maintain that it is the window width rather than the type of window that is important, since the different windows give much the same results. A Parzen window was used (see Chapter III) in this and subsequent analyses, as the form of this window prevents the introduction of negative power, and for a given width has the greatest number of degrees of freedom. The truncation point for the window, T_M, was chosen by reverting to the pilot analysis, trial-and-error method of window closing and fixed at 1/10th of the data length.

Therefore, with these parameters fixed, the number of degrees of freedom, v given by (Jenkins and Watts, 1969),

$$v = 2\ (T/T_M)\ b_1 \qquad (4.1)$$

was 37.2; where, T is the record length (in seconds) T_M is the truncation point (in seconds) and b_1 is the standardized bandwidth for the Parzen window (1.86). The resolution, a given by,

$$a = b_1/T_M\Delta t \qquad (4.2)$$

is 1.85 Hz. where, b_1 and T_M are as in (4.1) and Δt is the sampling interval.

The autocorrelation curve was calculated in each case with a truncation point T_M of 401 lags in order to observe its

behaviour outside the truncation point chosen for calculation of the power spectrum. Program AUTO was used to compute and plot the autocorrelation curves and SPEC to compute and plot the power spectrum. Program AUTO also incorporated a filtering routine FILT, which could remove a predominant frequency for further frequency analysis and program SPEC incorporated routine SMOOTH which applied the Parzen window (Fig. 4.6).

4.6 SOME THEORETICAL CONSIDERATIONS

In this section we shall briefly examine some of the processes by which the energy in an elastic wave propagating through a geologic medium is dissipated, and how the resultant signal detected at the surface is affected. In his paper on the diagnostic value of seismic energy, Hermont (1969) suggests that attenuation, partition at boundaries and geometric spreading are the important factors. So, we shall look at these in relation to the particular problem of the tunnelling machine at Warrington, and also include sections on the source and the effects of scattering.

4.6.1 The Tunnelling Machine As A Point Source

A tunnelling machine is a complex source of acoustic "noise" since it consists of not one, but several sources of vibration, in different positions and at different frequencies. In-tunnel vibration measurements, made by the Transport and Road Research Laboratories on the Warrington machine, (New, 1978) showed the

frequencies emitted to be mainly in the range of 10 to 50 Hz (see Table 4.1 below).

If we consider the tunnelling machine as an array of linear sources about 2 m long, we can adopt the approach of Beranek (1954). If the distance between the sources is small compared with the wavelength (approximately 30 m at the frequencies of interest) and the extent of the sources is small compared with the distance from them at which measurements are taken, then the tunnelling machine can be considered as a point (spherical) source. At distances of 40 to 60 m from the machine this is an assumption which may hold, but is not true for higher frequencies or for small distances from the machine.

So, the simplifying assumptions we are making in considering the tunnelling machine as a point source are; (1) that each source is a point source; (2) the distance between them is small compared with the distance to the point of observation (x); (3) the extent of the source array is small compared with x; and (4) the sources are identical.

Therefore, from these points alone, it can be seen that the tunnelling machine is a far from ideal source and for quantitative work may prove to be unsuitable. However, for our purposes we shall consider the machine as a point source, radiating several frequencies equally in all directions.

Probable Source Of Vibration Energy	Location Of Measurement	Peak particle velocity mm/s	Dominant Frequency Hz
Excavation	Shield tailskin (parallel to tunnel line)	0.1	15-50 (with other peaks between 150 - 900)
Excavation	Shield tailskin (normal to tunnel line)	0.08	20-40 (with other peaks between 200 - 800)
Excavation	Rear bulkhead of shield	0.12	15-100
Excavation	Last lining ring erected	0.08	10.35
No. 2 main motor	On motor	27	12.3
No. 2 main motor	Rail adjacent to motor	4.0	12.4
Erector pump	Rail adjacent to pump	0.25	24.5
Excavation?	Erector (parallel to tunnel line)	2.7	15
Excavation?	Erector (normal to tunnel line)	0.7	15-50
Main motors	Lining ring by main motors (parallel to tunnel line)	Below 0.05	-
Main motors	Lining ring by main motors (normal to tunnel line)	Below 0.05	-
Grout mixer	Rail by grout mixer	Below 0.05	-

Table 4.1 In-tunnel vibration measurements. (After New, 1978)

4.6.2 Attenuation

O'Brien (1957) suggested that by measuring the attenuation of seismic waves due to elastic imperfections of the media through which they travel, it might prove possible to identify the media.

However, the measurement of attenuation in the field is very difficult, in part because the mechanisms by which elastic energy is transformed into heat are not clearly understood. When an elastic wave passes through a medium, heat is generated during the compressive phase and absorbed during the expansive phase. Due to processes such as internal friction, viscous losses in the pore fluids, etc., this heat flow is not perfectly reversible. This absorption of energy gradually causes the complete disappearance of the wave.

Over the past 40 years or so there have been relatively few definitive studies of attenuation. This is due to the difficulty of performing controlled experiments to support theoretical work. All the labortory work has been performed at frequencies of several kHz, whilst seismic frequencies are in the range of 10-150 Hz. Thus, theories exist which explain the high frequency behaviour of attenuation but it is perhaps not valid to extrapolate these down to seismic frequencies. Some of the major studies are summarized and listed below in Table 4.2.

	EXPERIMENT	RESULTS	REFERENCE
1.	Pulses produced by electromagnetic shaker. Vertically travelling waves at 20-1400 Hz $A = A_0 x^{-1} e^{-ax}$	Found a and c for the area	Howell, Kean & Thompson (1940)
2.	Measured first pulse from explosion in range 10-3000 ft. $E = E_0 x^{-B}$ $E = E_0 x^{-C} e^{-ax}$ $V = V_0 x^{-D} e^{-ax}$	Results for B, C, D, showed great variation. Theory gives; C=2(body wave) C=1(surface wave) D=1(body wave) D=1/2(surface wave)	Howell Jr. & Kaukonen (1954)
3.	Measured first pulse from explosion in range 10-1172 ft. Frequencies 6-120 Hz. $V = V_0 x^{-B}$	Results for B varied from 3.0 to 6.9	Howell and Budenstein (1955)
4.	Measured phases and amplitudes from explosions. Plotted phase shift and attenuation versus frequency.	Found a approx. proportional to f	Collins and Lee (1956)
5.	Measured first, second and third peaks of first arrival of pulses produced by a vibrator. 200 ft. traverse $A = A_0 x^{-B} e^{-ax}$	B found to be approximately equal to 2.0	Collins and Lee (1956)
6.	Measured first refracted arrival from explosion at distances greater than 100 ft. $A = A_0 x^{-B}$	B found to be 2.16 ± 0.04 plus residual attenuation (proportional to f) of 1.96 ± 0.28 dB per 1000 ft.	O'Brien (1957)
7.	Seismo-acoustic field method, frequencies 100-4000 kHz.	Found a to be proportional to f	Karus (1958)
8.		Review of attenuation and Q	Knopoff (1964)
9.		Review of attenuation & definitions of Q.	Sato (1967)
10.	Measurements on plaster and plexiglass 2-D models at several kHz. Rayleigh, P and S waves. $A = A_0 e^{-ax}$	Found a to be proportional to f	Thapar (1972)

Table 4.2 Some studies of attenuation.

Where; B, C, A_0, E_0, V_0 and D are constants; A is amplitude; E is energy; x is distance; V is particle velocity; f is frequency; c is phase velocity; a is attenuation constant; and, Q is the dimensionless quality factor.

It appears from Table 4.2 above that the various workers do not agree on the nature of the fall-off of energy with distance. However, when one considers the different conditions, instrumentation, parameters measured, and assumptions made, it is not surprising that there is disagreement. From this it would seem that attenuation may not be a good indicator of local geology unless measurements can be made under carefully controlled conditions.

4.6.3 Scattering

Scattering of seismic waves by inhomogeneities in the earth can affect the signals recorded at the surface, but this effect may become negligible if the inhomogeneity is small compared with the wavelength.

At Warrington the velocity in the near-surface layers was about 600 m/s which, at the highest frequency of interest, gives a wavelength of about 6 m. Therefore, even the boulders encountered at the sand-sandstone interface (up to 500 mm in diameter) can be considered as small.

Little experimental work has been carried out on three-dimensional scattering apart from simple model experiments (Levin and Robinson, 1969) but, theoretical work has existed for a century. Rayleigh (1871) examined the problem of optical scattering, which is a satisfactory approach for order-of-magnitude estimations in the elastic case if the assumptions of small inhomogeneities and far field observation

are valid. Rayleigh found that on dimensional grounds, the scattered field was proportional to $VK^2\ x^{-1}$, where V is the volume of the inhomogeneity, x the distance to the point of observation, and K the wave number. Miles (1960) examined the scattering of plane P and S-waves in an elastic medium and found that his results differed from Rayleigh's only in the generation of an additional S-wave field in the P-wave case and vice-versa.

Therefore, at Warrington, the scattered field recorded at the surface is small enough to neglect in calculations of the dependence of amplitude upon distance and of the attenuation constant.

4.6.4 Interference

The proportion of an incident wave which undergoes reflection at an interface depends upon the density and velocity in the two media and on the angle of incidence. This is true for thick beds or for small wavelengths, but when the wavelength becomes large compared to the thickness of the beds, the reflection coefficients can become very small (Clewell and Simon, 1950) and have a dependence which is approximately inversely proportional to the wavelength. However, for the Warrington case the tunnelling machine (the source) is actually at the interface between alluvium and sandstone and so the angle of incidence is extremely small (grazing). Therefore, because of this and the large wavelengths produced by the machine, it is expected that very little reflected

energy would reach the surface when compared with the energy of the direct and surface waves.

Interference may also arise due to difference in path lengths between direct and refracted waves and between direct and surface waves, destructive interference occurring when the path difference is an odd number of half-wavelengths. However, the machine is so close to the surface that the maximum path difference, assuming straight ray paths and a maximum source to geophone distance of 60 m, is 0.2 m, which is nowhere near the smallest half-wavelength of interest of 3 m. Thus, the effect of interference due to the local geology (reflections and refractions) and the source (surface and direct waves) is expected to be small.

4.6.5 Geometrical Spreading

Geometrical spreading is the loss of energy due to the wave-front expanding as it moves away from the source. From pure geometry this effect must follow the inverse square law of radiation and should be frequency-independent. However, in our case this law does not apply exactly, since the surface geophones will record surface and refracted waves as well as the spherically expanding direct wave. Also there will be a frequency-dependent attenuation due mainly to solid friction in the surrounding rock. Whether geometric spreading or the other loss mechanisms are dominant will depend upon the distance of observation, the attenuation constant of the medium and the frequency. Let us compare the two effects by

considering the loss of energy experienced in travelling from the source to a point between 10 m and 80 m distant. Following the method of Telford et al. (1976), we assume the attenuation constant, a to be 0.25 dB per wavelength (an arbitrary value, thought to be tyical for sedimentary rocks). The results, shown in Table 4.3 below, were calculated using the following relations:

Absorption: Loss in dB $= 10 \log_{10} (I_o/I)$

$= 4.3\ ax$

$= 1.1\ x/\lambda$

$= 0.0018\ xf$ dB

Spreading: Loss in dB $= 10 \log_{10} (I_o/I)$

$= 20 \log_{10} x$

Where, x is the distance to the shotpoint (up to 80 m), and the velocity of the medium is 600 m/s.

	Frequency (f)	Distance from Shotpoint (x)				
		10 m	20 m	40 m	60 m	80 m
Absorption	1 Hz	0.02 dB	0.04 dB	0.07 dB	0.12 dB	0.14 dB
	3	0.05	0.11	0.22	0.32	0.43
	10	0.18	0.36	0.72	1.08	1.44
	30	0.54	1.08	2.16	3.24	4.32
	100	1.80	3.60	7.20	10.80	14.40
	150	2.70	5.40	10.80	16.20	21.60
Spreading	All	20.0 dB	26.0 dB	32.0 dB	36.0 dB	38.0 dB

Table 4.3 Losses by absorption and by geometrical spreading.

As can be seen from Table 4.3, at the distances and frequencies of interest at Warrington (0-60 m, 10-50 Hz), the losses by geometric spreading are much greater than those by absorption. In fact, considering the case for greatest absorption (60 m and 50 Hz), and the total losses to be absorption plus geometric spreading, the loss due to absorption is still only 13% of the total. Therefore, we would expect the measured losses to approximately follow an inverse square law, the deviation from this increasing towards the higher frequencies.

4.7 RESULTS

4.7.1 Introduction

The results presented in this section are selected examples from a total of over 50 digitized records. These records were selected by visual inspection from several hours of Warrington data collected during three visits to the site by the Engineering Geology Unit of the Institute of Geological Sciences.

Each record has a configuration number (see Table 4.4) which corresponds to a particular position of the tunnelling machine (chainage number) and/or configuration of geophones. Only one record for each configuration is shown here, for brevity and

to facilitate comparison of spectra. Each record shown was carefully chosen to be representative of a particular configuration. Configurations 1, 2 and 3 were recorded during the first visit to the site, 4 and 5 from the second visit and 6, 7 and 8 from the final visit.

Config-uration Number	Position of Machine in Metres from Start (Chainage)	Geophone Distances From Machine (Lateral)	Geological Medium	Record Name
1	185 m	0 m	Sandstone	T084CS5
2	185 m	0 m (background noise)	Sandstone	T074NP2
3	191 m	40 m	Sandstone	T064CP3
4	344 m	0 m 50 m 60 m	Drift	T158CP2
5	391 m	0 m 50 m 60 m	Drift	T148CP2
6	465 m	0 m 50 m 60 m	Drift	T138CP2
7	465 m	10 m(multigeophone)	Drift	T128CM6
8	470 m	0 m 45 m 55 m	Drift	T118CP5

Table 4.4 A list of records presented in the results.

4.7.2 Configuration 1

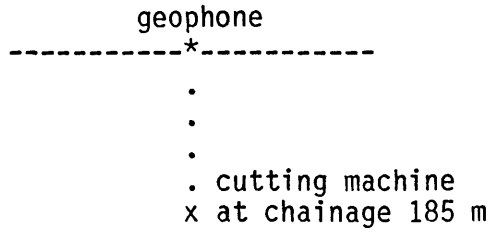

For this and the following two configurations, the recordings were of one geophone output only. For this record, T084CS5, a horizontal type geophone was used. The resulting auto-correlation and power spectrum (Fig. 4.7) do not exhibit any pronounced peaks but, indicate a broad spectrum from about 10 to 40 Hz. This frequency range, measured close to the machine, agrees well with that measured by New (1978) and listed in Table 4.1.

4.7.3 Configuration 2

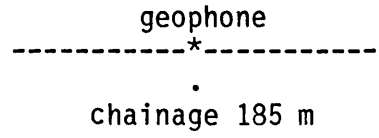

This record, T074NP2, is of background noise, recorded with a vertical-type 10 Hz geophone directly above the machine, which was not operating. As shown by the autocorrelation and power spectrum (Fig. 4.8), the noise is aperiodic and the power several orders of magnitude lower than that recorded when the machine is operating (cf. Fig. 4.9). So, background noise would not contribute significantly to any of the spectra of the machine recorded whilst it was excavating. Unfortunately, no other records of the background noise were available.

4.7.4 Configuration 3

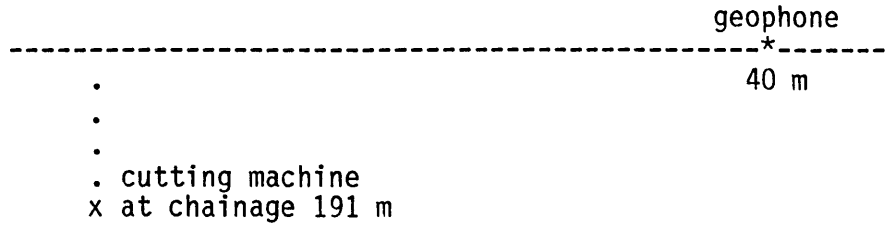

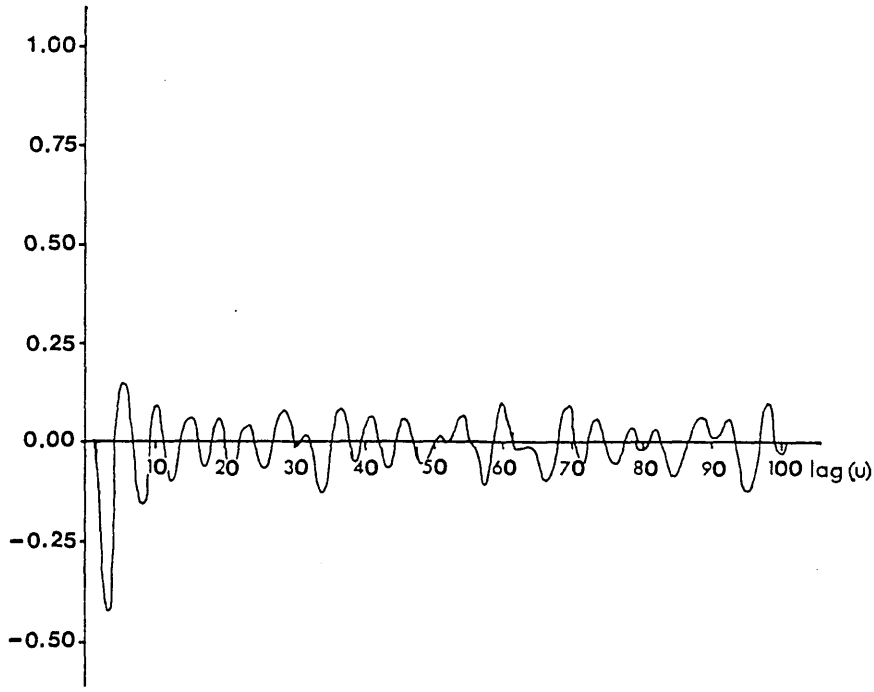

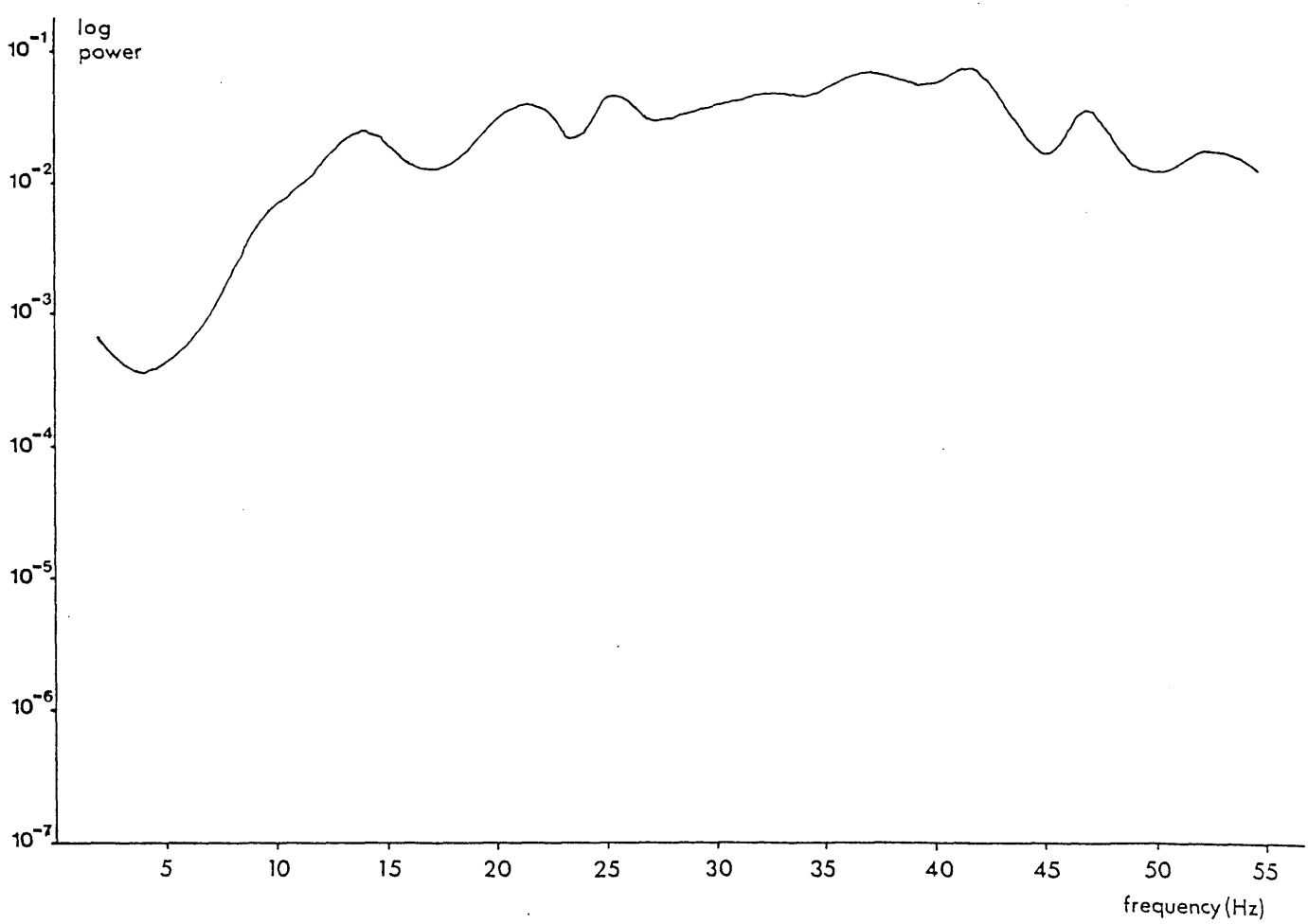

Figure 4.7 Autocorrelation and power spectrum for T084CS5 (one geophone only)

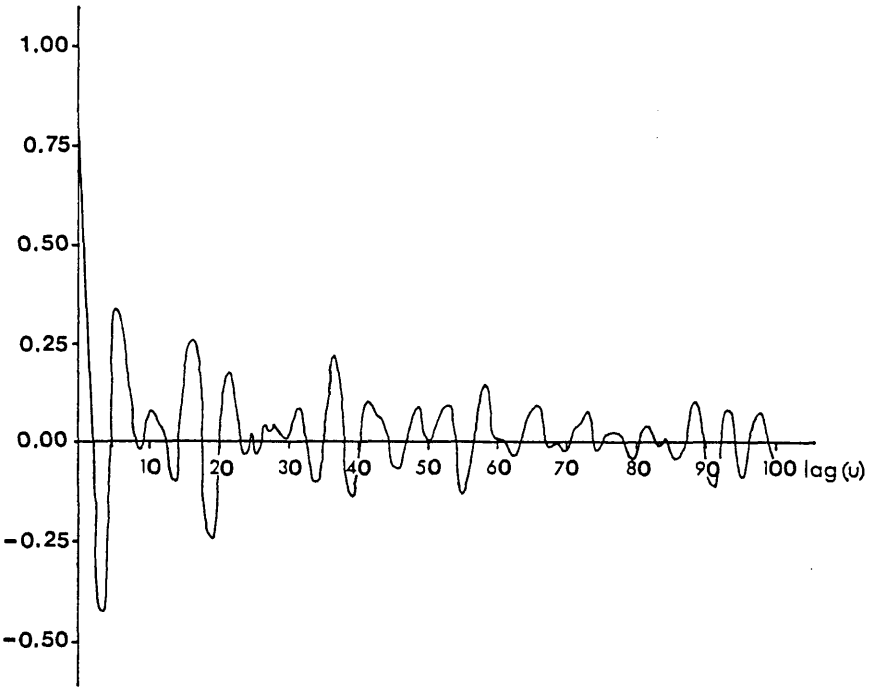

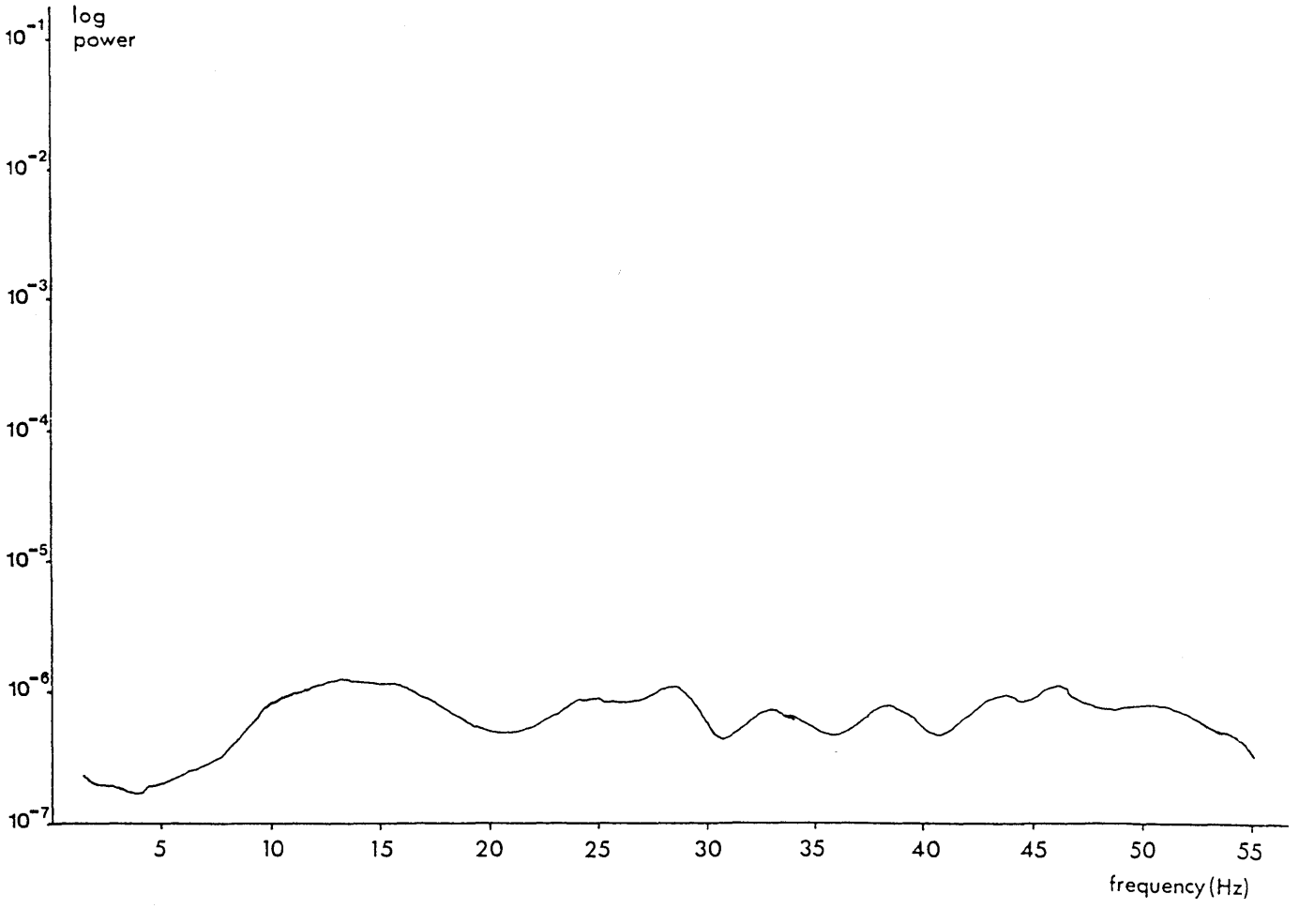

Figure 4.8 Autocorrelation and power spectrum for T074NP2 (background noise, one geophone only)

For this record, T064CP3, a vertical-type 10 Hz geophone was used and the resulting autocorrelation curve and power spectrum are shown in Fig. 4.9.

The results show a similar character to those from the previous recording of machine noise (Fig. 4.7). No major peaks are evident in the power spectrum and the majority of the power seems to be concentrated between 10 and 35 Hz at a fairly constant level. An additional difficulty, experienced at this early stage in the work, was that the observers were uncertain of the precise mode of operation of the machine, i.e., whether it was idling, cutting, etc.

4.7.5 Configuration 4

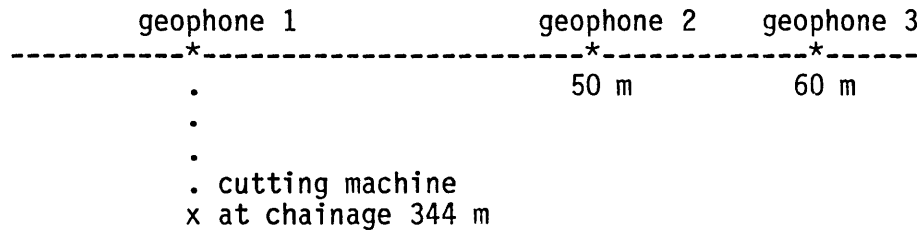

Configuration 4 is the first recorded during the second visit to the site and also the first in which the output from three geophones could be recorded simultaneously. The autocorrelation curves (Fig. 4.10) and power spectra (Fig. 4.11) for T158CP2 show a very pronounced 12 Hz signal. Table 4.1 shows that the 12 Hz signal may be ascribed to the No. 2 main motor of the machine. The 24 Hz signal is not evident in the autocorrelation but can easily be seen in the power spectra for geophones 1 and 2. When compared with the results for previous records it is possible to see a distinct change in the nature

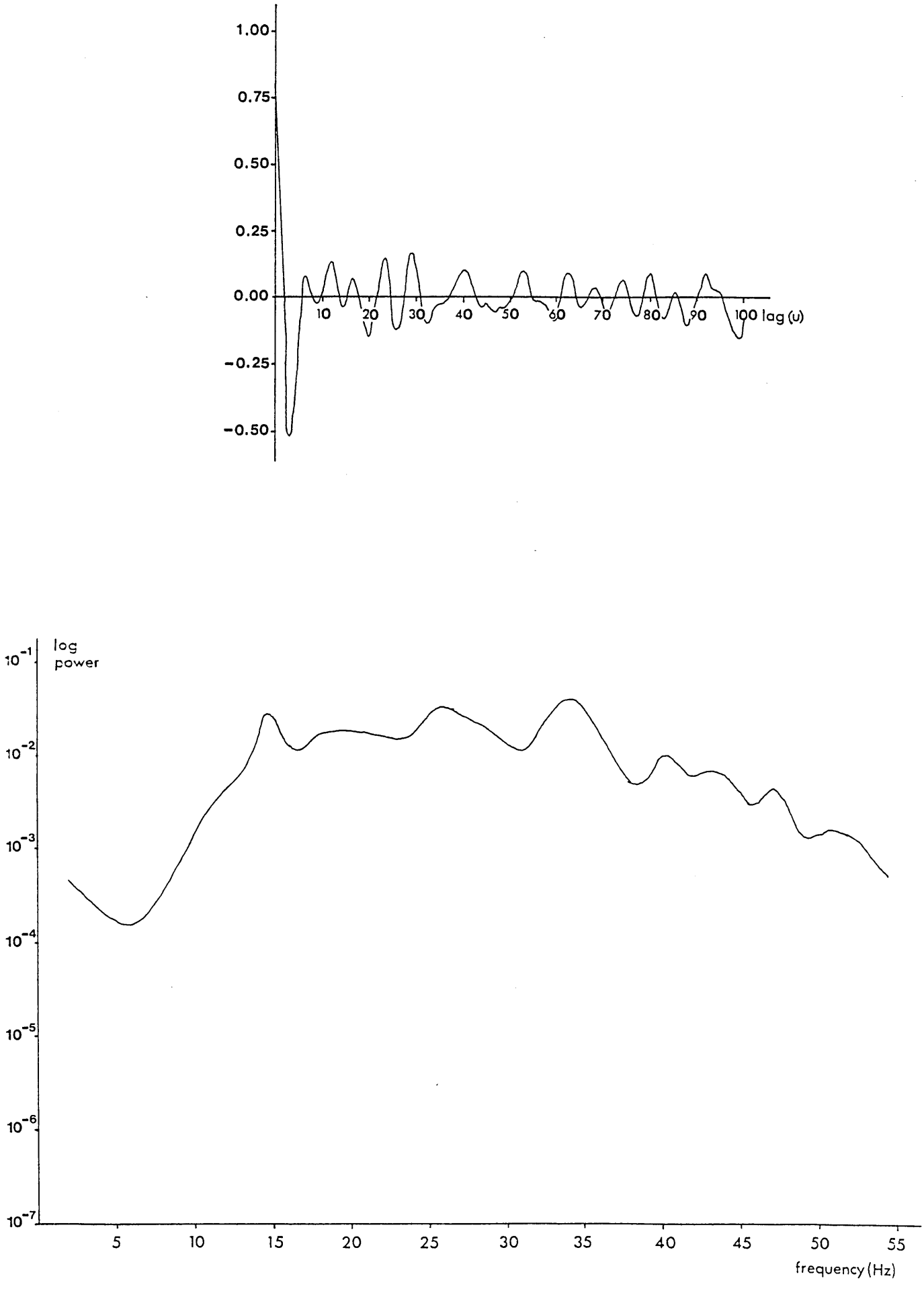

Figure 4.9 Autocorrelation and power spectrum for T064CP3 (one geophone only)

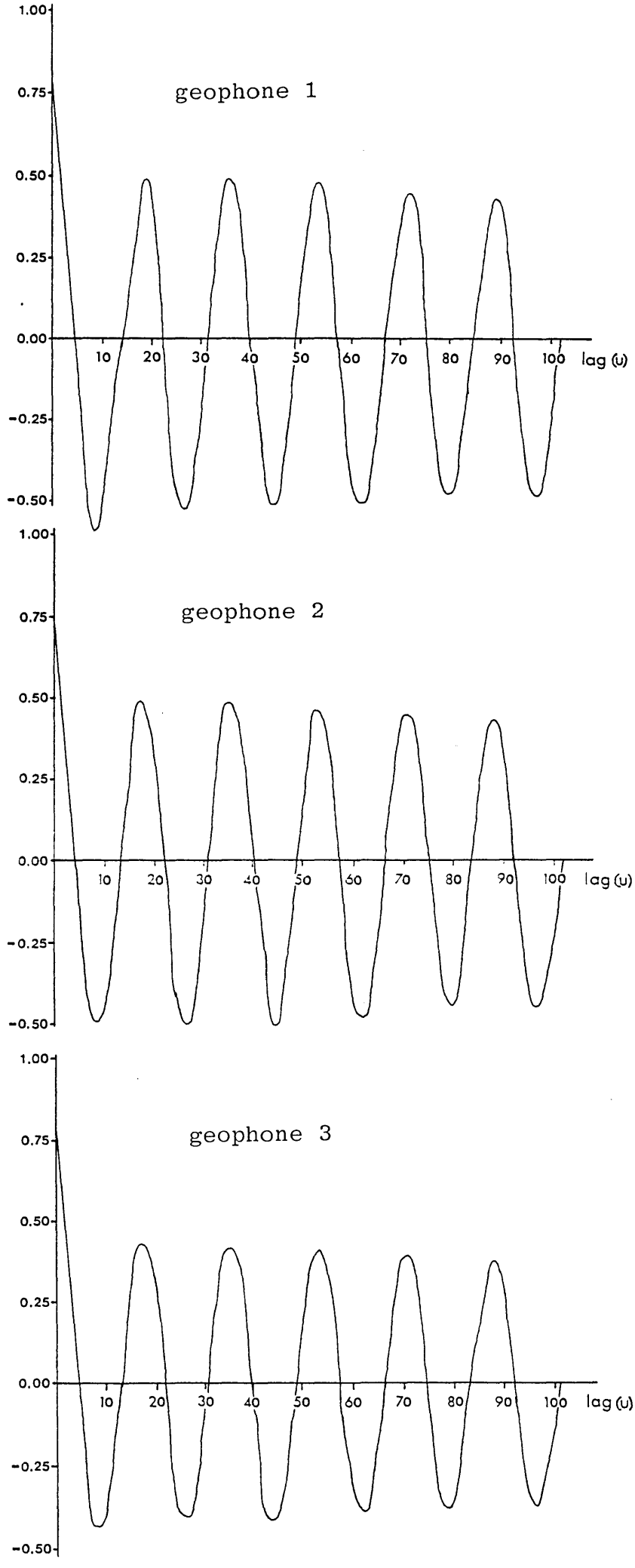

Figure 4.10 Autocorrelations for T158CP2

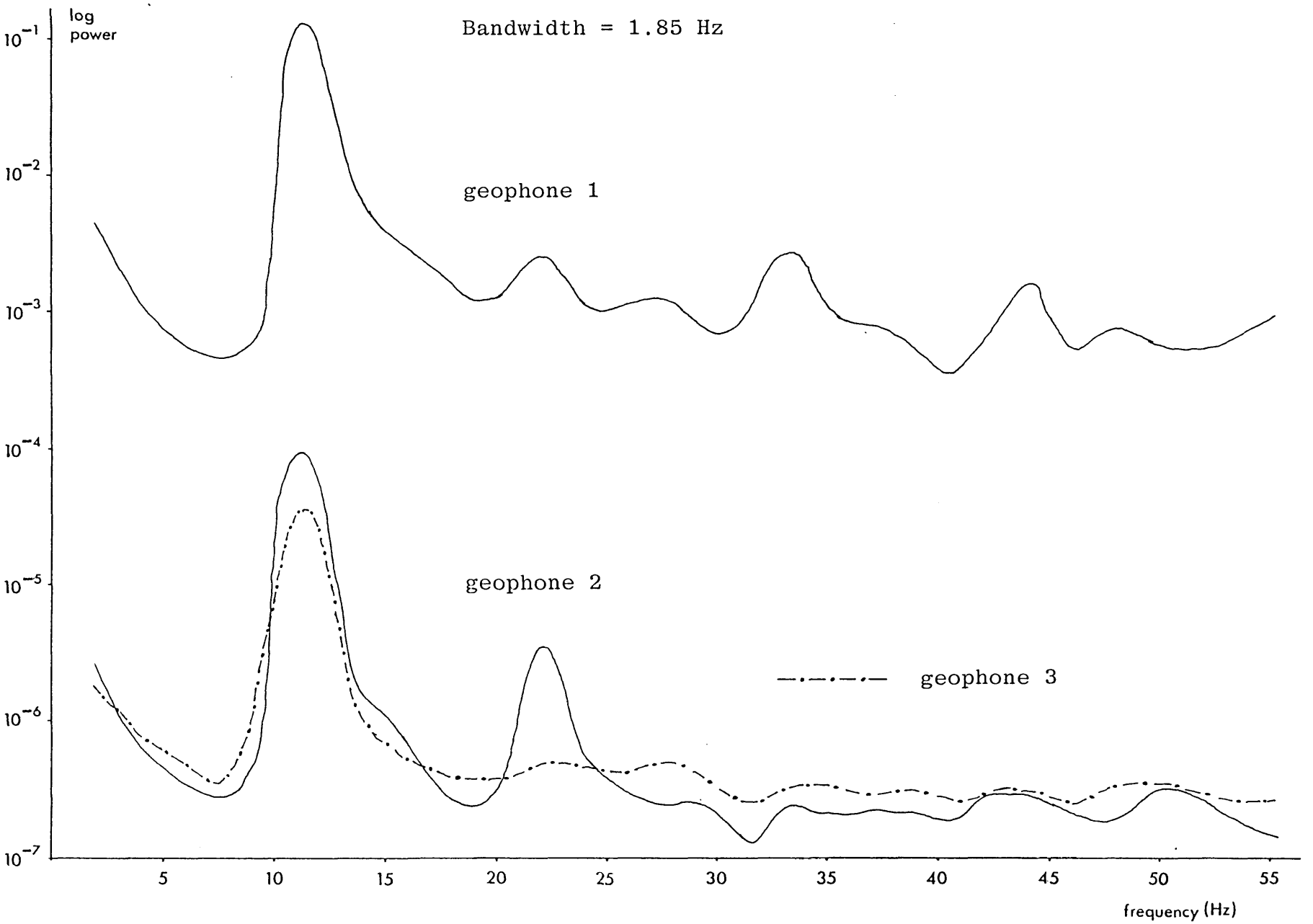

Figure 4.11 Power spectra for T158CP2

of the autocorrelation curves and the power spectra. As the chainage number increased from 191 m to 344 m, the predominant frequencies become much more sharply defined. This could be due to, a decrease in the amount of cover above the machine, or the change in geology at the tunnel face from sandstone to drift and sandstone,or to a change in the mode of operation of the tunnelling machine.

4.7.6 Configuration 5

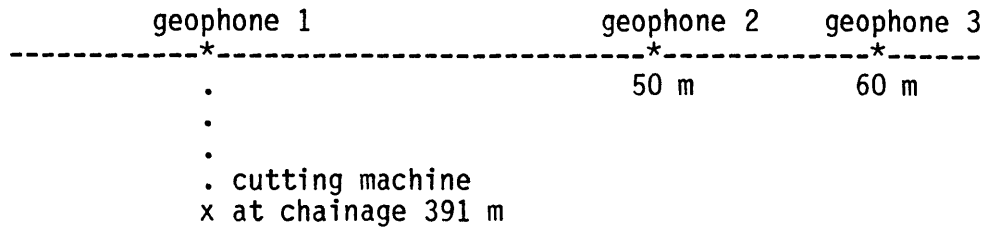

This configuration preserved the same spatial relationship between the tunnelling machine and the geophones as the previous one but, now the machine is some 47 m forward from its position of section 4.7.5. The autocorrelation curves for T148CP2 (Fig. 4.12) show an extremely well-defined 24 Hz signal. The power spectra (Fig. 4.13) show that the 24 Hz signal has a larger amplitude than previously, although the 12 Hz is still evident but at an amplitude less than that of the previous configuration. This indicates that the 24 Hz and 12 Hz signals have different sources. From Table 4.1 the erector pump appears to be the source of the 24 Hz signal. The increased power at 24 Hz indicates that for the duration of this record the pump may have been working for a longer period of the 10 second record length than previously, thus contributing more to the total power at that frequency.

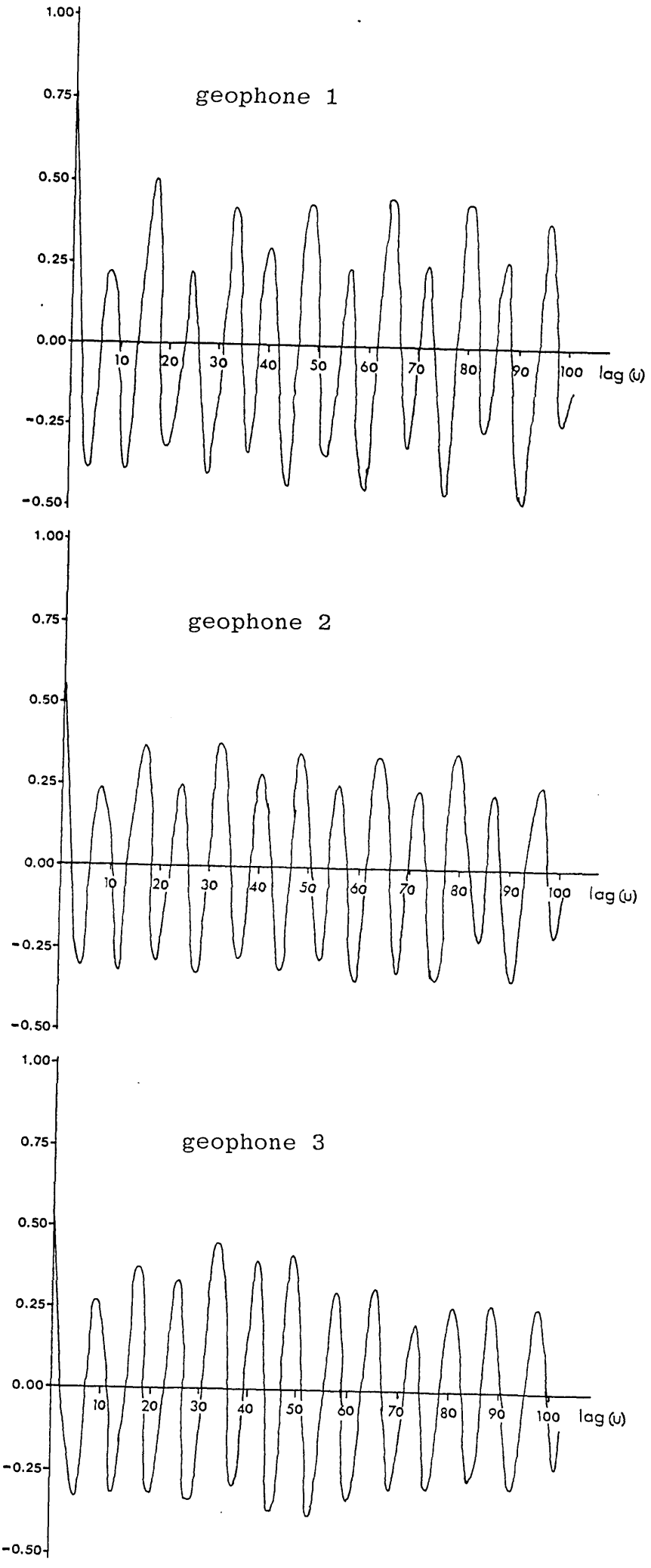

Figure 4.12 Autocorrelations for T148CP2

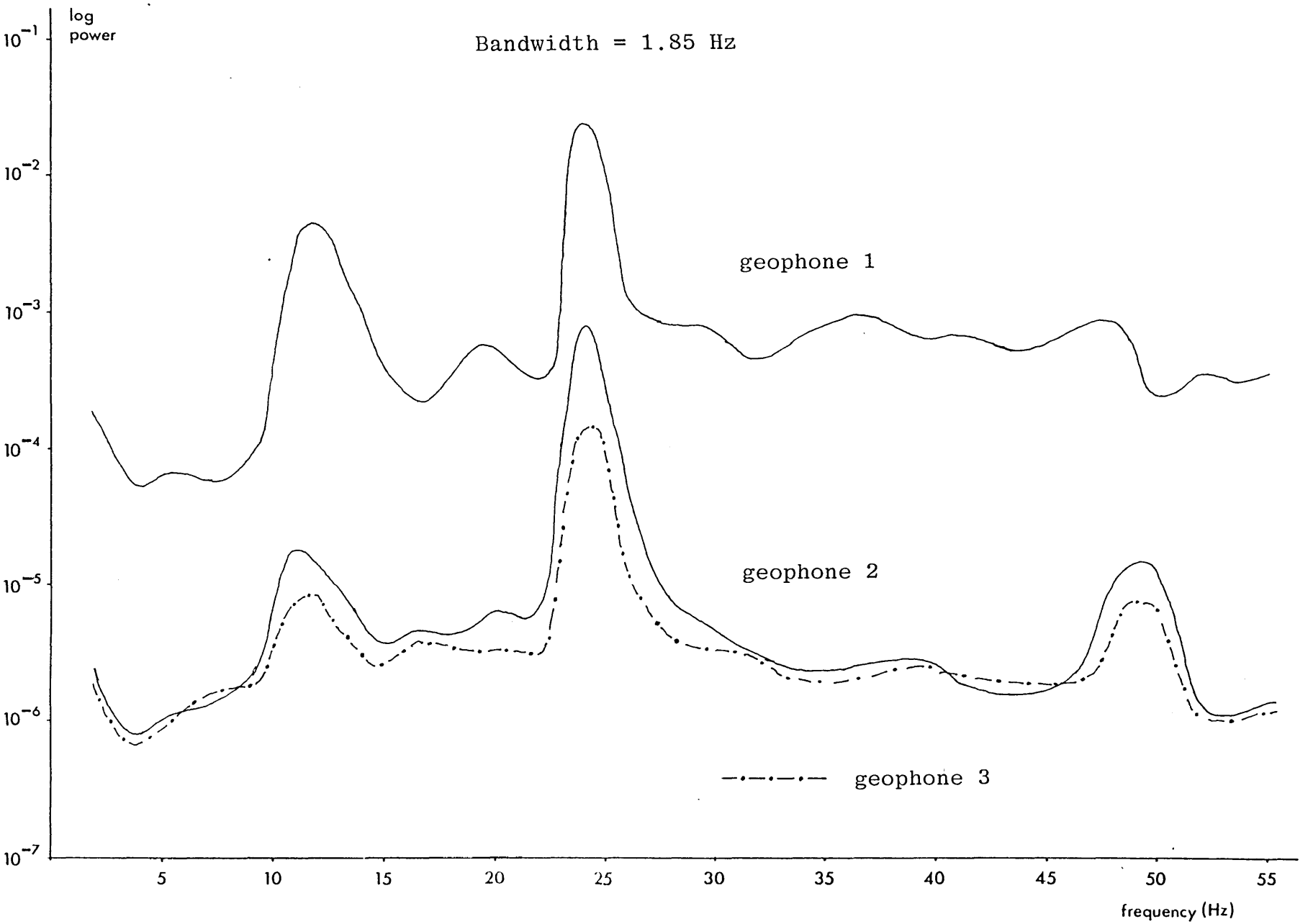

Figure 4.13 Power spectra for T148CP2

4.7.7 Configuration 6

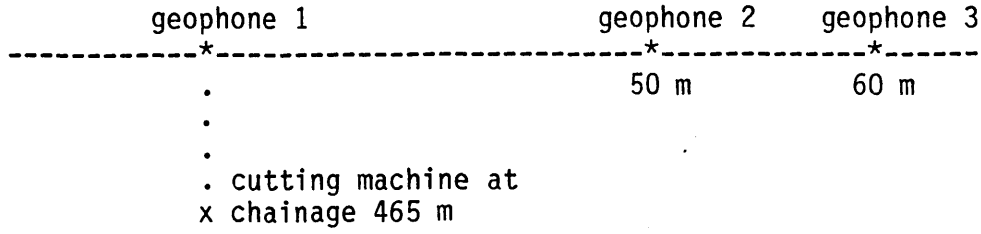

Configuration 6 marks the first recording of the third and final visit to the Warrington site. This configuration is the same as that for Configurations 4 and 5, except that the machine is now at chainage 465 m, some 74 m ahead of its position for the previous recording. As can be seen from the autocorrelation curves (Fig. 4.14) and power spectra (Fig. 4.15) for T138CP2, the character of these curves is quite different from those of Configurations 4 and 5 but, quite similar to that of Configuration 3 (Fig. 4.9), recorded by a single vertical geophone 40 m ahead of the machine.

4.7.8 Configuration 7

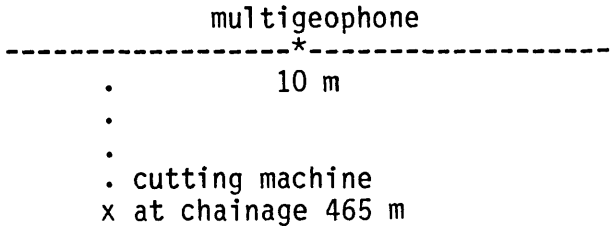

In this configuration a three-component geophone was set up on the surface close to the tunnelling machine and recordings of all three components taken simultaneously (record T128CM6). The geophones within a three-component geophone are orientated in three mutually perpendicular directions, two sensitive to horizontal motion and one to vertical. H1 was orientated

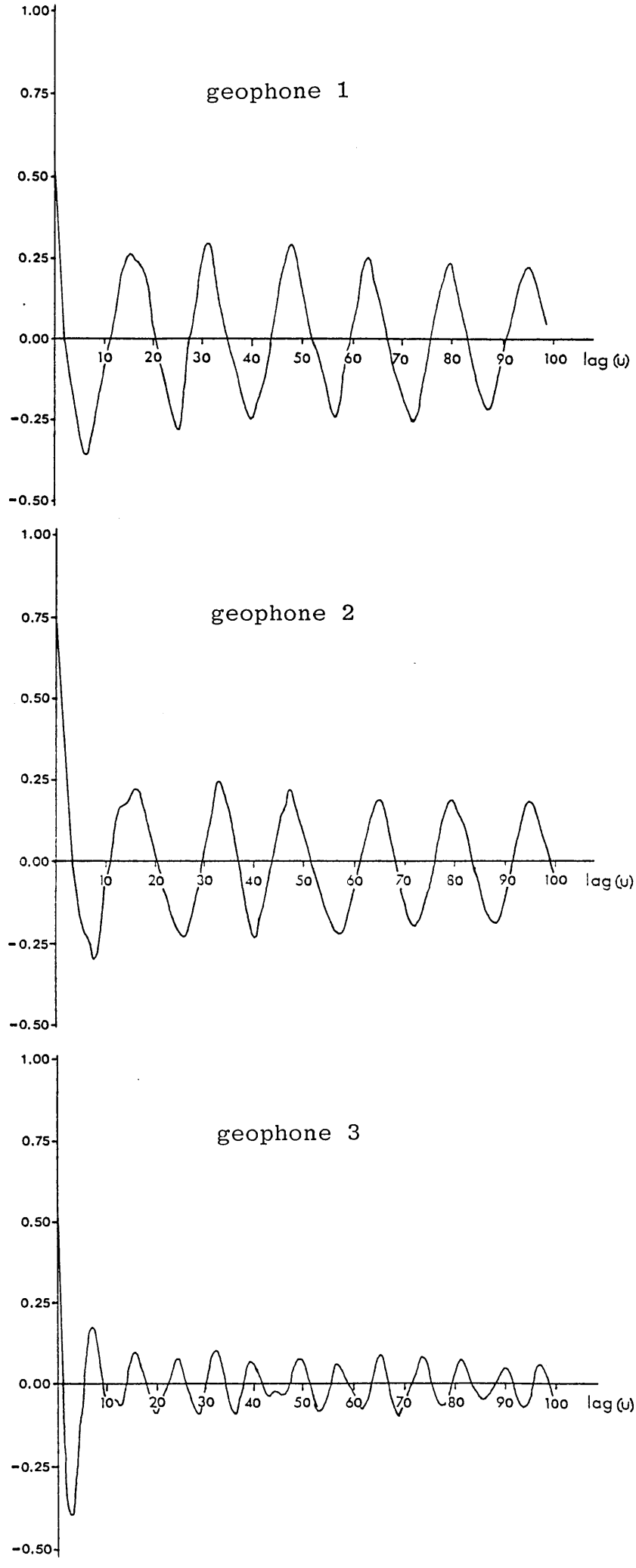

Figure 4.14 Autocorrelations for T138CP2

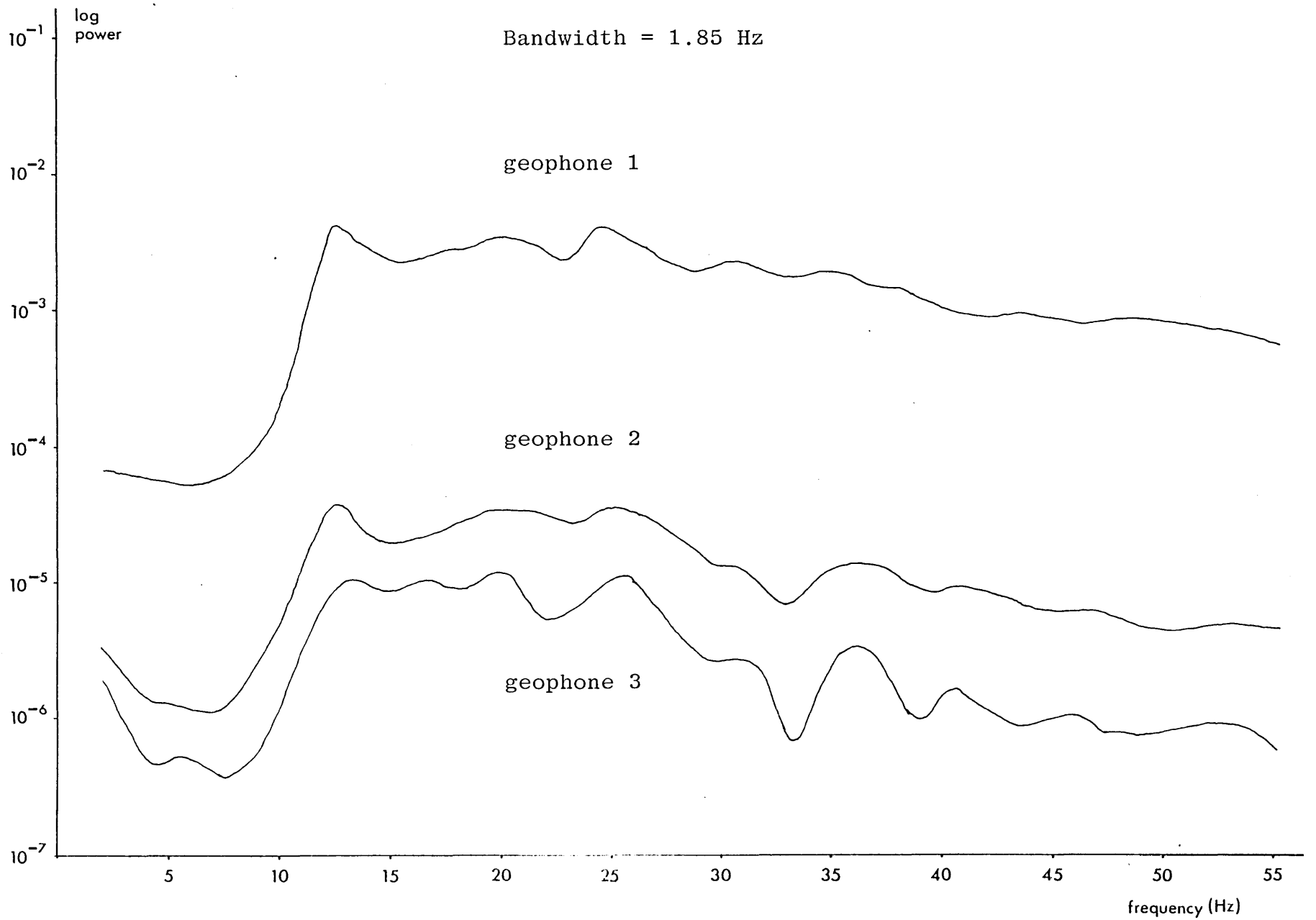

Figure 4.15 Power spectra for T138CP2

along the line of the tunnel and H2 at right angles to it. from the autocorrelation curves (Fig. 4.16) it would appear tht H1 has a greater low frequency content than H2 and V. Examination of the power spectra shows that H1 (parallel) has generally higher power over the 10 to 35 Hz frequency range than the H2 (perpendicular) and vertical components. It is also evident that the 24 Hz peak is absent from the H1 (parallel) component, suggesting that the recorded power at this frequency is made up of contributions from compressional and transversely polarized shear waves. The power spectra are shown in Figure 4.17.

4.7.9 Configuration 8

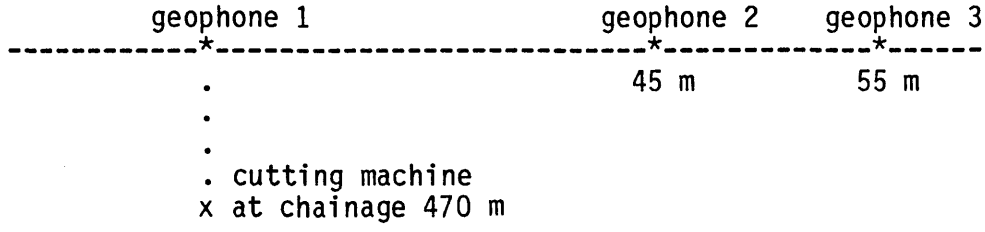

Record T118CP5 was chosen as representative of this configuration, the autocorrelation curves and power spectra are found in Figs. 4.18 and 4.19, respectively. The autocorrelation curves all indicate a predominant frequency of 12 Hz, which is assumed to be due to the main motors (see Table 4.1). The power spectra showed in all cases the dominant 12 Hz, with other peaks at 24 Hz and possibly at 36 hz. The character and calculated power for the three geophone positions were very similar to those recorded for configuration 6 which is to be expected, as geophones 2 and 3 have remained in exactly the same location on the ground whilst the machine (and therefore geophone 1 which was repositioned above the machine) has moved 5 m towards the positions of geophones 2 and 3.

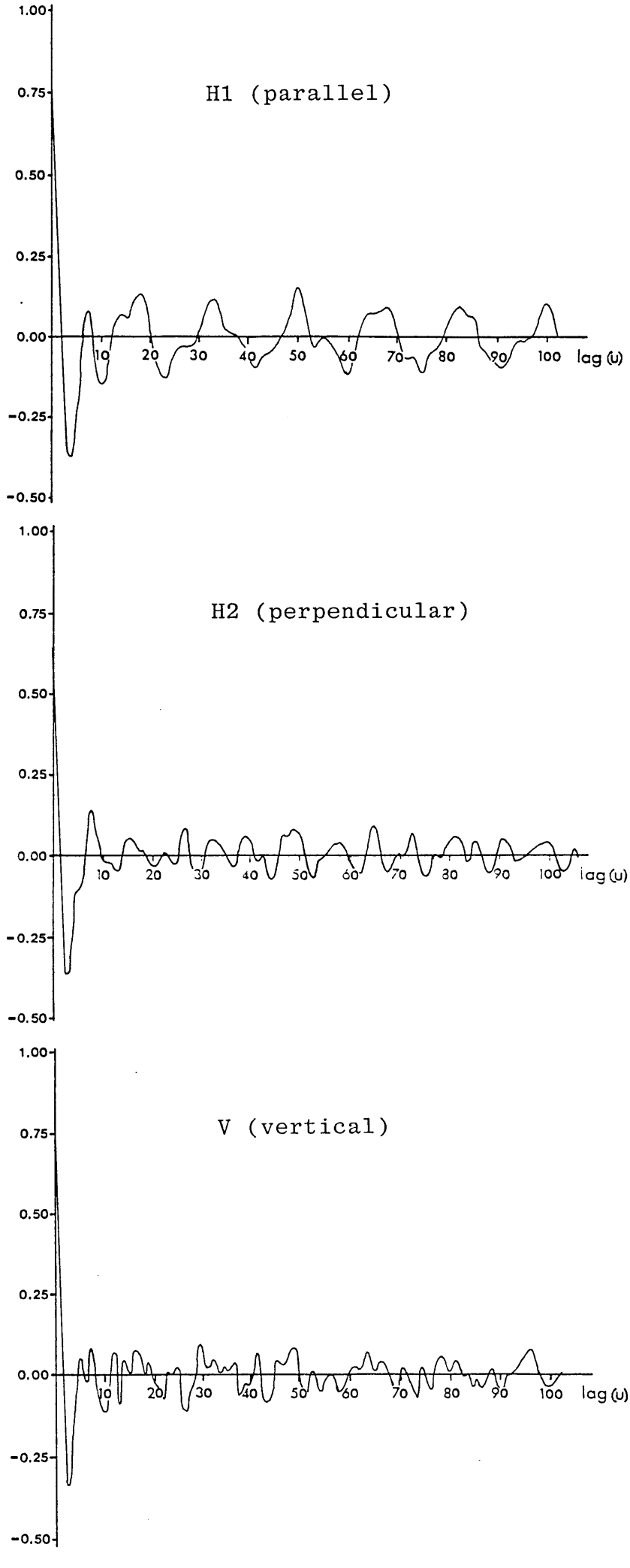

Figure 4.16 Autocorrelations for T128CM6

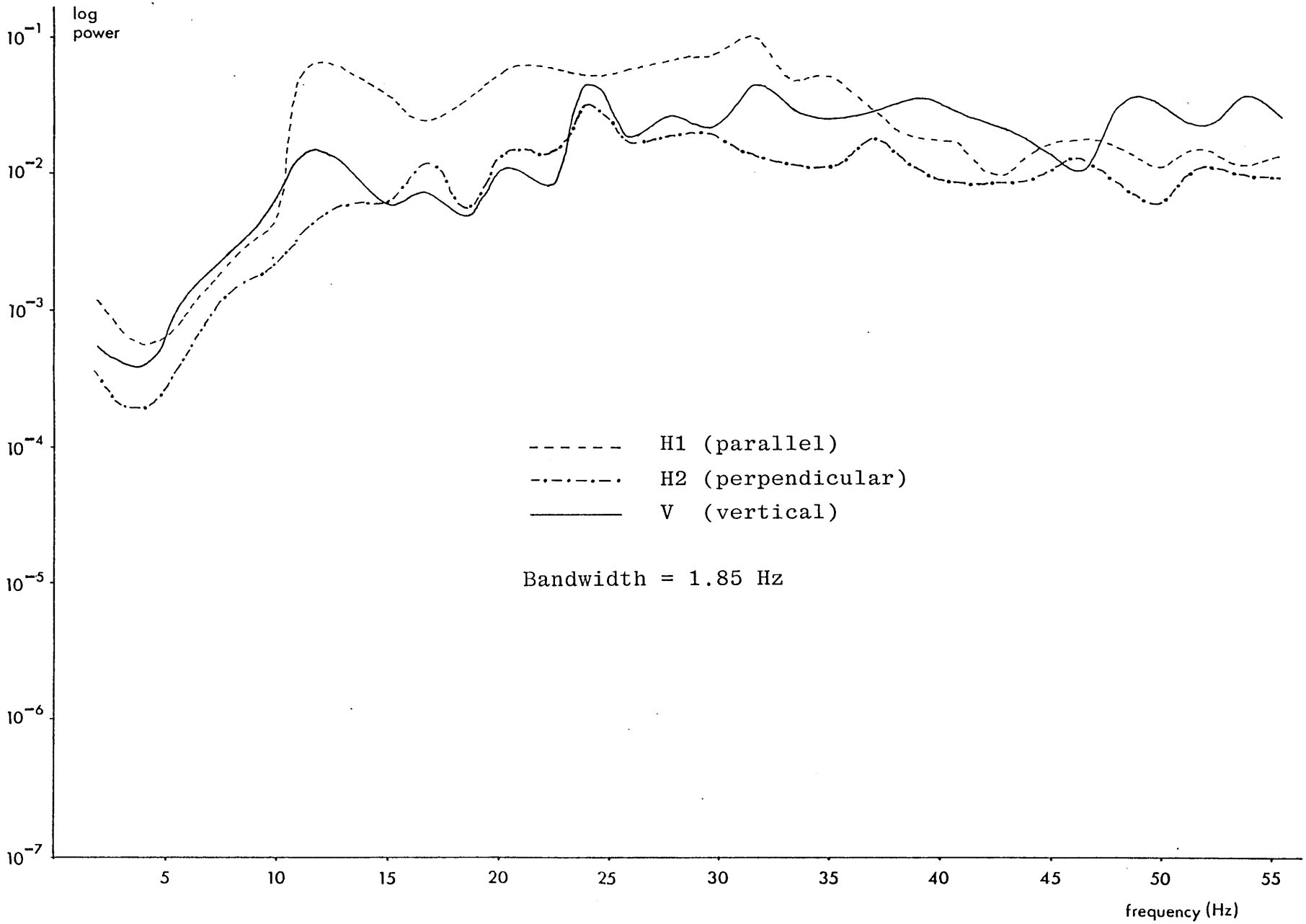

Figure 4.17 Power spectra for T128CM6

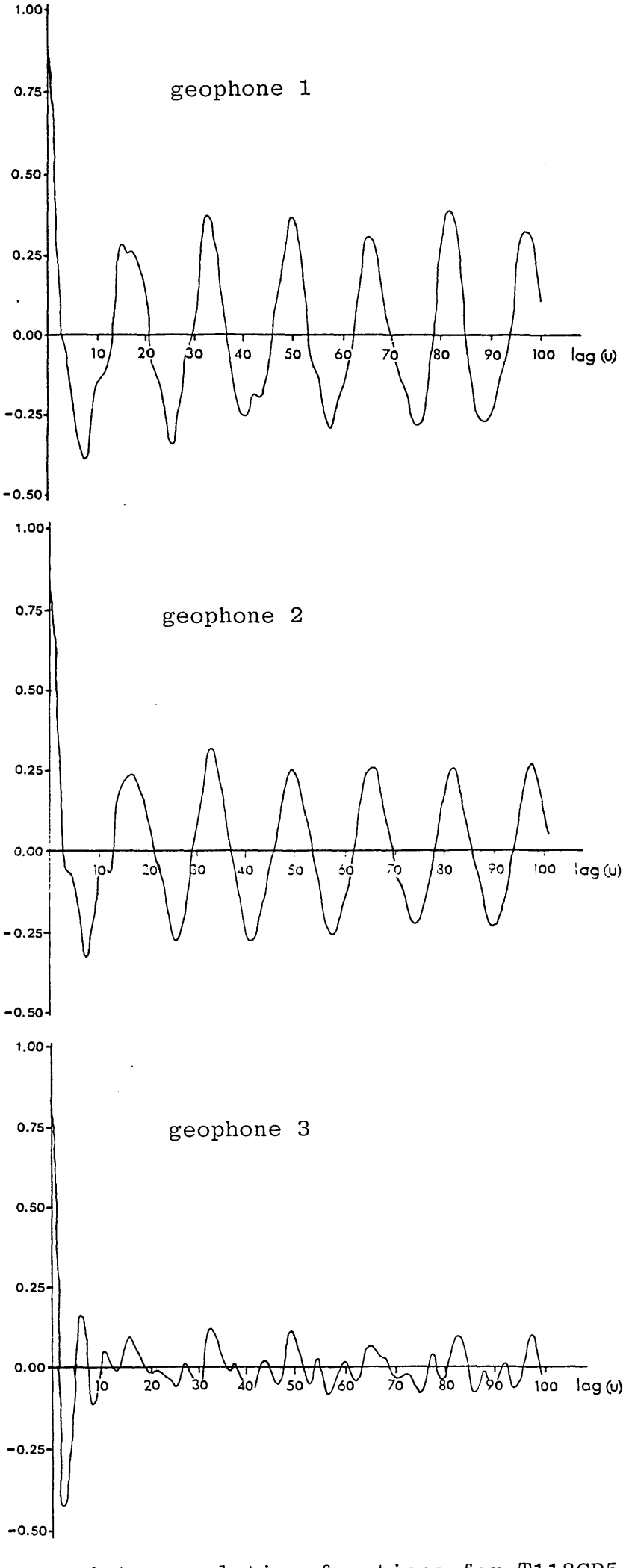

Figure 4.18 Autocorrelation functions for T118CP5

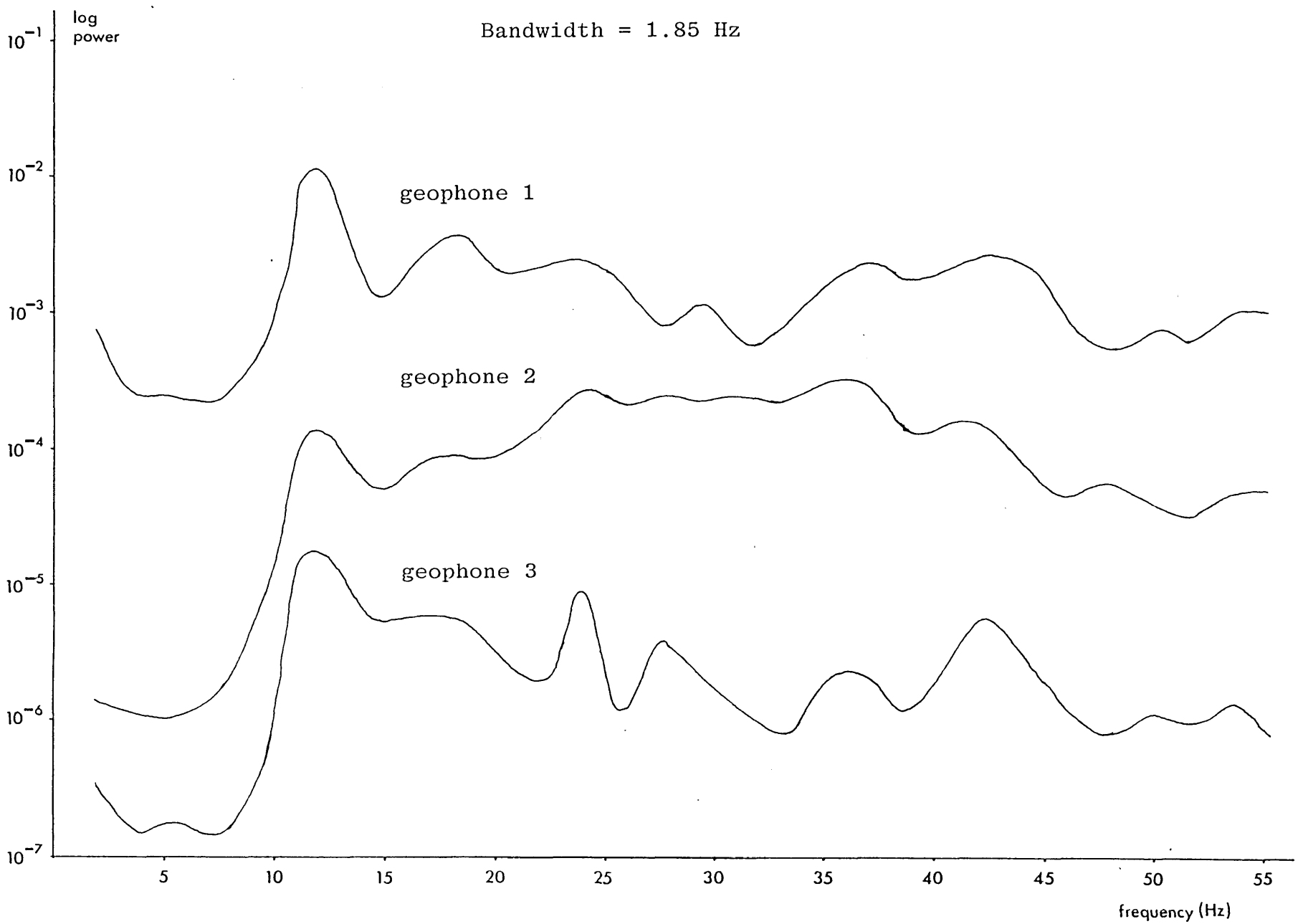

Figure 4.19 Power spectra for T118CP5

4.8 DISCUSSION

It is quite apparent from the results presented in Section 4.7 that the frequency spectrum of the tunnelling machine, as recorded by geophones at the surface, varied considerably within the 340 m length of tunnel for which recordings were obtained.

Configurations 1, 2 and 3 showed spectra obtained from a single geophone whilst the machine was operating in a full sandstone face. Of these, 1 and 3 exhibit spectra (Figs. 4.7 and 4.9) that do not show significant differences in frequency content although they were recorded by shear and vertical geophones, respectively. This result is not surprising as the rotary action of the tunnelling machine plus that of the main motors and pumps would be expected to produce both shear and compressive waves as well as Rayleigh and Love (SH) surface waves. The bandwidth recorded (15-45 Hz) agrees with that measured by New (1978) within the tunnel (as shown in Table 4.1). A spectrum of background noise shown in Figure 4.8 shows the power to be several orders of magnitude less than that when the machine is excavating and may be considered insignificant.

Configurations 4 and 5 (Figs. 4.10 to 4.13) show results from recordings made when the tunnelling machine is excavating mostly in drift or alluvium as the alluvium/sandstone interface has now dipped down until it remains only just above the invert of the tunnel bore. The spectra for these two configurations show a marked difference from those recorded previously. Both sets of spectra (Figs. 4.11 and 4.13,

respectively) exhibit strong maxima at 12 Hz and at 24 Hz. From in-tunnel measurements (New, 1978) these frequencies can be ascribed to the main motors and to the erector pump respectively. Examination of the individual spectra for Configuration 4 show the expected decrease in power with distance but the relative height of the 12 Hz and 24 Hz peaks for geophones 1 and 2 imply that the tunnelling machine is radiating a broad range of frequencies that are also several orders of magnitude above the ambient "background noise". It is not known why geophone 3 of Configuration 4 has not responded to the 24 Hz as have geophones 1 and 2. This may have been caused to some extent by destructive interference at this frequency within the uppermost layer of the road surface. Configuration 5 shows the strong 24 Hz peak at all 3 geophones (Fig. 4.13), the higher power at 24 Hz and lower power for the 12 Hz and other frequencies indicating that the erector pumps were operating at higher power or for more of the 10 second record length than in Configuration 4 or that the tunnelling machine was operating at relatively lower power.

The remaining Configurations, 6, 7 and 8 were recorded during the last visit to the site. Spectra calculated from Configurations 6 and 8 show (Figs. 4.15 and 4.19) greater similarity with that from Configuration 3 (Fig. 4.9) than those from Configurations 4 and 5. This could imply several things; 1) that during the recordings made of Configurations 4 and 5 the tunnelling machine was not excavating but, was merely operating with its motors and pumps idling; 2) that the lithology around chainage 300-400 m was different from that at the start of tunnelling and around chainage 470 m; or that the 12 and 24 Hz frequency maxima were caused by resonances

(constructive interferences) within the surficial layers. Point 1 would seem to be the most likely, that the tunnelling was operating in a different "mode" during recording of Configurations 4 and 5 as the lithology variations were gradational from the start to the end of the drive and it is unlikely that localized resonancies would cause the 12 and 24 Hz peaks at this location and nowhere else.

Configuration 7 was recorded using a multigeophone, the spectra in Figure 4.17 illustrating the recorded power in the three components as captioned. The spectra imply a generally higher contribution from the H1 (//) component. At the 12 Hz peak the greatest power comes from the H1 (//) and V (vertical) components, which may suggest a Rayleigh type surface wave, however, a true Rayleigh wave has a greater vertical component than horizontal. This configuration illustrates one of the drawbacks of studies in the frequency domain over those in the time domain in that velocity is a fundamental characteristic with which to distinguish certain types of arrivals whereas frequency is not. Although surface waves (ground-roll) generally have longer periods than body waves this is not necessarily true.

The peak at 24 Hz is shown by the V (vertical) component and the H2 (perpendicular) component but not significantly by the H1 (parallel) component. This could imply that both horizontally polarized shear waves and compressional waves contribute to the 24 Hz peak which may mean that the erector pump was mounted normally to the tunnel line.

These results may be further complicated by misalignment and imperfect levelling of the multigeophone. Howell and Budenstein (1955) calculated that a 5° misalignment will cause a 0.4% decrease of sensitivity to the component being sought and cause a response to 8.7% of the motion at right angles in the plane of misorientation. We are also assuming that all the geophones have equal sensitivity, which tests showed was true to within a few percent. It is also possible that simultaneous recording of both surface and direct waves could distort the results. Without some kind of simultaneous recording from multigeophones at various distances from the tunnelling machine it is not possible to distinguish the contributions from different wave types.

4.8.1 The Variation Of Total Power With Distance

The preceding results showed that it was not possible to perform quantitative analysis on individual frequencies. An attempt was made, by measuring the total input power at each geophone of each of the three-geophone configurations (Nos. 4, 5, 6, 8), to determine the nature of the variation of total power with distance.

The total input power is defined as,

$$\frac{1}{N} \sum_{t=1}^{N} m^2_t \qquad (4.3)$$

where, m is the magnitude of the digitized value at time t and N is the number of digitized values. The input power for each of the three geophones in a configuration is plotted as $\log_e$ power versus $\log_e$ distance and as $\log_e$ power versus distance (Fig. 4.20). The power fall-off could be described by a power law if a straight line was given in the first case and by an exponential law if a straight line was given in the second case.

As can be seen in the example in Figure 4.20, in neither case do the three points describe a straight line. Attenuation curves for three other relationships between distance and power are shown in Figure 4.21. None of these relationships exhibit a straight line which would indicate some kind of linear relationship.

4.9 CONCLUSIONS

These results have shown that the power spectrum of the tunnelling machine, as recorded by geophones at the ground surface, is not stationary in the context of the definition given in Section 4.1. It is perhaps intuitively obvious that the total power and that of the contribution of individual frequencies will vary with time but we have shown that the spectral content may vary by an amount greater than that attributable to variance for a 95% confidence limit (see section 3.3.3). Thus, it would not be possible to use the tunnelling machine for attenuation studies as we could not be sure whether recorded variations were due to lithology or to changes in the output spectrum of the tunnelling machine.

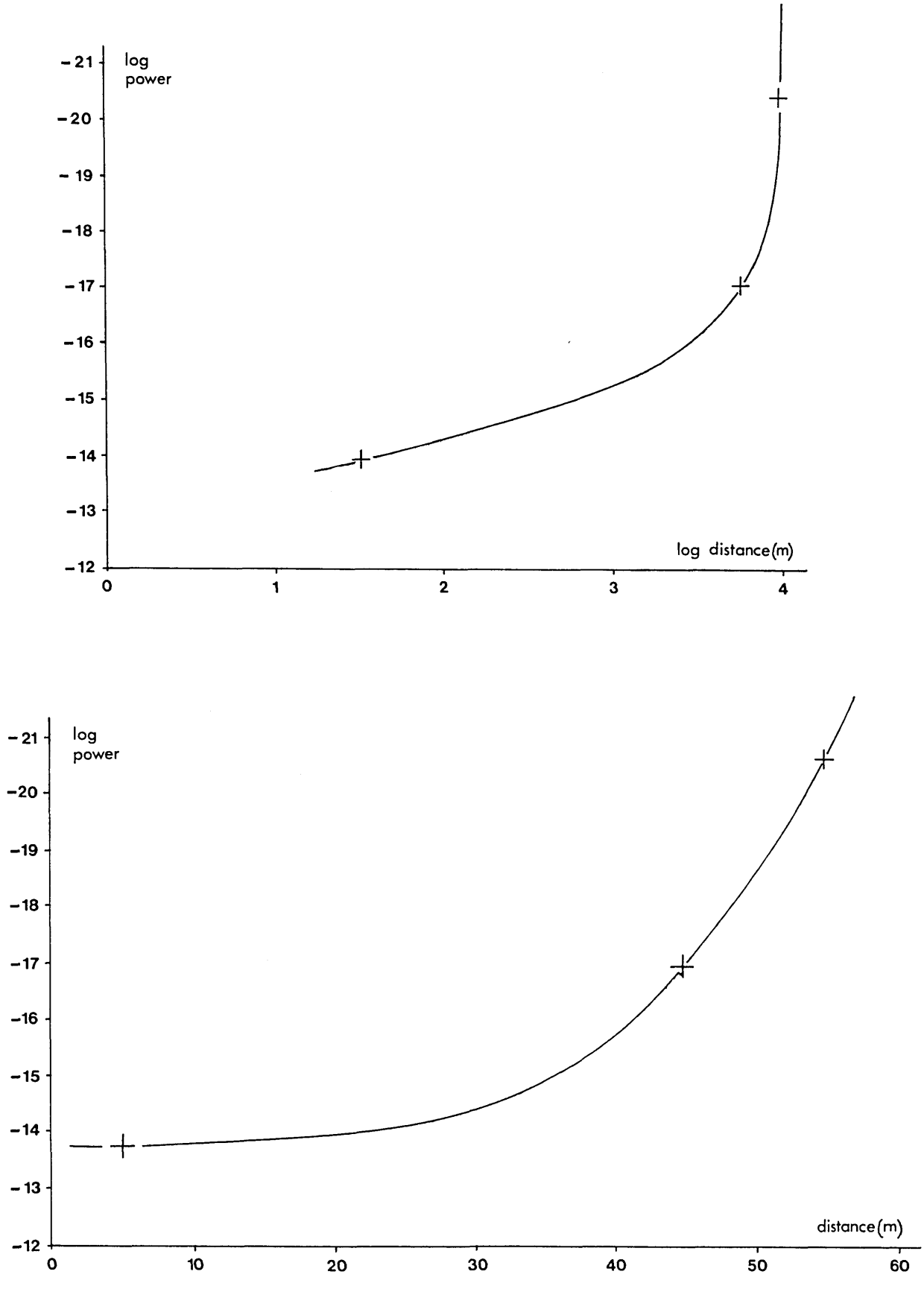

Figure 4.20 Plots to investigate the nature of power fall-off; assuming, a power law (top) and an exponential law (bottom).

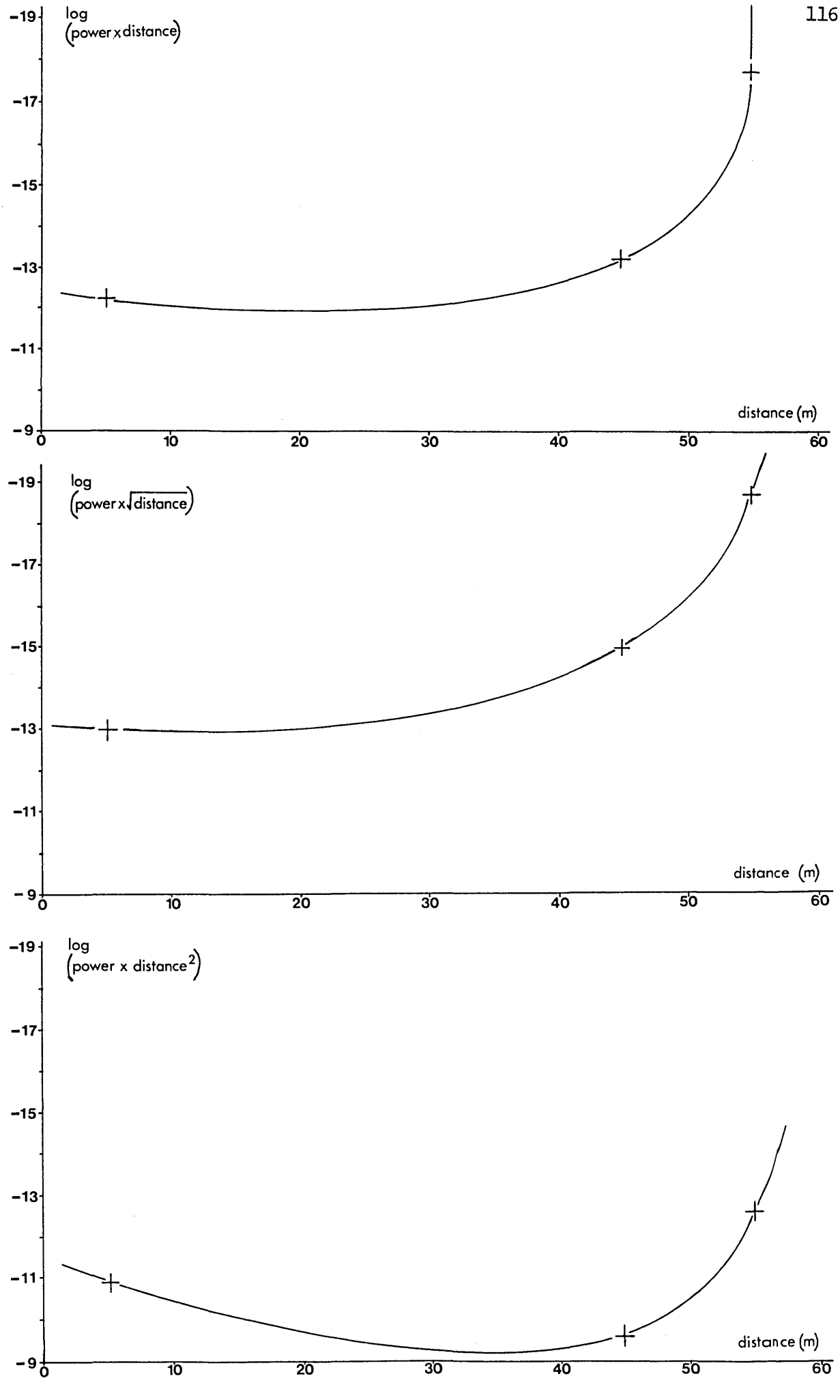

Figure 4.21 Three different relationships between distance and power

Whilst it was true that certain predominant frequencies could be consistently seen in the autocorrelation curves and power spectra, it is not possible to "normalize" the input of these frequencies into the ground as any geophone in close proximity to the tunnelling machine will no longer see it as a point source. The "near-field" signature will be obtained under conditions that do not pertain to the "far-field" thus making normalization impossible.

Had it been possible to obtain access to the machine and attach geophones to it, we would have been able to determine the variation in output of the "noise" generated by the machine. Using bandpass filters to isolate the predominant frequencies seen at the surface geophones, a partial correction for the normal variation of "noise" output by the machine could be made. Of course a common time frame between the surface and in-tunnel recording would need to be established. The correction would be a partial one only as it would still not be possible to determine the time variation in the coupling of the machine "noise" into the ground.

It is also true that the geophones were recording a complicated mixture of surface, refracted and possibly reflected arrivals which one cannot distinguish using vertical geophones and frequency analysis alone.

It is possible, from the one multigeophone recording (Configuration 7), that the 12 Hz frequency was caused by a Rayleigh type surface wave, although the horizontal and vertical components did not exhibit the correct amplitude ratio for this type of wave.

We may conclude that seismic "signals", as generated by a tunnelling machine, are unsuitable for quantitative or qualitative analysis to determine hazardous ground conditions ahead of the tunnel face, or to determine lithology.

CHAPTER V

COCKING - DETECTION OF CAVITIES PART 1

5.1 INTRODUCTION

The Warrington work demonstrated that it is not feasible to use a tunnelling machine as a seismic source because its frequency spectrum is not statistically stationary. This chapter describes an experiment to show how a different type of machine "noise" might be used to detect subterranean voids. In the context of this work we shall consider the total frequency spectrum of the machine, whilst operating, to be the "machine noise" and the useful part of this spectrum to be the "signal". All extraneous sources shall be deemed background noise.

The source chosen was a petrol-driven, portable earth-tamper of the type known as a Warsop, which weighs approximately 35 kg. The Warsop was operated by means of a hand-held throttle and imparted its energy to the ground as a periodic impulse via a rigid circular baseplate of about 15 cm diameter. By operating it with the throttle in a fixed position the Warsop gave a continuous and repeatable signal. A certain measure of frequency control was possible by altering the position of the throttle.

The site chosen for this experiment was one used by the Institute of Geological Sciences, situated in West Sussex.

The site consisted of a small area of uncultivated farmland beneath which ran a disused railway tunnel of approximately circular cross-section and with a diameter of about 5 metres. The aim of this experiment was to determine whether the presence of such a void would affect the characteristic frequency spectrum of the Warsop and in what way.

The Warsop was operated in three different positions around the tunnel, the signal being detected by various spreads of surface mounted geophones, (see Table 5.1 and Fig. 5.7). Only three geophones were allowed in each spread since the recording capacity was four channels, the fourth channel being used for a 1 kHz reference signal, as previously (see Section 4.3). Geophone spreads were laid at several different positions and orientations to the line of the tunnel. Depending upon the position of the source, some configurations did not traverse the tunnel, thus acting as a control for comparison with configurations in which the signal did traverse the tunnel before being recorded at the geophones. It was realized from previous experience at Warrington that absolute measurements of attenuation factors and signal levels would not be possible with our limited recording capability. Thus, relative measurements were the only means of observing any effects of the cavity on the signal and some form of control was essential.

The experiment was performed over several days and numerous recordings were made using geophones on the surface and within the tunnel. The effects that we hoped to observe were, cavity

resonance as reported by Watkins et al. (1967) and anomalous attenuation.

The site had a high level of ambient noise due to other work being done there, but some encouraging results were obtained. It proved possible to detect the signal of the Warsop up to a distance of 70 m, even in the presence of several sources of coherent noise. The autocorrelation function proved very useful in identifying predominant frequencies and in estimating the relative contribution of other frequencies in some cases. Cavity resonance was not observed, but in the absence of any theory in the literature, it was not possible to predict at what frequencies this might occur. Anomalous attenuation was observed in the vicinity of the cavity but it was probable that this was not due to the cavity, but to the surrounding disturbed ground.

5.2 THE SUITABILITY OF THE WARSOP AS A SEISMIC SOURCE

Evison (1957) stated in his paper that non-explosive sources are better for fundamental studies of propagation of seismic waves because of the potential for control of the waveform and energy. Whilst it is true that the Warsop did not have that potential, it did provide the kind of machine "noise" that was the object of study in this work.

An advantage of this type of vibratory source is that it is many times more powerful when operated at the surface of the ground than on bedrock. This is because for a vibrator acting

by vertical translation of a base in contact with the surface of the ground, the power is proportional to the square of the frequency and proportional to the inverse cube of the velocity of propagation (Miller and Pursey, 1955), (see also Appendix 1). The power radiated is given approximately by,

$$W = 15\ F^2\ f^2/pV^3\ \text{erg/sec} \qquad (5.1)$$

where, F is the peak force applied to the ground (dyne), f is the frequency, p is density (gm/cm^3) and V is the velocity of compressional waves. This equation is not strictly true for the Warsop, as the base will not be in constant contact with the ground and the energy will thus be imparted as a series of impulses. Therefore, the total power radiated will be somewhat less than that given by Equation 5.1. The amount of power radiated into the ground was maximized by applying downwards pressure whilst operating the Warsop, thus keeping the base in contact with the ground for the maximum time possible.

5.2.1 Testing The Warsop

Before being used in the field, the Warsop was taken to the Imperial College Research Station at Silwood Park, near Ascot for testing. The site chosen for the test was a level, grassy area well away from extraneous sources of noise.

A conventional refraction survey was done in the area proposed for the test using a 12-channel Dresser SIE RS44 seismic recording system and a sledgehammer source. This gave very satisfactory seismograms and a four-layer model could be calculated from the distance-time plot. The results are shown in Figure 5.1. The top 2 metres, which have a very low velocity, consist of very loose, dry sand covered by a 30 cm thick layer of topsoil. These results are in close agreement with the log of a borehole which is situated about 20 m away from the refraction line. The log shows 12 m of Bagshott sands overlying a bed of Oxford clay of more than 15 m thickness. The log also shows the top 2 m to consist of very loose sand.

The data for the test were recorded using an in-line spread of 12 geophones connected to the RS44 seismic recording system. The first geophone was planted 15 m from the source position and geophone separation was 5 m, thus giving a maximum source-to-geophone distance of 70 m. The geophones used were of 10 Hz natural frequency sensitive to vertical vibration. The recording was done without using filters and the gains were set to give greatest clarity on the twelve trace seismograms. The Warsop was also recorded using a three-component geophone, whose outputs were fed to three channels of the four-channel Fenlow F.M. tape recorder. The multi-geophone was buried in turn at a 1/2 m offset from each of the positions of the vertical geophones, a new recording being made for each position. The Warsop was operated in a hole about 50 cm deep to provide better coupling.

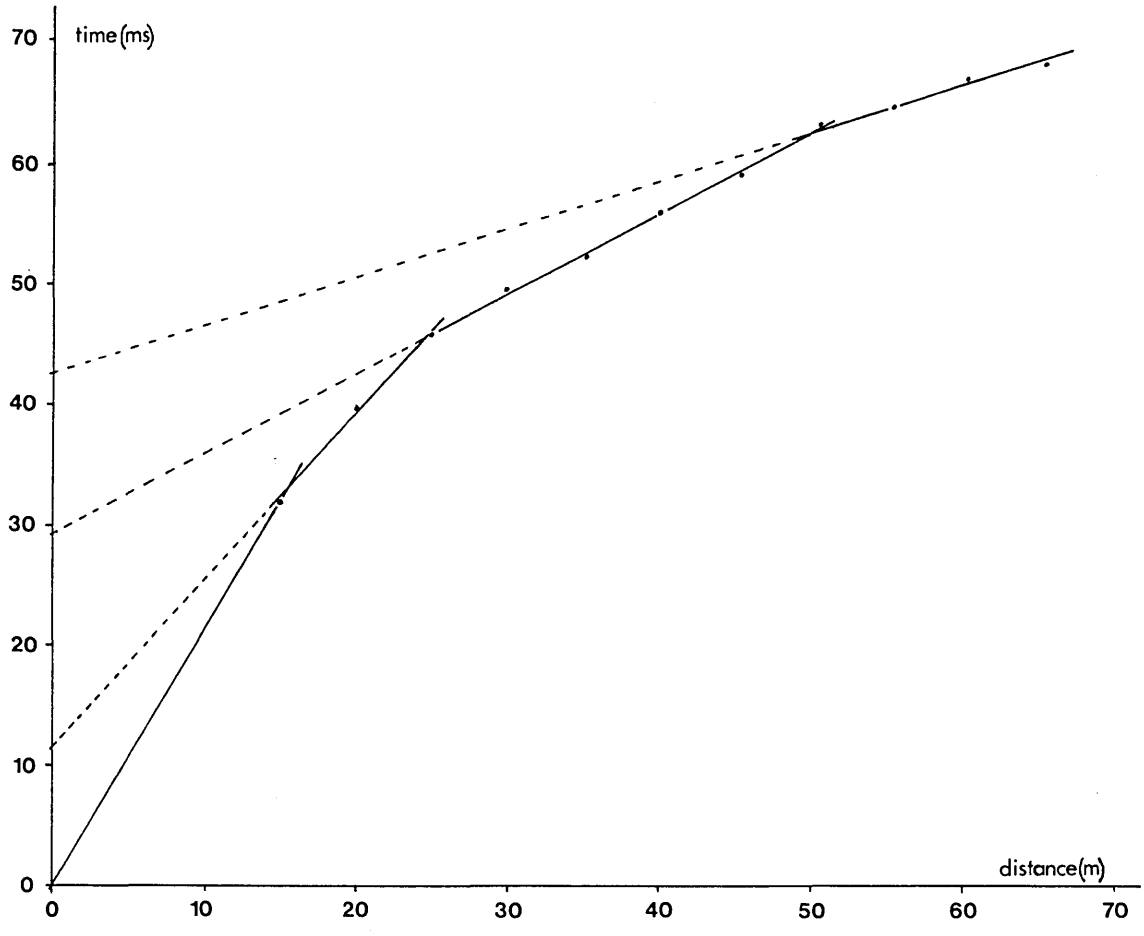

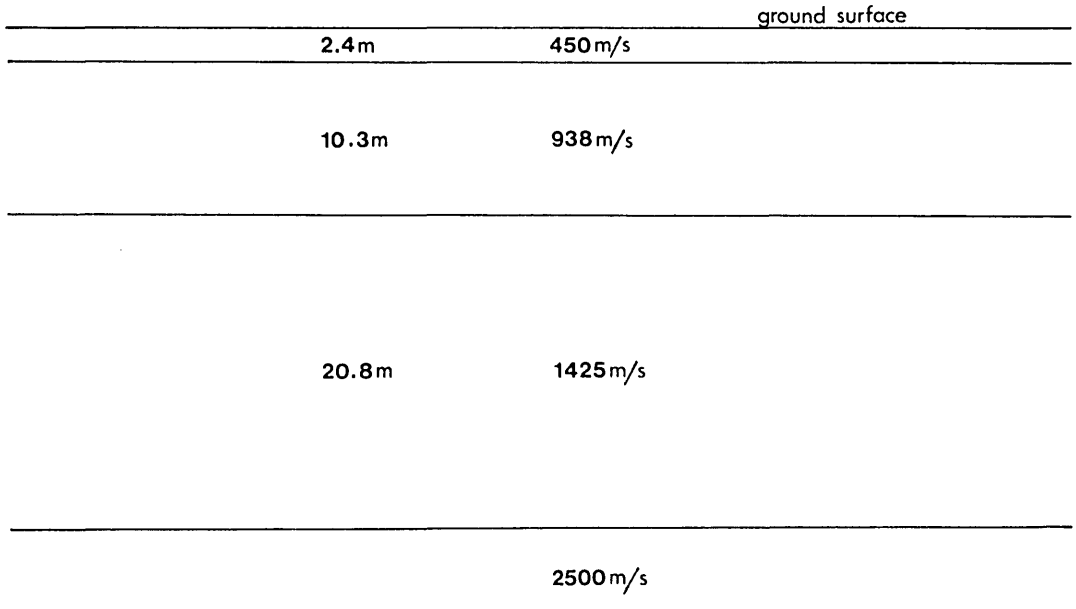

Figure 5.1 Distance-time graph and depth section for Silwood Park.

A typical seismogram recorded with the Warsop in operation as recorded by the RS44 is shown in Figure 5.2. The timing lines are at 10 ms intervals enabling the approximate predominant frequency of the signal to be measured visually, using 20 cycles per trace. The predominant frequency is the frequency of maximum amplitude on the seismograms and is assumed to be the frequency at which the Warsop radiates most energy into the ground. This came out to be approximately 48 Hz in each case, although evidence of other, higher frequencies could also be seen. Figure 5.2 also shows a typical recording from the three-component geophone. H_2 is oriented along the geophone spread and H_1 perpendicular to it. As can be seen, the amplitude of H_1 and H_2 components is greater than that of the vertical, indicating the predominance of surface and shear waves. This is consistent with the theory of a rigid, circular plate undergoing vertical translation in contact with a semi-infinite solid medium (Miller and Pursey, 1955); see Appendix 1. Miller and Pursey calculatd the power radiated from such a source for compressional, shear and surface waves to be in the ratio 1:3.74:9.78.

The three-component records were obtained by playing back the magnetic tape recordings through a Medelec oscilloscope which had a built-in hard copier. The predominant frequency of each component was measured and found to be approximately 48 Hz in each case.

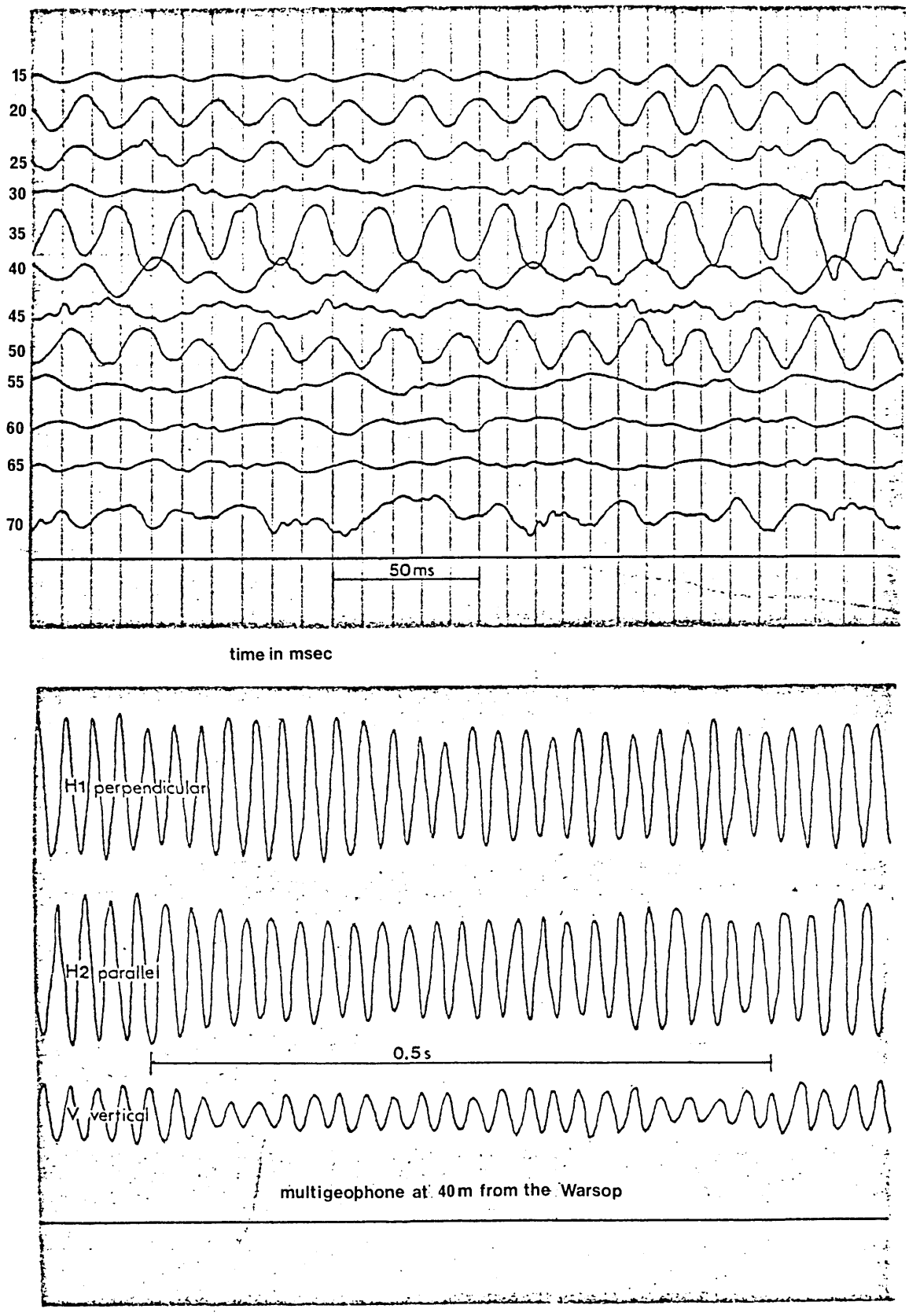

Figure 5.2 Recordings of the Warsop from the RS44 (top) and three-component geophone.

5.3 THE COCKING SITE

The site was situated about 1.5 km south-west of Cocking Village in West Sussex (Grid Ref., 870160 on 1:50,000 O.S. sheet 197). It was a small, uncultivated area lying between two large fields, partly surrounded by bushes and trees and with a disused railway tunnel running directly beneath it (Fig. 5.3). The tunnel was 5 m high, 5 m wide and the crown was at a depth below ground level of approximately 9 m. The tunnel began about 42 m to the south of the site and so most geophone lines were restricted to the east-west direction.

A cored borehole, which was about 30 m to the east of the tunnel (BH3, see Fig. 5.3), and drilled to a depth of 30 m, showed the geology of the area to be fractured chalk at least to that depth (Baria and McCann, 1977). Measurements of the geophysical properties of core samples taken from this borehole showed a small increase with depth for the compressional and shear velocities of approximately 2.9 to 3.0 km/s and 1.3 to 1.6 km/s respectively in going from 4 m to 26 m below ground level (Green, 1976). However, a seismic refraction survey, carried out by the I.G.S. (Institute of Geological Sciences) using a 24-channel ABEM seismic set and falling weight source in the immediate vicinity of the tunnel, showed a three layer structure (Fig. 5.4). The refraction line was laid parallel to the tunnel and about 12 m to the east of it. The geophone spacing was variable but usually 2.5 m and the line was shot from both ends. The first geophone (G1) and shotpoint (SP1) were about 5 metres north from the tunnel portal.

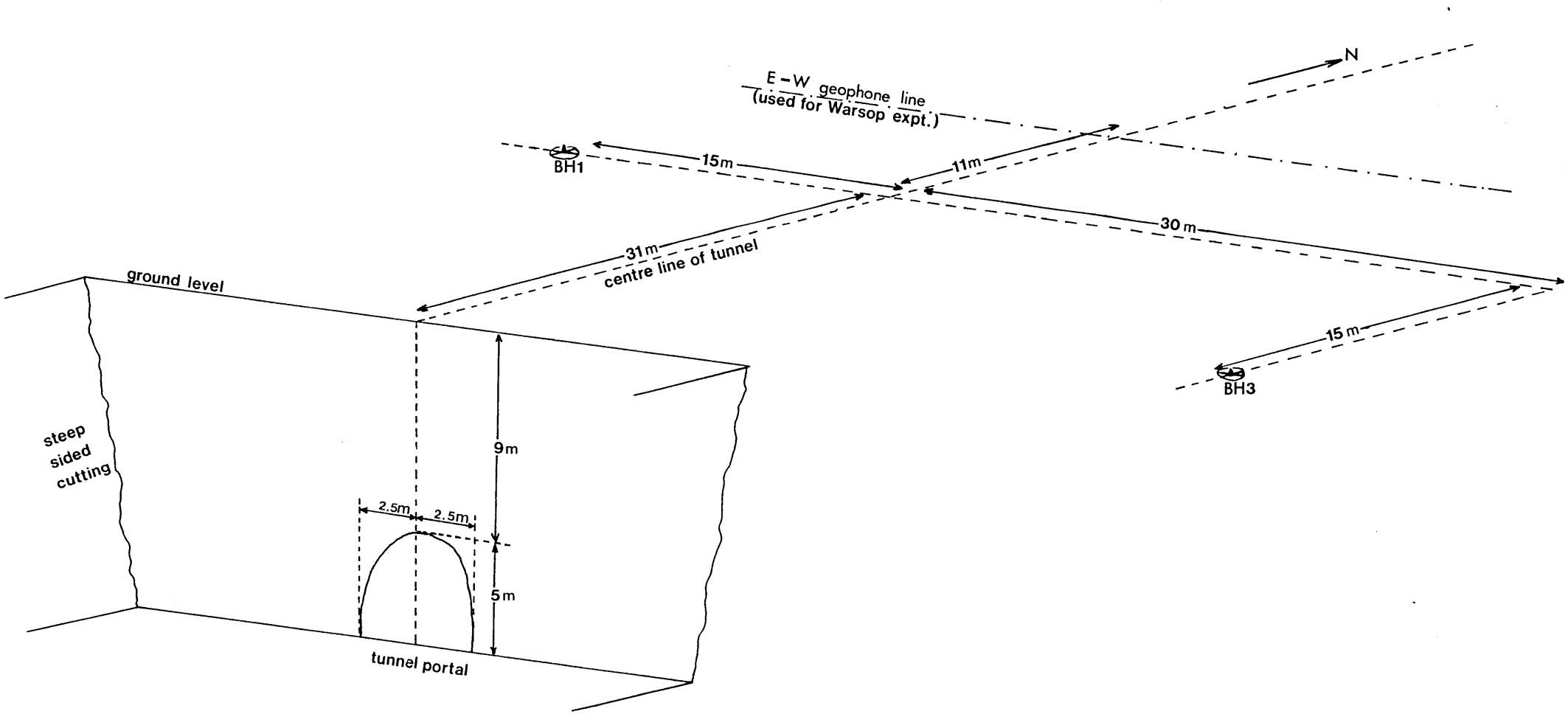

Figure 5.3 A plan of the Cocking site showing the relative positions of the tunnel, boreholes (BH) and east-west geophone line. (see also Figure 5.7)

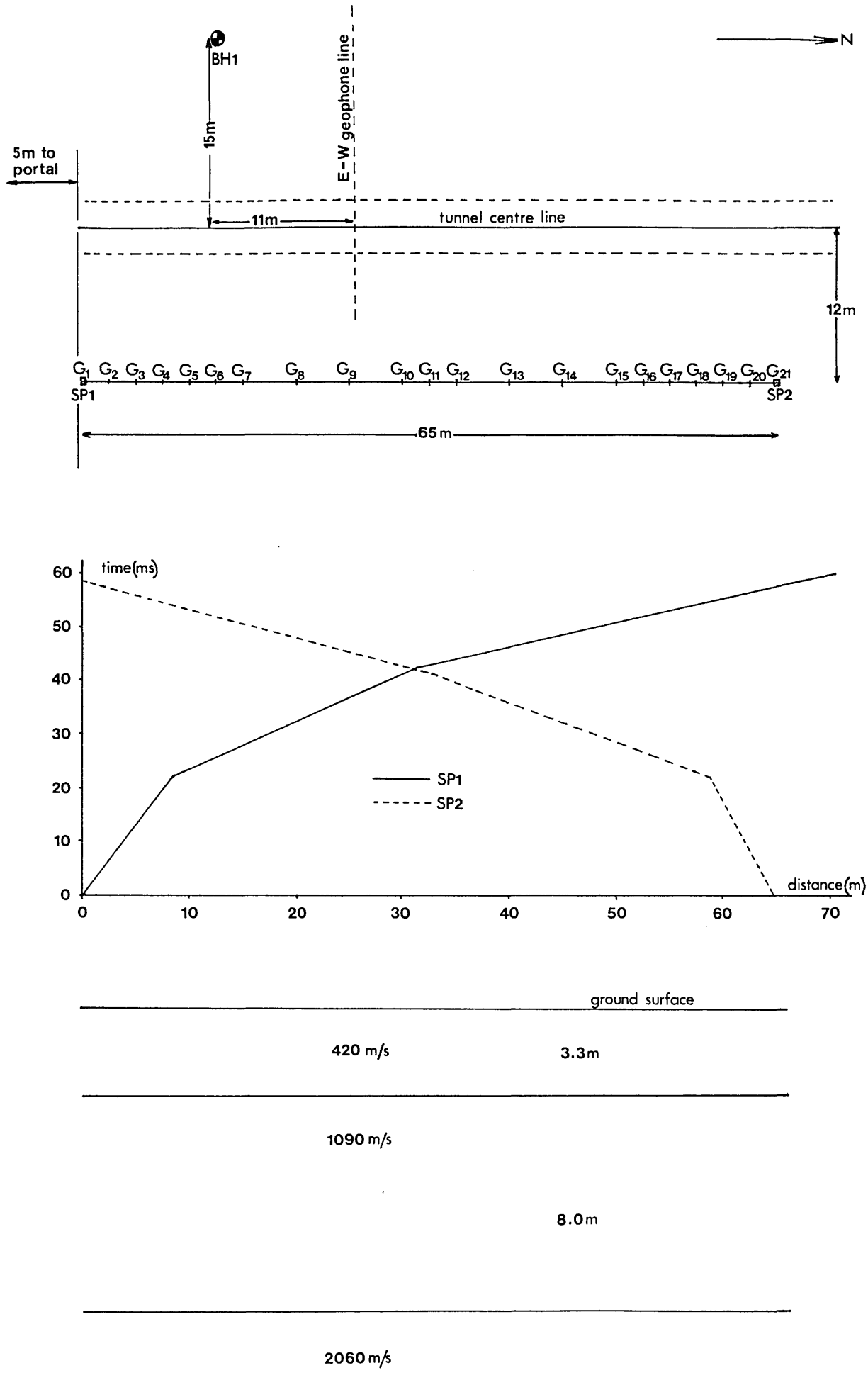

Figure 5.4 Plan and results of the Cocking refraction survey.

A further seven boreholes were drilled around the tunnel during the next year, one whilst this experiment was taking place, and they showed that the geology around the tunnel was more complicated than had previously been supposed. The chalk in the vicinity of the tunnel was highly fractured, and it was concluded that this section of the tunnel had been constructed by the cut-and-fill method, rather than by boring as had been thought from original enquiries (Baria et al., 1978).

The site was very noisy during the experiment due to the constant operation of a small generator, and intermittent operation of a large generator, sparker, compressor and a drill rig. The small generator was used to supply electricity for the recording equipment and all the other machinery was operated by the I.G.S. for their experimental work. However, the presence of these sources of noise probably simulate the conditions on a real tunnelling site.

5.4 THE EXPERIMENTAL WORK

The principal aim of this experimental work was to see whether the presence of a large cavity (depth to size ratio of approximately 1.5) would have a discernible effect on the characteristic spectrum of the Warsop. From the theoretical work of Miller and Pursey (1955) it was expected that the Warsop would radiate most of its available power as surface waves. However, a five year study conducted by R. D. Rechtien (Symposium on detection of subsurface cavities, 1977) concluded that surface waves were the most effective for

detection of near-surface cavities because; (1) surface wave energy dominates seismograms in the region where near-surface reflections occur; (2) surface wave energy is confined to propagate in the shallow layers within which the cavities are found; and, (3) surface waves are easy to generate. But, the resulting seismograms are very complex and the interaction of seismic waves with cavities has not been theoretically investigated, therefore, the interpretation is difficult.

5.4.1 Acquisition Instrumentation

The instrumentation used was similar to that used by the I.G.S. at Warrington (see Section 4.3). The system comprised of; detectors (three geophones), amplifier (three-channel), a Fenlow F.M. tape recorder (four-channel), monitor oscilloscope and frequency generator. The fourth channel of the tape recorder was used for voice commentary and to record a precise 1 kHz signal for later checking and calibration.

5.4.2 Data Preparation

As previously, the first step was a visual inspection of the recordings and then selection of suitable sections for digitizing. From this point the preparation and analysis system is different from that used for the Warrington work. The paper-tape and GE08 facility were no longer used and the playback amplifier was extensively modified to improve its frequency response and incorporate low-pass filters.

5.4.3 Playback and Digitization System

The playback system was essentially the same as that used for the Warrington data (see Section 4.4) except for some modifications to the amplifiers. These modifications comprised, resetting the gains to x15 and incorporating a two-stage, passive, low-pass filter into each channel to act as an anti-alias filter. The frequency response was tested and found to be flat from 10 to 100 Hz. The minus 3 dB points were at 2 Hz and 200 Hz (see Fig. 5.5). A small amount of aliasing was therefore expected but, confined to the upper end of the frequency range analyzed and of low amplitude compared with the signal.

The digitizing system consisted of a Kennedy A/D converter, a pulse generator, pulse doubler and tape drive.

The four output channels of the playback amplifier were directly connected to the first four channels of the A/D converter. The four channels were sampled in ascending order, each sampling command being provided by a pulse from the pulse generator and doubler. The pulse generator provided a burst of two pulses each burst having a user determined separation in time. In this case the sampling interval was set to be 3 ms, thus, giving a Nyquist frequency of 167 Hz. The additional two pulses required to sample the four channels were provided by the pulse doubler which added a "ghost" pulse to each of the pulses provided by the generator.

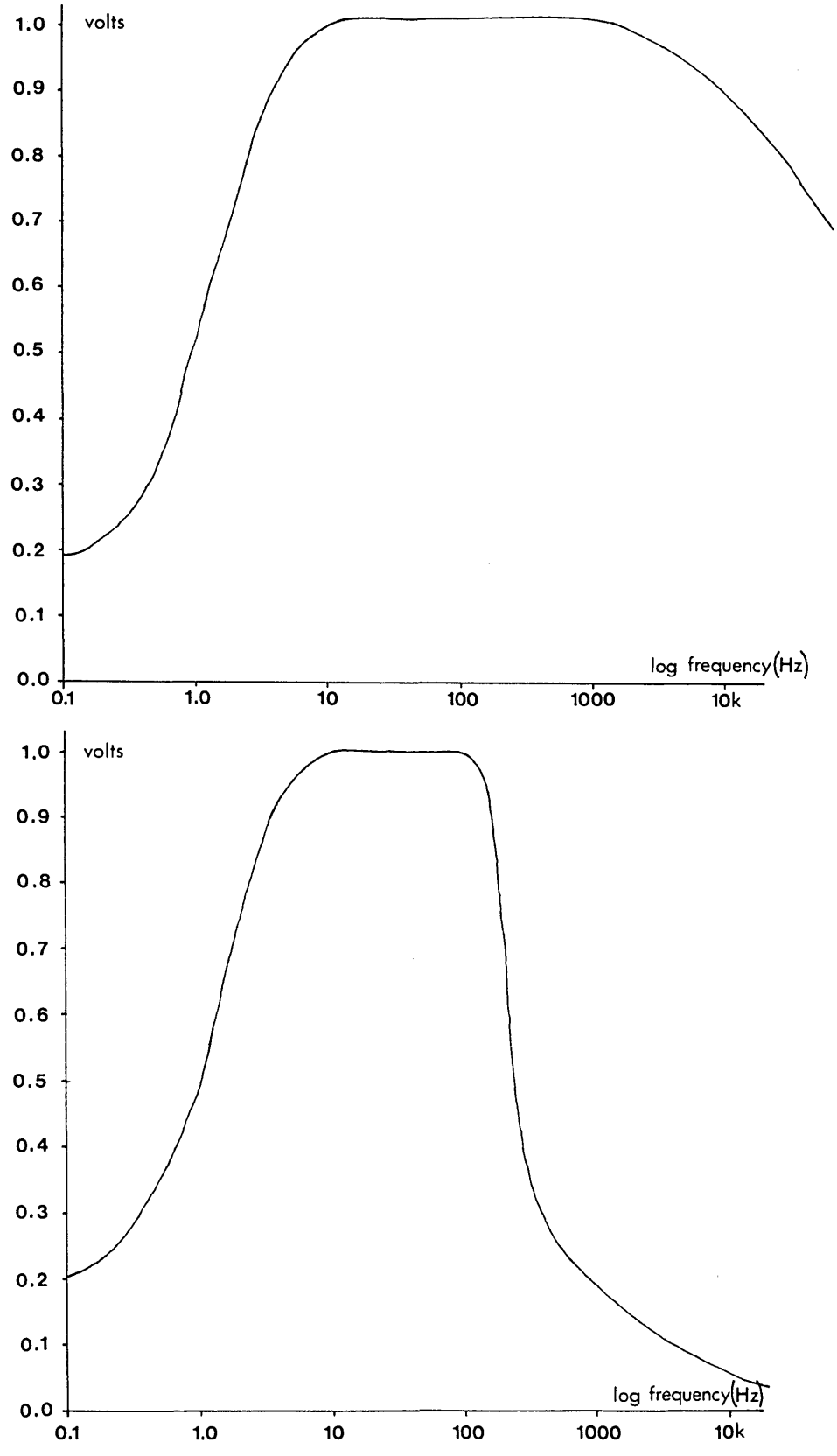

Figure 5.5 Frequency response of the four-channel playback amplifier without (top) and with low pass filters.

The Kennedy digitizing system is a sophisticated, portable A/D converter which can accept up to 16 channels. It has a direct link to a tape drive which accepts computer-type seven-track magnetic tape. The system has two buffers each having a storage capacity of 1024 words, each word being equivalent to 12 bits, which is equivalent to an accuracy of one part in 4096 for each word. Thus, the resolution over the 10 V range of the digitizer is approximately 2.5 mV.

5.4.4 Kenndy to CDC Format Conversion

Although the tape itself was compatible with the mainframe computer tape drives, the format of the data was not. Whereas the Kennedy system uses 12-bit words, the CDC system uses 60-bit words. This incompatibility was overcome by the use of program KTOCDC which first repacks the data into 60-bit words and then demultiplexes it. Thus, four separate files were produced from each third of a digitized record. The three separate parts of each channel were then repacked to form four files, each corresponding to the 9.98 second, digitized record of the output from one channel (see Fig. 5.6). Great care was taken at each stage to ensure that the right pieces of data were put together; printing out the data values at each stage helped in this.

5.4.5 Editing The Data

Unfortunately, the way in which the file for each channel was crated left small gaps between the three sections making up

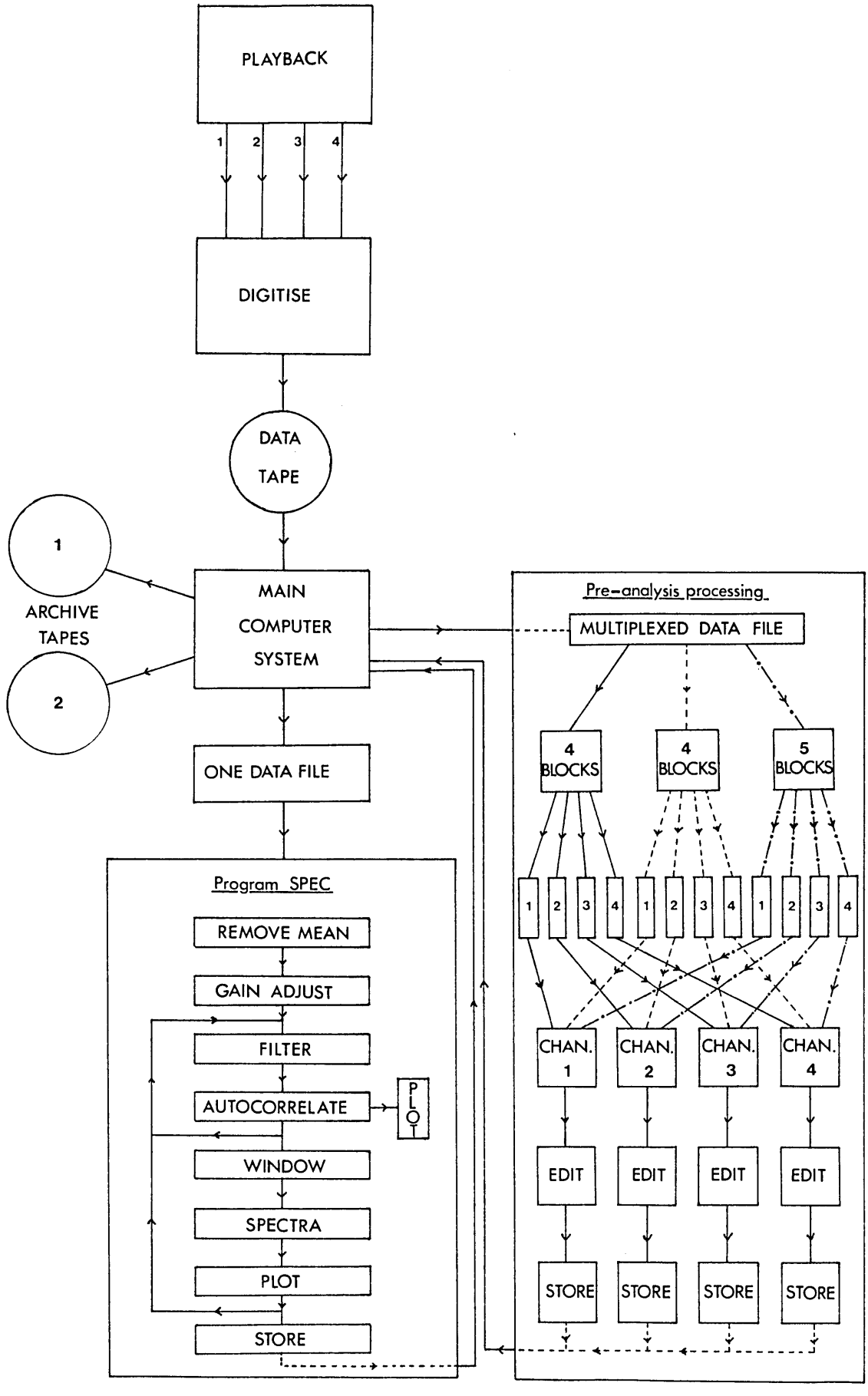

Figure 5.6 Data preparation and analysis scheme.

the whole file. This gap amounted to four data points in each case, equivalent to a time of 12 ms or 0.12% of the total data length. As these gaps in the data were small, it was possible to join them by a straight line (Beavan, 1976).

5.5 DATA ANALYSIS

The analysis was performed in much the same way as for the Warrington work except that a completely new computer program was used. The program (ISPEC) incorporated several new features, such as plotting options for any or all of the autocorrelation function, power, amplitude and log amplitude spectra, least squares removal of a linear trend, high-pass, low pass and notch filters and a choice of different windows.

The spectra were calculated via the autocorrelation function but, some of the parameters of the analysis were no longer the same as before. The number of data points per channel was now 3336 for a record length of 10 secs. The Parzen window was again used with a truncation point of 333 or 1/10th the data length. Thus, the number of degrees of freedom was 37.2 and the resolution 1.86 Hz (see Section 3.3). The resolution was improved over the prevous analysis by plotting more points. The increase in efficiency of ISPEC over SPEC meant that although more autocovariances were calculated, no increase in computer time resulted, unless the filtering routines were used. A schematic of the data preparation and analysis is found in Figure 5.6.

5.6 CHECKING OF THE COMPUTER PROGRAMS

Due to the extensive modifications to both the preparation and analysis of the data a number of tests were initiated to check the performance of each stage.

The first series of tests were on the system as a whole, from tape recording right up to final production of the spectra. For this, an accurately calibrated frequency generator was used to record monofrequency signals exactly as for an experiment, the generator replacing the geophones. Several different recordings were made; (1) 20 Hz on all channels; (2) 150 Hz on all channels; (3) 80 Hz on channel 1, 54 Hz on channel 2, 15 Hz on channel 3 and 105 Hz on channel 4, with all channels recorded sequentially; and, (4) using the same frequencies, but with all channels recorded simultaneously (using four generators). In all cases the spectra gave a single peak which was at the correct frequency within the resolution capability of the system.

The next series of tests were performed directly on program ISPEC and consisted of inputting to the program deterministic functions (sine waves), theoretical earth tidal data (line spectra) and some real data (seismic time series) for which the spectra were known. The time series generated were all of the same length and produced with the same sampling interval as the real data to be analyzed. In the case of the earth tidal data, where both the frequencies and amplitudes were accurately known, the frequencies were given exactly and the

amplitudes were correct to within 1%. As a final check, programs SPEC and ISPEC were compared by using the same set of data on each. Although both gave very similar spectra, ISPEC gave estimates which were generally within 1% of the true amplitude as compared to the 2-3% of SPEC (as measured from theoretical test data).

Additionally, the same checks were run on a program based on the Fast Fourier transform routine N log N. This was faster than, but not as accurate as ISPEC (see Section 3.3.6).

Some data from Cocking was selected prior to general analysis to determine the need for trend removal and prewhitening. There was found to be no requirement for prewhitening, nor any trends in the data. As for the analysis of Warrington data, some window-closing (Jenkins and Watts, 1969) tests were performed and a window width of 1/10th the record length was found to be optimal.

5.7 RESULTS

The results presented in this section are representative of a total of 66 digitized records (164 individual geophone records) or 6 per configuration. A plan of the geophone and source configurations is given in Figure 5.7 and listed in Table 5.1 below. For each configuration an associated recording of background noise is also shown.

In order to facilitate comparison between spectra, all the figures referred to in Section 5.7 (except Fig. 5.7) are grouped together at the end of the section.

5.7.1 The Geophone and Source Configurations

A total of eleven different source and geophone configurations were used, of these, nine were recorded with the geophones on the ground surface and two were recorded with the geophones clamped to the tunnel wall. For the nine different surface geophone configurations, some were laid parallel to the tunnel (north-south) and some perpendicular to it (east-west) as indicated in Table 5.1. Surface access above the tunnel was restricted, except to the west and so most of the geophone positions were on that side of the tunnel. Two source positions were used for the surface configuratons, designated S_1 and S_2 in Figure 5.7. Position S_1 was used for configurations 1 to 7 (excluding 3, the source for this being the rig drilling at BH1) and position S_2 was used for configurations 8 and 9.

Configurations 10 and 11 were recorded with geophones bolted to the tunnel wall at a distance of 30 m to 60 m from the portal. For configuration 10 the Warsop was operated at position S_3 (Fig. 5.7), about 12. 5 m east of the point on the ground surface directly above the position of the geophone furthest into the tunnel. The rig, drilling at BH3, was used as the source for configuration 11, the geophones remaining within the tunnel as for configuration 10.

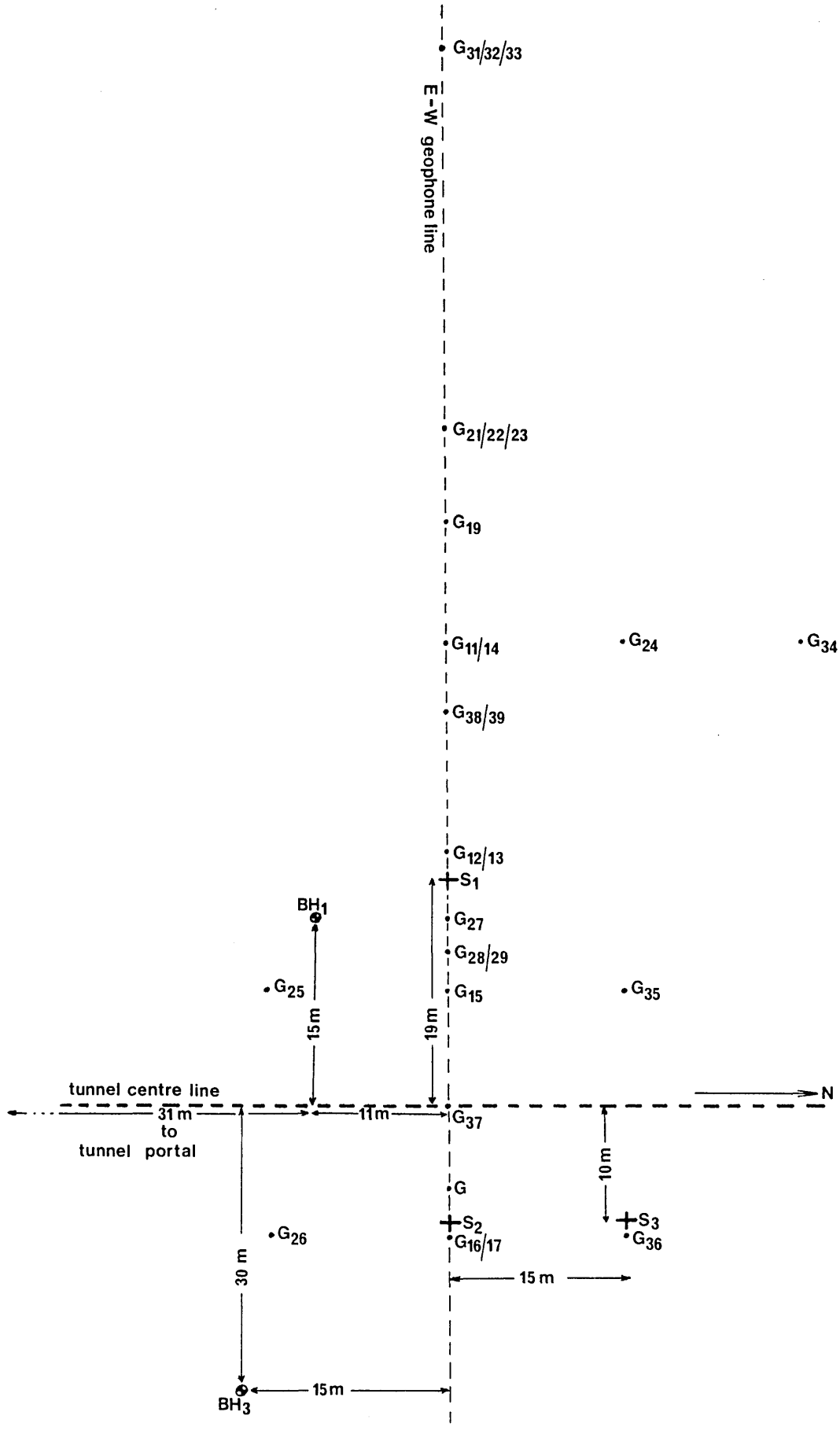

Figure 5.7 Geophone and source configurations. (Geophones are numbered according to geophone number followed by configuration number; e.g. G_{31} is geophone 3 from configuration 1)

Configuration Nummber	Source and Position	Geophone Distances from Source (m)	Geophone Spread	
			Crosses Tunnel	Orientation to Tunnel
1	Warsop, S_1	20.0 m, 38.0 m, 70.0 m	No	$\perp$
2	Warsop, S_1	2.0 m, 38.0 m, 71.0 m	No	$\perp$
3	Drill, BH_1	12.0 m, 39.5 m, 71.0 m	No	$\perp$
4	Warsop, S_1	20.0 m, 25.0 m, 36.0 m	No	//
5	Warsop, S_1	9.0 m, 17.5 m, 17.5 m	No	//
6	Warsop, S_1	30.0 m, 33.5 m, 33.5 m	No	//
7	Warsop, S_1	3.0 m, 19.0 m, 30.0 m	Yes	$\perp$
8	Warsop, S_2	3.0 m, 23.0 m, 43.0 m	Yes	$\perp$
9	Warsop, S_2	23.0 m, 43.0 m, 59.0 m	Yes	$\perp$
For configuratios 10 and 11 the geophones are wall mounted within the tunnel.			Geophone distances from South Portal	
10	Warsop, S_3	18.8 m, 21.5 m, 31.5 m	31.0m, 46.0m, 56.5m	
11	Drill, BH1	18.5 m, 25.0 m, 33.0 m	31.0m, 46.0m, 56.5m	

Table 5.1 A list of geophone and source configurations ($\perp$ means perpendicular to, and // means parallel to).

5.7.2 Configuration 1

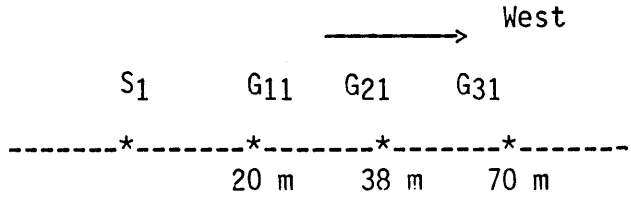

This geophone configuration does not cross the area of the tunnel. Its principal purpose is to act as a control for later configurations and to see if the signal was still easily distinguishable from the noise at 70 m, especially as there were several powerful sources of noise on site.

For all three channels the results were very much as expected. The predominant frequency on the autocorrelation curves is approximately 48 Hz, which is the same as that measured from the recordings of the Warsop made at Silwood Park. The spectra show a large peak at 48.6 Hz which is due to the Warsop. There is a slight shift in the frequency of this peak in going from geophone 1 (G_{11} above) to geophone 3, but as this shift is less than the resolution of ISPEC (about 1 Hz), no significance can be attached to it. The signal from the Warsop is well above the general noise level, even at 70 m the signal amplitude is about three times larger than that of the noise. The falloff of amplitude with distance of the signal appears to approximately follow an inverse square law, but with only three geophones any quantitative measurements are not accurate and only a qualitative assessment can be made.

Other peaks appear in the spectra at frequencies of 36 Hz and 99 Hz. These also appear on the spectra of the background noise so it would appear that there are several sources of coherent noise. On site there were two generators, a compressor and the drill rig, and it is most likely that the peaks on the noise spectra are due to these. It also appears that the noise frequencies do not attenuate as rapidly as the

signal, suggesting that the noise is confined to propagate in the surface layers in a kind of waveguide effect. However, it is not possible to say what type of ground motion is involved without the use of three-component geophones.

The autocorrelation, amplitude spectrum and log amplitude spectrum obtained from geophones 1, 2 and 3 are given in Figures 5.8, 5.9 and 5.10, respectively. The amplitude spectra for the corresponding noise records are given in Figure 5.11.

Channel four with the 1 KHz signal on it was also analyzed to make sure that none of the observed peaks was the result of data preparation or analysis and to check the operation of the anti-aliasing filter. The spectrum was found to be uniformly flat thus confirming the analysis above.

5.7.3 Configuration 2

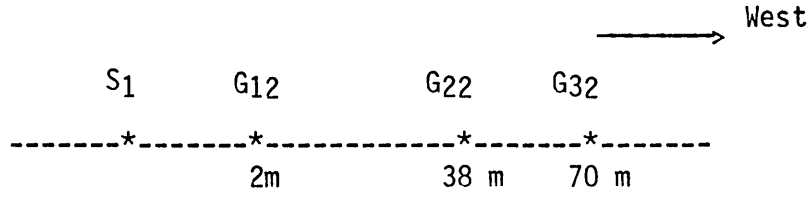

This configuration is essentially the same as that for configuration 1 except that geophone 1 is now only 2 metres from the Warsop. Geophones 2 and 3 occupy the same positions as previously and the similarity in the spectra for these two geophones is remarkable. Both the amplitudes and frequencies of the spectra are nearly identical which shows the very good repeatability of the Warsop. However, the spectrum for geo-

phone 1 shows the introduction of a new band of frequencies between 70 and 77 Hz. It is highly likely that this is due to the proximity of the geophone to the Warsop since the noise spectra do not show these frequencies. The noise spectrum (Fig. 5.15) for geophone 1 has also changed from that seen in configuration 1 (Fig. 5.11). This is due to geophone 1 being much closer (by 18 metres) to the major sources of background noise, namely the drill rig and compressor at BH1. The auto-correlations were the same as previously, with a predominant frequency of 48 Hz. The results are shown in Figures 5.12 to 5.15.

5.7.4 Configuration 3

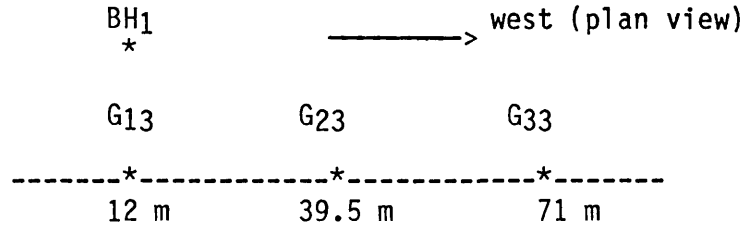

For this configuration, recorded with the drill rig in operation, the signal levels were very low and only one peak showed significantly on the spectra at about 45 Hz. This was assumed to be due to the drill rig. The drill rig was only operating intermittently which would explain the low levels, which were comparable with noise levels in previous configurations when the drill rig was not operating. The auto-correlations show a mixture of frequencies, especially on geophone 1 which is closest to the source. This is also an indicator of the low level of signal from the drilling rig

since previous autocorrelations showed only the predominant frequency of the Warsop. The frequency previously seen on noise spectra at 99 Hz can be seen, plus other frequencies of 12 Hz, 27 Hz, 63 Hz and 87 Hz. The autocorrelations and power spectra can be seen in Figures 5.16 to 5.18. Since this is essentially a noise record, no other spectra are shown.

5.7.5 Configuration 4

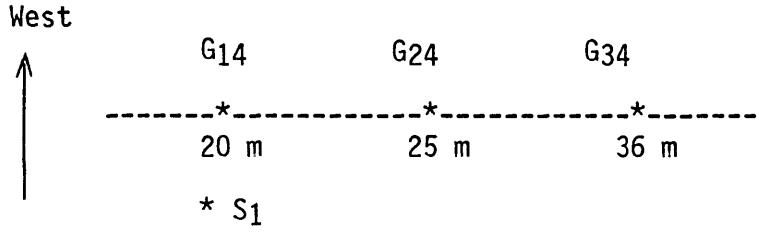

Once again the spectra and autocorrelation curves are similar to those in configurations 1 and 2. The predominant frequency is again 48 Hz and at a level comparable with those at similar distances from the source in previous configurations. For this configuration the site was noisy and consequently noise levels are high, as can be seen from the noise records (Fig. 5.22). Peaks at 27 Hz were seen which were repeated on the noise spectra. Their source could not be identified but as there were many possible sources of noise on the site, some working intermittently, it is expected that the noise spectra would not remain constant. Comparing the amplitudes of the signal and noise from different geophones, it again appears that the signal attenuates more rapidly than the noise. Figures 5.19 to 5.22 show the autocorrelation curves and the signal and noise spectra.

5.7.6 Configuration 5

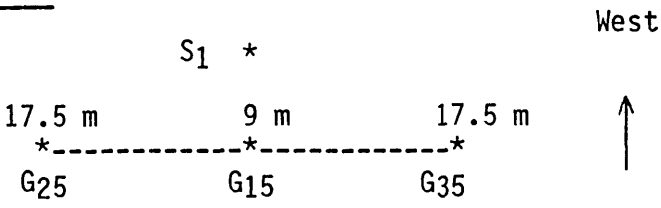

As this geophone spread is very close to the machinery on site, the noise levels are extremely high. One major difficulty for this configuration is that one source of noise has a frequency very close to that of the predominant frequency of the Warsop at 48 Hz. This is shown by the enhanced autocorrelation and also by the peak at 48 Hz on the amplitude spectra. This was formerly a single peak and has now become a double peak. The peak due to the Warsop is highest on geophone 1 and comparable on geophones 2 and 3 which is consistent with their spatial relationship. However, the noise levels of geophones 1 and are higher than on 3, and are especially high on geophone 2 at 24 Hz and 43 Hz. Geophone 2 was in fact close to a generator and the drill rig, and geophone 1 was closer to these than geophone 3, which explains the difference in noise level. Figures 5.23 to 5.26 show the autocorrelations and spectra for this configuration.

5.7.7 Configuration 6

Unfortunately, it was not possible to obtain results for this configuration as the tape was found to be "bad" over this section during digitization.

5.7.8 Configuration 7

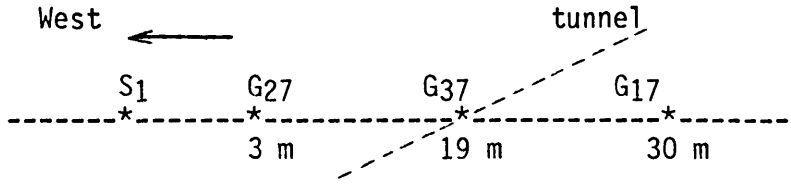

This is the first of the configuratons which cross the tunnel and in the discussion of this and following configurations much reference will be made to previous spectra. To aid the reader in this comparison, where a geophone number in a previous configuration is mentioned, the corresponding figure will be given in brackets.

Comparing geophone 2 with that at a similar distance, geophone 1 of configuration 2 (5.14), there is only a 4% difference in amplitude of the Warsop signal for a 1 m difference in distance. Then, comparing the spectra of geophones 1 and 3 with those of similar distance the similarities and differences are immediately apparent. For geophone 3 (which is directly over the tunnel) and comparing this with geophone 1, configuration 1 (5.10) and geophone 1, configuration 4 (5.21) there is an order of magnitude increase in the amplitude between 57 Hz and 70 Hz, whereas the amplitudes for other frequencies are nearly identical (on all geophones). However, this configuraton is closer to sources of noise than others and thus could be noise. But, it may also be due to the presence of the tunnel and may possibly be cavity resonance as seen by other workers (Watkins et. al., 1967; Godson and Watkins, 1968) and believed to be initiated by Rayleigh waves. When comparing geophone 1 (at 30 m) with other spectra at a similar distance and nearly identical source amplitude (geophone 2, configurations 1 and 2; Figs. 5.10 and 5.14), the amplitude at geophone 1 is half that of the other two. This greater attenuation of the signal could be because it has to travel through the volume of ground containing the tunnel. It is not possible to say whether it

is the tunnel itself causing this attenuation or the disturbed ground around it. However, it is more likely to be due to the latter. The results for configuration 7 can be seen in Figures 5.27 to 5.29.

5.7.9 Configuration 8

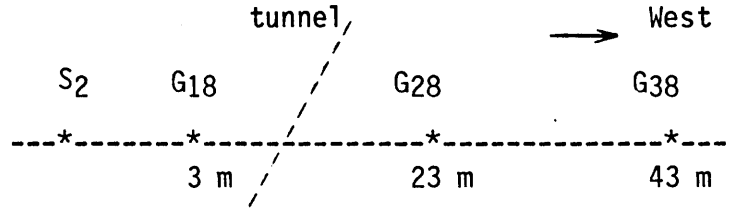

The Warsop was moved to a position approximately 10 m east of the tunnel for this and the next configuration. The tunnel now lies between geophones 1 and 2. The noise levels for this configuraton are particularly high, especially on geophones 2 and 3 as the generators and the compressor are near geophone 2 on the west side of the tunnel. At geophone 3 the noise level is comparable in amplitude with that of the signal, but at geophone 1 the noise is about 1% of the level of signal plus noise. It is interesting to compare geophone 1 with geophone 1, configuration 2 (5.14), geophone 2 with geophone 1, configuration 1 (5.10) and geophone 3 with geophone 2, configuration 2 (5.14), which are nearly equal distances from the Warsop. The differences and similarities are immediately apparent, even allowing for the differences in the source positions and noise levels. Comparing the two geophnes close to the source (2 m and 3 m), the spectra are very similar both in shape and amplitude. The extra frequencies previously seen around 70 Hz are now also seen and believed to be due to the

the proximity of the geophone to the Warsop, since they are also observed on geophone 2 but not with any appreciable amplitude on geophone 1, configuraton 1 (5.10). Comparing the amplitudes of the frequencies which are believed to be noise (24 Hz, 57-70 Hz, 73 Hz, 97-99 Hz) and the amplitudes of the signal (48 Hz) for the three pairs of geophones (those for configuration 8 and those mentioned above), shows that the signal amplitudes for configuration are very low for geophones 2 and 3, whereas the noise amplitudes are nearly identical. As the signal traverses the tunnel and the noise does not, the sources of noise being to the west of the tunnel, it is reasonable to assume that the attenuation is greater in the vicinity of the tunnel. No frequencies were observed which could be unambiguously ascribed to cavity resonance. The spectra are shown in Figures 5.30 to 5.33.

5.7.10 Configuration 9

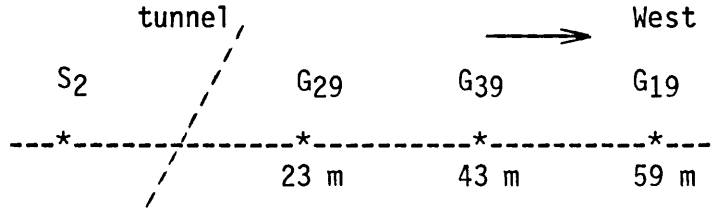

For this configuration the tunnel lies between the source and all three of the geophones. Geophone 1 of configuration 8 was moved to a position 59 m west of the source. If the outputs of geophones 2 and 3 are compared with 2 and 3 of configuration 8 (5.32) the similarities are obvious; so are the differences for geophone 1. This difference is not just due to the change in distance from the source. For example,

if one compares geophone 1 with geophone 3, configuration 1 (5.10), which is even further from the source, (showing the difference in amplitude), it is seen that the amplitude for geophone 1 is about 30% of that for geophone 3, configuration 1, even though geophone 1 is 11 m closer to the source. This confirms the results of configuration 8, which indicated that the area around the tunnel caused a rise in attenuation of the signal from the Warsop. The results are shown in Figures 5.34 to 5.37.

5.7.11 Configuration 10

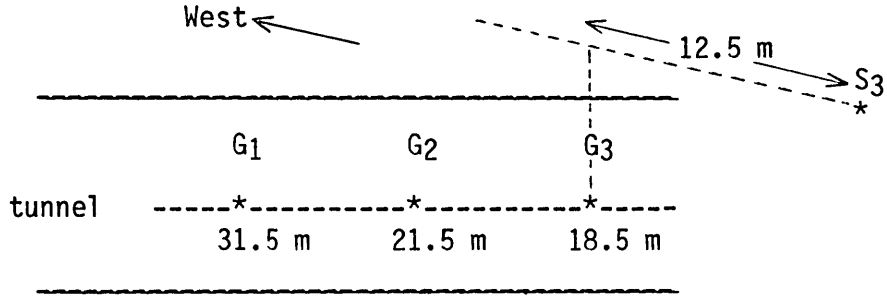

For this configuration the geophones are mounted on angle iron which has been firmly bolted to the brick lining of the tunnel approximately 1.4 m from the floor on the west side. The Warsop was moved to position S_3, about 10 m west of the tunnel or 12.5 m east of the vertical projection to the surface of the position of geophone 3.

Unfortunately, recording conditions in the tunnel were bad due to the damp and crumbling brick tunnel lining and a two-foot deep layer of cow manure on the tunnel floor. Also, the cable

to geophone 3 was found to be defective. Thus, only two geophones were operative since a replacement cable of the required length was not available.

The spectra for the two geophones are very similar, showing significant peaks at 23 Hz, 30 Hz, 48 Hz and 99 Hz. The peak at 48 Hz, due to the Warsop is the largest in amplitude, the other peaks being due to the drill rig and other sources of noise. No other peaks are observed and therefore it must be assumed that there is no resonance. The autocorrelation curves show the 48 Hz of the Warsop as the predominant frequency. The results are shown in Figures 5.38 and 5.39.

5.7.12 Configuration 11

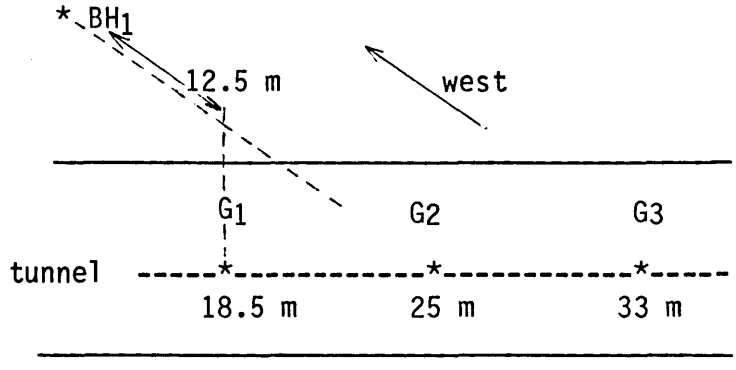

Geophone 3 is again non-operational. The autocorrelations for the recording of the drill rig and other background show no predominant frequency, indicating that several frequencies are at a comparable level. The spectra show peaks at 20 Hz, 33 Hz, 70 Hz and 99 Hz which correspond to those of the previous configuration, neglecting the contribution due to the Warsop. The autocorrelations and spectra are shown in Figures 5.40 and 5.41.

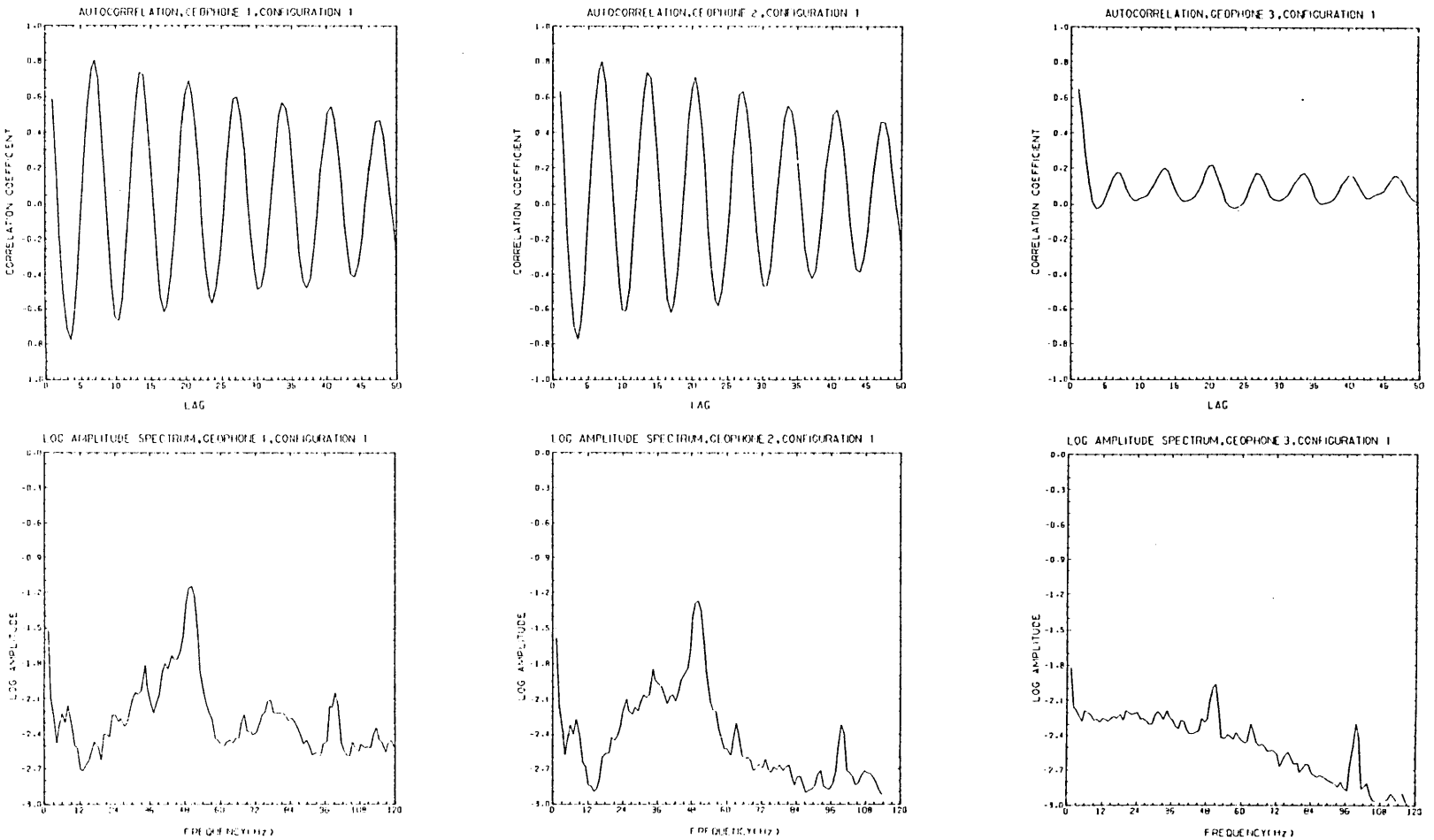

Figure 5.8 (top) Autocorrelation curves for configuration 1

Figure 5.9 (bottom) Log amplitude spectra for configuration 1

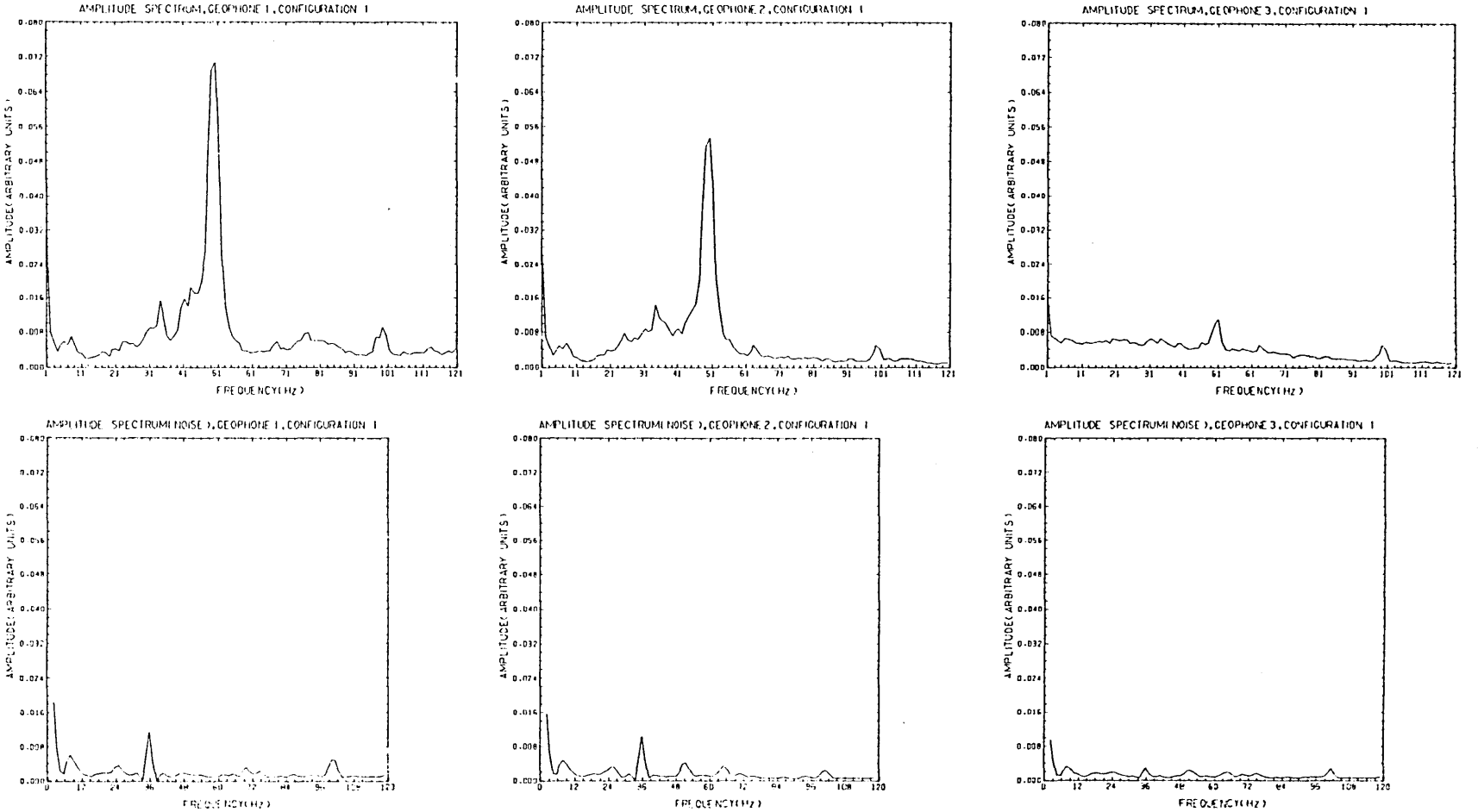

Figure 5.10 (top) Amplitude spectra for configuration 1

Figure 5.11 (bottom) Noise amplitude spectra for configuration 1

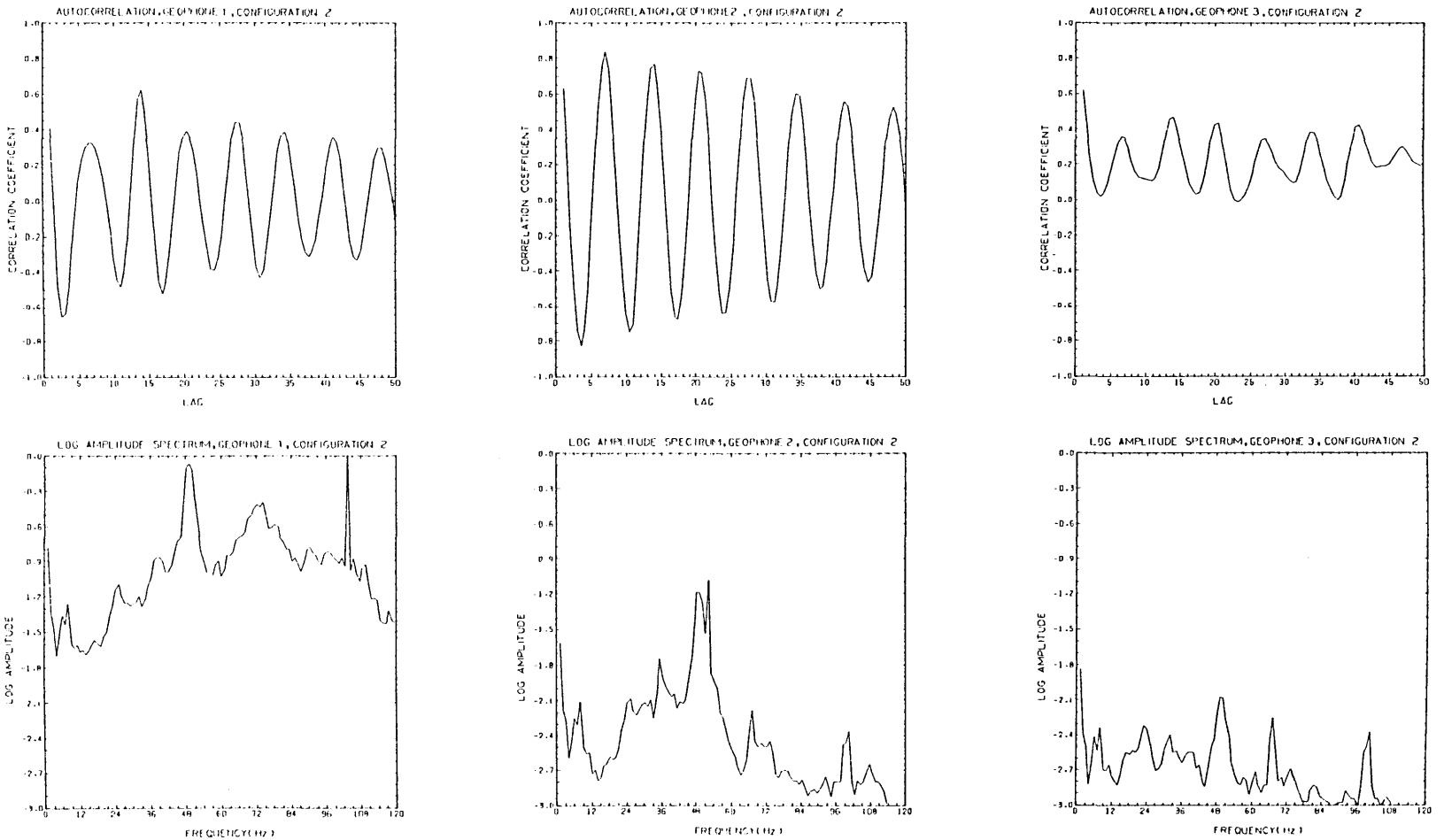

Figure 5.12 (top) Autocorrelation curves for configuration 2

Figure 5.13 (bottom) Log amplitude spectra for configuration 2

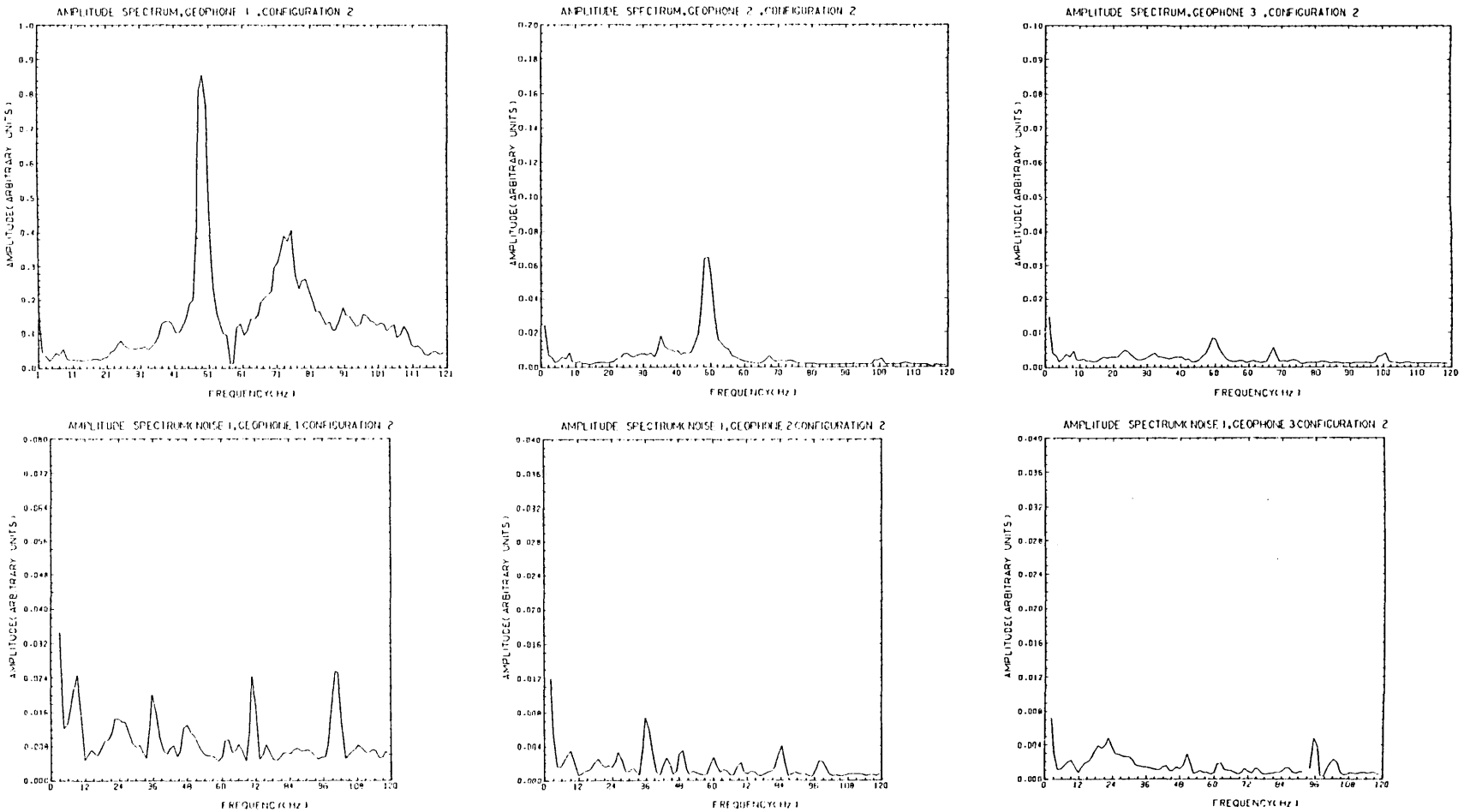

Figure 5.14 (top) Amplitude spectra for configuration 2

Figure 5.15 (bottom) Noise amplitude spectra for configuration 2

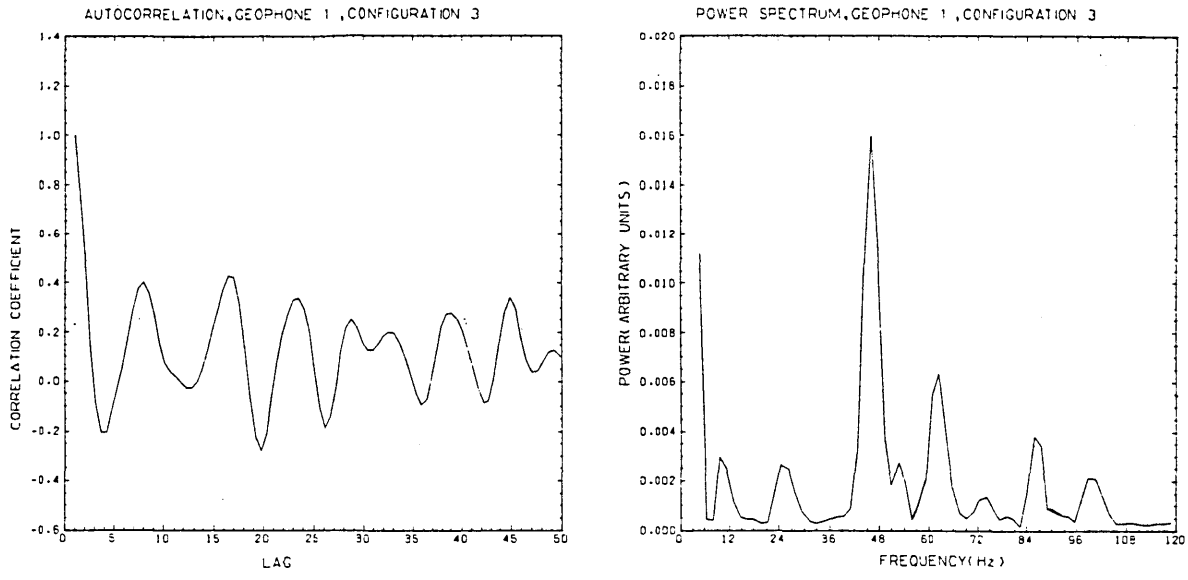

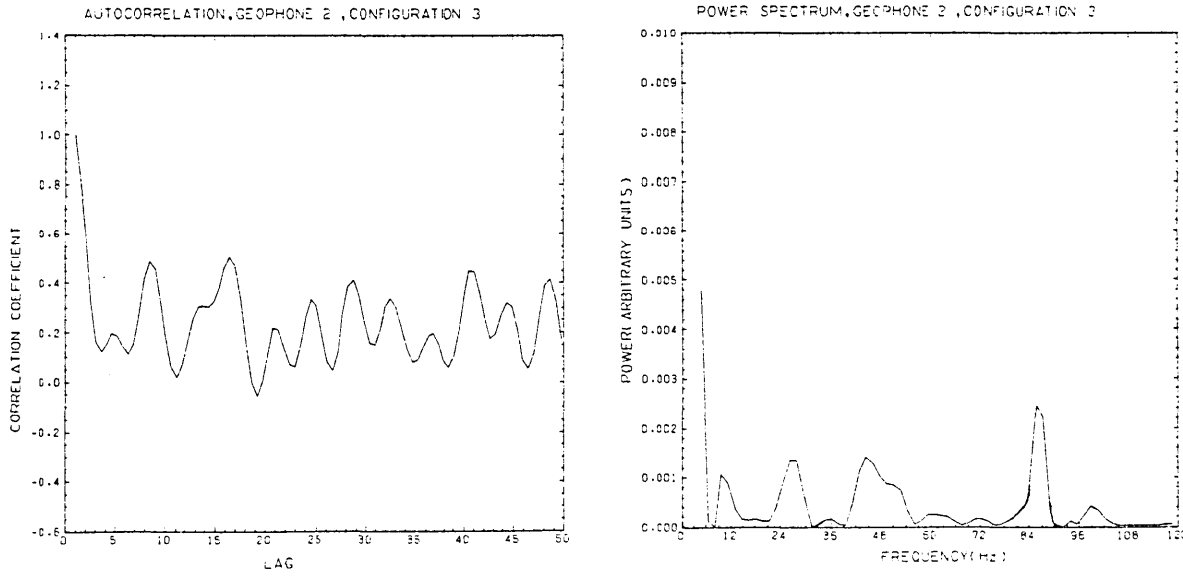

Figure 5.16 (top) Autocorrelation and power spectrum for geophone 1, configuration 3

Figure 5.17 (bottom) Autocorrelation and power spectrum for geophone 2, configuration 3

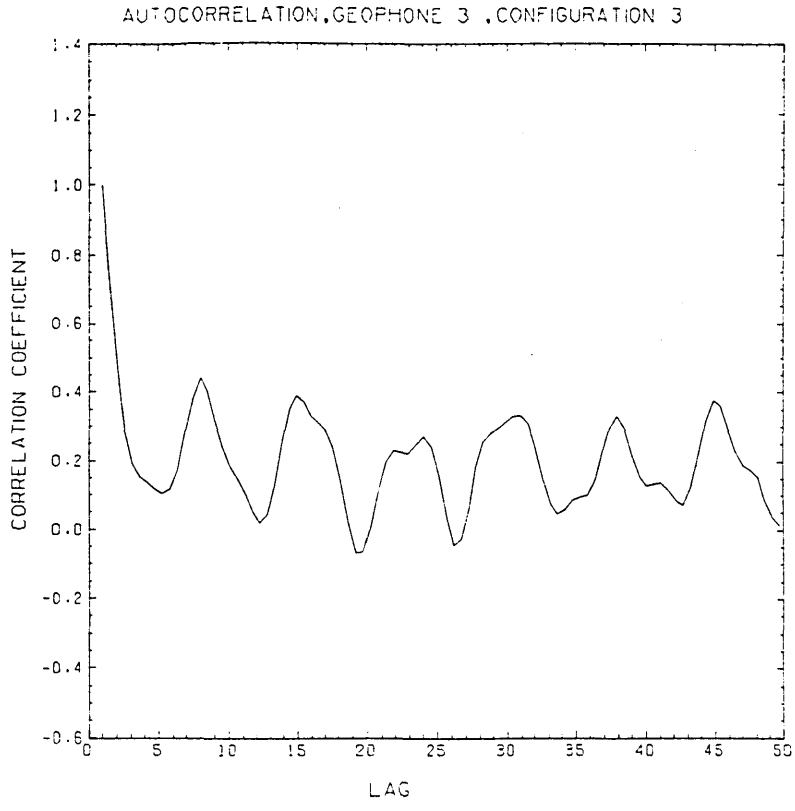

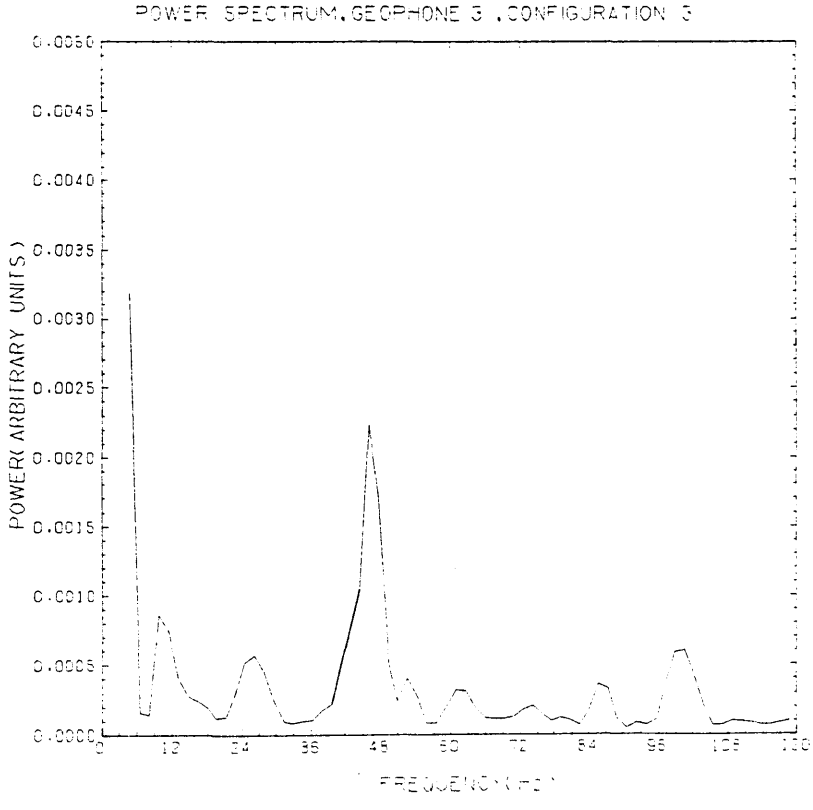

Figure 5.18 Autocorrelation and power spectrum for geophone 3, configuration 3

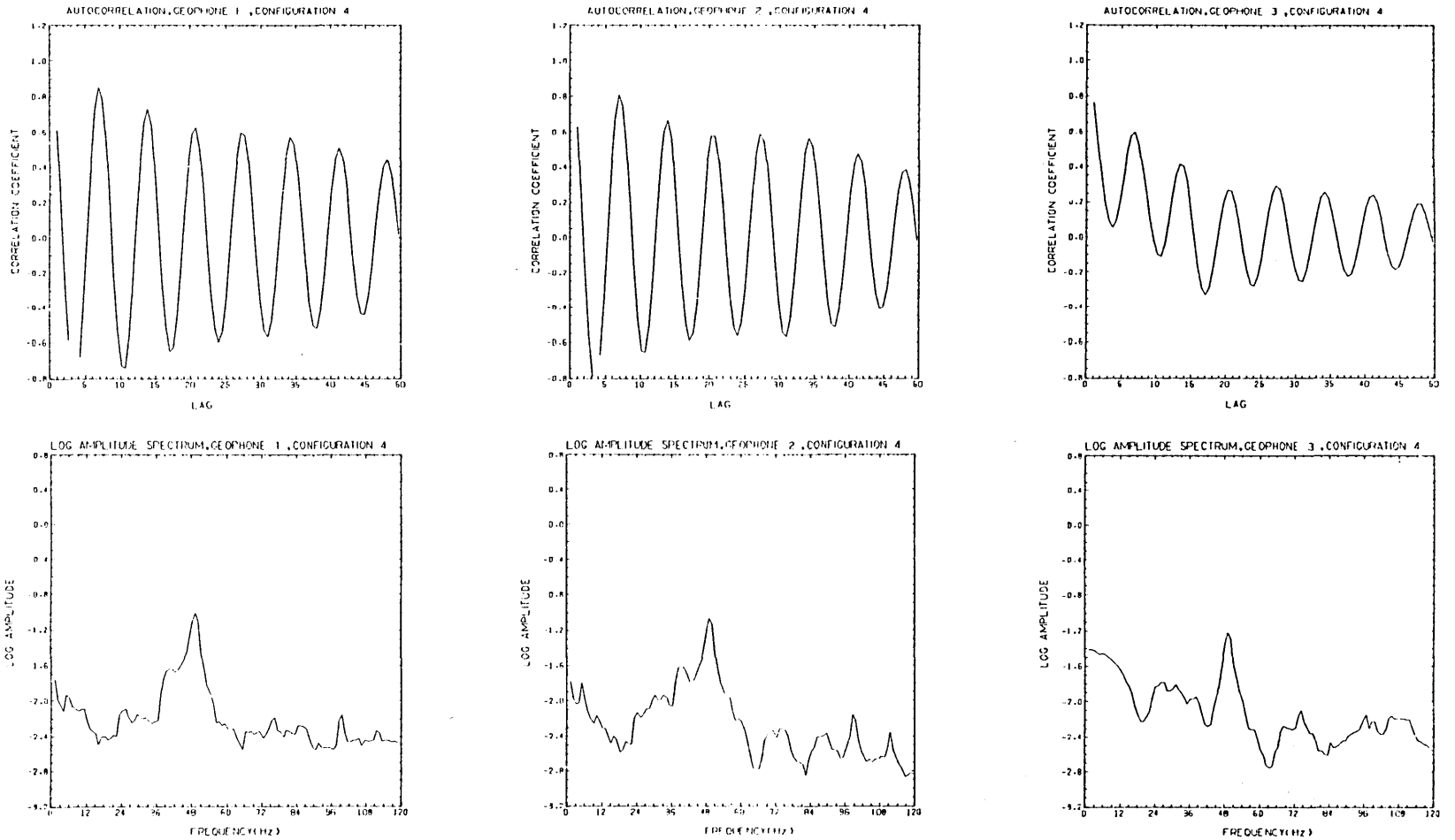

Figure 5.19 (top) Autocorrelation curves for configuration 4

Figure 5.20 (bottom) Log amplitude spectra for configuration 4

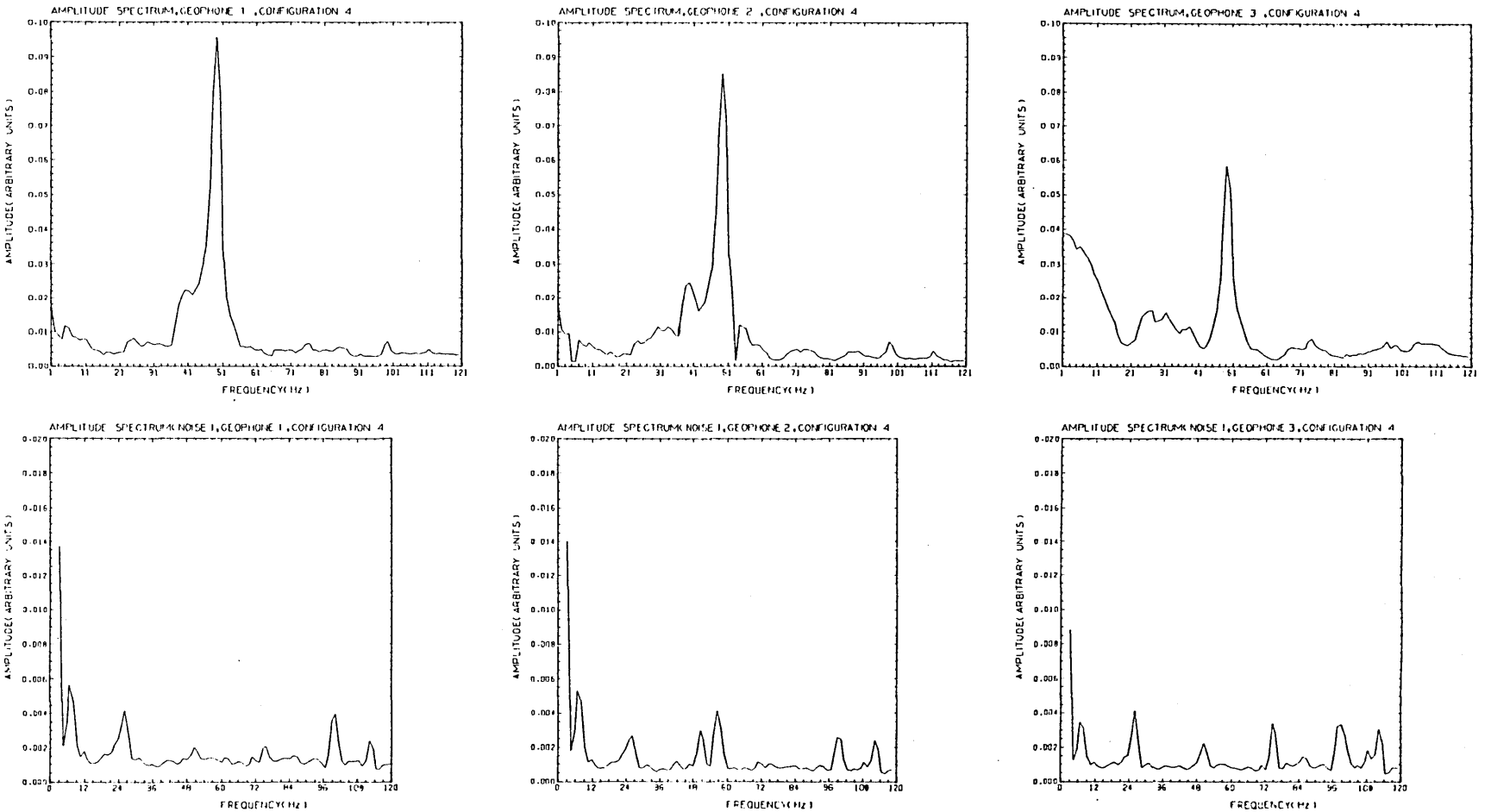

Figure 5.21 (top) Amplitude spectra for configuration 4

Figure 5.22 (bottom) Noise amplitude spectra for configuration 4

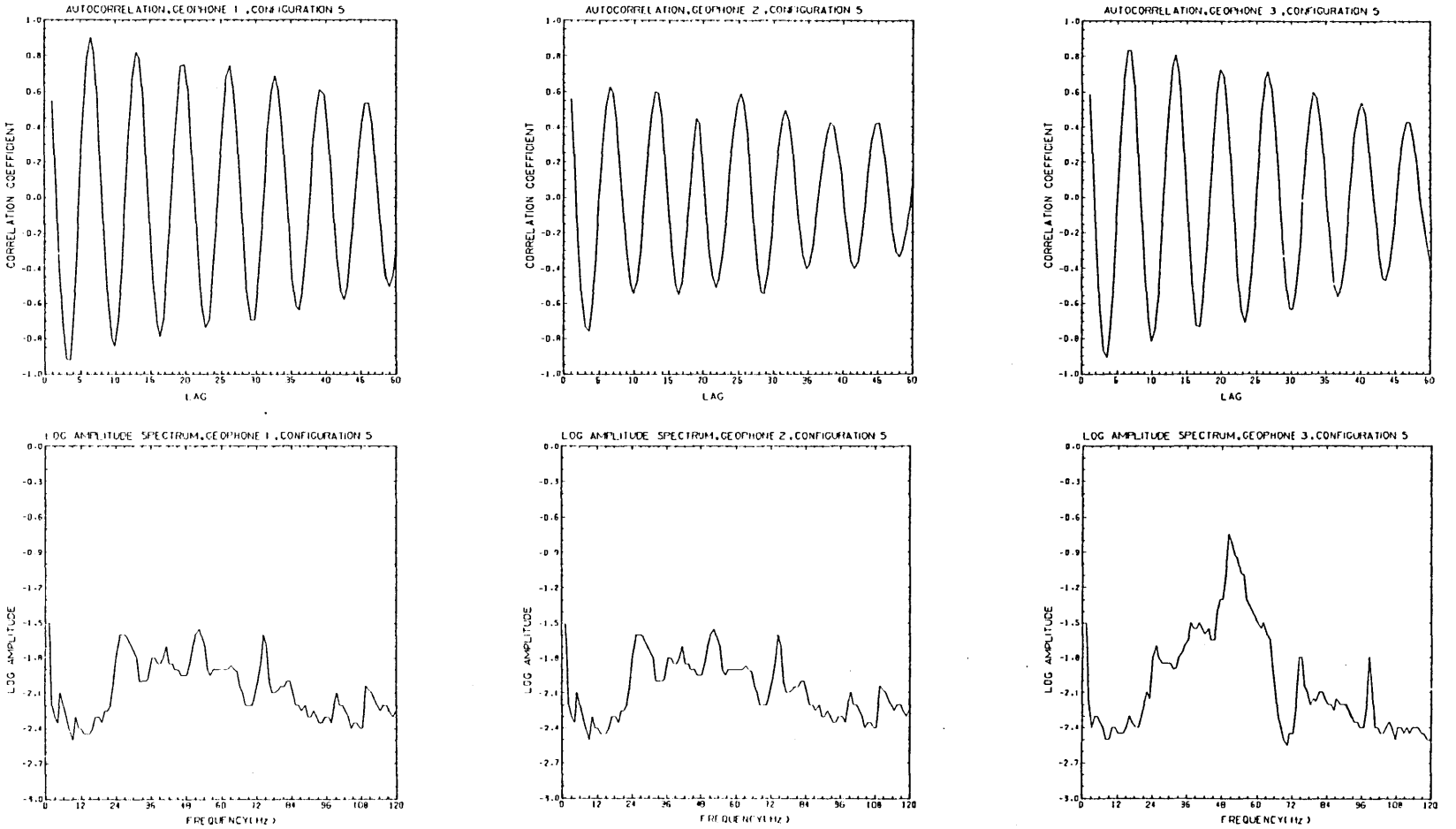

Figure 5.23 (top) Autocorrelation curves for configuration 5

Figure 5.24 (bottom) Log amplitude spectra for configuration 5

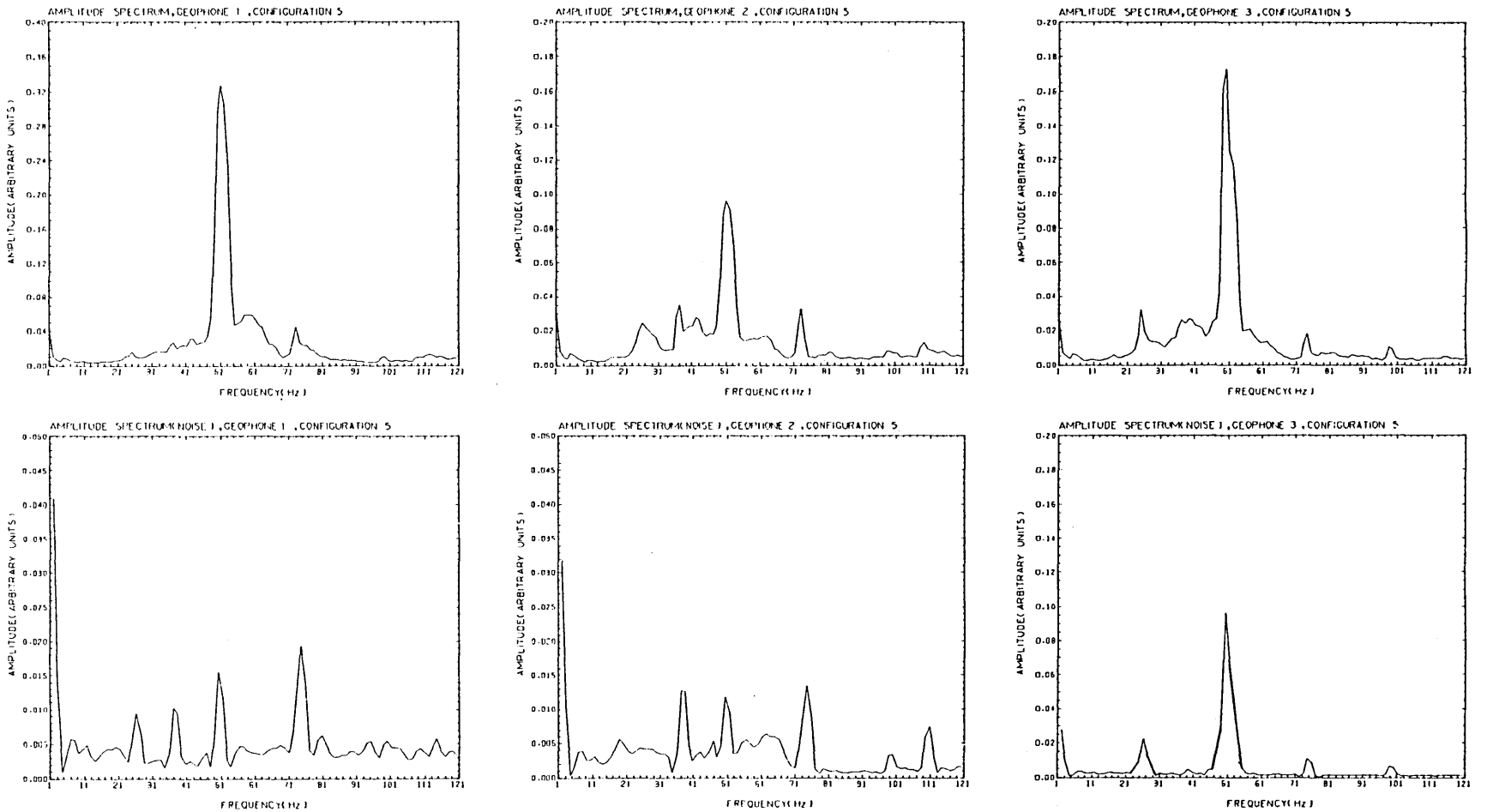

Figure 5.25 (top) Amplitude spectra for configuration 5

Figure 5.26 (bottom) Noise amplitude spectra for configuration 5

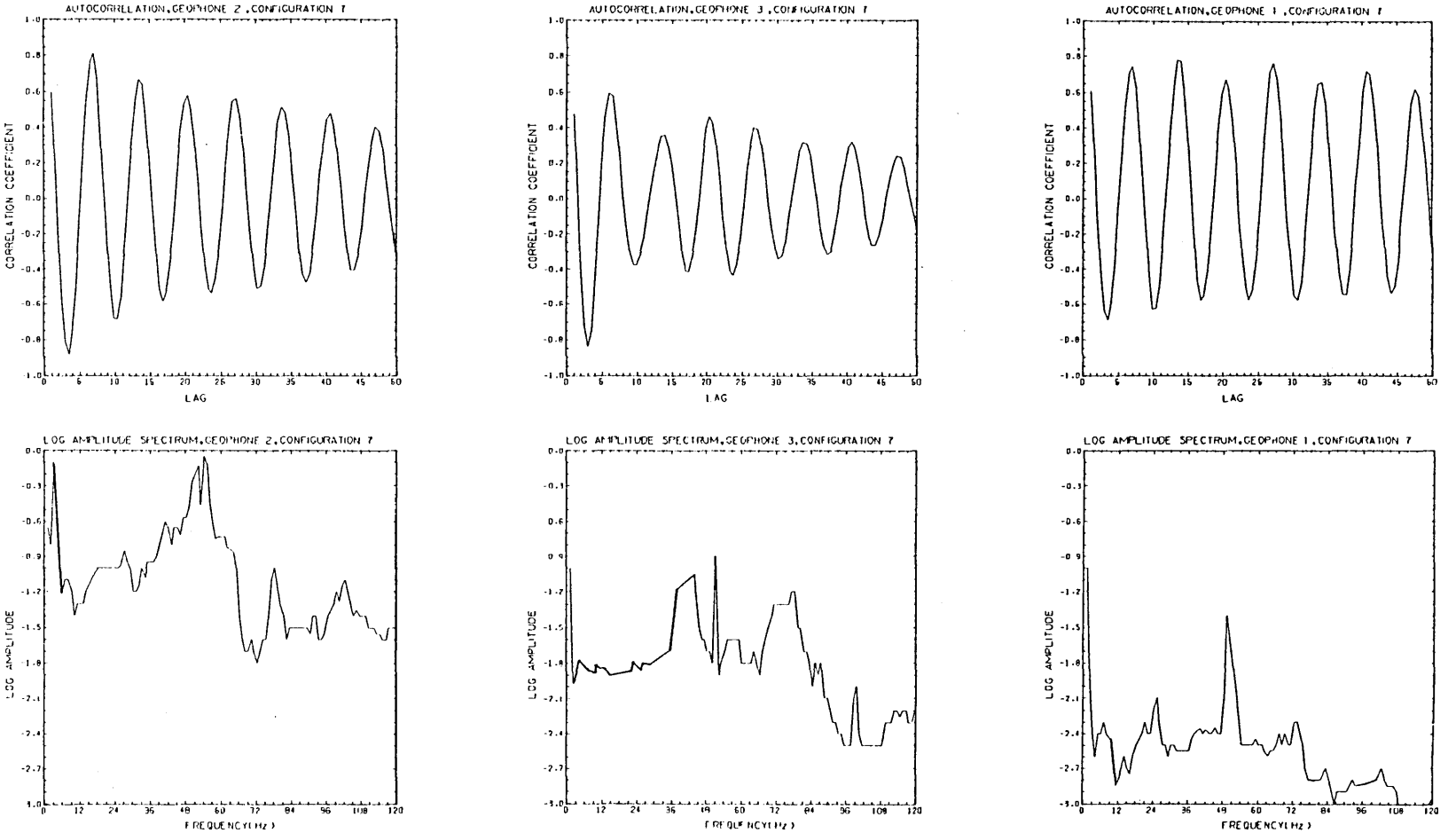

Figure 5.27 (top) Autocorrelation curves for configuration 7

Figure 5.28 (bottom) Log amplitude spectra for configuration 7

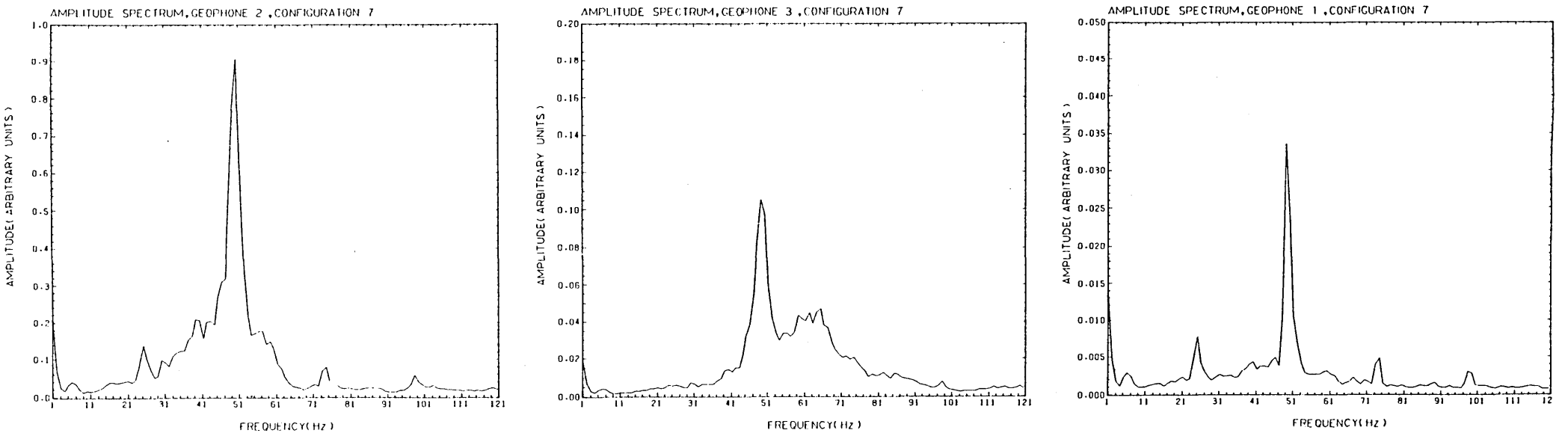

Figure 5.29 Amplitude spectra for configuration 7

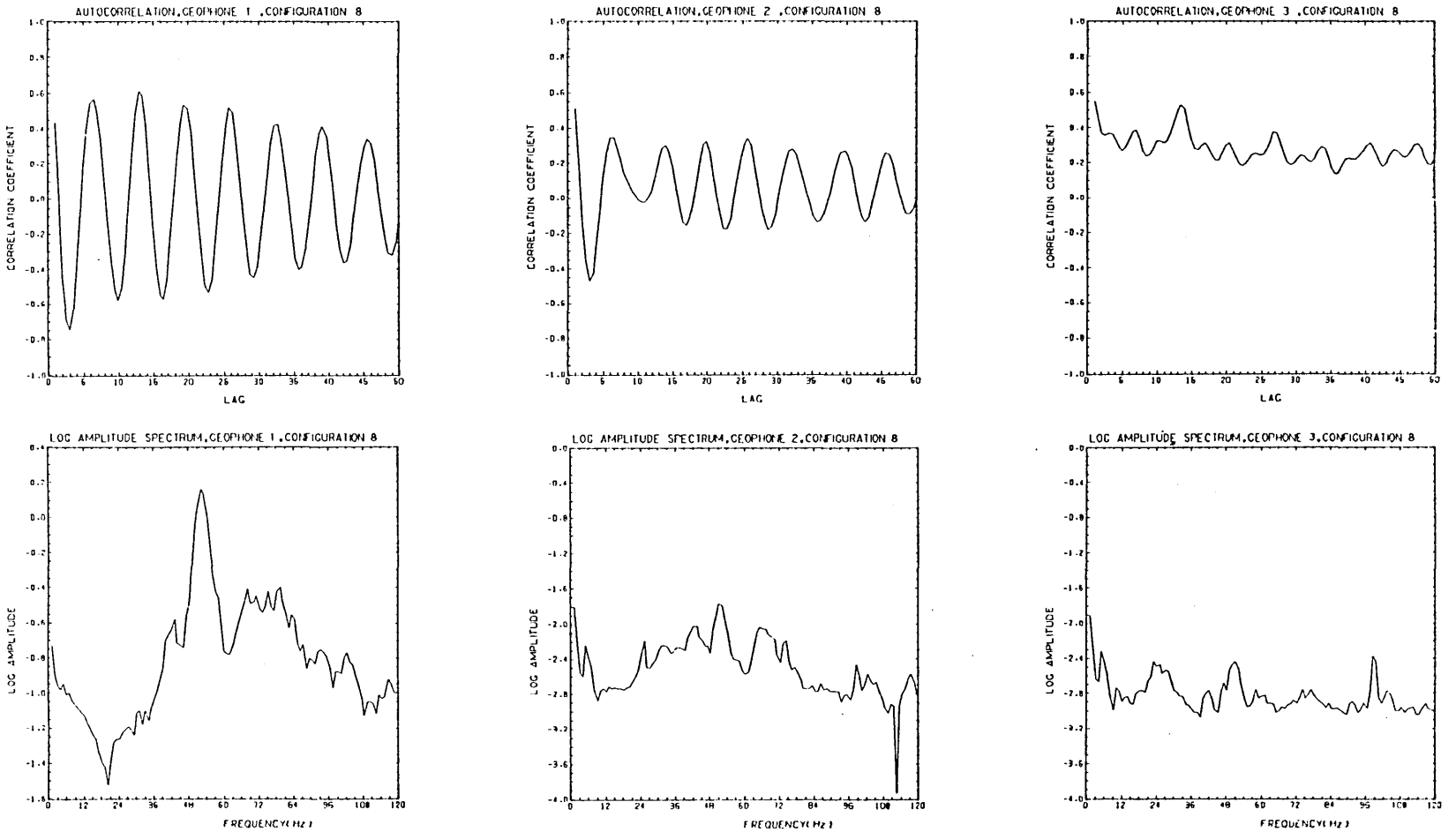

Figure 5.30 (top) Autocorrelation curves for configuration 8

Figure 5.31 (bottom) Log amplitude spectra for configuration 8

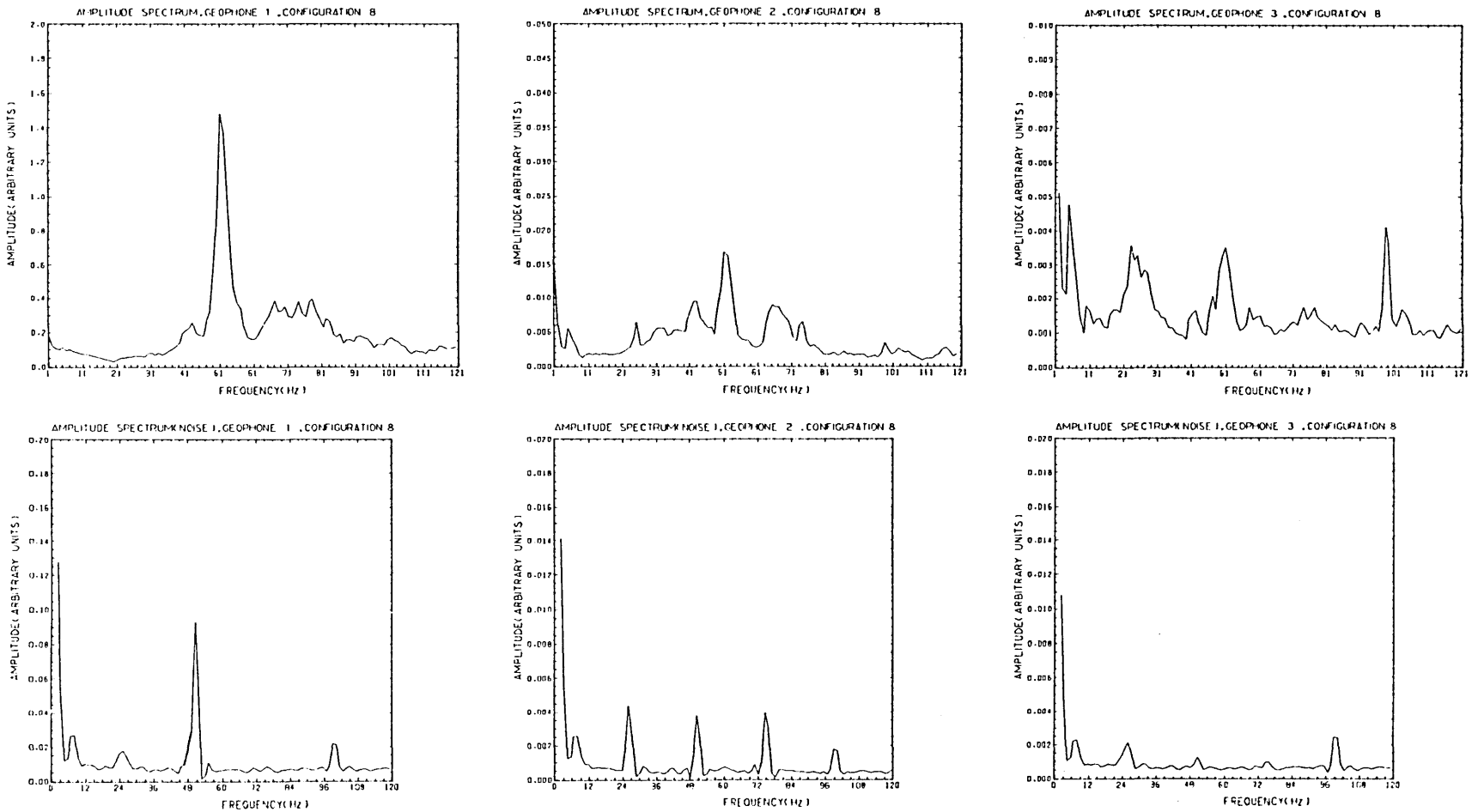

Figure 5.32 (top) Amplitude spectra for configuration 8

Figure 5.33 (bottom) Noise amplitude spectra for configuration 8

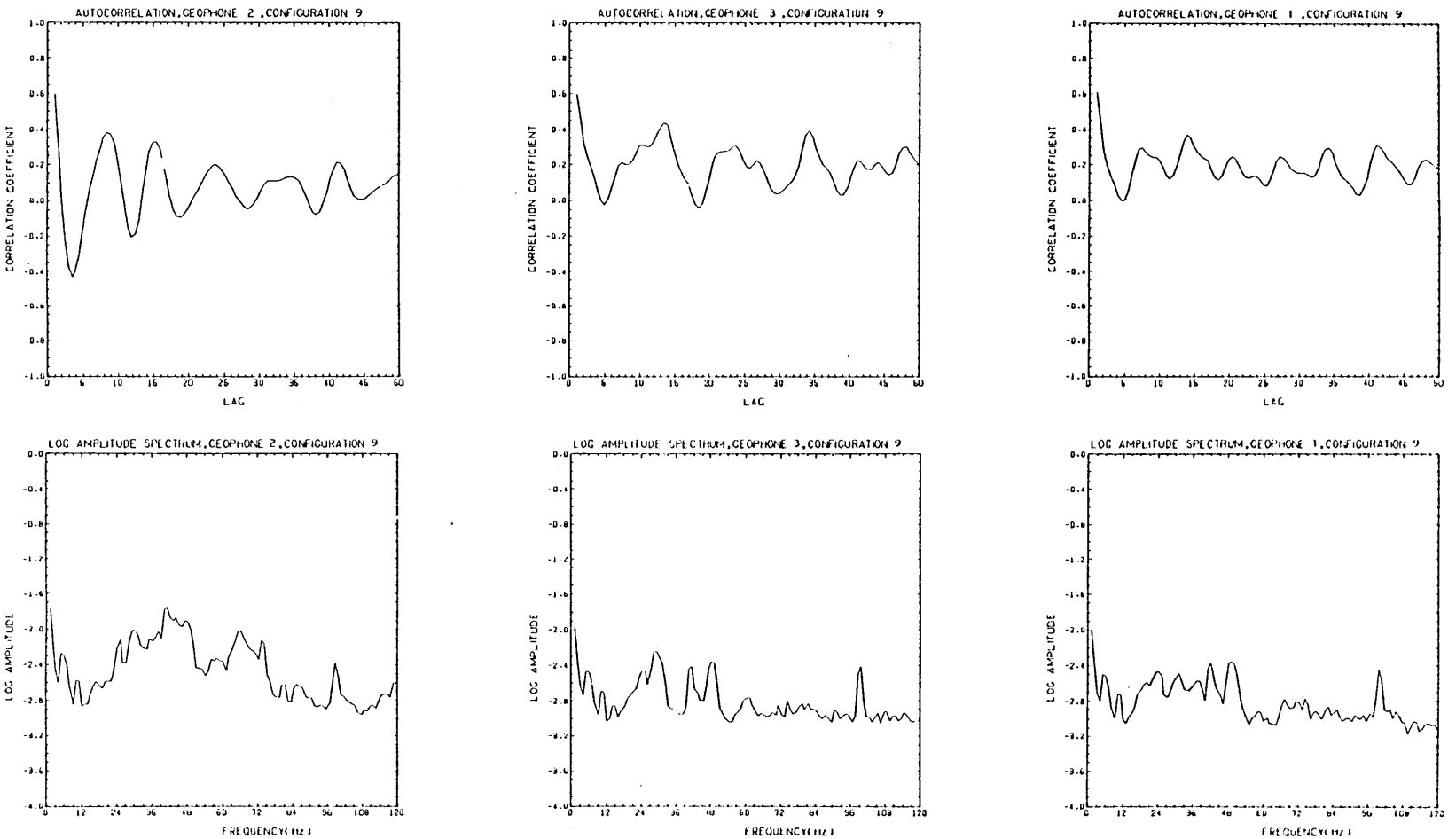

Figure 5.34 (top) Autocorrelation curves for configuration 9

Figure 5.35 (bottom) Log amplitude spectra for configuration 9

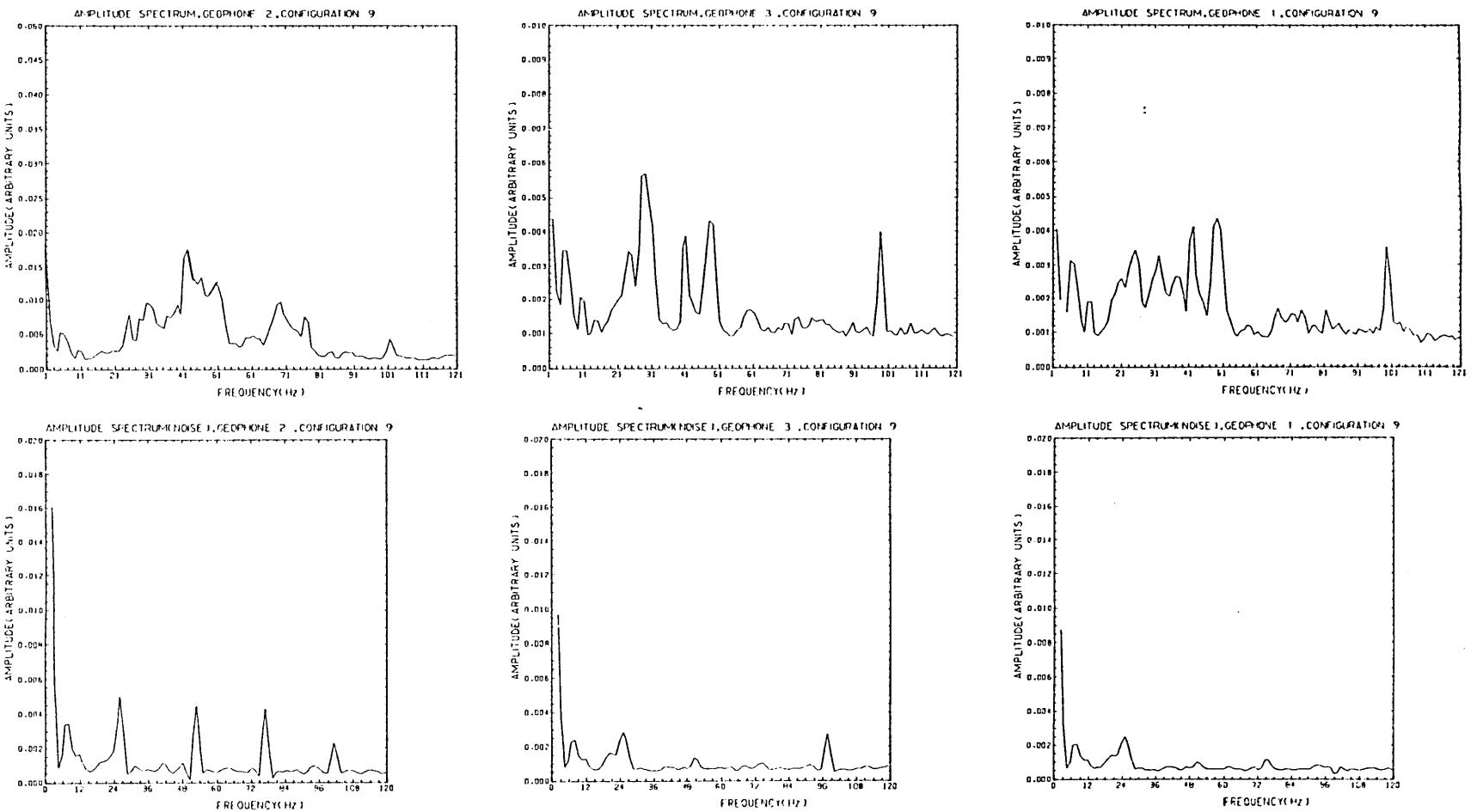

Figure 5.36 (top) Amplitude spectra for configuration 9

Figure 5.37 (bottom) Noise amplitude spectra for configuration 9

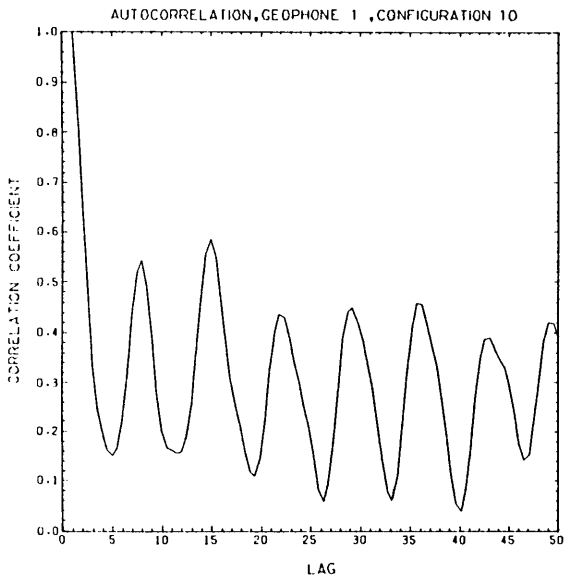

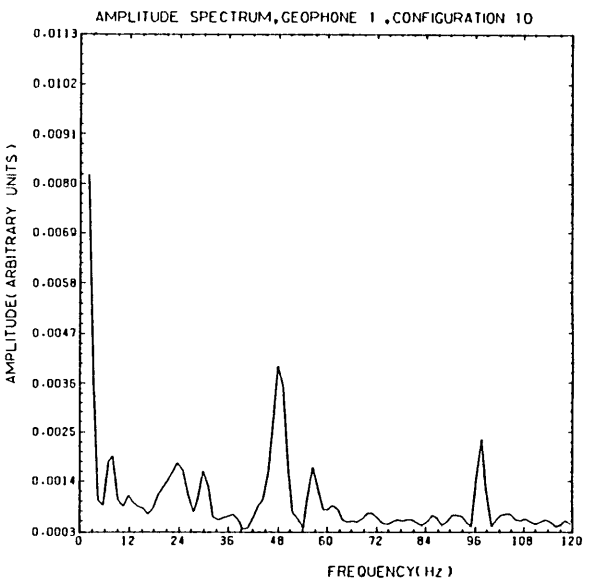

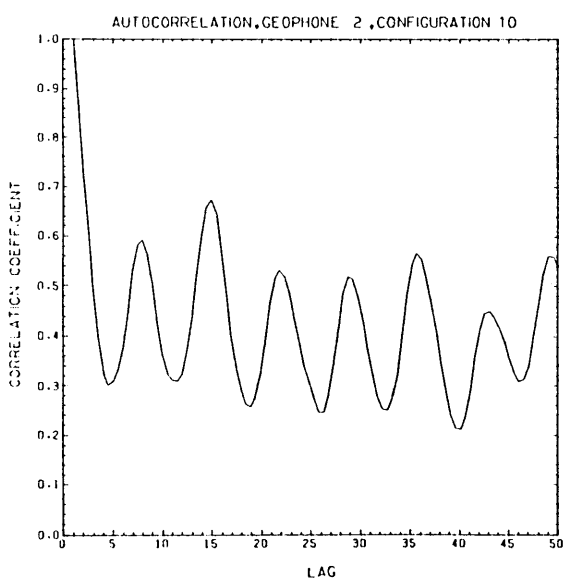

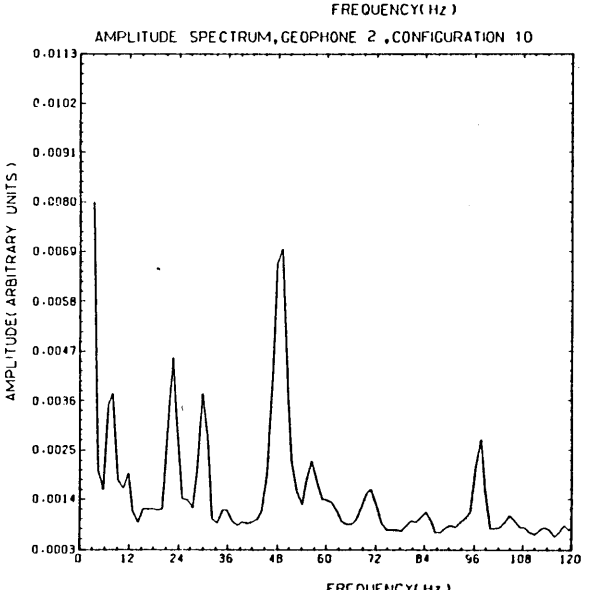

Figure 5.38 (top) Autocorrelation and amplitude spectrum for geophone 1, configuration 10
Figure 5.39 (bottom) Autocorrelation and amplitude spectrum for geophone 2, configuration 10

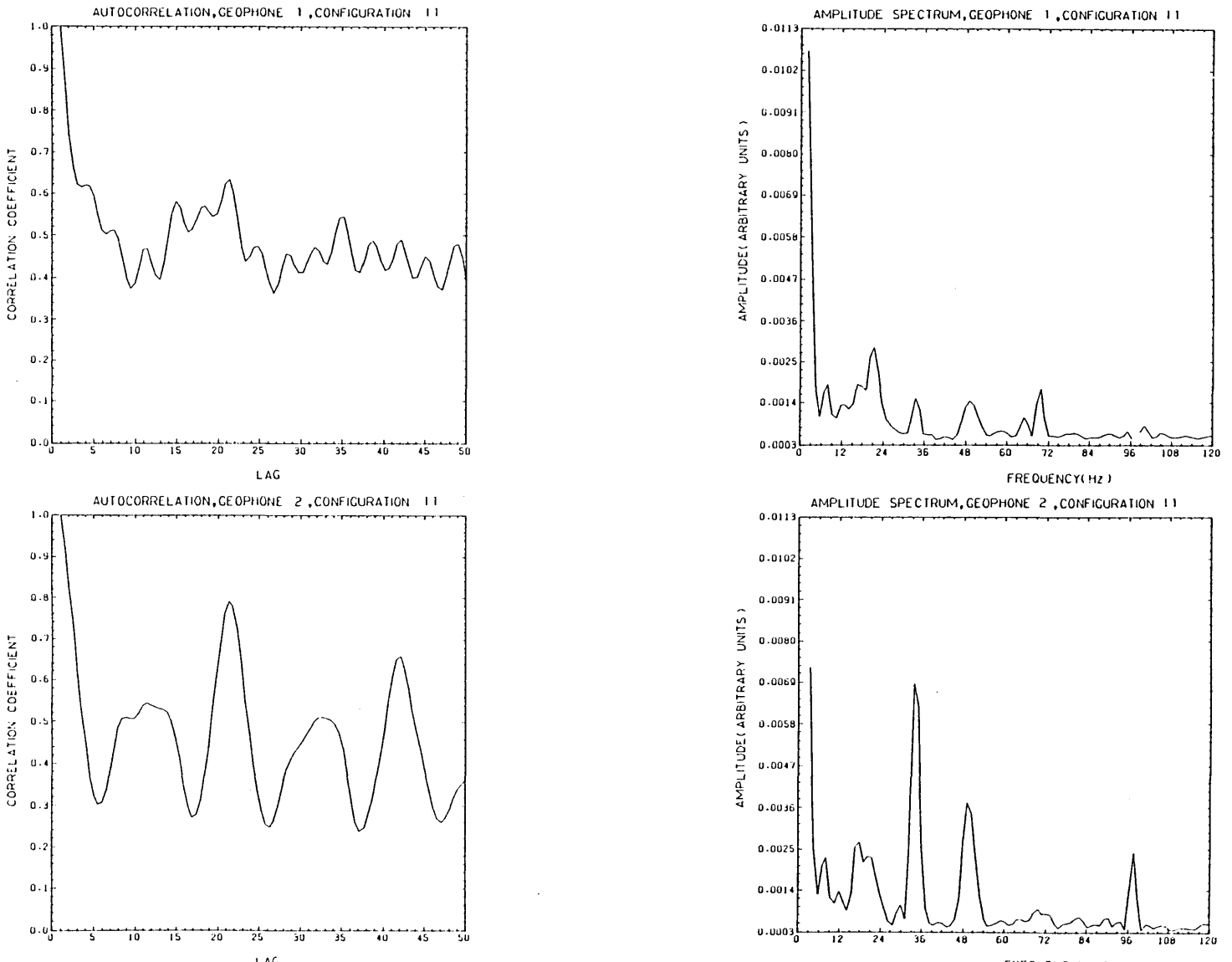

Figure 5.40 (top) Autocorrelation and amplitude spectrum for geophone 1, configuration 11
Figure 5.41 (bottom) Autocorrelation and amplitude spectrum for geophone 2, configuration 11

5.8 FURTHER ANALYSIS OF THE COCKING RESULTS

Some additional analyses were performed on selected data in an attempt to extract more useful information than could be provided using the autocorrelation and amplitude spectrum. The anlyses performed were crosscorrelation, phase differencing and a study of the frequency-dependence of attenuation. The crosscorrelation and phase differencing were done in an attempt to find subsurface velocities and the attenuation study to determine whether the cavity (railway tunnel) produced a frequency-dependent amplitude anomaly.

5.8.1 Crosscorrelation

In order to examine the crosscorrelation, a program was written which would list the coefficients and plot the crosscorrelation function. The program also included a digital notch filter for which the centre frequency and half-bandwidth could be specified.

The input to the program was a portion of the output from two geophones of the same configuration which had been digitized simultaneously. Thus, the two records, each of 451 lags length (1 lag equals 0.003 seconds) had a time origin which was coincident. A propagating event recorded by the two geophones would produce a positive peak of the crosscorrelation function, the time lag at which the peak occurred being the time taken for this event to travel from one geophone to the other. Therefore, with a knowledge of the distance

between the geophones, the apparent velocity could be calculated (assuming straight raypaths).

Unfortunately, the results were disappointing. As expected, the crosscorrelation function before filtering merely reflected the form of the predominant frequency (Solodonikov, 1960). However, filtering out this frequency resulted in a crosscorrelation which showed no significant peak from which a determination of the velocity could be achieved (Fig. 5.42).

5.8.2 Phase Differencing

The phase differences of the outputs from two geophones were calculated from phase spectra derived from a fast Fourier transform program based upon the subroutine N log N (Robinson, 1967). If the phase difference of the same frequency at two geophones are known, then by assuming a number of wavelengths between the two geophones, the apparent velocity could be calculated in a similar way to that of Ward and Hewitt (1977). It is only possible to do this if the outputs from the two geophones have the same time origin.

The idea was first tested using some deterministic data; two sine waves, each with a frequency of 0.074342 Hz and with a phase difference of $\pi/2$, were assumed to be the outputs from two geophones. The distance between the two geophones was made to be 100 m and this was also assumed to be less than one wavelength. Thus, a phase difference of $\pi/2$ is equivalent to a quarter wavelength and since this equals 100 m, the wave-

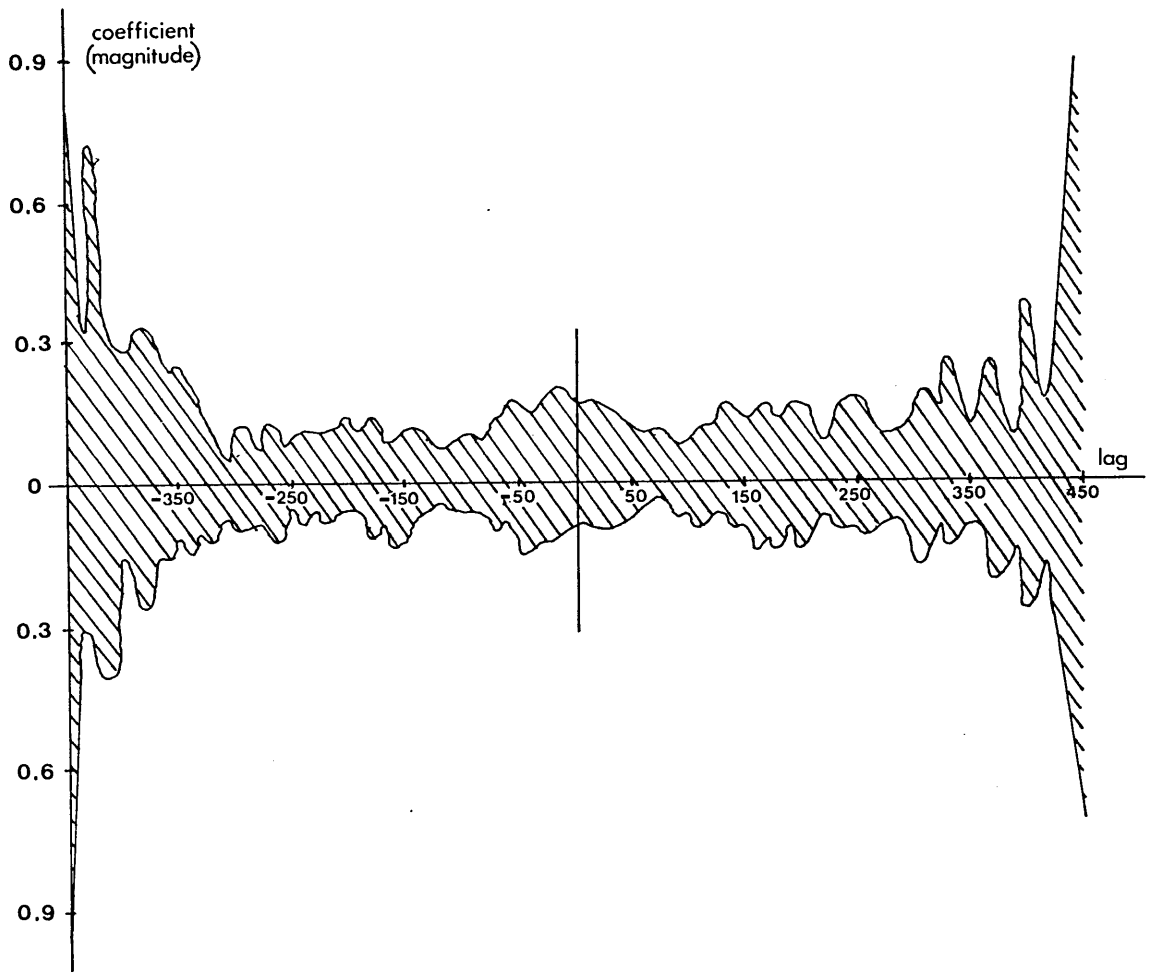

Figure 5.42 A typical example of the crosscorrelation function after filtering.

length must be 400 m. The program gave the velocity of 0.073242 Hz as 29.285 m/s which is very close to the calculated velocity of 29.297. The program was then applied to some real data, but the phase differences were so scattered that it was not possible to arrive at a value for the velocity (Fig. 5.43).

5.8.3 Frequency-Dependent Attenuation

Although it would not be possible to arrive at an absolute value for the attenuation constant using only three geophones at short distances from the source, it was possible that comparing plots of attenuation for configurations across and away from the tunnel may show differences which could be ascribed to the tunnel.

Conventionally, attenuation is calculated graphically using the equation;

$$A = A_o x^{-1} e^{-ax} \qquad (5.2)$$

and then plotting $\log_e Ax$ v. x to avoid using the constant A_o, the attenuation constant a being given by the slope of the graph. Since the outputs from numerous geohones at a wide variety of distances is usually known, this method is the most accurate. However, this was not the case here and the attenuation constant was calculted from

$$a = -\log_e \frac{Ax}{A_o} .x^{-1} \qquad (5.3)$$

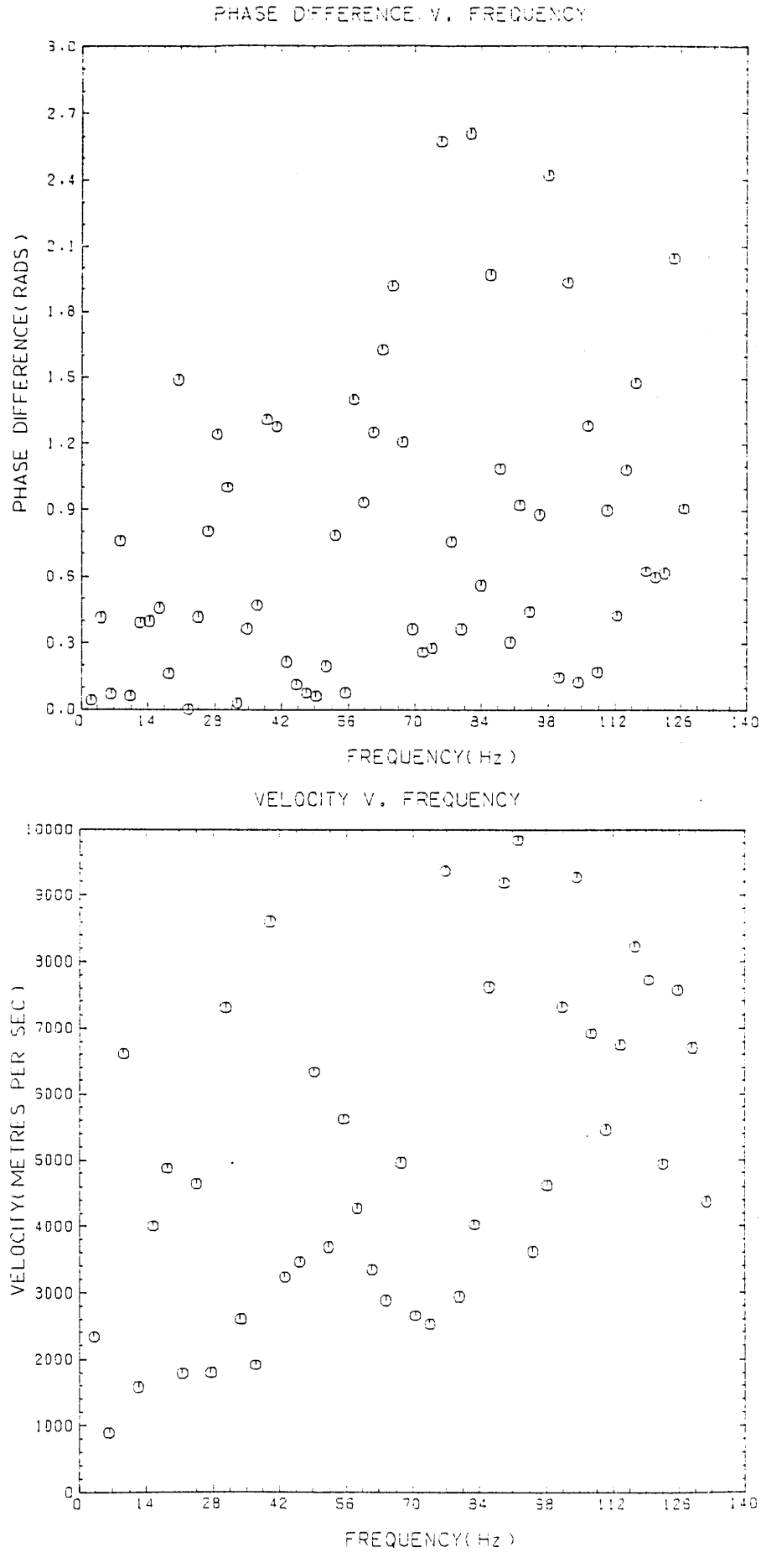

Figure 5.43 Scatter of phase difference and velocity plotted versus frequency

for the configurations where A_0 was known (from a geophone close to the source) and then a plotted v. frequency. However, the values for a (attenuation const.) showed a strong correlation with distance and so the exponential term in the equation (5.3) was dropped, giving,

$$A = A_0 \, x^{-n} \tag{5.4}$$

where n is known as the divergence factor. So, n is calculated from,

$$n = \frac{-\log_e \frac{A}{A_0}}{\log_e x} \tag{5.5}$$

and plotted v. frequency. The results are shown in Figure 5.44; Table 5.2 shows the divergence factor averaged over all frequencies. Although the divergence factor is higher for the configuration which crosses the tunnel, the errors are such that this difference may not be significant.

Configuration	Geophone Distance	Divergence Factor	
2 (not across tunnel)	38 m 70 m	1.79 1.74	0.49 0.44
8 (across tunnel)	23 m 43 m	2.26 2.25	0.49 0.53

Table 5.2 A comparison of divergence factors for different configurations.

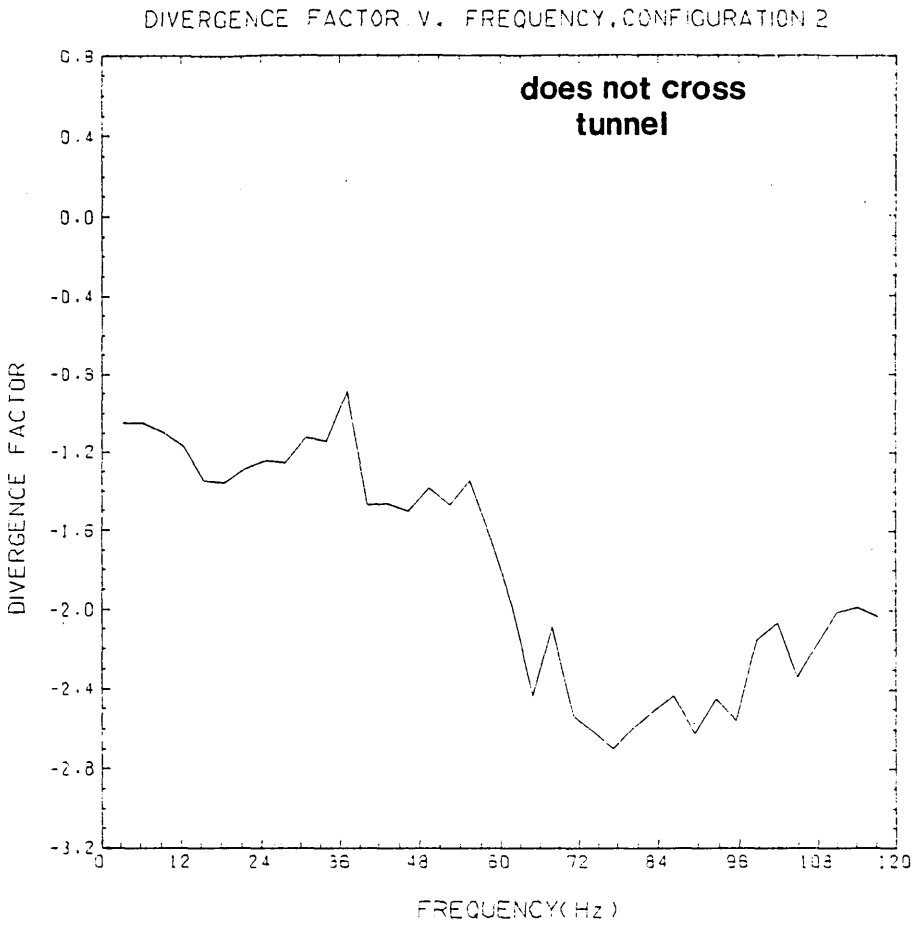

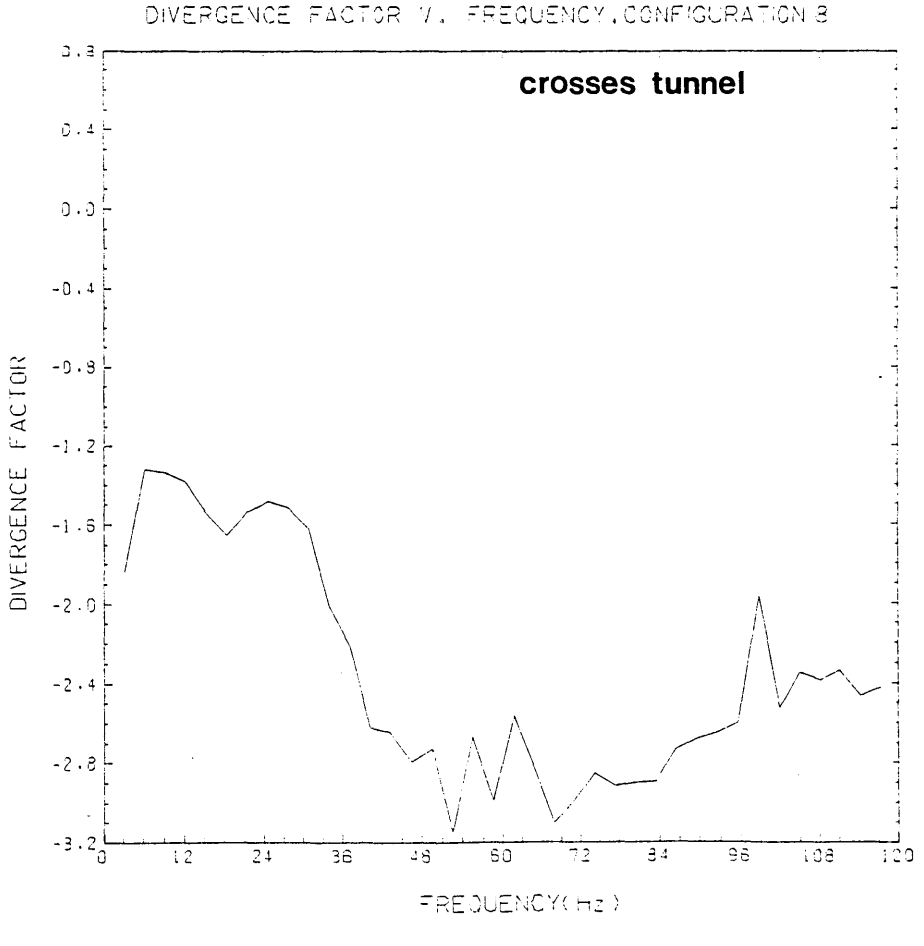

Figure 5.44 Divergence factor versus frequency for configurations 2 and 8

It is possible that much of the energy radiated into the ground by the Warsop was in the form of Rayleigh waves (see Appendix 1), which are affected by elastic properties down to a depth of approximately one wavelength (Sheriff, 1973). Figure 5.44 shows an abrupt increase in the divergence factor at 60 Hz for the configuration which does not cross the tunnel (2), compared with that at 36 Hz for the configuration which does cross the tunnel (8). This implies that the increase in divergence factor occurs at a greater depth for configuration 8 than for configuraton 2.

Using the P-wave velocity for the first layer to calculate the Rayleigh wave velocity (Poisson's ratio = 0.31; Green, 1976) gives a figure of 202 m/s. Therefore, the wavelength at 60 Hz is 3.37 m and that at 36 Hz is 5.61 m, both somewhat less than the depth of 9 m for the tunnel. Thus, the increase in divergence factor for a configuration crossing the tunnel and seen by comparing configurations 2 and 8, is unlikely to have been caused by the tunnel itself but most likely by the disturbed ground above it.

Although the error in the calculation of divergence factors is large enough to question their significance, the increase in divergence factor for configuration 8 is supported by a significant decrease in the Warsop signal measured from the amplitude spectra for that configuration (see Section 5.7.9).

5.9 DISCUSSION

It has already been shown that the anomalous attenuation in the vicinity of the tunnel was probably caused by the disturbed ground above and around the tunnel as a result of the cut-and-fill method of construction.

Anomalous amplitudes were recorded at frequencies of 57-70 Hz on geophone 3 (configuration 7) which was directly over the tunnel. Originally this was thought to be possibly due to cavity resonance. Subsequent recordings by geophones clamped to the tunnel wall showed no frequencies which had not been previously observed as due to the Warsop or to background noise.

Thus, it was concluded that cavity resonance had not been observed. This may have been due to several factors; (1) the bandwidth of the energy radiated into the ground by the Warsop was not broad enough to provide the necessary excitation frequency; (2) the power of the Warsop was not great enough at any frequency to cause resonance; or (3) cavity resonance occurred but was not recognized as such. The lack of any theoretical work on cavity resonance reported in the literature precludes any calculations of the energy required, the frequency dependence or even the precise mechanism by which cavity resonance is initiated. Thus, none of the above three points may be excluded, but, as previous reports showed cavity resonance, recognised on seismic monitor records as a low frequency wave lasting several seconds, (Rechtien and Stewart, 1975) to be initiated in very shallow cavities by an explosive

source, it is most likely that the first two points are true and that cavity resonance did not actually occur.

Most frequencies seen as peaks on the amplitude spectra recorded whilst the Warsop was operating could, by comparison with the corresponding recordings of background noise, be ascribed either to the Warsop or to various sources of noise on the site. Occasionally, extra frequencies, such as those around 70 Hz on configurations 2, 7 and 8 could be seen. These may be due to intermittent sources of background noise or could be due to other modes of energy radiated by the Warsop.

The Warsop will produce a mixture of surface, shear, and compressional waves. The shear and compressional waves will have small amplitude compared with the surface waves.

A further complication may be caused by modes of propagation other than those propagating directly through the sub-surface and these are due to the nature of the source. These can be grouped under two headings; resonances and air-wave coupling.

5.9.1 Resonances

For a source-soil system, such as that provided by the Warsop operated at the ground surface, resonance can occur between the baseplate and the ground (Warburton, 1957). For a light base the resonance will be broad and have little effect on the waveform. The sharpness, s, of the resonance is given by,

$$s = M/pr^3 \qquad (5.6)$$

where, r is the radius of the base, M is its mass and p is the density of the soil. If s is less than 0.66 then the effect is negligible; at Cocking s was approximately 0.5.

Resonance may also occur when the frequency is such that the thickness of the LVL (low velocity layer) is equal to an odd number of quarter wavelengths. This was obviously not a significant effect whilst the Warsop was operating as no peaks were consistently present on the amplitude spectrum except for that of the predominant frequency of 48 Hz.

5.9.2 Air-wave Coupling

When using a vibrating source at the surface of the ground it must be expected that energy will be radiated into the air as well as into the ground. Three types of air or air-coupled wave may be generated. These are; (1) a direct air-wave, which will travel with the speed of sound in air (335 m/s); (2) a ground-coupled air-wave (Mooney and Kaasa, 1962); and (3) resonant coupling of Rayleigh waves and atmospheric compressional waves. (Press and Ewing, 1951; Jardetzsky and Press, 1956).

The direct air-wave was probably not a significant contributor of energy during recording of the Warsop except when the geophones were a few metres or less away, as other sources of noise on the site which sounded as loud as the Warsop, gave orders of magnitude lower amplitude, as shown by recordings of background noise. It is possible that much of the background

noise may have been caused by air-waves as this would explain the less rapid attenuation observed. The ground-coupled air-wave, as recorded by Mooney & Kaasa (1962), is manifest as a surface wave produced by direct coupling of the air-wave to the ground, although the primary propagation path is through the air. This type of signal was shown to consist of a short pulse which contains a broad range of frequencies and thus would not contribute to the spectra as a significant peak but rather as a general increase in the background noise.

Resonant coupling of ground roll (Rayleigh waves) and compressional air-waves can only occur if the phase velocity of Rayleigh waves is less than or equals the speed of sound in air. The near surface layer at Cocking was measured to have a compressional wave velocity of 420 m/s (Section 5.3) thus, it is likely that a dispersive Rayleigh wave having the speed of sound in air could be produced. The result of such coupling gives a train of approximately constant frequency waves. Although such waves are possible and may cause some of the frequencies seen on the recordings of background noise, it is mostly likely that such resonant coupling would have small effect compared with the predominant frequency of the Warsop but may be significant elsewhere in the spectrum. There was no way to distinguish such a wave type on the basis of frequency alone.

5.10 CONCLUSIONS

Tests of the Warsop at Silwood Park (Section 5.2) and results of the experimental work performed at Cocking demonstrated the capability of the Warsop to produce a repeatable signal,

detectable at a distance of at least 70 m. Theoretical work by Miller and Pursey (1954, 1955) showed that most of the energy radiated by such a source would be in the form of surface waves.

Cavity resonance was not observed, either by geophones at the ground surface or clamped to the tunnel wall. The most likely cause is that the Warsop did not radiate enough energy into the ground to excite such a resonance within the tunnel wall.

Anomalous attenuation, measured directly from amplitude spectra and indirectly from calculations of divergence factors, was seen in the vicinity of the tunnel. This was shown to be due to the disturbed ground above the tunnel rather than caused by the tunnel itself.

Quantitative analysis of the phase difference of various frequencies arriving at two or more geophones within the same configuration was unsuccessful in determining apparent velocities of horizontally propagating energy. Crosscorrelation was also used unsuccessfully to try to distinguish discrete arrivals for velocity analysis.

Examination of various types of direct and ground coupled air-waves showed that although their effects on the amplitude spectra could not be predicted, they were likely of little significance except perhaps on recordings of background noise.

CHAPTER VI

CRESWELL - DETECTION OF CAVITIES PART 2

6.1 INTRODUCTION

The experimental work at Cocking demonstrated the use of a surface operated, portable, soil-compaction tool (Warsop) as a seismic source and how, using frequency analysis, anomalous attenuation in the vicinity of a subterranean cavity was detected. However, it was concluded that the anomalous attenuation was caused by disturbed ground around the cavity and no conclusions could be reached concerning the effect of the cavity itself. Thus, further experimentation was necessary, preferably at a site of a more suitable nature; that is, one containing a shallow cavity (depth to size ratio of about 1:1) of natural origin.

Such a site was found at a place called Creswell Crags in Derbyshire. It consisted of a large sloping field next to agricultural land, bounded on three sides by a fence and on the other by a water treatment plant, which was approximately 100 m away. A cylindrical cavity ran some way beneath the field, entering at the northern end of the experimental site and running southwards. This was a natural formation and so it was reasonable to assume that the ground around the cavity was in an undisturbed state.

The source used for this experimental work was a Kango hammer with soil compaction attachment. The Kango operated in an identical manner to the Warsop (which was used at Cocking) that

is, it imparted a periodic impulse to the ground via a rigid, circular baseplate. The Kango hammer was tested at Silwood Park and found to be more convenient to use than the Warsop as it was lighter and electrically driven, yet still gave a detectable signal at a distance of 70 m.

The experimental work was divided into two parts; the first using a three-component geophone and the second using spreads of six vertical geophones. For the first part of the experiment thirty geophone positions around the tunnel, on a regular 4 m grid, were occupied in turn with the three-component geophone. For the second part, eleven geophone spreads, each of six vertical geophones were laid perpendicularly to the centre line of the tunnel on a regular 2 m grid. A seventh vertical geophone was incorporated into each line but, was kept in a fixed position 20 m from the source to act as a reference and to monitor the performance of the Kango. The Kango was kept in the same position, offset 30 m west of the cavity for the duration of the experimental work.

A conventional refraction survey was also carried out over the area, using a 12-channel Nimbus system and dropped-weight source, to ascertain the local near-surface velocities.

6.2 THE SUITABIITY OF THE KANGO AS A SEISMIC SOURCE

The Kango has a mode of operation identical to that of the Warsop; that is, a periodic vertical translation, thus it was expected to give a similar kind of signal. The theoretical basis for this kind of source has been discussed previously in Section 5.2, to which the reader is referred. However, it was

necessary to confirm that the Kango produced a broad "noise" bandwidth encompassing the frequency range of the analysis; that is, up to 167 Hz. It was also necessary to determine the distance at which useable signal could be detected.

6.2.1 Testing the Kango

The Kango was tested in a similar way to that performed on the Warsop (see Section 5.2.1). This test also took place at the Imperial College Research Station near Ascot in Berkshire.

Recordings of the Kango were made using an in-line spread of twelve vertical-type geophones plus an uphole geophone and RS44 seismic recording gear. The first geophone was planted 15 m from the source position and the geophone separation was 5 m, giving a maximum source-to-geophone distance of 70 m. the uphole geophone was planted about 1/2 m from the source.

The Kango was operated in three different positions; (1) suspended in the air, (2) on the surface, and (3) within a half-metre deep hole, to observe what effect this might have on the amplitude and frequency content of the recorded signal. Analysis of the resulting seismograms (Fig. 6.1) showed; (1) that the air-wave had a predominant frequency of about 50 Hz with a low amplitude component at approximately 160 Hz superimposed on this. The higher frequency is seen only at the far offsets where the gains are high; (2) that the repetition rate of the periodic impulse as seen on the uphole geophone and channel one (Fig. 6.1, middle and bottom) is approximately 33 Hz; (3) when operated on the surface or within the hole, the Kango produces both 33 Hz and 100 Hz, the higher frequency

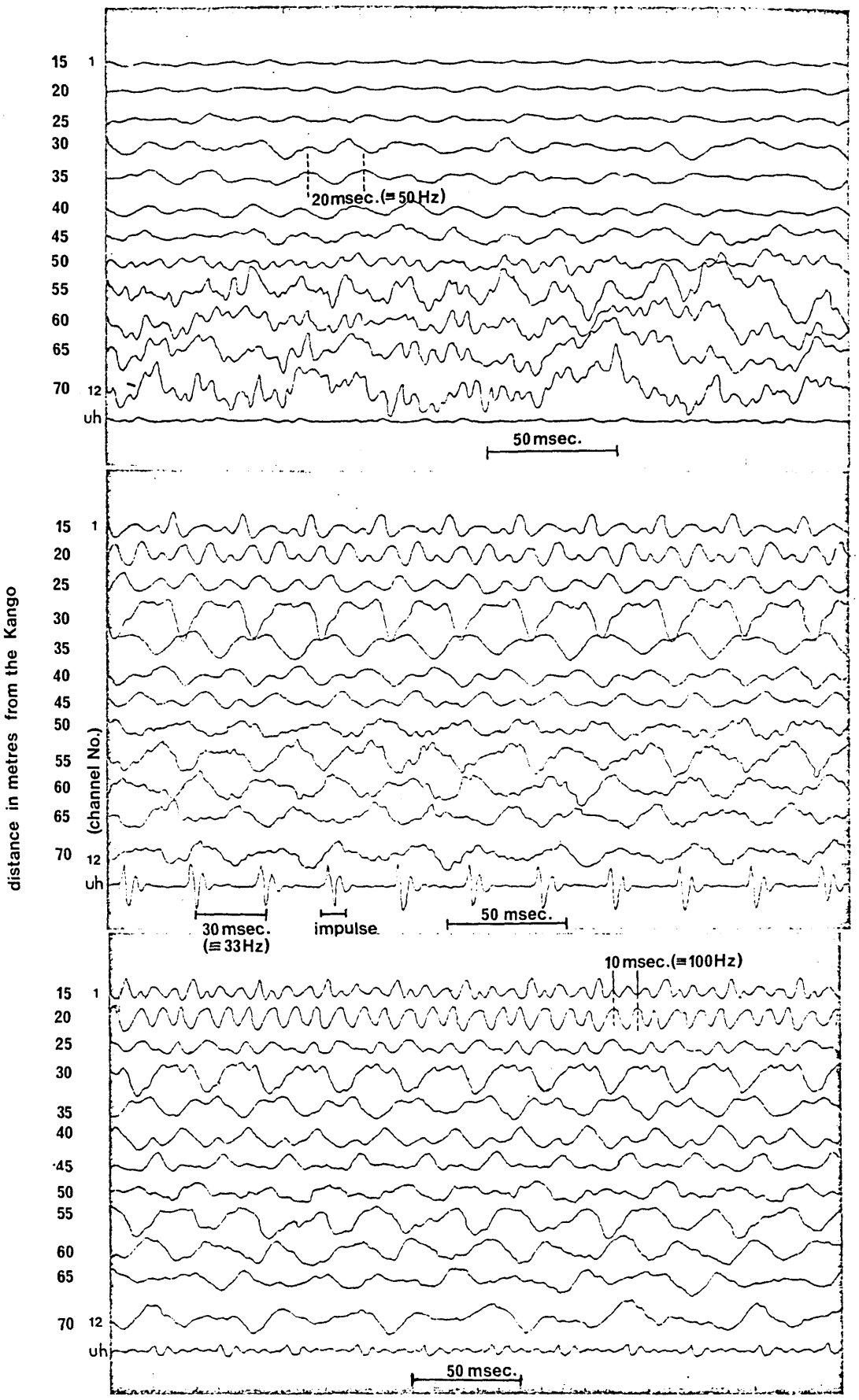

Figure 6.1 Recordings from the RS44 of the Kango operating in the air (top), on the surface (middle) and in the hole (bottom)

being most easily seen on channel 2; (4) the predominant frequency of the impulse itself, as measured peak-to-peak on the recording from the uphole geophone, (Fig. 6.1, middle) is about 200 Hz.

Thus, it can be seen that the Kango produced a number of frequencies from 33 Hz up to 200 Hz. It is difficult to establish true amplitude relationships between the different frequencies from the paper records as the ampifier gains vary from channel to channel, however, we may make some general observations. The air-wave (50 Hz) appears to be of low amplitude compared with the other frequencies of interest as it is not seen on recordings made when the Kango is in contact with the ground. The 100 Hz and 200 Hz frequencies appear to attenuate rapidly and cannot be distinguished beyond the seventh geophone, a distance of 45 m from the source. So, for the field experiment the maximum source-to-geophone distance should be somewhat less than 45 m to ensure that the higher frequencies remain above the noise level.

The impulse, produced by the actual impact of the Kango baseplate with the ground shows that the baseplate may only be transferring energy to the ground during a small part of its 33 Hz cycle of vertical translation. This would considerably reduce the amount of energy radiated by the source, as discussed in Section 5.2, and will also change the ratio in which this energy is divided between surface, compressional and shear waves (see Section 5.2.1 and Appendix 1), probably increasing the proportion radiated as compressional waves. The difference in the amplitude of the impulse as recorded by the uphole geophone, it being less when the Kango is in the hole,

may be explained by the directivity of the source. The uphole geophone is so close to the Kango (1/2 m away) that when the Kango is 1/2 m below ground level less energy will be radiated "backwards" than will be radiated "sideways" when the Kango is at the ground surface. This effect will diminish with distance from the source and is hardly evident on geophone 1, 15 m away from the Kango.

No three-component geophone was available at this time for recordings of the three mutually perpendicular components of ground motion as was done for the Warsop.

6.3 THE CRESWELL SITE

The site chosen for the experimental work was situated about 500 m east of Creswell Crags in Derbyshire (Grid Ref., SK538743, O.S. sheet No. 120, 1:50,000 series). It was a large grassy field situated next to a water treatment plant, surrounded by woods and agricultural land. The area of the field used for this study is shown in Figure 6.2 below.

The field sloped gently to the north towards the mouth of the cavity at which point it dropped off sharply to form a bank. At this point the cavity was approximately cylindrical with a diameter of almost 2 m. The crown of the cavity was 1 m below ground level but this depth increases as the cavity progresses southwards (Fig. 6.3). Access to that part of the field directly above the cavity was restricted some 5 m east of the cavity by a large fence and so most of the area over which measurements were taken was to the west (Fig. 6.4).

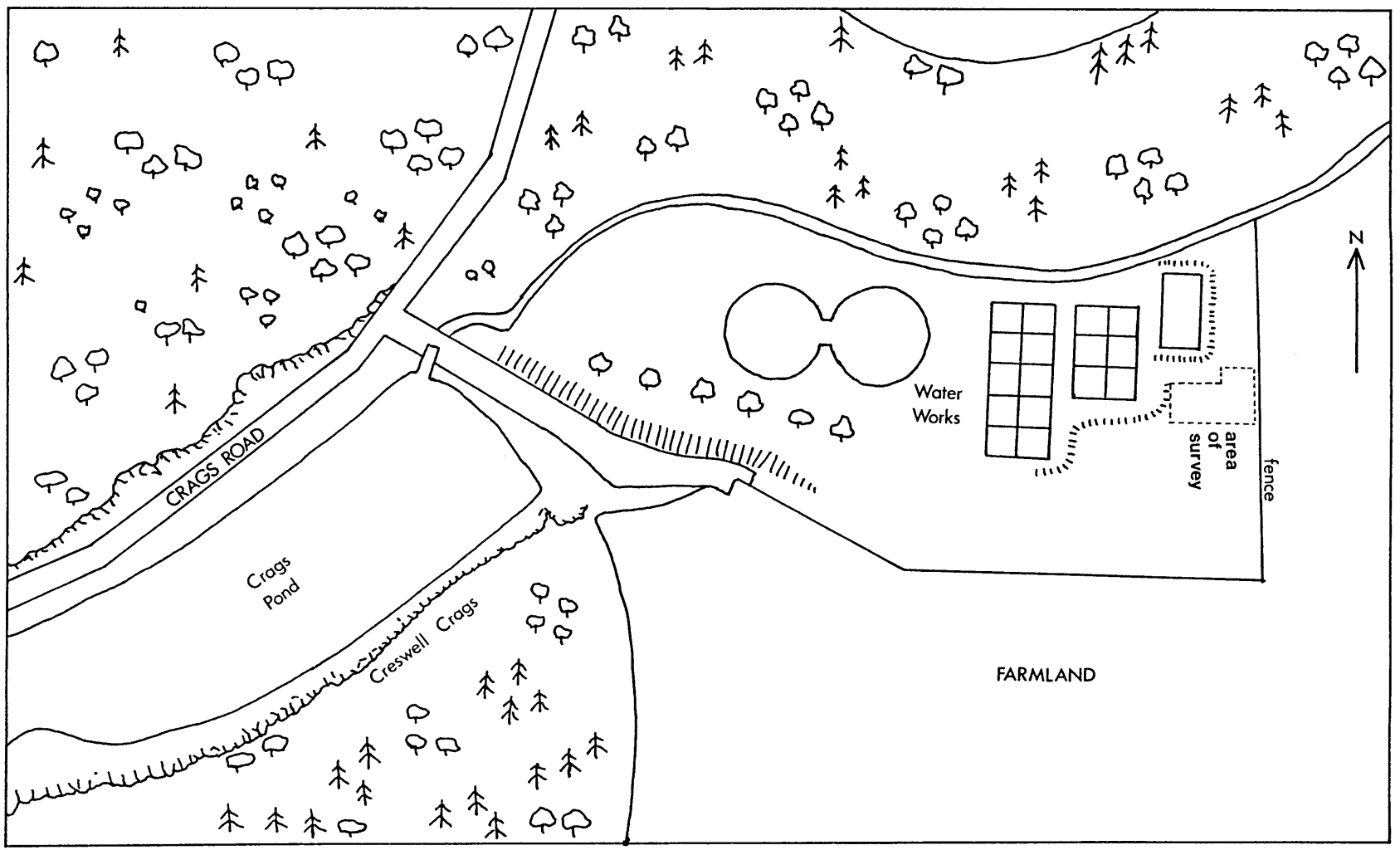

Figure 6.2 A plan of the site and the surrounding area

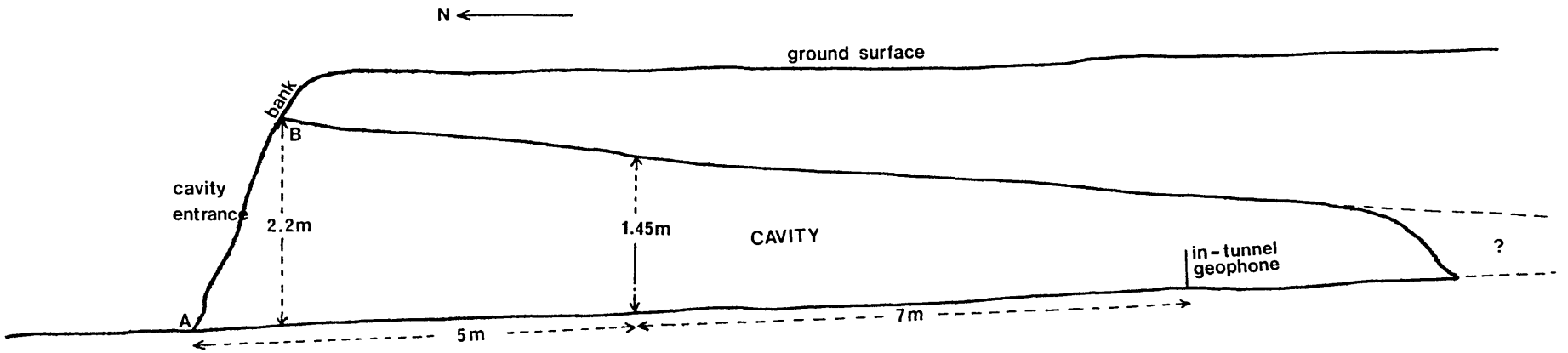

Figure 6.3 A section showing the side view of the cavity.

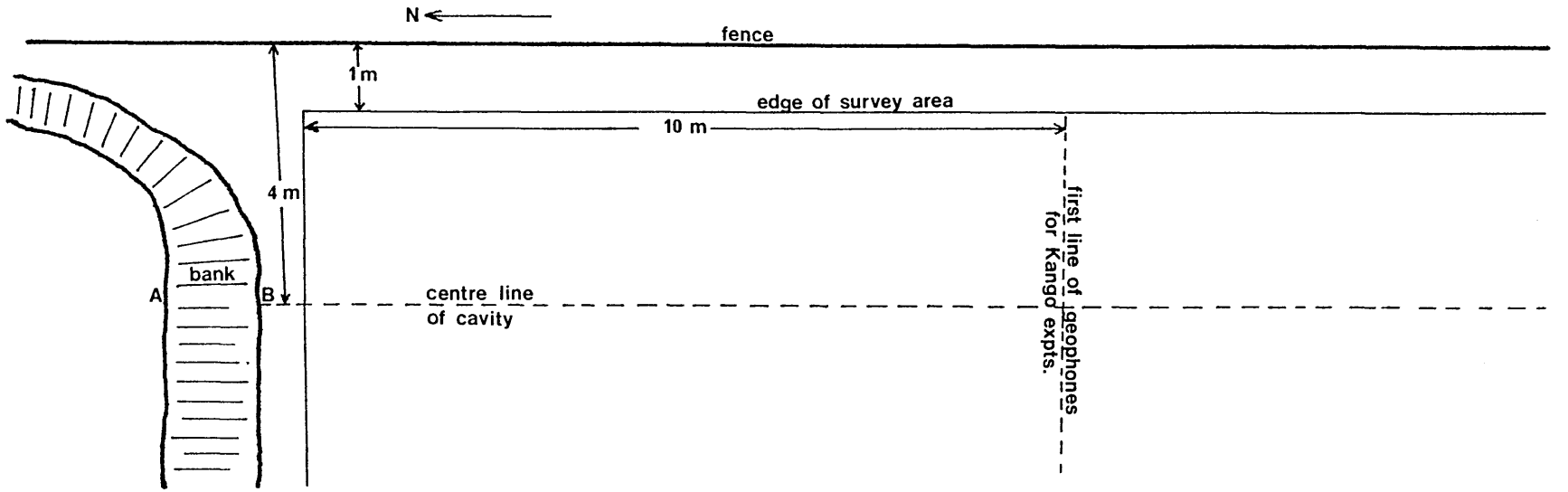

Figure 6.4 A plan of the site corresponding to Figure 6.3.

The geology of the area consisted of a thick (at least 10 m) limestone section overlain by 2-3 inches of soil. The limestone outcrop on the north side of the site, to the west of the cavity, showed that the top 1-1/2 to 2 m of the limestone was severely weathered. Also there was evidence of a large vertical fracture which may run beneath the field on a line parallel to that of the cavity. The true extent and direction of the fracture could not be determined as this was the only outcrop within the immediate vicinity of the site.

6.3.1 How Features of the Site Might Effect the Results

In this section we examine the effect that certain features of the site might have on the amplitude of surface and air-waves at different ranges and frequencies.

The effects of topography were minimized both for the refraction survey and subsequent work with the Kango by orientating the spreads along the strike of the slope. Conveniently this orientation was also perpendicular to the cavity.

The cavity itself, being shallow and, at certain frequencies, (up to approximately 135 Hz, assuming V_R = 265 m/s and 2 m depth) within the depths whose elastic properties determine the velocity of surface (Rayleigh) waves, may have some measurable effect on the amplitudes of surface waves recorded in the vicinity of the cavity. This effect will diminish with increasing frequency, as the depth of the cavity increases and as its size decreases. Therefore, we might expect any observed effect to be a maximum at the northern edge of the site where

the cavity is at its largest and shallowest, and diminish towards the south.

The direct air-wave, as recorded at Silwood Park, occurred at a frequency of 50 Hz at the ranges subsequently used at Creswell. It was at low amplitude compared to those frequencies recorded when the Kango was coupled with the ground. Thus, it was anticipated that the direct air-wave and the ground-coupled air-wave of the type recorded by Mooney and Kaasa (1962) (see Section 5.9.2) would not be of significance at Creswell.

The near-surface layer, consisting of heavily weathered limestone is likely to have a Rayleigh-wave (V_R) velocity less than the speed of sound in air. Thus, it is possible that resonant coupling of Rayleigh-waves and air-waves could occur. It is difficult to predict at what frequencies this might occur as Howell et. al. (1953) measured a large spread in periods for the air-coupled wave. This is in contrast to the work of Press and Ewing (1951) who predicted a single period for the air-coupled wave. It is also difficult to predict the amplitude of the air-coupled wave, although work by Howell et. al. (1953) showed very low amplitudes recorded at the ground surface for an air shot and a similar amplitude to the direct air-wave for a hole shot recorded by an air microphone. We can therefore say that although an air-coupled wave may occur, it is likely to have an amplitude no greater than that of the direct air-wave. Therefore, even at the maximum range of interest at Creswell (34 m) the air-coupled wave is unlikely to have significant amplitude compared with other types of waves.

The large vertical fracture, seen in outcrop approxmately 16 m west of the cavity, may have some effect if it extends across the site. Such a fracture could act as a reflector, retransmitting high frequency shear and compressional waves back towards the source whilst having less effect on the lower frequency surface waves. It is not possible to measure any effect the fracture might have but, as the reference geophone and the geophone spreads are to the east of its position, the possible effects may be neglected when comparing records from different geophones. This may not be true if the fracture crosses part of the site only, but this was not known.

6.4 THE REFRACTION SURVEY

A high-resolution seismic refraction survey was performed over the site by the Engineering Geology Unit of the I.G.S. and myself. A total of 15 shot-points were occupied, their positions being shown in Figure 6.5. All the lines were shot in an east-west direction, along the strike of the slope, in order to reduce any effects of topography.

The instrumentation used was a Nimbus 12-channel stacking seismograph, twelve vertical geophones of 10 Hz natural frequency and a dropped weight source. The dropped weight was a cylindrical piece of steel weighing about 10 Kg and machined to a point at one end. The shot was provided by allowing the weight to fall vertically through a 10 ft. tube and impact upon a small steel plate. The shot instant was provided by a small inertial switch attached to the steel plate. Best possible coupling to the limestone was provided by digging away the soil

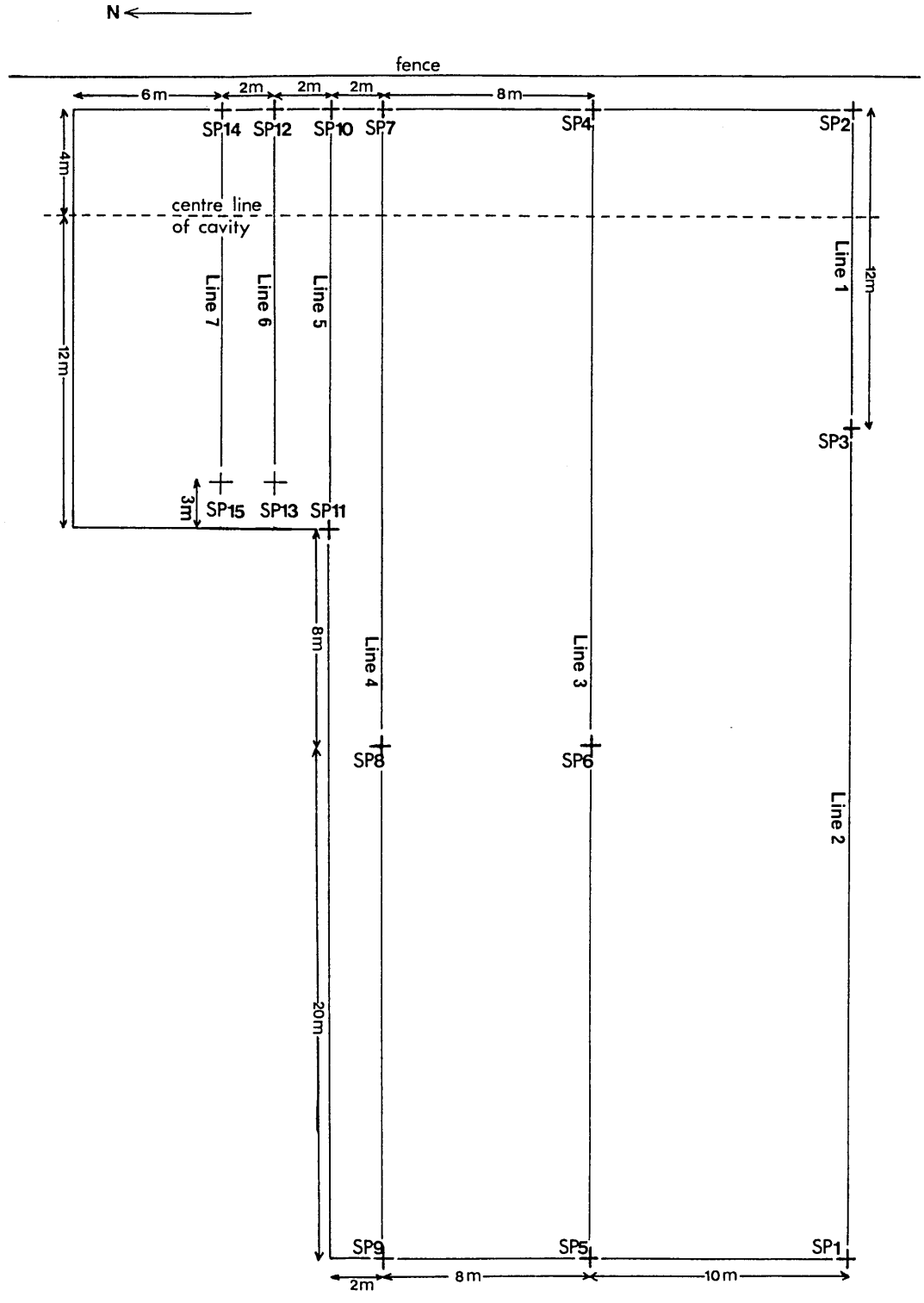

Figure 6.5 The site grid showing the refraction shotpoints (each shotpoint is shown by a +)

cover (about 2-3 inches) and jamming the plate into the hole, making sure it was in good contact with the rock.

A total of seven lines were shot; lines 1, 5, 6 and 7 with a geophone spacing of 1 m and lines 2, 3 and 4 with a geophone spacing of 4 m (Fig. 6.5). All the lines were shot in both directions to allow the calculation of true velocities and depths.

Unfortunately, the resulting seismograms were of poor quality and first breaks were difficult to pick. This was due to; (1) problems were experienced with the seismograph in that a large amount of internal noise was generated, this had the effect of smearing the first breaks; (2) the shot itself was smeared to a certain extent by rebound of the weight; and (3) the shallow soil cover made the geophone coupling less than ideal. We attempted to get around the weight rebound problem by using a sledgehammer source but, this did not result in any noticeable improvement.

An attempt was made to do a shear wave survey using a piece of angle iron hammered vertically into the limestone as the source. This was struck by a sledgehammer in the direction of the vertical plane containing both the source and geophones. This then generated vertically polarized shear waves (SV-waves) to which the vertical geophones could respond. The same problems were experienced as for the P-wave survey except that the low amplitude of SV-waves generated made the first breaks even more difficult to pick.

6.4.1 Results and Interpretation of the Refraction Survey

Due to the reasons mentioned above, the results obtained from the refraction survey varied from line to line, especially the velocity of the first layer. The shear wave results also varied considerably and so only three lines were attempted. Figure 6.6 shows two examples of time-distance plots from the P-wave survey and one example of a time-distance plot from the SV-wave survey.

The first plot (1) shows the interpreted results from refraction line 3, which was shot in each direction from SP4 and SP5 (Fig. 6.5). Geophone separation was 4 m except for the first and last geophones which were 2 m from the source positions. The first arrivals showed considerable error (± 2ms), although a best straight line fit indicated a two-layer case. Velocities were calculated from the slopes of these lines and are displayed on the plot. The forward and reverse velocities calculated for the second layer are close enough that dip may be neglected, thus the true velocity is the arithmetic mean of the two values (1665 m/s). For layer 1, the value of 436 m/s given by the forward spread from SP4 is probably correct, the velocity of 333 m/s given by the reverse spread is most likely the direct air-wave, 335 m/s being the approximate speed of sound in air. Using the equation.

$$z_1 = 1/2 \; t_1 \; V_1/\text{Cos}\,\Theta \qquad (6.1)$$

where, z_1 is the depth to the first reflector, t_1 is the intercept time, V_1 is the velocity of the first layer and Θ is the critical angle, the depth to the first reflector was

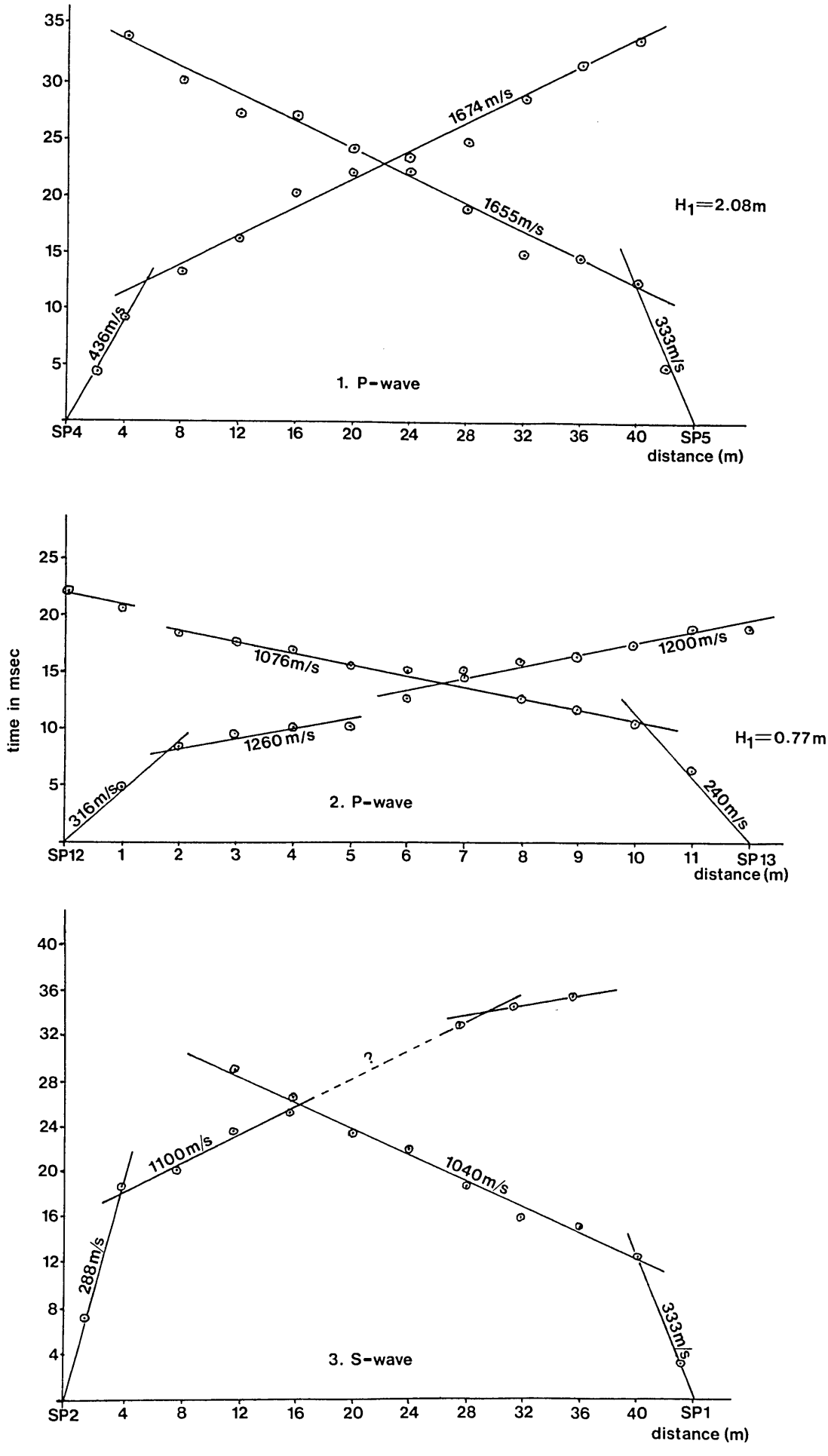

Figure 6.6 The results of the refraction survey.

calculated to be 1.8 m. This is close to the thickness of severely weathered limestone seen at the outcrop and probably represents the boundary between the weathered and unweathered rock.

The second plot (2) shows the interpreted results from line 6, which was shot in each direction from SP12 and SP13. The geophone spacing is 1 m for all geohones. This short spread is 12 m to the north of line 3 and the cavity is known to lie beneath geophone position number 4. The exact depth of the cavity is unknown but it is approximately one metre.

Both the forward and reverse profiles appear to exhibit discontinuities or anomalous delay times of approximately 2 msec. This may have been caused by the cavity as its position falls between the apparent discontinuities seen on the time-distance plots. However, record quality was such that this may have been caused by picking on a different part of the cycle, as the first breaks were not "clean". The very low velocities recorded for the first layer are probably due to surface waves as they are lower than the speed of sound in air. Lines 5 and 7 did not show the same discontinuities seen on line 6, thus making it less likely that this effect was due to the cavity. The two velocities measured for the second layer are again close enough that the angle of dip is small enough to neglect.

The depth to the first reflector was calculated to be 0.77 m, which is consistent with the decreasing amount of cover over the stratum containing the cavity, seen at the northern side of the site.

The third plot (3) in Figure 6.6. shows the results of a shear (SV)-wave profile, shot using line 2 and shot points SP1 and SP2. These results are shown for illustraton only as the high gains needed to observe the SV-wave made a consistent pick of the first break almost impossible.

Unfortunately it was not possible to obtain copies of the seismograms for inclusion in this thesis as they were the property of the Institute of Geological Sciences and were "mislaid" once the interpretations had been made.

6.5 INTRODUCTION TO EXPERIMENTAL WORK INVOLVING THE KANGO

The aim of this experimental work was to perform a detailed seismic study over a natural cavity, using the Kango as the source and a grid of vertical geophones and a three-component geophone as receivers.

The instrumentation used for the experimental work was limited to that kindly made available by the I.G.S. and so the vertical geophone survey and the three-component geophone survey were done as two separate surveys. Hardware problems with the digitizing system at Imperial College also resulted in the two surveys being analyzed on different systems. Therefore, as the work seems to split quite naturally into two parts, I shall describe the surveys and present the results in separate sections and then bring the two together in the conclusions at the end of this chapter.

6.6 THE THREE-COMPONENT GEOPHONE SURVEY

Instrumentation used for the three-component geophone survey was, a three-in-one geophone plus the three-channel amplifier and Fenlow four-channel tape recorder that were used at Cocking and Warrington (described in Section 4.3).

The three-component geophone consists of a cylindrical case about 18 cm long and 5 cm in diameter containing three geophones, each of which is sensitive to motion in one direction only. The geophones are oriented at right angles to each other within the case so that one is sensitive to horizontal radial motion (H1), one to horizontal tangential motion (H2) and one to vertical motion (V).

6.6.1 Geophone and Source Configurations

The three-component geophone occupied in turn each position of a regular 4 m grid, covering an area of 20 m by 16 m around the centre line of the cavity (Fig. 6.7). For each position of the geophone (30 in all) the Kango was operated in the same position, offset 30 m to the west of the centre line of the cavity. Ideally, the survey should have been repeated with the source 30 m to the east of the cavity, but we were prevented from doing so by the large fence encircling the site.

Due to the very thin soil layer the geophone could not be buried in the ground. Good coupling was provided by hammering a thick metal stake into the underlying limestone to which the geophone could be firmly attached using jubilee clips. Great care was taken to ensure that the metal stake was vertical and

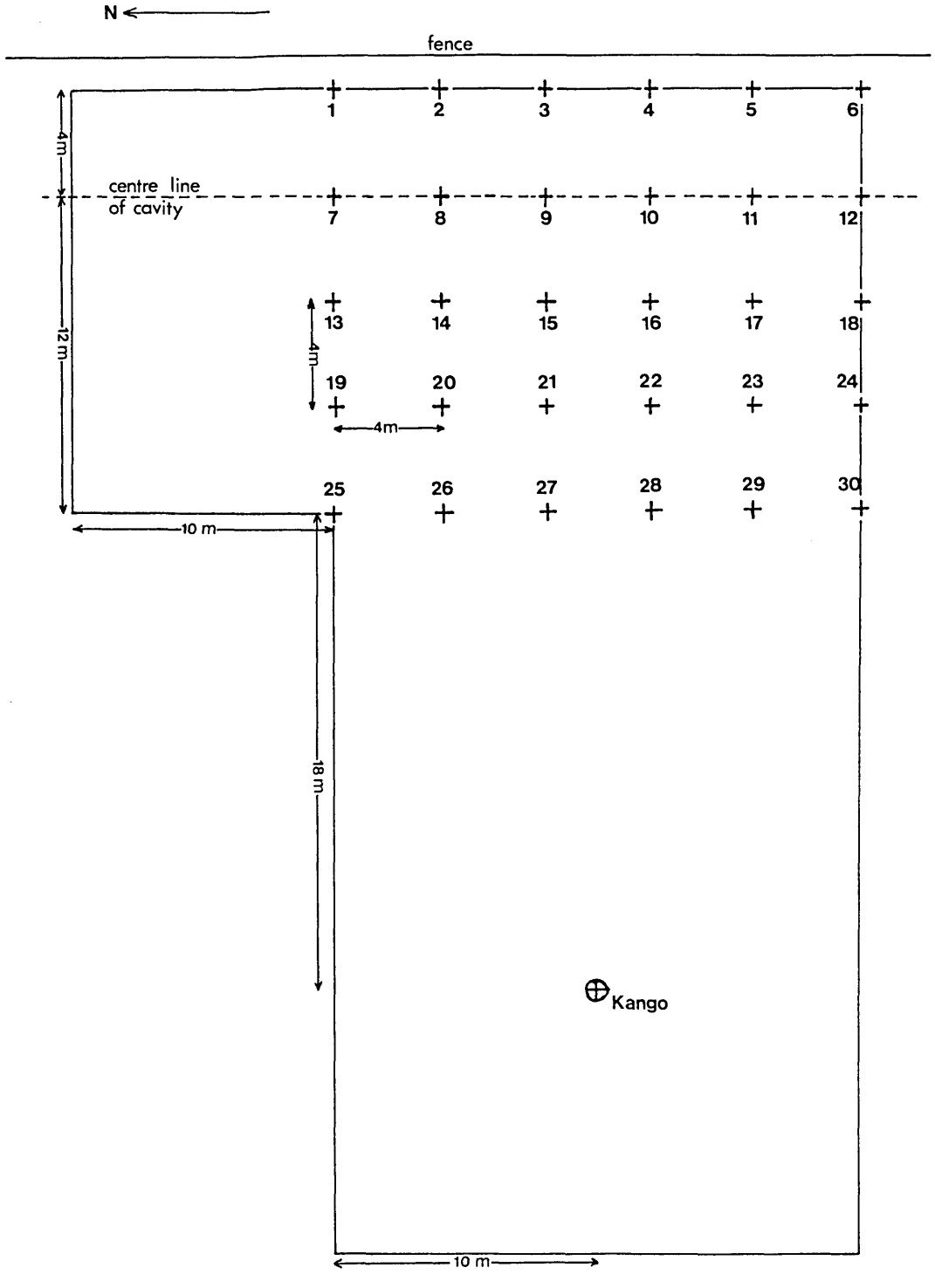

Figure 6.7 The 3-component geophone grid showing the geophone and source positions (the geophones are shown by a + and the source by a ⊕)

that the geophone was properly oriented. Orientation of the geophone was achieved by sighting along marks scribed onto the outer casing for that purpose. H1 was oriented along the straight line from the source to the geophone and was thus the radial component, approximately perpendicular to the centre line of the cavity. Thus, H2 became the tangential component, approximately parallel to the centre line of the cavity.

The Kango was operated directly on the limestone where a small patch of soil had been cut away. This served to provide good coupling and also ensured that the Kango was operated in the same position each day.

It was also possible to take the geophone 12 m into the cavity and secure it using the metal stake as before. Several recordings of the Kango were made with the geophone within the cavity.

6.6.2 Preparation and Analysis of the Three-Component Data

The preparation and analysis of this data was performed in a similar way to that of the Warrington and Cocking data. The equipment and general procedures have been described in Sections 4.4, 5.4 and 5.5 and so only the main points will be given here.

Data was selected by visual inspection using an oscilloscope with hard-copy facility and calibration was checked using channel 4 on which was recorded a 100 Hz signal and voice commentary. The Fenlow four-channel tape-recorder, four-channel playback amplifier and Kennedy digitizer were used

as before. A sampling frequency of 333 Hz, record length of 10 seconds and window length, T_M of 1/10th the data length were used. It was not possible to increase the sampling frequency to 500 Hz (giving a Nyquist frequency of 250 Hz) as data storage and handling problems would have resulted. Thus, the Nyquist frequency was 167 Hz and using a Parzen window during analysis gave 37.2 degrees of freedom and a frequency resolution of 1.86 Hz for the resulting amplitude spectra.

In all, 75 records were digitized, each record consisting of 3 channels (plus the calibration channel), giving a total of 225 spectra. Analysis was done using program ISPEC, as for the Cocking data (Section 5.5).

6.6.3 Results

As the number of spectra produced from the three-component survey was large, these results are presented in a novel way to aid comparison and interpretation. The spectra for each of the thirty geophone positions occupied are first grouped according to their component of motion. This results in three groups each of thirty spectra. The spectra are then ordered in the numerical order of the geophone positions one to thirty as shown in Figure 6.7. In this manner the amplitude value for each frequency could be stored on the computer as a third-dimension superimposed upon a two-dimensional matrix consisting of frequency in the y-direction and geophone number (position) or space in the x-direction. The result of this is a three-dimensional surface, stored and plotted by the computer, which represents a frequency-space-amplitude diagram.

The frequency-space-amplitude (FSA) diagrams for the radial (H1), tangential (H2) and vertical (V) components are shown in Figures 6.8, 6.9 and 6.10, respectively. The brackets containing two figures, situated at each corner of the diagrams, indicate the number of rows and columns of the surface respectively. In all cases the row number is equivalent to the geophone number (position) and the columns refer to frequency, each column representing 1 Hz. The large spike at the top right-hand corner is an artifical value introduced for the purpose of scaling.

Scaling is internal to the plotting routine so, this value was made to be just larger than the highest amplitude encountered in any of the three diagrams. Thus, each diagram is plotted from zero to this value and amplitudes can be visually compared between the different components.

Although the Nyquist frequency of the spectral analysis was 167 Hz, examination of the original spectra showed no anomalous amplitudes between 108 Hz and 167 Hz, so only 1-120 Hz is shown in the following figures representing the results of the three-component survey.

A comparison of Figures 6.8, 6.9 and 6.10 reveals the features of the amplitude spectra as recorded at the thirty geophone positions and the similarities and differences between the three components of motion. It is immediately apparent that the recorded "noise" is a complex mixture of the three-components and that the FSA surfaces contain both regular and irregular features. The main features of the surfaces are large peaks which occur irregularly between 30 Hz and 55 Hz and

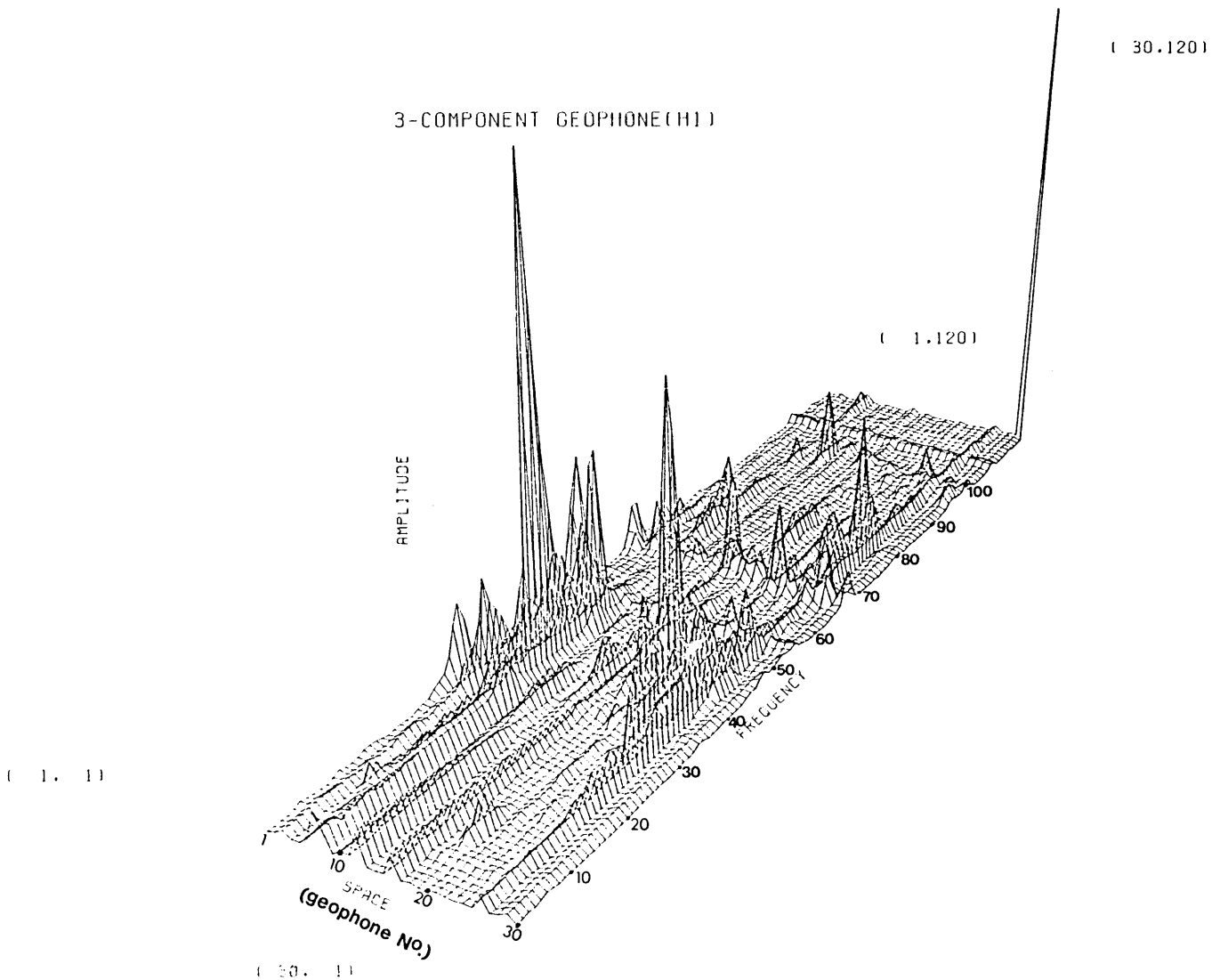

Figure 6.8 Frequency-space-amplitude surface for the H1 (radial) component

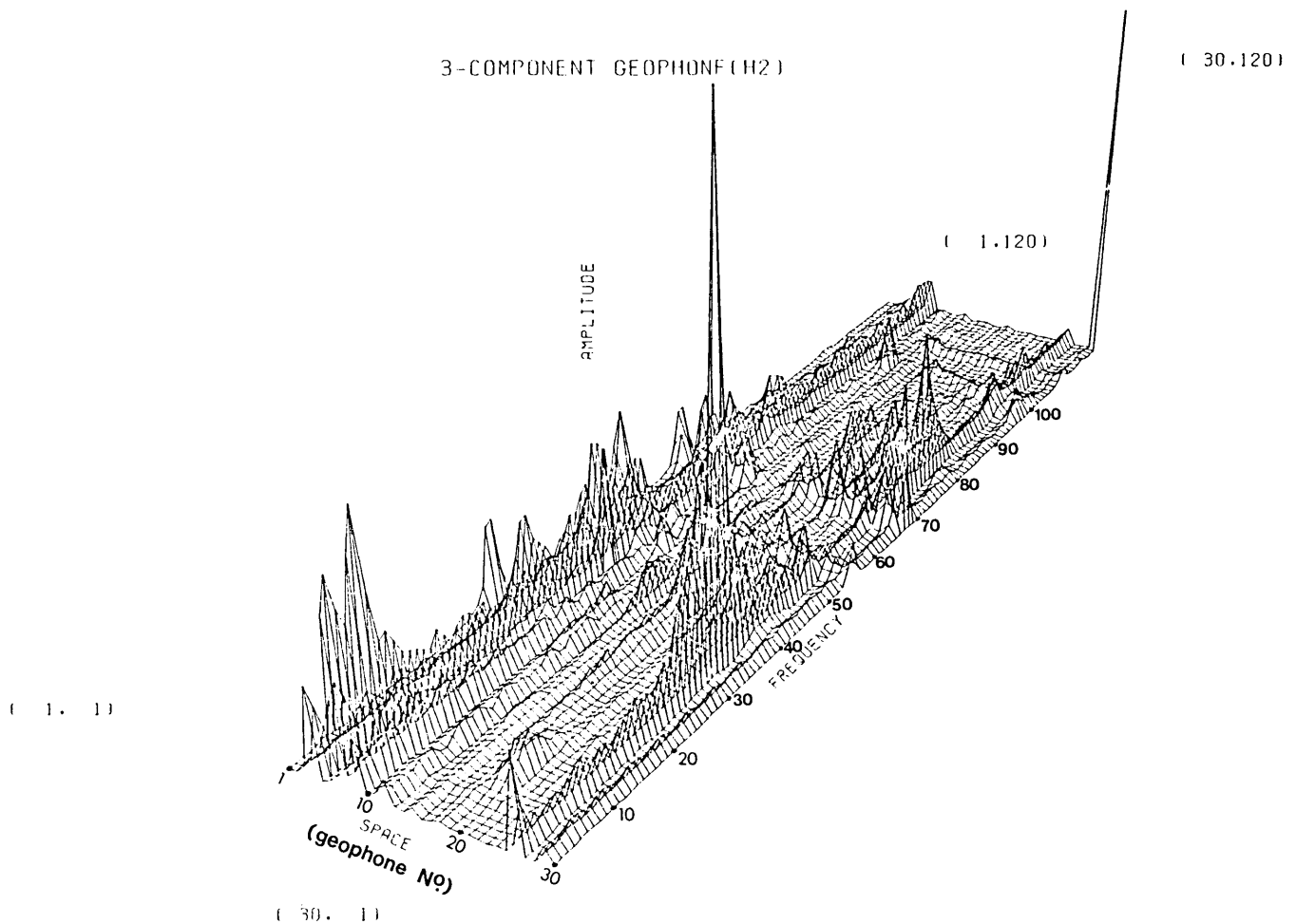

Figure 6.9 Frequency-space-amplitude surface for the H2 (tangential) component

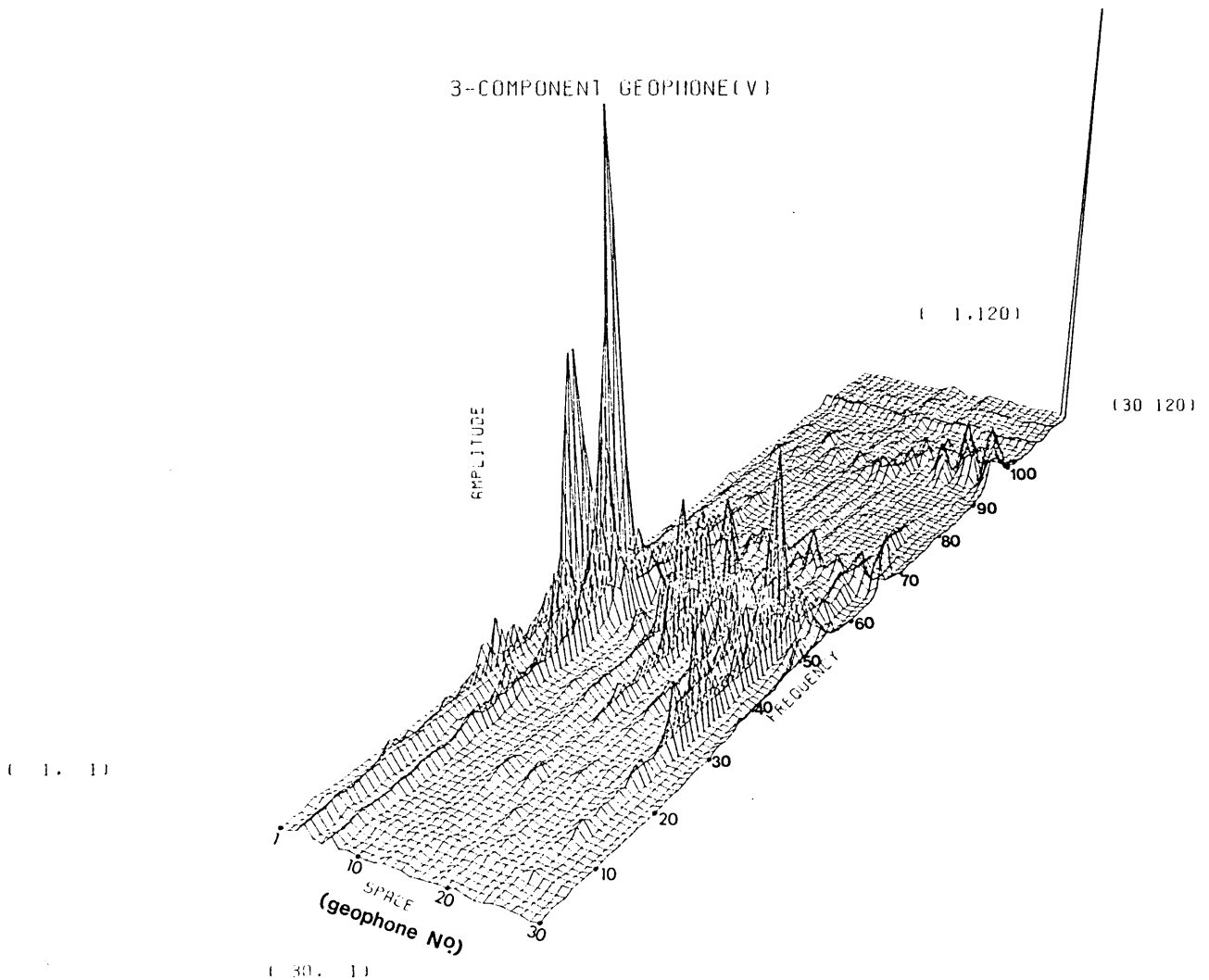

Figure 6.10 Frequency-space-amplitude for the V (vertical) component

regular features seen on all components at 68 Hz and 100 Hz. There is also a small peak at 108 Hz which occurs at the same amplitude on all three components and on all thirty geophones. This is, therefore, most likely a spurious frequency introduced by the instrumentation or during processing. Over the complete frequency range (1-120 Hz) there appears to be more energy in the radial component than in the tangential, whilst the vertical component has the least of the three.

Table 6.1, below, is a summary of the peak frequencies seen on the amplitude spectra which comprise the FSA surfaces. The numbers within the columns representing the three components of motion refer to the geophone numbers as detailed in Figure 6.7. Designation of a particular frequency as a "peak" at any one geophone position is somewhat subjective as it was not possible to normalize the spectral output of the Kango for the three-component survey.

Frequency (Hz)	COMPONENT OF MOTION		
	Radial (H1)	Tangential (H2)	Vertical (V)
33	1, 3, 26	1, 3, 26	1, 3, 26
40	7	7	7
50	7, 26		3, 7, 13, 14, 17, 21, 23, 26
68	1-10, 15-30	1-10,15-22,26-30	9,10,26,27,29,30
75	7, 26		
80	26	26	
100	8,9,10,16,26,29	26-29	26, 27, 29, 30
108	1-30	1-30	1-30

Table 6.1 A summary of peak frequencies seen on the frequency-space-amplitude surfaces (Numbers within the three component columns refer to geophone numbers).

The 33 Hz frequency, shown to be the repetition rate of the periodic impulse imparted by the Kango (Section 6.2.1), is only seen to have significant amplitude for geophones 1, 3 and 26. Thus, it is evident that the repeatability of the Kango is not as good as was originally thought. The large peak seen at 40 Hz on geophone 7 appears to have the majority of its energy in the radial and vertical components. The peak seen on the tangential component may be spurious as it appears that all frequencies have been increased in amplitude at geophone 7 for this component, which could have been caused during acquisition or processing. Geophone 7 is positioned directly above the cavity, approximately 10 m south of the entrance. The predominance of radial and vertical motion for the 40 Hz frequency suggest a Rayleigh-wave, which may be caused by cavity resonance.

The 50 Hz frequency, previously shown to be an air-wave, is seen predominantly on the vertical component which would support this interpretation. It is possible that there is some coupling of this air-wave with the ground. Some component of radial motion would also be caused by a spherically expanding air-wave and which is seen on geophones 7 and 26. Significantly, geophones 7 and 26 also exhibit higher amplitudes for other frequencies. As previously mentioned this may be spurious (caused by the acquisition or processing) or it could be a function of the operation of the Kango.

The 68 Hz appears on all three components but with larger amplitude on the radial and tangential than on the vertical. The amplitude of this frequency does not appear to vary in a

consistent manner with distance from the source, but this may be due to our inability to detect a change across the 16 m width of the grid. The 100 Hz frequency appears to have its largest amplitude on the vertical component but attenuates rapidly with distance, the higher geophone numbers (positions) being closest to the source. This is in agreement with the results of the Kango test (Section 6.2.1) for this frequency. The 100 Hz is also seen on the horizontal components but at low amplitude and a regular amplitude-distance relationship is not apparent.

Figures 6.11 and the first part of 6.12 show amplitude spectra of background noise recorded both on the surface and within the tunnel. For comparison purposes the scaling spike seen on each of these diagrams is of the same size as that used in Figures 6.8, 6.9 and 6.10. Each of the three frequency-amplitude plots show one recording of background noise recorded at the surface (row 1) and two recordings of background noise within the tunnel. The surface mounted geophone recorded both 40 Hz and 50 Hz components on both the radial and vertical components. The tangential component shows no significant background noise on the surface or within the tunnel. Within the tunnel the three-component geophone recorded 55 Hz and what appears to be a harmonic at 110 Hz.

The second part of Figure 6.12 and Figure 6.13 show recordings made with the geophone 12 m within the cavity whilst the Kango is in operation. The results of two similar recordings show the previously recorded 55 Hz ad 110 Hz (background noise) on the radial and vertical components plus a 68 Hz signal seen on all components. The 68 Hz peak has its largest amplitude on

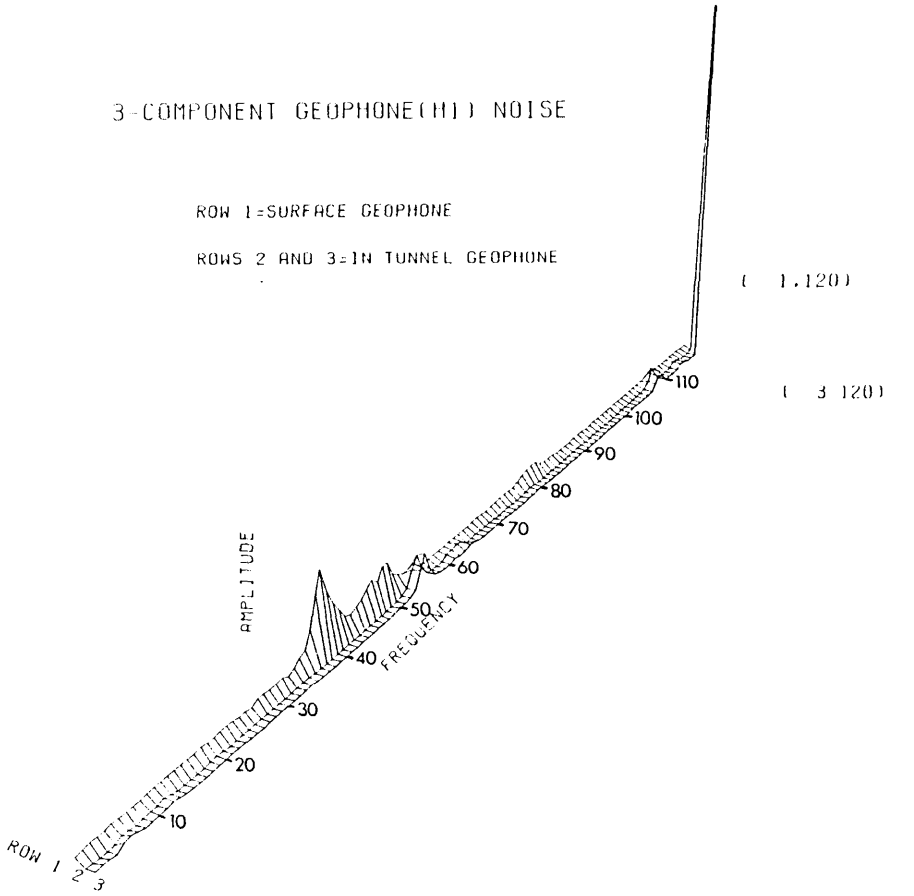

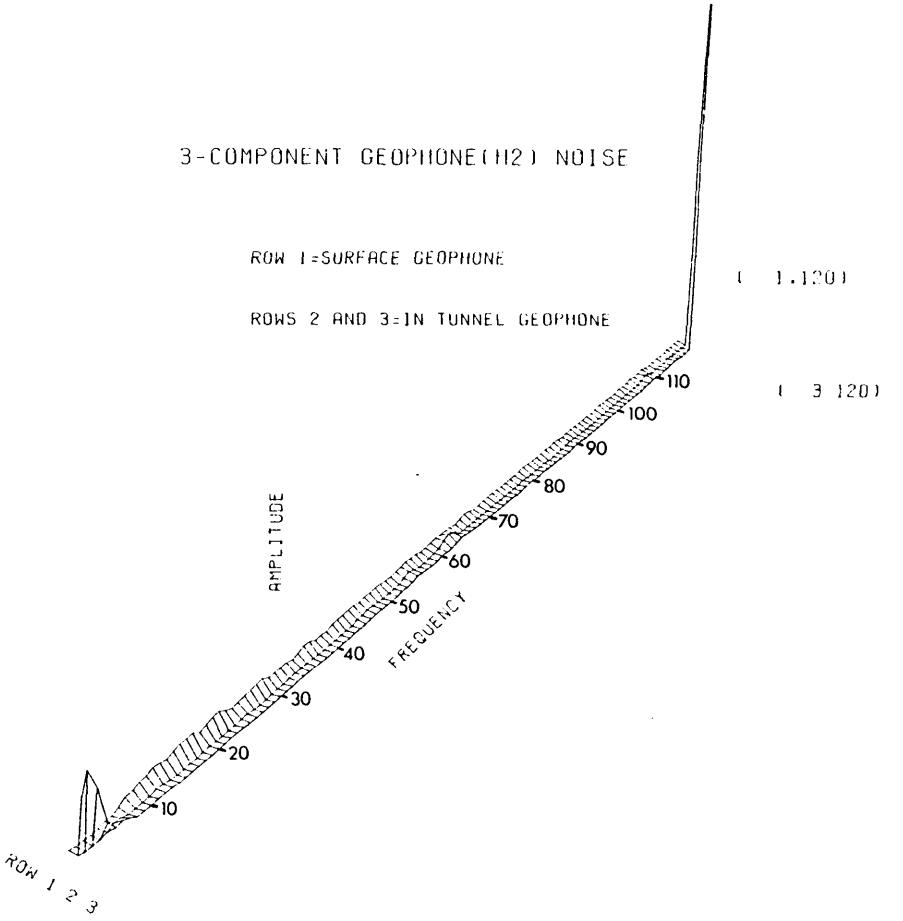

Figure 6.11 Frequency-amplitude plots of background noise for the radial and tangential components

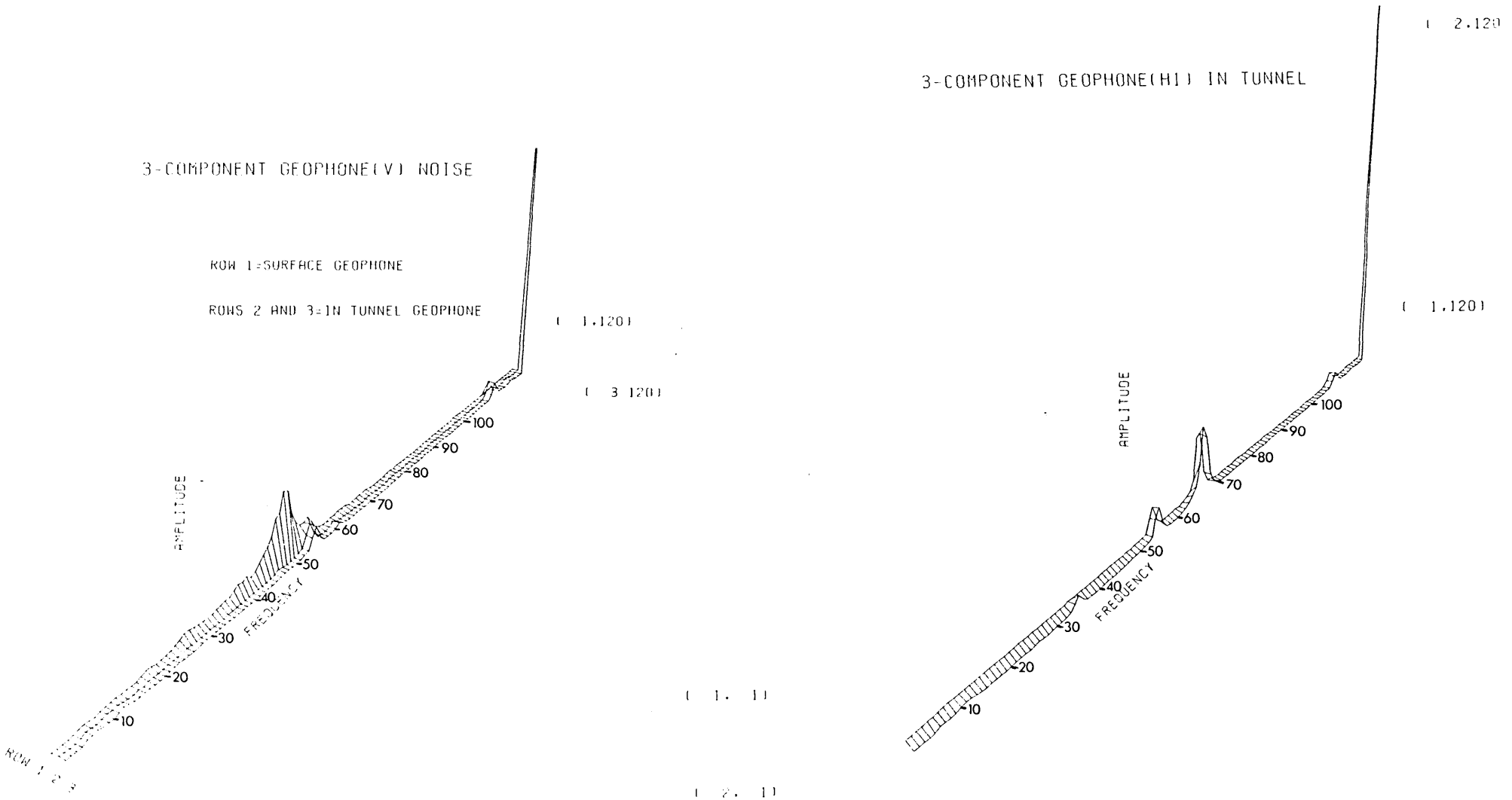

Figure 6.12 Frequency-amplitude plots of background noise for the vertical component and of in-tunnel recordings of the Kango (radial component)

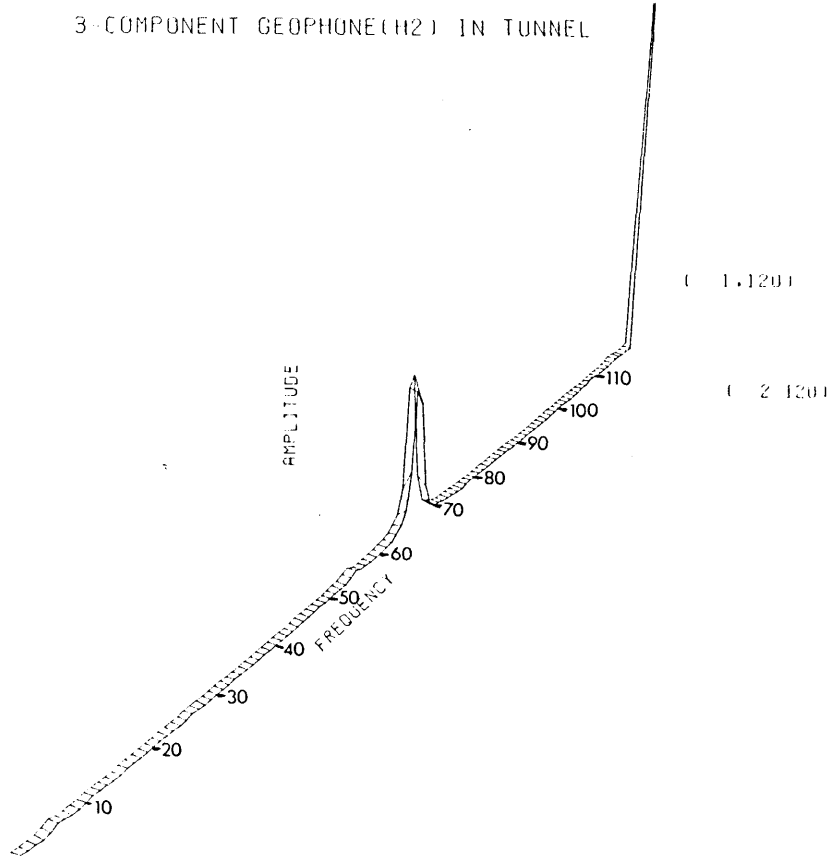

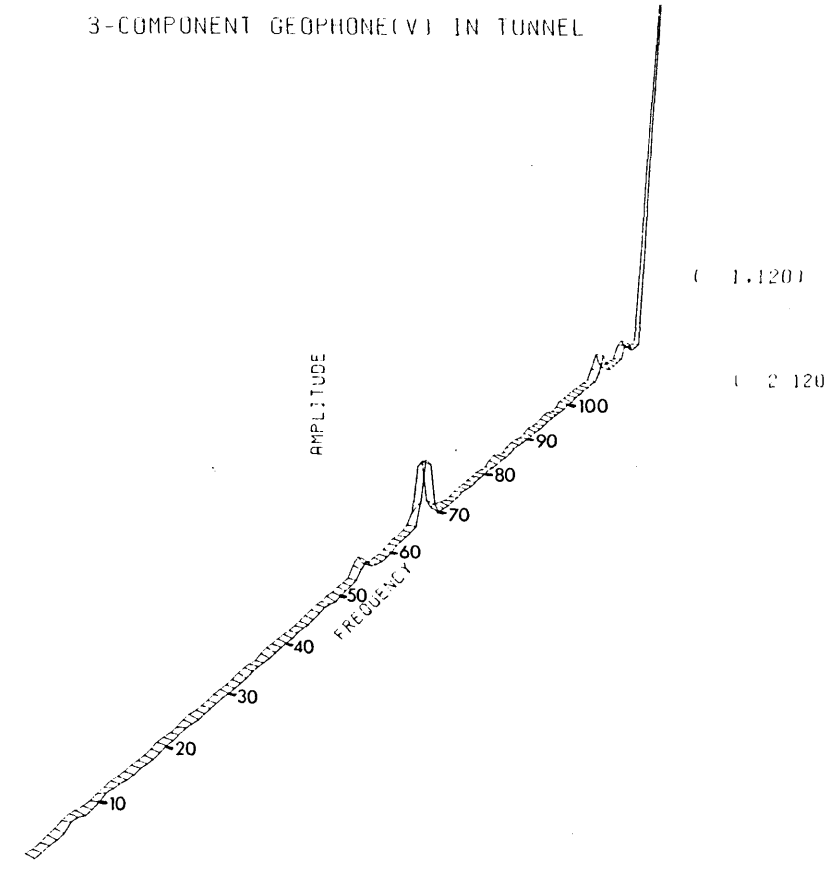

Figure 6.13 Frequency-amplitude plots of in-tunnel recordings of the Kango (tangential and vertical components)

the tangential component and smallest on the vertical component. This agrees with the amplitudes seen on the full surfaces in Figures 6.8, 6.9 and 6.10. It would appear that the 68 Hz is a shear wave and may be the only wave-type radiated into the rock by the Kango that is not a surface-wave which, can be recorded at a distance of 30 m from the source.

For a more detailed look at some of these frequencies, portions of the FSA diagrams grouped by position and by frequency are shown in Appendix 2.

6.6.4 Discussion

The frequency-space-amplitude diagrams allowed easy identification of frequencies recorded on several geophones. Grouping the spectra according to geophone position also allowed some idea of how the amplitude varied with distance (the space axis of the FSA diagrams show geophone positions from 1 to 30; each position may be related to a perpendicular distance from the source by referring to Figure 6.7) and how the relative amplitude changed with component of motion. It was not possible to make any definitive statements regarding amplitudes as it was not possible to normalize the spectra for each geophone position.

It was apparent from the variation of the frequency spectra for different geophone positions that the output from the Kango was quite variable. It is probable that both the frequency spectrum and the partition of energy between components of motion can be affected in a fundamental way by the Kango operator. The amplitude of the air-waves and frequencies

propagated through the ground will be affected by the length of time the baseplate is in contact with the ground which is controlled to a certain extent by the amount of downwards pressure applied by the operator. This may also affect the partition of energy which, in any case, will be affected by the angle the baseplate makes with the ground; that is, whether the Kango is held vertical or not. Both of these factors may vary between and during recordings in an indeterminant way.

The 40 Hz peak seen at geophone 7 is probably a Rayleigh-wave because of the predominance of the radial and vertical components but is not due to cavity resonance as it was not recorded by the geophone placed within the cavity. Recordings made within the cavity show that only a 68 Hz shear-wave is recorded. As the Kango radiates most of its energy as surface-waves and these were not recorded within the cavity it is probable that much of this energy was confined to propagate within the low velocity layer which extends to a depth of about 1-2 m below the ground surface.

Recordings of background noise within the tunnel show differences from that recorded at the surface. It is possible that a frequency such as the 40 Hz recorded at the surface (Fig. 6.11) may be caused by resonance set up within the geophone-metal stake-ground system by an external agency such as the wind. It is true that the geophone, clamped to the end of a metal stake, would be particularly susceptible to this type of background noise. The background noise seen at 55 Hz, with a probable harmonic at 110 Hz, on the radial and vertical components may originate from the water treatment plant close by. It might have been a good idea to create a FSA diagram from recordings of background noise at each geophone position

but, our computer resources (allocation of CPU time) did not allow for this as graphic devices are heavy users of the central processor.

The general observation that the horizontal (radial) component has more energy than the horizontal (tangential) component, which in turn has more than the vertical component, supports the theory that vertical translation of a circular plate in contact with the ground will radiate most of its energy as surface and shear waves.

6.7 THE VERTICAL GEOPHONE SURVEY

For the survey using vertical geophones the instrumentation consisted of seven vertical geophones, seven geophone amplifiers and a Racal Store-7D tape recorder. The vertical geophones were the same as those used at Cocking (Chapter V), which were selected for their similar frequency/sensitivity characteristics. The geophone amplifiers were specially constructed to be compatible with the Racal tape recorder and incorporated a variable input impedance and variable low-pass (anti-alias) filter. The Racal Store-7D is an F.M. type recorder and was used at a tape speed of 1 7/8 i.p.s. which gave a recording bandwidth from 0 Hz (D.C.) up to 1.25 kHz.

The geophone amplifiers were calibrated using a frequency generator and oscilloscope and each channel of the Store-7D was set to have zero offset for a peak voltage of 1V. The output was set to this level in order to be similar to that of the Fenlow tape recorder (used for the three-component survey) in anticipation of using the same system for data analysis. The low-pass filter on the geophone amplifiers was set at 500 Hz

and the variable coupling resistor to 1kΩ which provided 68.5% damping as at Cocking.

6.7.1 Geophone and Source Configurations

The vertical geophone survey was done on a regular 2 m grid around the centre line of the cavity, encompassing an area 20 m by 10 m (Fig. 6.14). Each geophone line contained seven geophones laid perpendicularly to the cavity in an east-west direction. There were eleven lines in all, spaced 2 m apart, line 1 being the northernmost as shown in Figure 6.14. For each line, geophones 2-7 were spaced at 2 m intervals whilst geophone 1 was kept in a fixed position, 20 m east of the Kango, for the duration of the survey to act as a reference. A recording of background noise was made for each line. No recordings were made with the geophones within the cavity.

The Kango was operated in the same way as for the three-component geophone survey, from a position 30 m west of the cavity.

6.7.2 Preparation and Analysis of the Vertical Geophone Data

Due to a serious hardware failure of the Kennedy digitizer, the data was analyzed on a different system than that used previously. Playback was via the Racal Store-7D tape recorder, each channel being fed in turn through a Kemo type VBF/1 low-pass, active filter to a Datalab type DL922 transient recorder. The transient recorder acted as the digitizer and interface to a Hewlett-Packard 9845A microcomputer. It was only possible to digitize one channel at a time as a seven-channel interface to the transient recorder was not available. This was not serious as far as the spectral analysis was concerned since the statistical properties of stationary time series do not depend

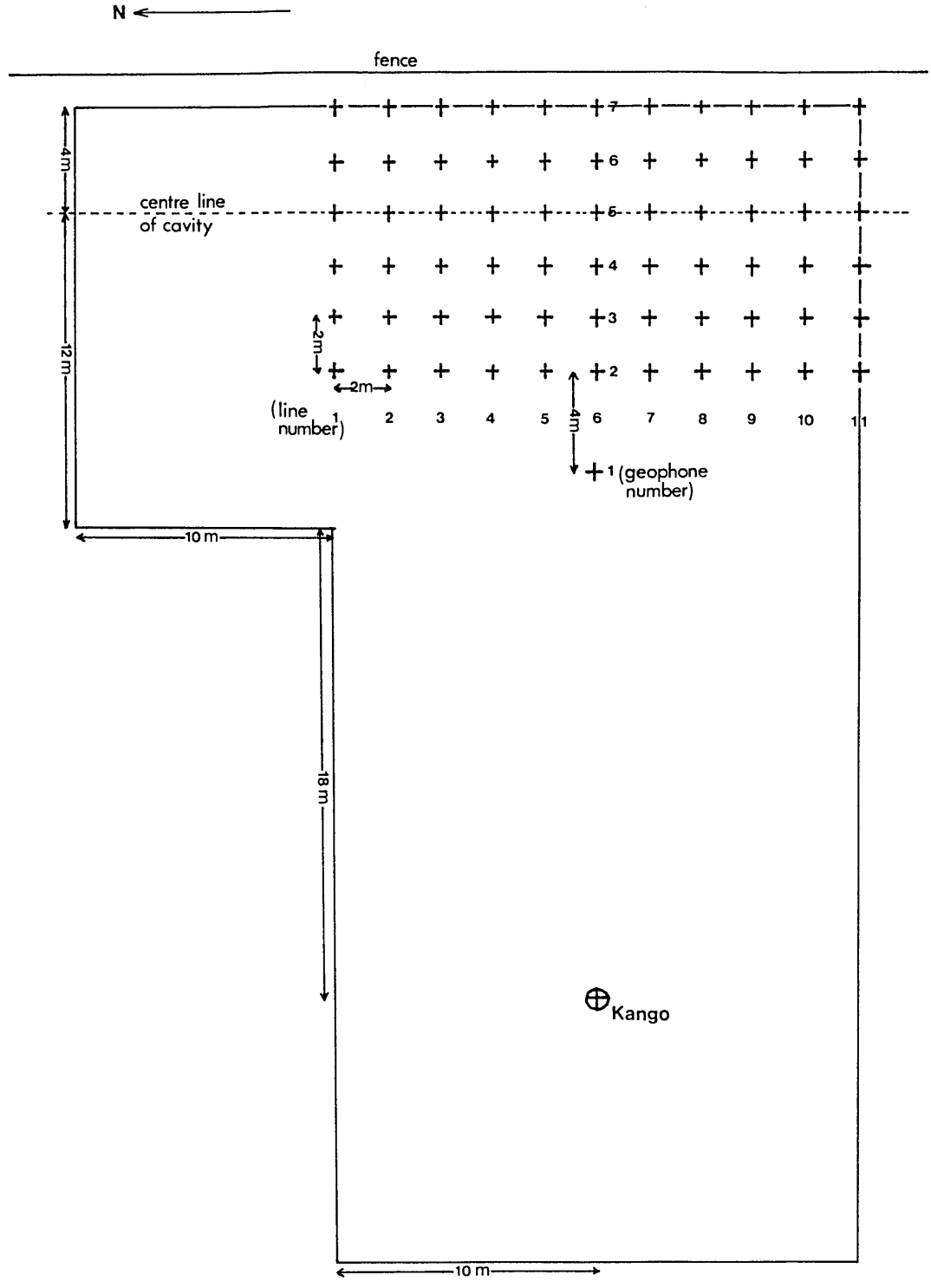

Figure 6.14 The vertical geophone grid showing the geophone and source positions (the geophones are shown by a + and the source by a ⊕)

upon the time origin and it was possible to manually choose almost exactly the same section of tape for the playback and digitizing of each channel. However, it was then not possible to use this data for timing events by cross-correlation since the time origin of events from different geophones was no longer coincident.

Limitation of the record length was provided by the transient recorder which had a maximum sweep length of 8 seconds. Using the full accuracy of the recorder gave a sampling interval of 8/4096 or 1.953125 msec. This gave a Nyquist frequency of 256 Hz; thus the low-pass filter was set to begin its roll-off just above 200 Hz, with maximum slope to avoid aliasing.

Data analysis was performed using a modified form of the spectral analysis package available on the HP9845A. Modifications made included; changing the data arrays to accept 4096 words, addition of a routine to calculate and remove the mean value of each channel (removal of bias) and up-grading of the plotting routines. Co efficients were calculated using the fast Fourier transform and smoothing was performed by a Hanning window. Altogether eighty-four records were analyzed in this way.

6.7.3 Results

Examination of the amplitude spectra calculated from recordings made whilst the Kango was in operation revealed four peak frequencies which were consistently present. These frequencies are; 33 Hz, 50 Hz, 100 Hz and 200 Hz. A typical spectrum, recorded at geophone 1, illustrating the relative amplitudes of

these frequencies is shown in Figure 6.15. The spectrum has been normalized to the maximum value of amplitude seen over the 256 Hz bandwidth. These peak frequencies are the same as those measured from the paper records made during the Kango test (see Section 6.2.1) and may correspond to the repetition rate of the Kango (33 Hz), an air-wave (50 Hz) and Rayleigh-waves (100 Hz and 200 Hz).

Figure 6.16 shows a typical spectrum of the background noise which was also recorded at geophone 1 (the reference geophone). The peak frequency in this case is seen at 50 Hz. A closer inspection of the maximum value seen on each of the two spectra shows that the 50 Hz peak in Figure 6.16 has an amplitude about 78% of that of the 100 Hz in Figure 6.15. This is somewhat misleading as different gains were used when recording the background noise and the maximum value should be scaled down by a factor of 2.5. This reduced the amplitude of the 50 Hz background noise to about 80% of that seen whilst the Kango is operating.

The 50 Hz, 100 Hz and 200 Hz frequencies were chosen for closer analysis; the 33 Hz was not used as its amplitude was generally not very much above the background noise and the amplitude showed large variation on geophones at the same distance from the Kango, even after normalizing the spectra. The spectra were normalized by dividing the amplitude at a particular frequency by the amplitude of that frequency calculated for geophone 1. This was done on a line-by-line basis in an attempt to compensate for differences in the output from the Kango, each line (consisting of seven geophones) being recorded separately.

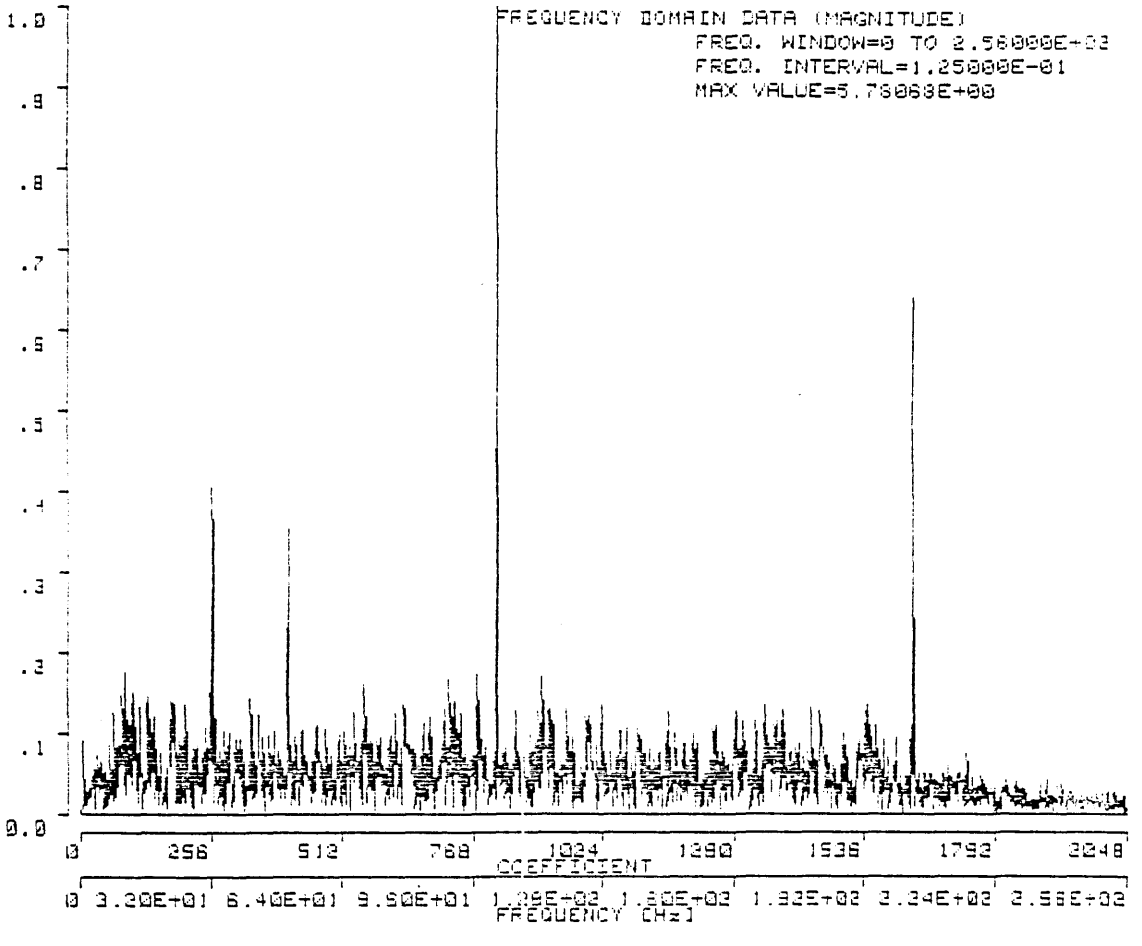

Figure 6.15 Amplitude spectrum with the Kango in operation (geophone 1)

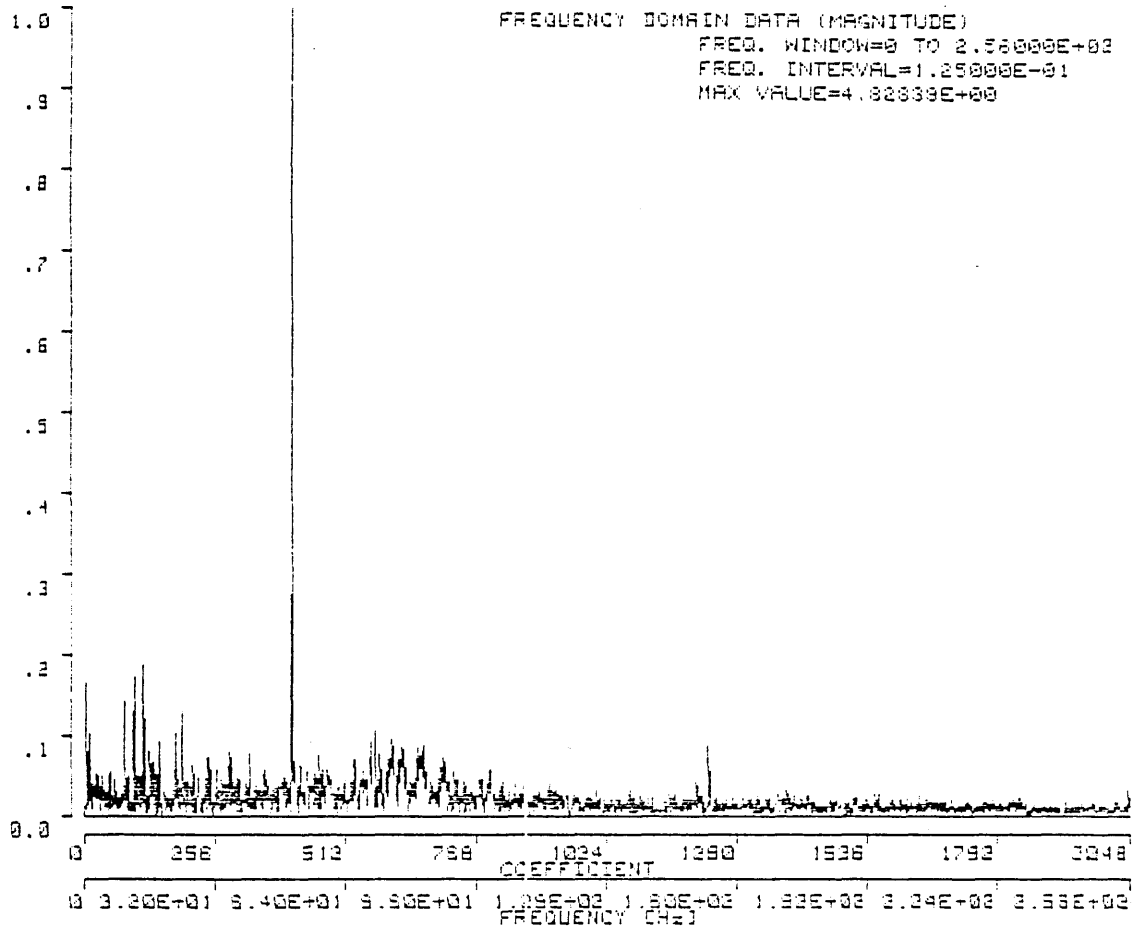

Figure 6.16 Amplitude spectrum of background noise (geophone 1)

Figure 6.17 shows three space-amplitude surfaces which correspond to the three frequencies chosen for further analysis. The surfaces as shown correspond to the vertical geophone grid (see Figure 6.14), each junction point on the surface representing a geophone position. The east-west direction is left to right across the page so, line 1 is at the bottom or northernmost part of each surface. The two crosses to the right of each surface represent the positions of the Kango and the fixed geophone (number 1 in each line); the figures have not been drawn to scale.

The three surfaces shown in Figure 6.17 all show anomalous behaviour; that is, there does not appear to be a normal fall-off of amplitude with distance. Over the geophone grid the minimum amplitude for the 100 Hz and 200 Hz frequencies occurs at geophone 5 on each line which corresponds to the approximate position of the cavity (see Fig. 6.14), whilst for the 50 Hz it occurs at geophone 2 or 3 on each line. The form of the surfaces appears very similar for the 100 Hz and 200 Hz, it is possible that the higher frequency is a harmonic of the 100 Hz.

Figure 6.18 shows plots of amplitude versus distance for the unnormalized data plotted in a more conventional fashion. Distance in Figures 6.18 and 6.19 refers to the perpendicular distance from source to receiver; the difference between this and the radial distance would merely cause a small bulk shift of the curve. Lines 1-10 only are shown as the plotting routines would not accept any greater volume of data. The points are joined by smooth (cubic spline) curves generated by curve fitting routines available on the Imperial College Interactive Graphics System.

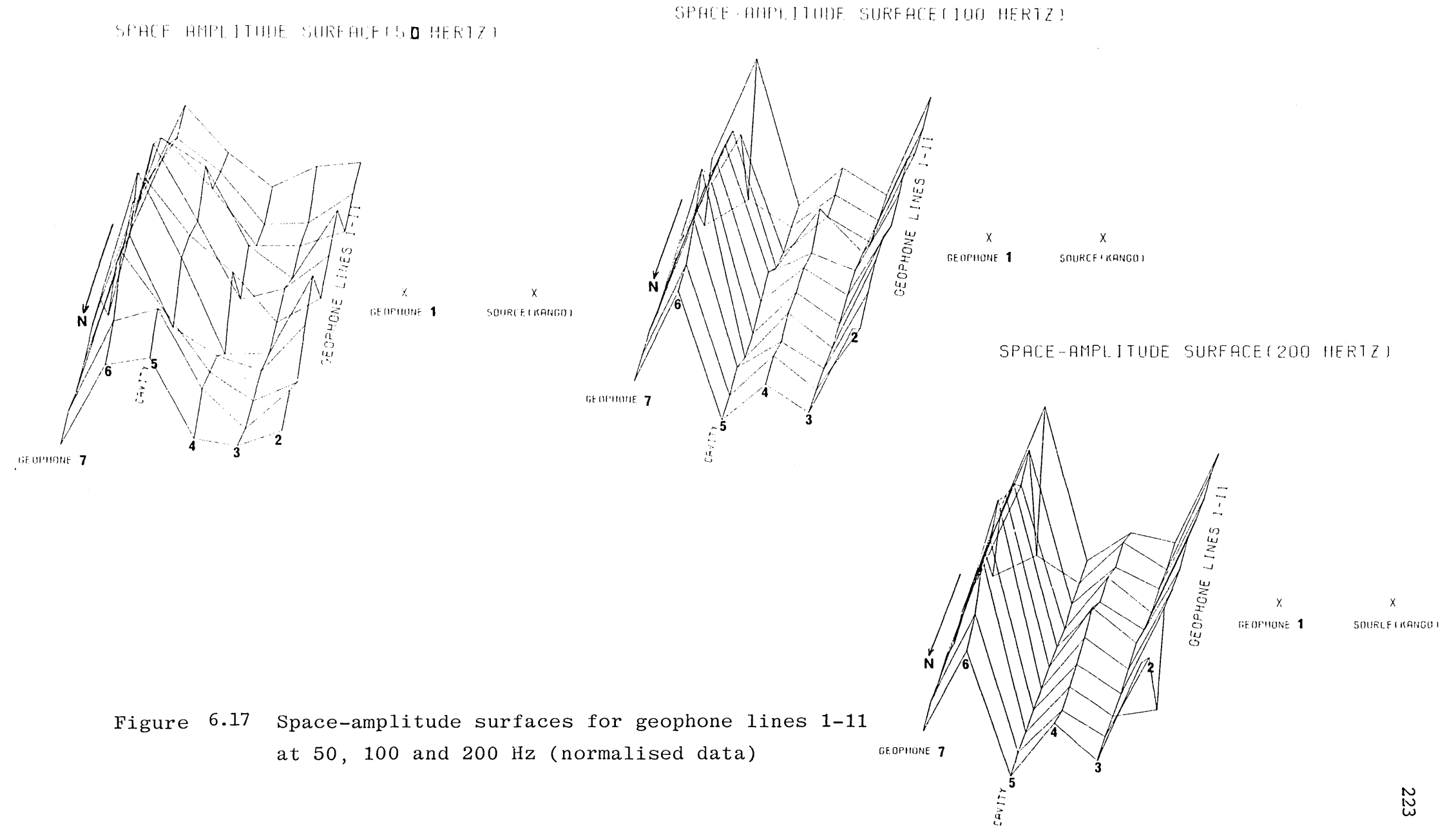

Figure 6.17 Space-amplitude surfaces for geophone lines 1-11 at 50, 100 and 200 Hz (normalised data)

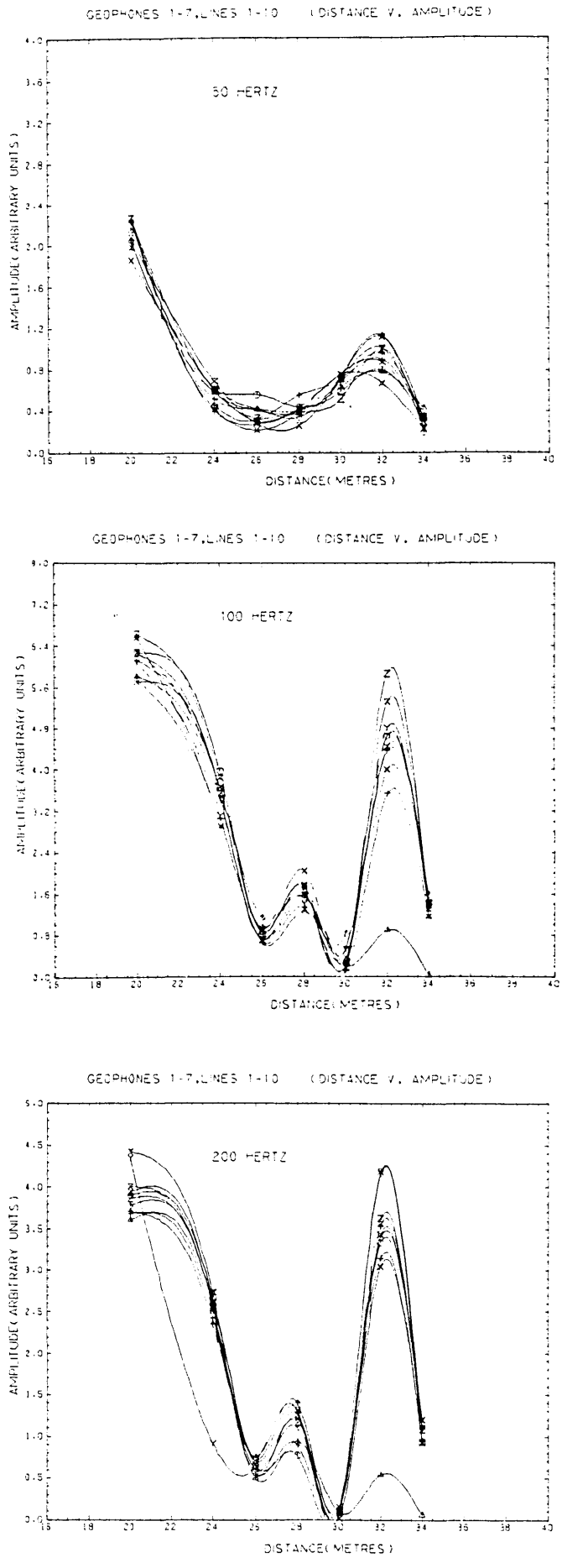

Figure 6.18 Amplitude versus distance for lines 1-10 at 50, 100 and 200 Hz (unnormalised data)

Apart from one line on the plots of 100 Hz and 200 Hz, all the lines show a remarkable similarity for all three frequencies. Plots of amplitude versus distance for the background noise are shown in Figure 6.19. These amplitudes have been scaled to allow comparison with Figure 6.18. As shown previously, at 50 Hz the background noise has an amplitude comparable to that seen whilst the Kango is operating but, is generally much less for 100 Hz and 200 Hz.

It is quite apparent from Figure 6.18 that the variation of amplitude with distance of all three frequencies will not fit an equation of the form,

$$A = A_0 \, x^{-n} \qquad (6.2)$$

or

$$A = A_0 \, e^{-ax} \, x^{-1} \qquad (6.3)$$

where, A is the amplitude at distance x, A_0 is the amplitude close to the source, n is the divergence factor and a is the attenuation constant. Thus, it was not possible to make any calculations of the divergence factor or the attenuation constant.

6.7.4 Discussion

The fact that the 33 Hz frequency, which represents the period of the impulse provided by the Kango, shows considerable variation in amplitude on geophone 1 implies that there was considerable variation in the coupling of the Kango with the ground. However, the predominant frequencies of 50 Hz, 100 Hz and 200 Hz showed very similar amplitudes recorded at equivalent distances from the Kango.

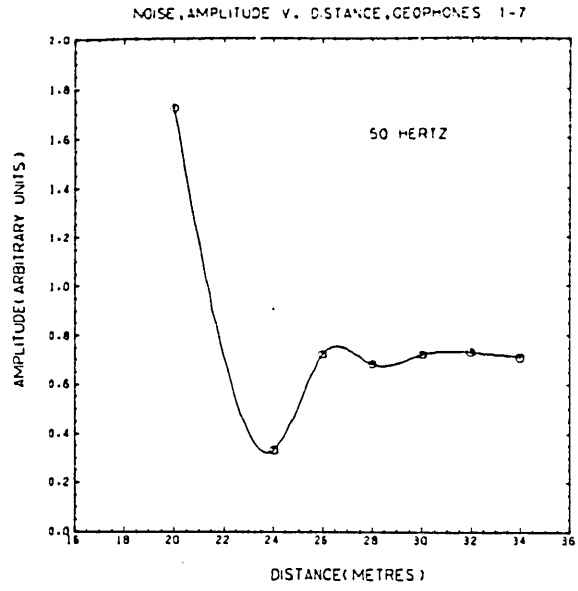

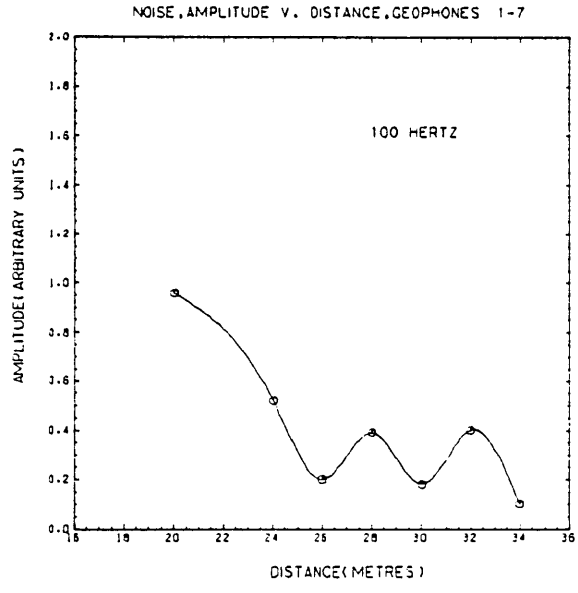

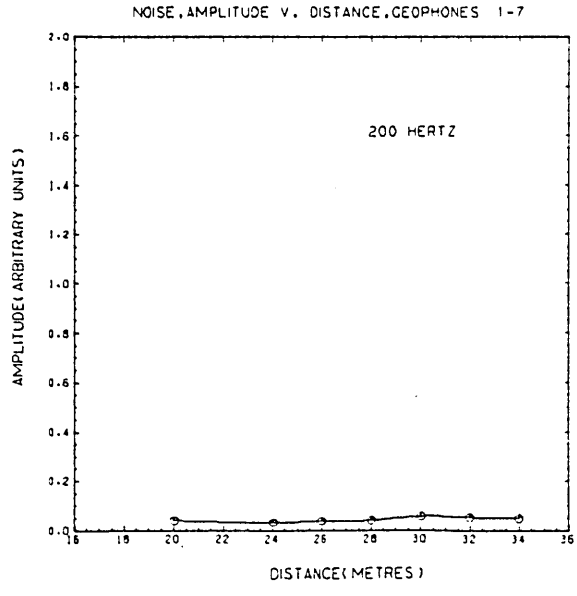

Figure 6.19 Amplitude versus distance, background noise at 50, 100 and 200 Hz (unnormalised data)

For the 50 Hz frequency much of the variation in amplitude has been shown to be due to background noise, which is probably due to electrical interference caused by the mains supply to the instrument truck and to the Kango. It is possible that the original testing done with the Kango suspended in the air (Section 6.2.1) also recorded mains interference and that there is no air-wave at that frequency. Comparison of amplitude spectra of background noise and with the Kango operating does show small differences in amplitude, but this could be due to the statistical nature of the analysis. If an air-wave does exist at a frequency of 50 Hz it is of very low ampliutde and practically indistinguishable from the background noise.

Variations in the amplitude of the 100 Hz and 200 Hz frequencies cannot be explained in terms of background noise. There are several possible explanations for this amplitude variation which we shall now examine.

Firstly, these frequencies could be composed of simple, direct air-waves, only propagated when the Kango is doing work, that is, operating at the ground surface rather than suspended in the air, as was done during initial testing. This is not possible, as it would require the generation of standing waves in the air and the conditions necessary for this do not exist at the Creswell site. Standing waves require a reflecting surface in order to establish the well understood patterns of destructive and constructive interference. Thus, the net result of the propagation of an air-wave would be a recorded signal which would remain relatively consistent from geophone to geophone apart from

a small decrease in amplitude with distance from the Kango.

Secondly, the variation in amplitude could have been caused by interference between direct, surface and refracted waves. These could be confined to propagate within the uppermost 1-2 m, bounded by the velocity contrast at that depth, which is detailed in Secton 6.4 (which shows results of the refraction survey). Again, this explanation is unlikely as it is highly improbable that virtually the same interference pattern would be seen for all eleven lines. Also, even if these waves were all confined within the uppermost layer, at the higher amplitudes observed, there would probably have been some leakage across the acoustic impedance boundary which the geophone within the cavity would have detected during the three-component survey. No frequencies were seen within the cavity except a 68 Hz shear-wave.

The most likely explanation is that the amplitude variation is caused by resonant air-wave coupling. Since air-wave coupling can only occur in the near surface when the Rayleigh-wave velocity is less than or equal to the speed of sound in air (Section 6.3.1), it is evident that variations in the velocity of the very near surface would cause variation in the amplitude of the resonant coupling. Thus, in the region of geophone 6 at a distance of 32 m from the Kango (Fig 6.18) there is a decrease in the near-surface velocity allowing resonant coupling to take place. The low velocity zone in the near surface may be a fracture zone or a more heavily weathered zone associated with the cavity, which runs beneath the fifth geophone. Therefore, it is believed that the Kango radiates a very low amplitude surface

wave at 100 Hz that is confined to the near-surface and is not detectable above the background noise within the cavity. This surface wave has a velocity just above the speed of sound in air. A 200 Hz harmonic of the 100 Hz surface wave is also propagated at a similar velocity. These frequencies rapidly attenuate as seen on the first five geophones. Then a low velocity area is encountered just beyond the cavity, which lowers the velocity of the surface waves below that of the speed of sound in the air, allowing resonant coupling with the air-wave to take place, which causes higher amplitudes to be recorded.

One must remember that although the plots in Figure 6.18 appear to exhibit some kind of spatial frequency which might be measured to obtain apparent velocities, this is not the case. On a seismogram the wiggle traces preserve the phase of the recorded energy, a downwards excursion of the wiggle being equivalent to a particular direction of ground motion. In spectral analysis this is not true since it is the absolute amplitude which is measured and a phase rotation of 180° will make no difference to the calculated amplitude. Therefore, we cannot calculate the apparent velocities of the 100 Hz and 200 Hz frequencies by assuming a peak-to-peak distance is one wavelength.

6.8 CONCLUSIONS

A high resolution refraction survey carried out over the site showed the existence of a shallow reflector at a depth of 1-2 m. The velocity of the shallow layer appeared to be highly variable but, this was due in part to the poor quality

seismograms which made picking of the first breaks difficult. One of the refraction lines showed a delay in the first arrivals which may have been caused by the cavity. Two other lines in the near vicinity did not show the same delay however.

An attempt to generate and use vertically polarized shear (SV)-waves was unsuccessful due to the low amplitude of these arrivals and the consequent uncertainty of picking the first breaks.

A three-component geophone survey over that part of the site containing the cavity showed that the output from the Kango varied in an inconsistent manner. This was believed to be due to the way in which the operation of the Kango affects the partition of energy between the modes of propagation of seismic waves and how it also affects the coupling of the baseplate with the ground. The partition of energy between the components appeared to conform approximately to that predicted by theory.

Cavity resonance was not detected by the three-component geophone placed at the surface or within the tunnel. The only frequency detected within the tunnel was at 68 Hz, which was believed to be a shear-wave. Consequently, it was supposed that much of the energy radiated by the Kango was confined to propagate within the near-surface layer as surface waves of an amplitude too low to be detected within the cavity.

A survey over the same part of the site using lines of vertical geophones also failed to detect cavity resonance. Only three

frequencies of any significance were consistently detected, at 50 Hz, 100 Hz and 200 Hz. It was found that the 50 Hz component was mostly comprised of background noise, probably electrical in nature. Amplitudes over the geophone grid did not vary with distance in a manner that could be fitted to any linear equations of attenuation or divergence. Thus, it was not possible to make any calculations of these factors. It was believed that the variations in amplitude were caused by resonant coupling between the surface waves and air-waves. The consistency in the pattern of resonant coupling was believed to have been caused by a low-velocity area of the near surface associated with the position of the cavity. Thus, it was apparent that the Kango radiated more energy as air-waves than was originally thought.

So, we may conclude that this experiment using the Kango and grids of three-component and vertical geophones failed to detect any anomalous effects which may only be attributable to the presence of the cavity.

CHAPTER VII

SUMMARY OF CONCLUSIONS AND RECOMMENDATIONS FOR FURTHER WORK

7.1 SUMMARY OF CONCLUSIONS

The feasibility study of a tunnelling machine showed that the power spectrum of seismic waves generated by the machine varied with time. It was not possible to continuously monitor the machine at the surface or to gain access to the tunnel but, it was believed that the variation in power spectra recorded at the surface was related to the mode of operation of the machine and not to the lithology ahead of the tunnel face.

Due to the variability in the recorded power spectrum at certain peak frequencies, an attempt was made to measure the total power at each geophone and perform attenuation measurements on this. The results showed a lack of linearity which rendered quantitative measurements of attenuation impossible.

Thus, it was concluded that the tunnelling machine would not be a suitable source of seismic energy to use for determining ground conditions ahead of an advancing tunnel face.

Two further experiments, using two types of portable, surface -operated machines to act as the seismic soure, were performed. These were done in an attempt to show how such machine noise may be used to detect cavities.

The first experiment showed that the machine was capable of producing a repeatable signal upon which attenuation measurements could be performed. Anomalous attenuation was detected in the vicinity of the cavity but, this was shown to be due to disturbed ground around and above the cavity and not due to the cavity itself.

Cavity resonance was not observed either at the surfae or within the cavity. This was believed to be due to the lack of sufficient energy radiated by the source to excite such a resonance.

The second experiment, over a very shallow cavity was performed utilizing a three-component geophone as well as the normal vertical type. The three-component study showed that the partition of energy between the three components of motion was not consistent but, over the whole survey, appeared to conform approximately to that predicted by theory.

It was shown that the variation in output of the source was probably due to the way in which it was operated; that is, the partition of energy between surface, shear and compressional waves was effected by the amount of downwards pressure applied when operating the source and by the angle to the horizontal made by the baseplate.

A frequency of 68 Hz was detected within the cavity but was not believed to be cavity resonance as its major component of motion was transverse horizontal and cavity resonance is believed to be caused by Rayleigh-waves.

A grid of vertical geophones over the cavity showed a great variation in the amplitude of two frequencies believed to be Rayleigh-waves. It was believed that a sudden increase in amplitude of these frequencies was caused by resonant coupling with air-waves which occurred when a low velocity zone was encountered, allowing the Rayleigh-wave velocity to fall below that of the speed of sound in air.

A normal, dropped-weight refraction survey carried out in the vicinity of the cavity showed a delay in arrival time which was originally thought to be due to the cavity. Other lines close by failed to observe this effect, which in fact may have been due to improper picking of the seismogram. The seismograms were of poor quality due to geophone coupling and instrumentation problems.

Thus, it may be concluded that the use of machine noise and the techniques of spectral analysis are not suitable for the determination of lithology or hazardous conditions ahead of a tunnel face. This is due to the mutual incompatibility of the source and method of analysis. Whilst spectral analysis requires long records for a meaningful statistical solution, it has been shown that seismic waves generated by machines do not generally exhibit the required stationarity.

7.2 RECOMMENDATIONS FOR FURTHER WORK

It is not recommended that further work be carried out using machine noise as a seismic source. It is recommended that a

similar type of work be pursued using some other form of source. An impulsive source or one with a controllable and correlatable sweep of frequencies as in VIBROSEIS appear to offer the best hope of a useable seismic method for hazard detection in a tunnelling environment.

Impulsive sources offer some distinct advantages especially in shallow environments where explosive sources need not be used.

1. Boreholes used for a previous site investigation may be utilized.

2. A simple refraction survey can be interpreted on-site.

3. Currently available technology may be easily adapted for the task.

4. The acquisition effort may be easily tailored to meet the required objectives.

5. The impulse response of the ground is well understood and on a sound theoretical footing.

Thus, it is recommended that studies be carried out to investigate the prediction of shallow lithology and the detection of near-surface hazards using a seismic method which incorporates an impulsive source. There are numerous

surface operated, impulsive sources that may be used including:

1. Small air-guns.
2. Water guns.
3. Various sophisticated weight-drop methods; usually hydraulically, mechanically or vacuum assisted.

It is possible with these methods to achieve high frequencies (up to 150 Hz) and good penetration.

Theoretically, work needs to be done on the phenomenon of cavity resonance. The precise mechanism by which this effect is generated is still in doubt and therefore the best method by which it may be induced is not known.

Model studies of the effects of various hazards such as fracture zones, faults and cavities would also be beneficial. A useful spin-off of this work on the near-surface could be a better understanding and new methods of static corrections for petroleum exploration.

APPENDICES

APPENDIX I

FORCED VIBRATIONS OF A RIGID CIRCULAR PLATE

The Warsop and Kango hammer were both mechanical devices which imparted a periodic force to the ground via a rigid circular plate undergoing vertical translation. The theory of the forced vibration of this type of body on an elastic stratum is given by Warburton (1957) and developed from papers by Miller and Pursey, (1954, 1955); Arnold et. al., (1955); and Bycroft (1956). Their work arose from the interest at that time in using transducers for dynamic investigation of soils for engineering and geophysical applications (Evison, 1956).

Miller and Pursey (1954) derived expressions for the stress field and radiation impedance produced in the earth by a circular plate vibrating normally to the surface of a semi-infinite isotropic solid. The plate provided a stress which varied sinusoidally with time. The radiation impedance, defined as the ratio of stress to mean displacement velocity under the plate was evaluated numerically and expressions derived for the field at infinity for points on and within the solid. The plate is assumed to be in continuous contact with the ground and the stress over the area of the surface beneath the plate is assumed constant, whilst zero elsewhere. The expressions were only valid for large distances and small plate size. Further developments by Miller and Pursey (1955) showed that the vibrations produced by the plate could be divided into three parts known as compressional, shear and surface waves. The partition of energy between such waves was found to be in the ratio of 1:3.74:9.78, respectively and when added were consistent with the total energy radiated by such a source into a half-space.

This theory was further extended by Warburton (1957), who considered a body with a circular base resting on an elastic stratum of infinite area and constant depth (Fig. A1.1).

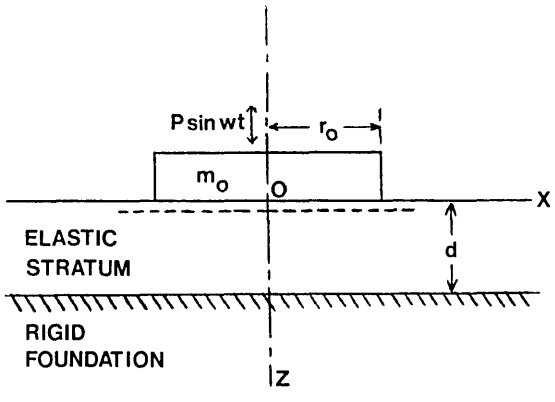

Figure A1.1 Mass on an infinite elastic stratum (After Warburton, 1957).

This is a mixed boundary-value problem, as the conditions to be satisfied for a body with a rigid circular base of radius r_0 resting on a stratum are (1) zero stress at the surface for $r > r_0$; (2) constant amplitude of displacement of the surface for $0 < r < r_0$; and (3) no reflection of waves from the boundaries at infinity ($r = \infty$). The assumptions are (1) the stratum rests on a rigid infinite foundation; (2) no friction exists between the stratum and the foundation; (3) no friction exists between the circular base and the surface of the stratum; and (4) the distribution of

the distribution of direct stress under the base is similar to that between a rigid base and a semi-infinite medium for a static load (which is known exactly). However, applying asumption (4) means that the surface does not remain plane for $r < r_o$ and so condition (2) is violated.

But, it is possible to obtain a weighted average displacement by integrating over the circular area and then the true displacement lies between this average and that obtained for $r = r_o$. The average displacement is given by a complicated integral expression (Arnold et. al., 1955) which diverges at frequencies given by,

$$f = \frac{(2n-1)\pi}{2d} \left[\frac{E(1-v)}{p(1+v)\ (1-2v)}\right]^{\frac{1}{2}} , \quad n = 1,2,3.... \qquad (A1.1)$$

where, d is the depth of the stratum, E is Young's modulus, p is the density and v is Poisson's ratio. Thus, infinite amplitudes occur at these frequencies but the effects of the mass of the plate and of damping in the stratum, which have been neglected, will reduce the resonant amplitudes to finite values and may change the resonant frequencies.

By including a mass m_o, the integral is modified (Warburton, 1957) and diverges at frequencies given by

$$a_o = (2n-1)\pi /2mR, \quad n = 1,2,3.... \qquad (A1.2)$$

where a_o is known as the Frequency Factor and is equal to the frequency multiplied by a factor including the density and modulus of rigidity; m is a function of Poissons' ratio and R is the depth factor, equal to d/ro.

In order to verify these theoretical results, an experiment was performed using a small plastic disk which was excited by a small oscillator. The stratum was modelled by a layer of foam rubber (Arnold et. al., 1955). the results agreed well with those given by theory and are shown in Figure A1.2.

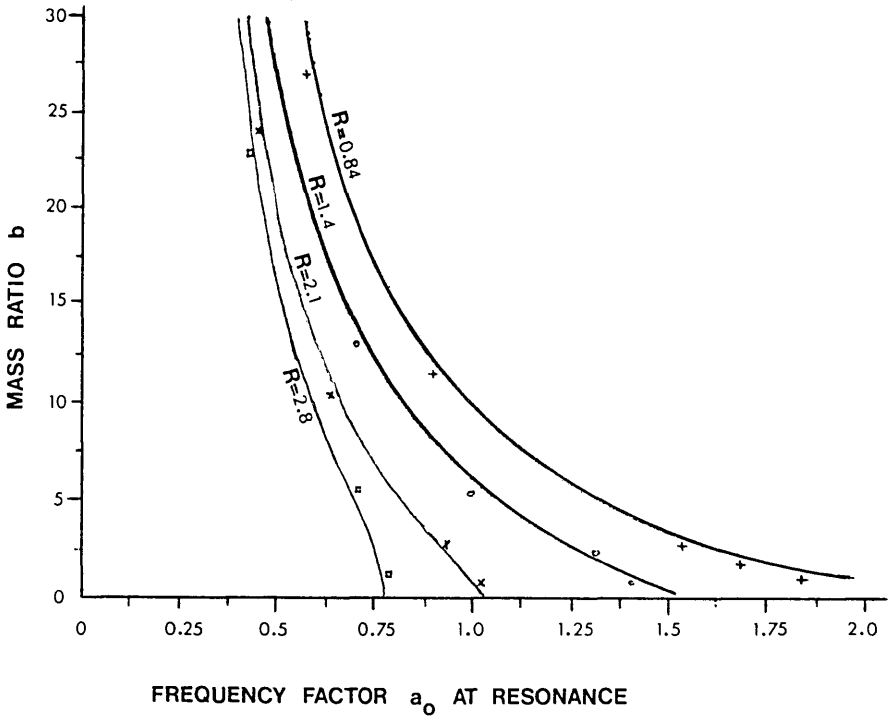

Figure A1.2 Variation of Frequency Factor at resonance with b and R, (v=0)

b is the mass ratio and is equal to m_o/pro^3.

There are two major sources of error in the derivation of the theory; the assumed stress distribution will lead to errors that will increase as the depth factor R decreases; also damping has been neglected. The presence of damping should not affect the resonant frequencies for low R, but will for high R, since moderate damping will prevent the return of reflected waves to the surface. Nevertheless, in real media it is usually the case that waves are reflected from the base of the first layer and reach the surface. Substituting values of the elastic constants of rock samples from the Cocking site, (Green, 1976) into equation A1.2, gave values of the resonant frequencies for which no anomalous amplitudes were observed.

APPENDIX II

PORTIONS OF THE FREQUENCY-SPACE AMPLITUDE DIAGRAMS OF CHAPTER VI

This Appendix shows portions of the FSA diagrams from Chapter VI grouped by position and by frequency.

Those portions that are grouped by position each contain the spectra from six geophones. Thus, geophones 1-6, 7-12, 13-18, 19-24 and 25-30 are grouped together. This was done because each group of six geophones shares a common perpendicular distance from the source (see Fig. 6.7). The first eight figures (Figs. A2.1 to A2.8) show the five groups of six spectra for each of the three components. They are shown in order of ascending geophone number, the radial component (H1) first, followed by the tangential (H2) and then the vertical (V). As each portion does not contain a scaling spike, the amplitudes between geophone groups may not be directly comparable. Reference to Figures 6.8, 6.9 and 6.10 as appropriate will help establish proper amplitude relationships.

Those portions grouped by frequency show 10 Hz "slices" for all thirty geophone positions. Five of these slices are shown for each component and comprise the frequencies 30-40 Hz, 40-50 Hz, 50-60 Hz, 93-103 Hz and 103-113 Hz. These frequencies were chosen because they cover the frequencies of interest seen on the full diagrams (see Section 6.6.3). The frequency slices are shown in order of ascending frequency for each component, radial (H1) first followed by the tangential (H2) and the vertical (V). They may be found in

Figures A2.9 to A2.16. As for Figures A2.1 to A2.8, each slice does not have a scaling spike and reference should be made to the appropriate figure in Chapter VI to establish the true amplitude relationships between them.

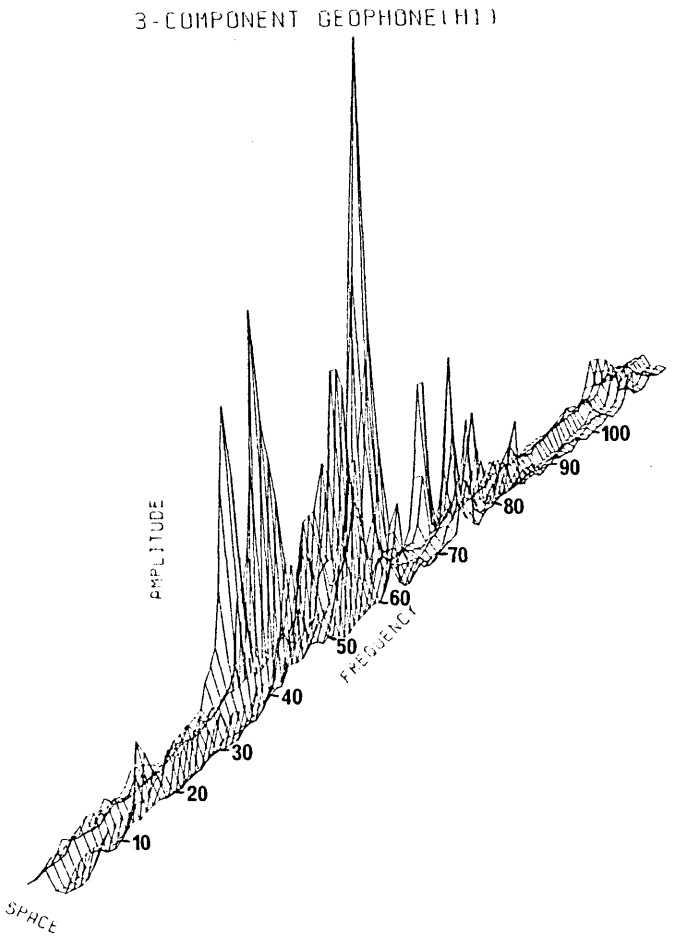

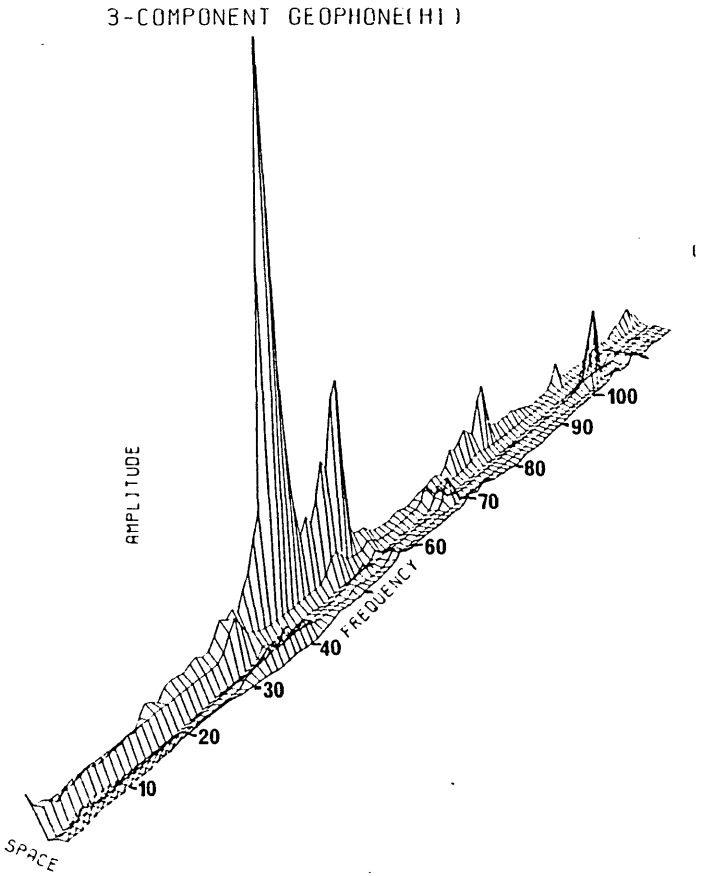

Figure A2.1 Geophone positions 1-6 and 7-12 for the radial component

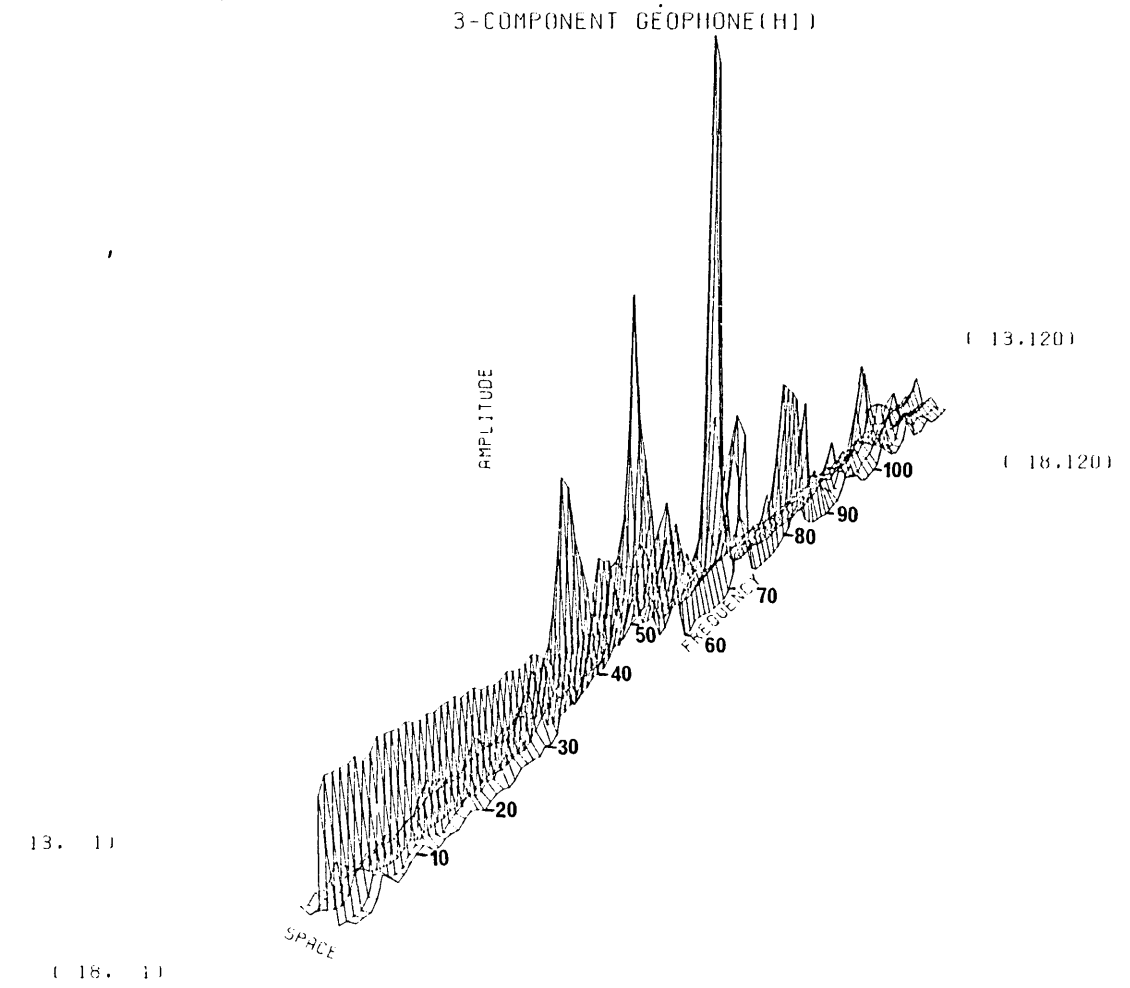

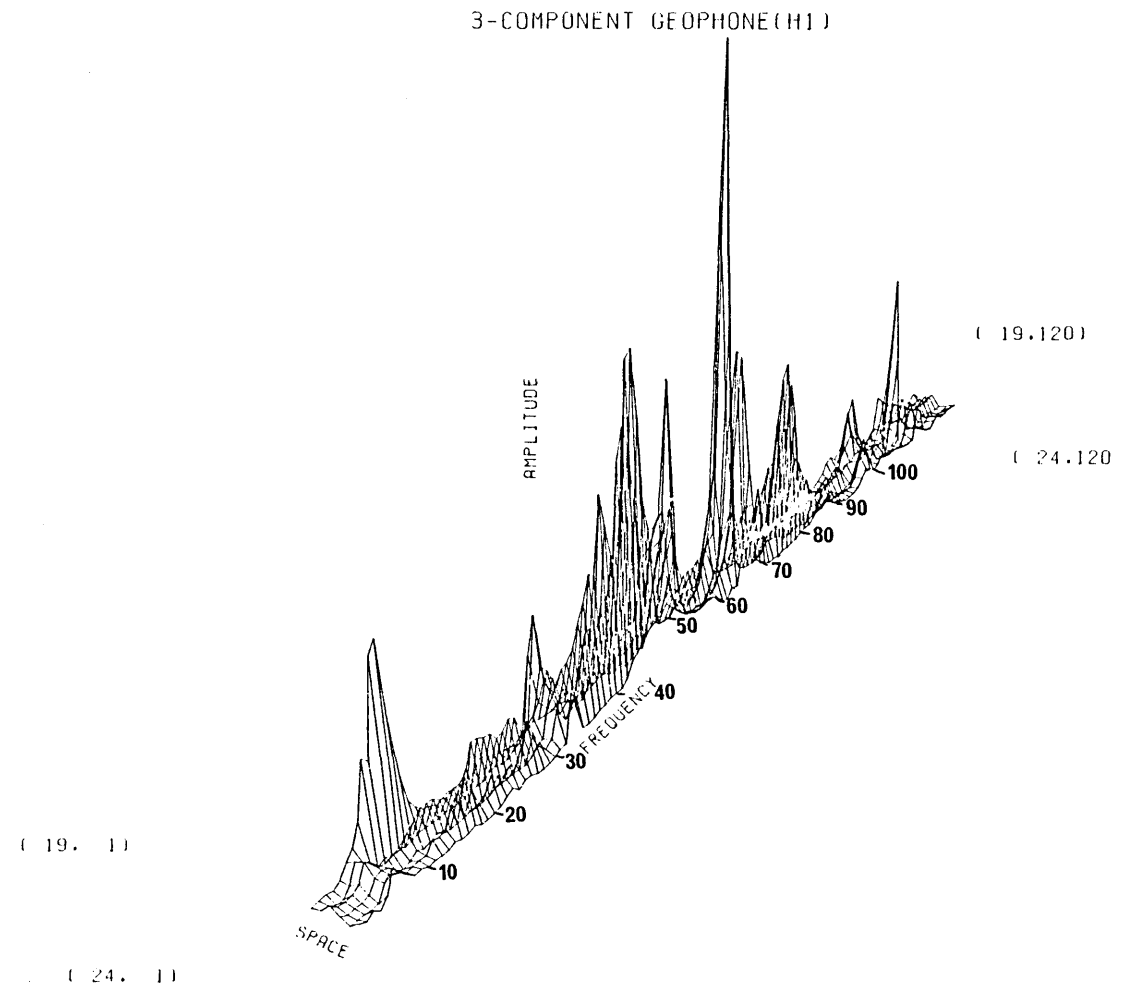

Figure A2.2 Geophone positions 13-18 and 19-24 for the radial component

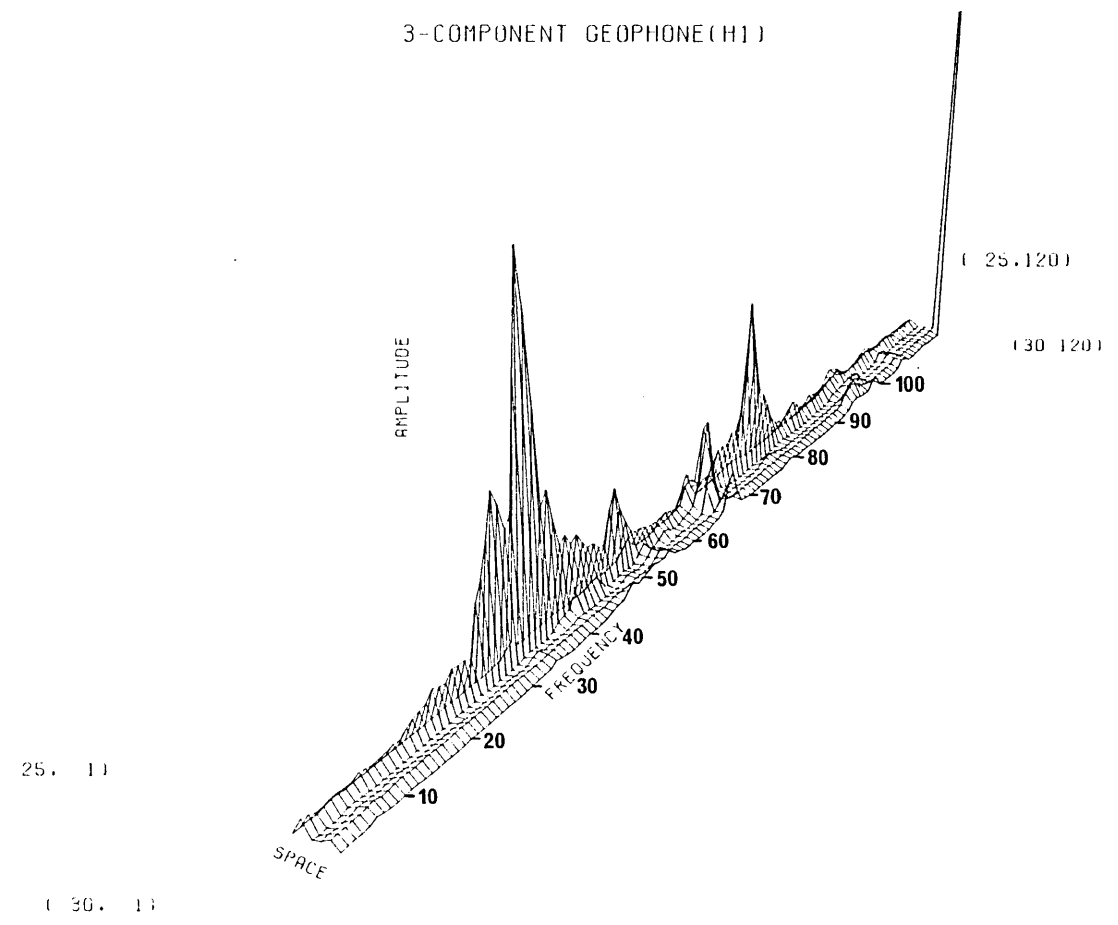

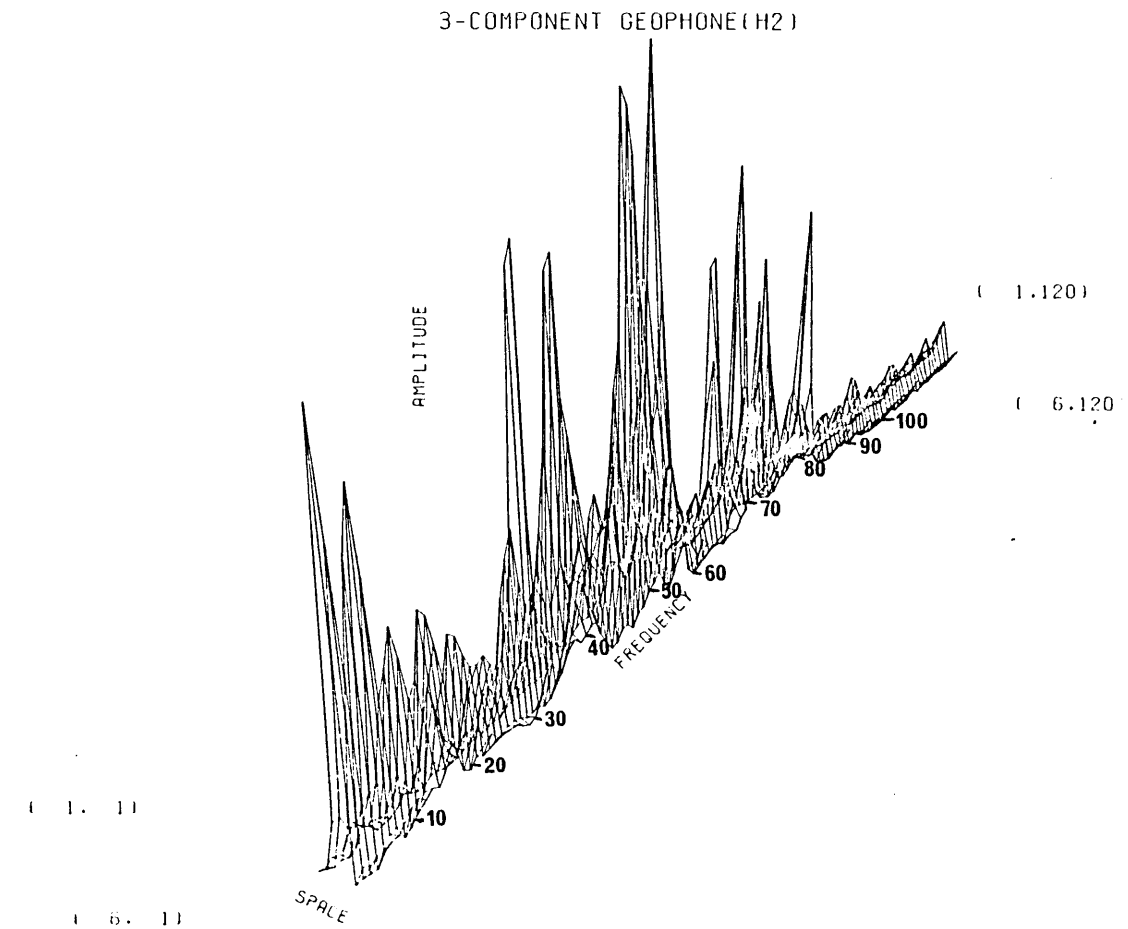

Figure A2.3 Geophone positions 25-30 for the radial and positions 1-6 for the tangential component

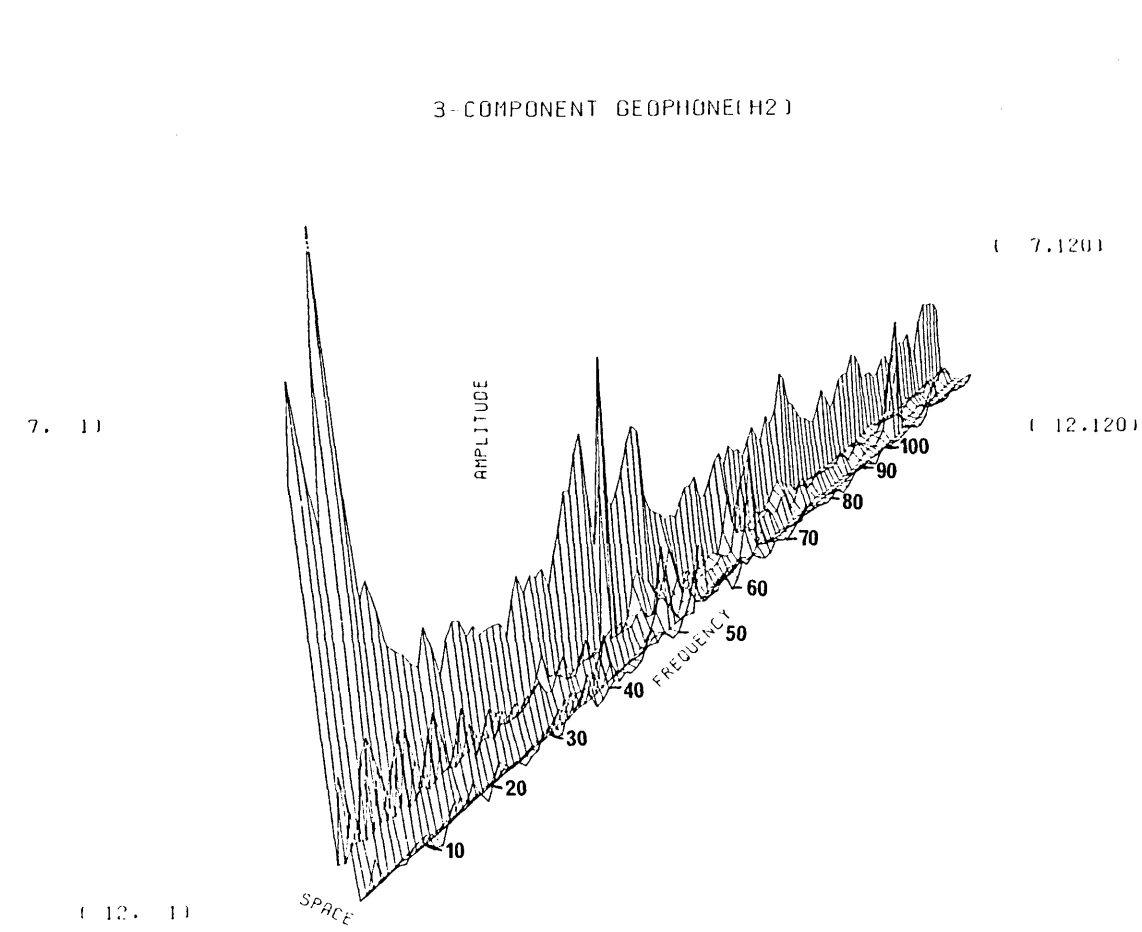

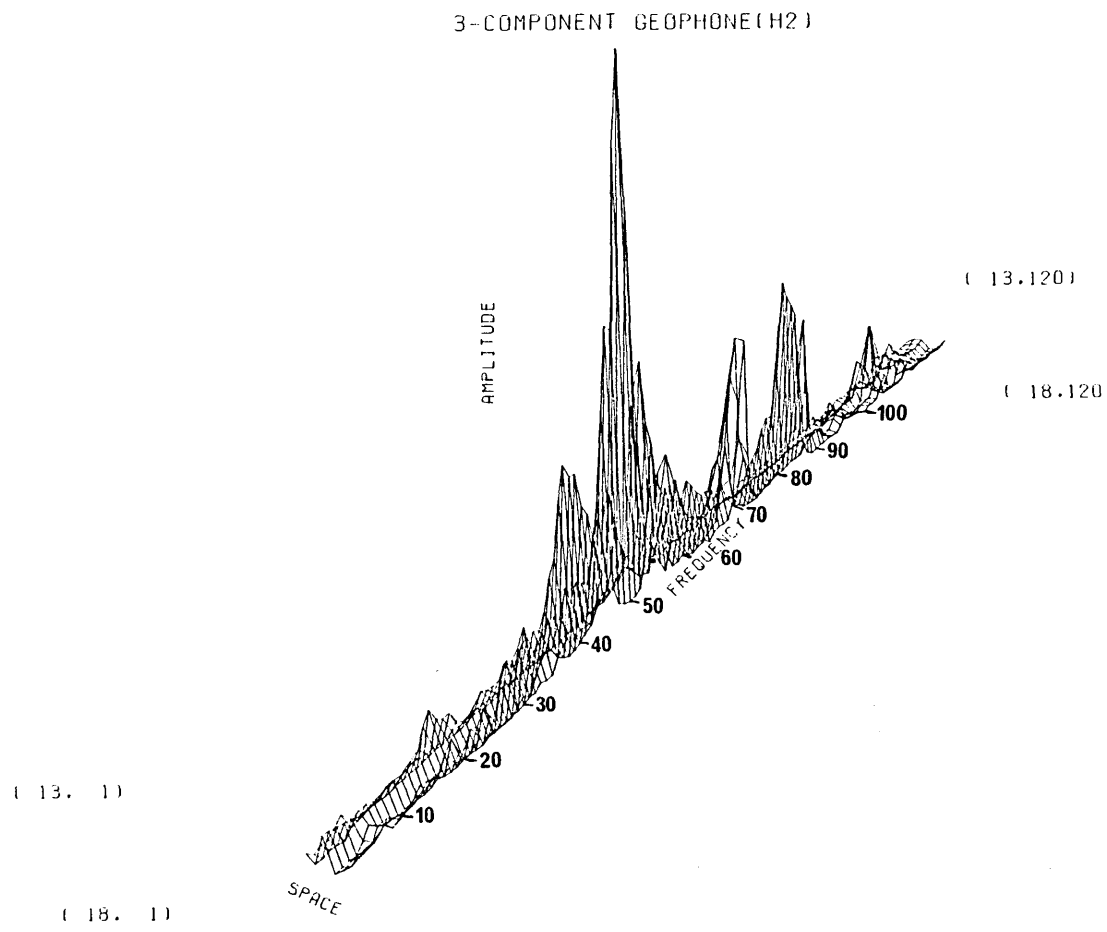

Figure A2.4 Geophone positions 7-12 and 13-18 for the tangential component

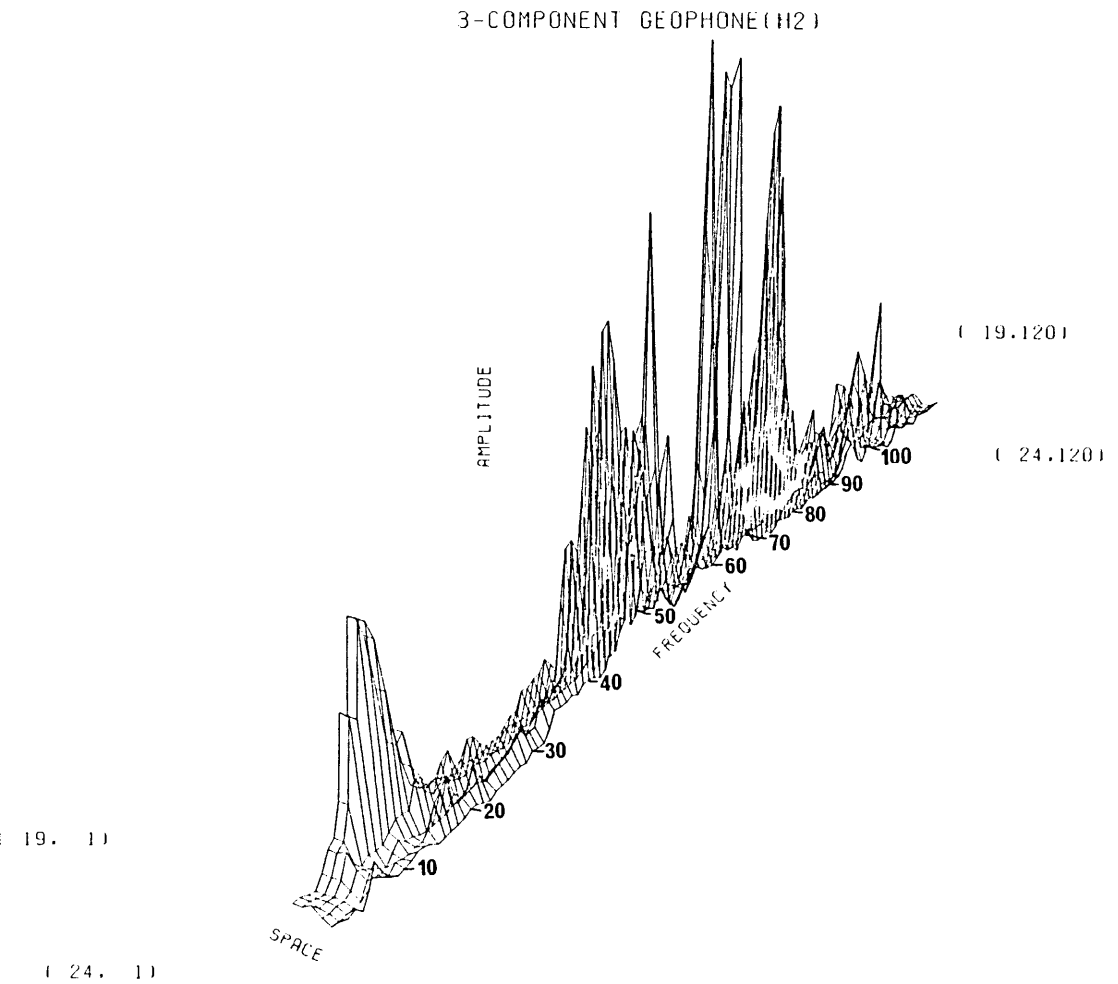

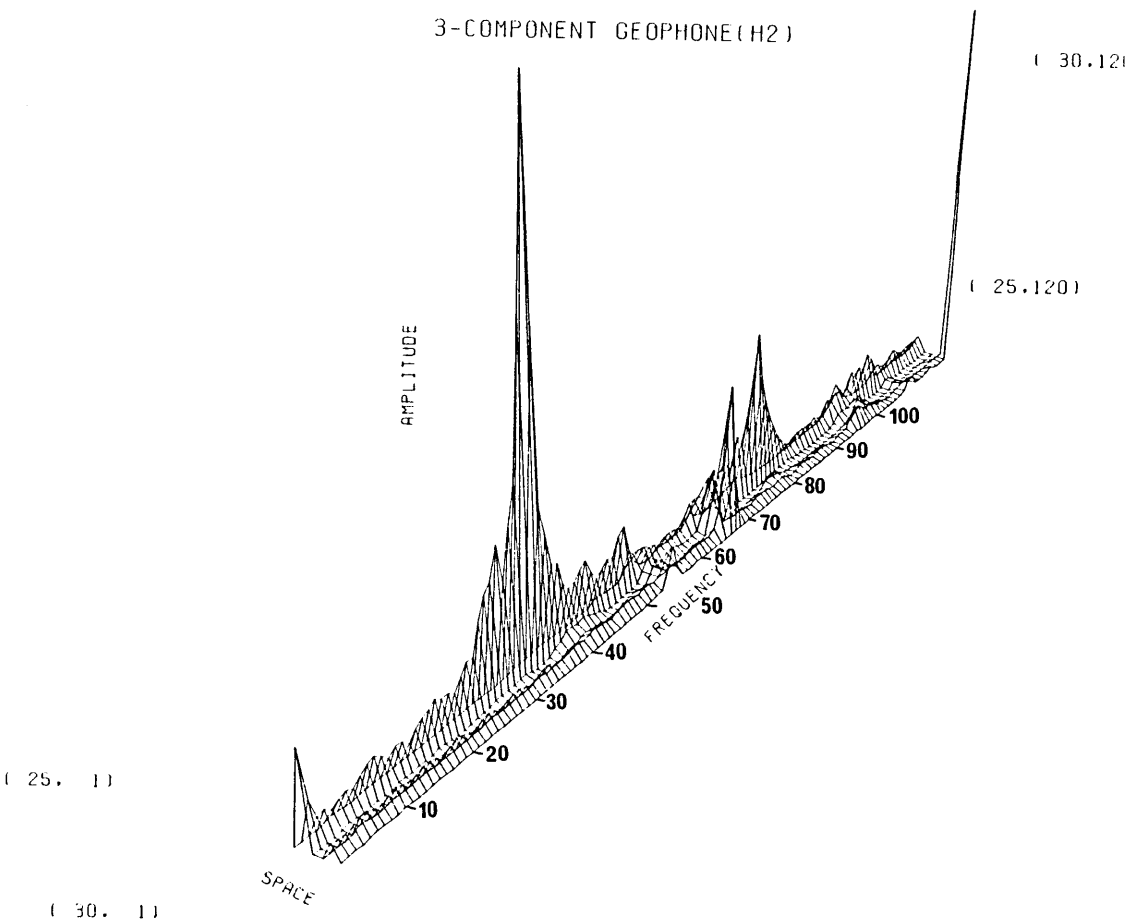

Figure A2.5 Geophone positions 19-24 and 25-30 for the tangential component

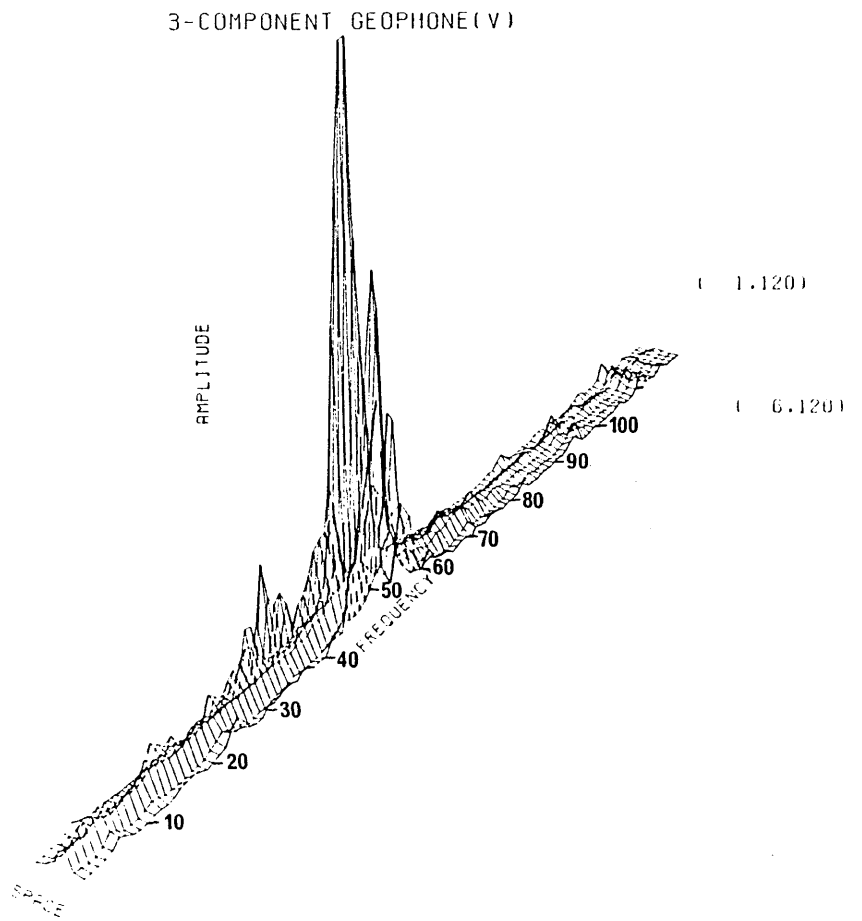

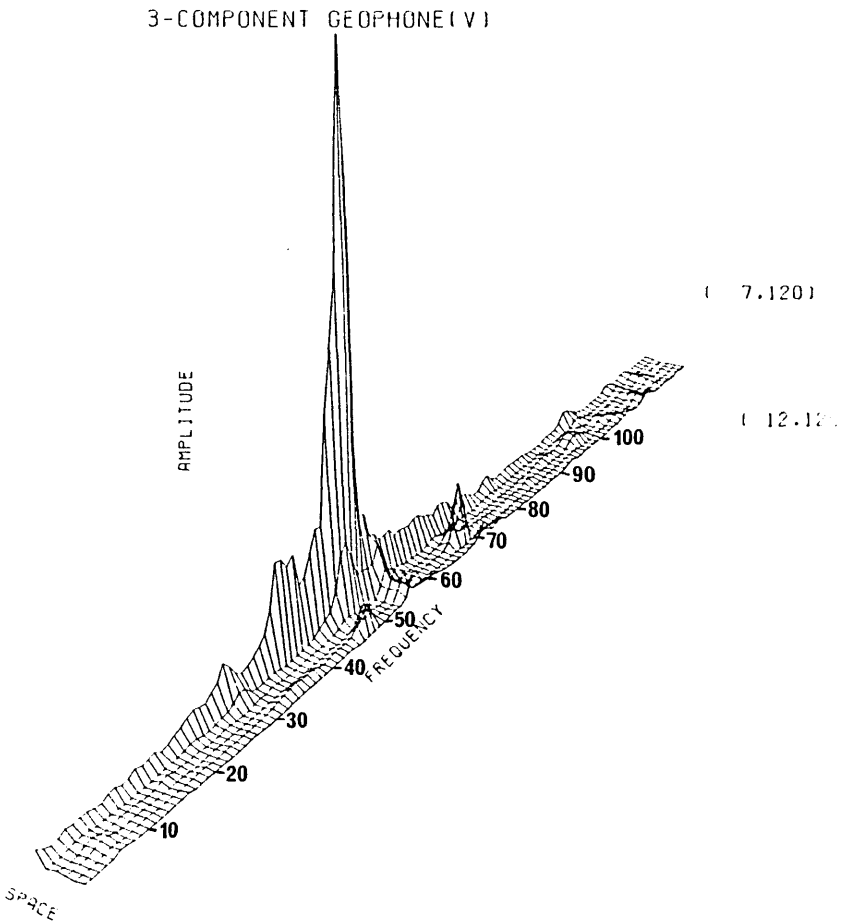

Figure A2.6 Geophone positions 1-6 and 7-12 for the vertical component

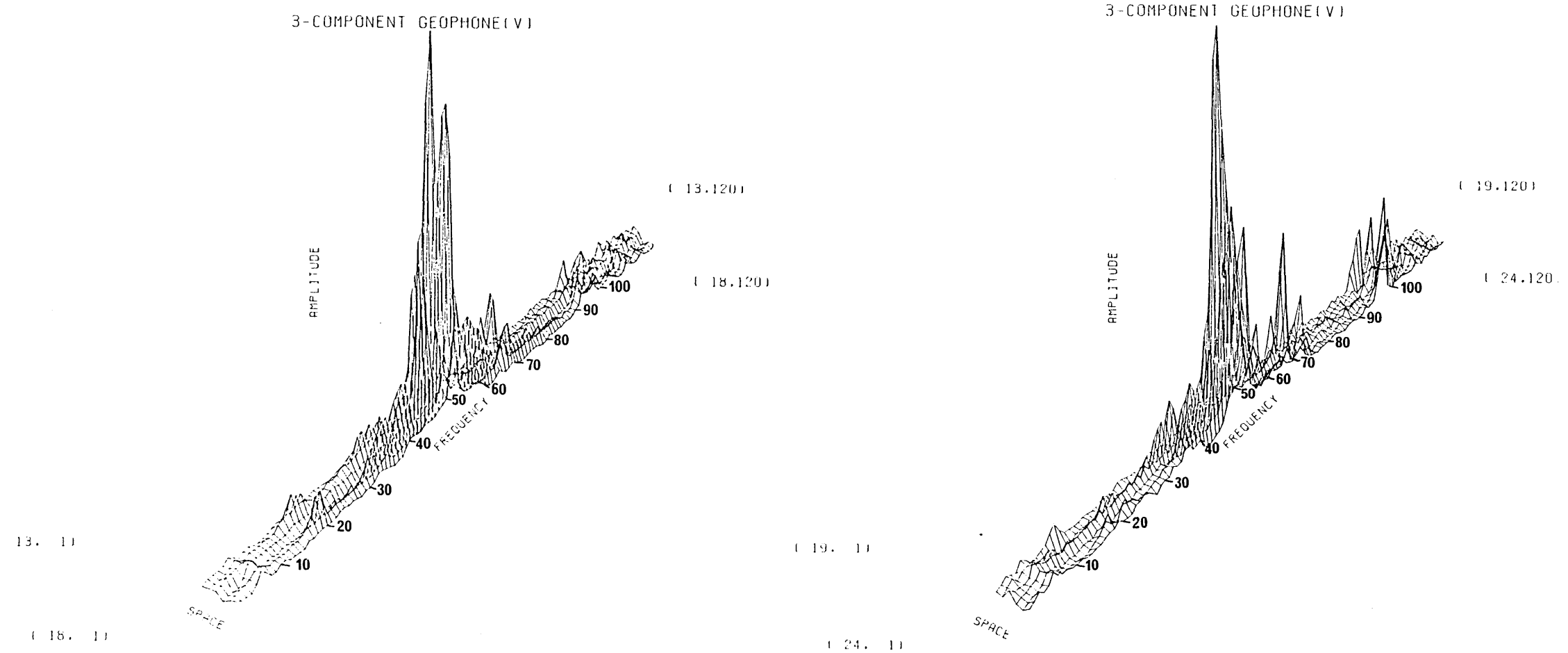

Figure A2.7 Geophone positions 13-18 and 19-24 for the vertical component

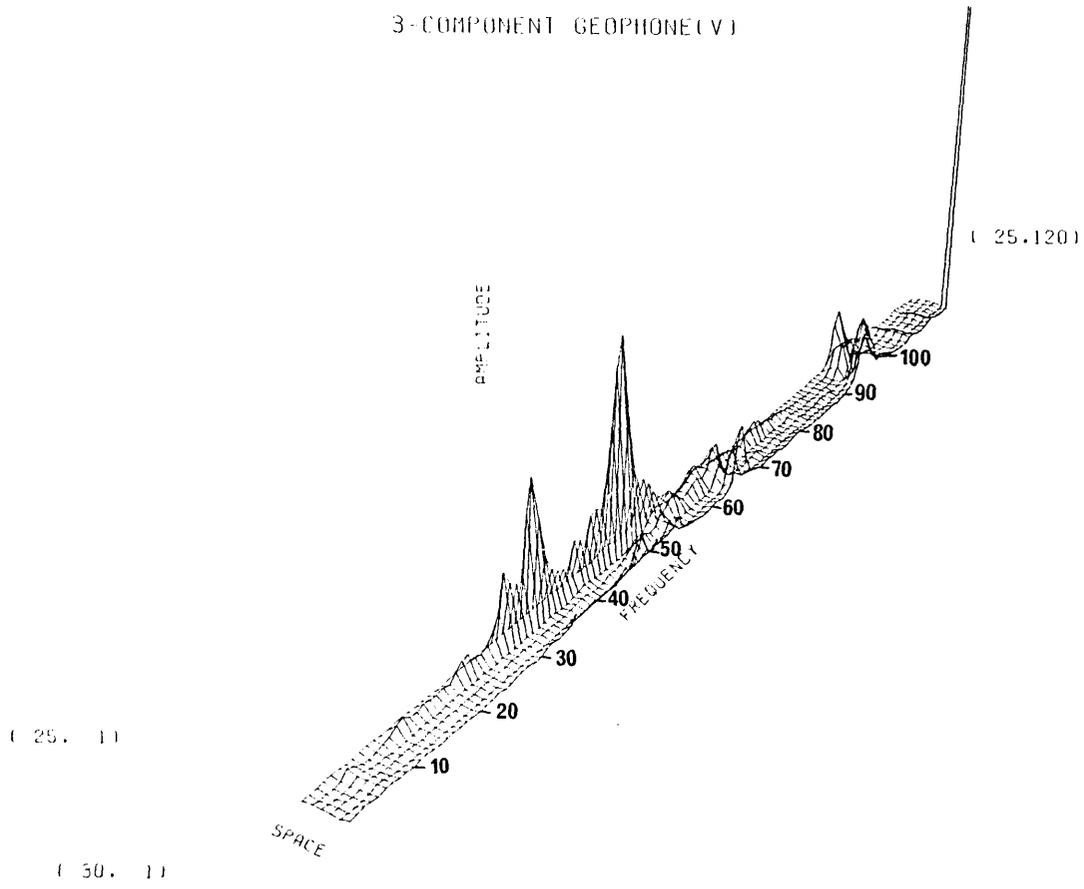

Figure A2.8 Geophone positions 25-30 for the vertical component

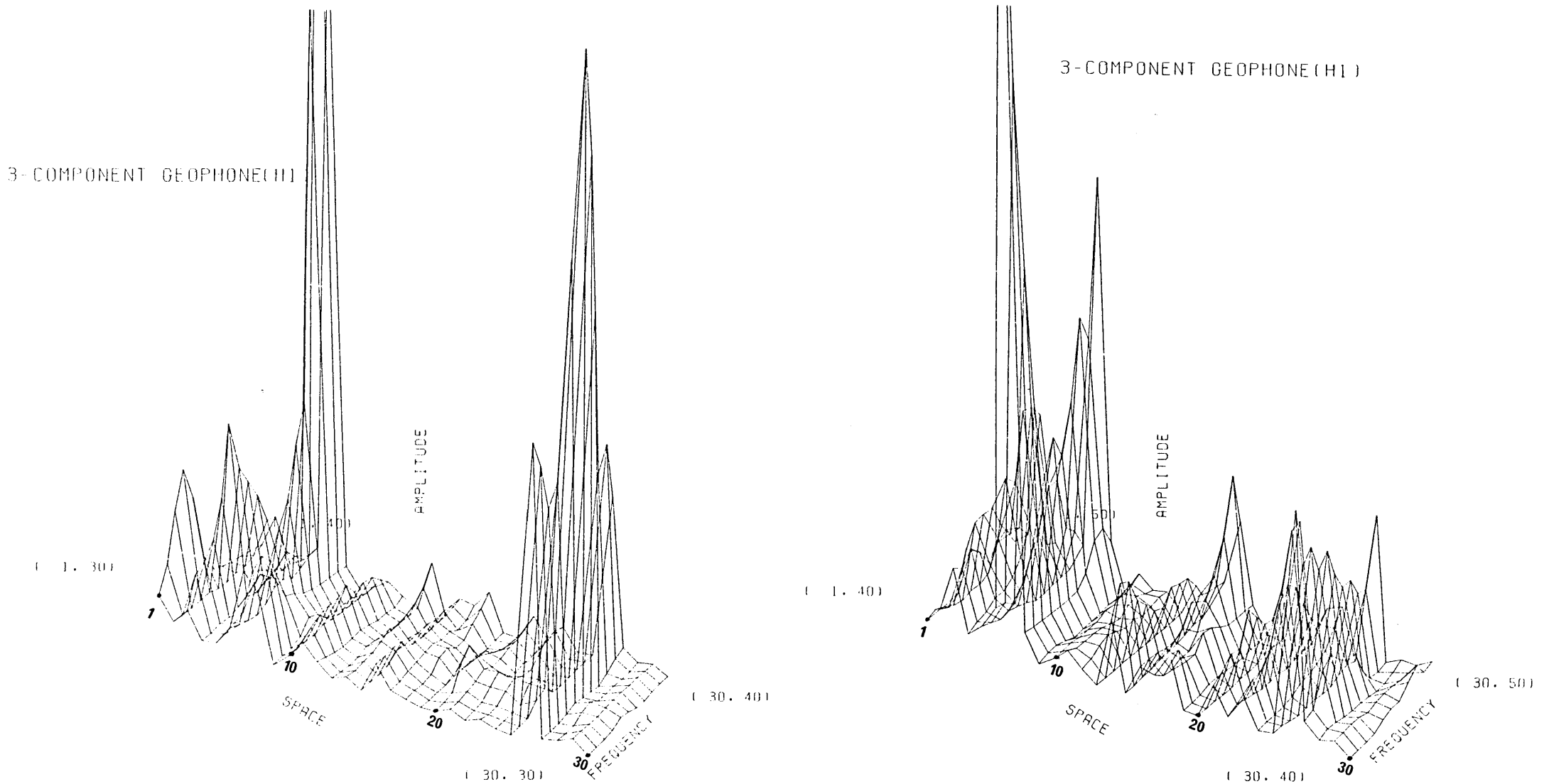

Figure A2.9 Frequencies 30-40 Hz and 40-50 Hz for the complete grid (radial)

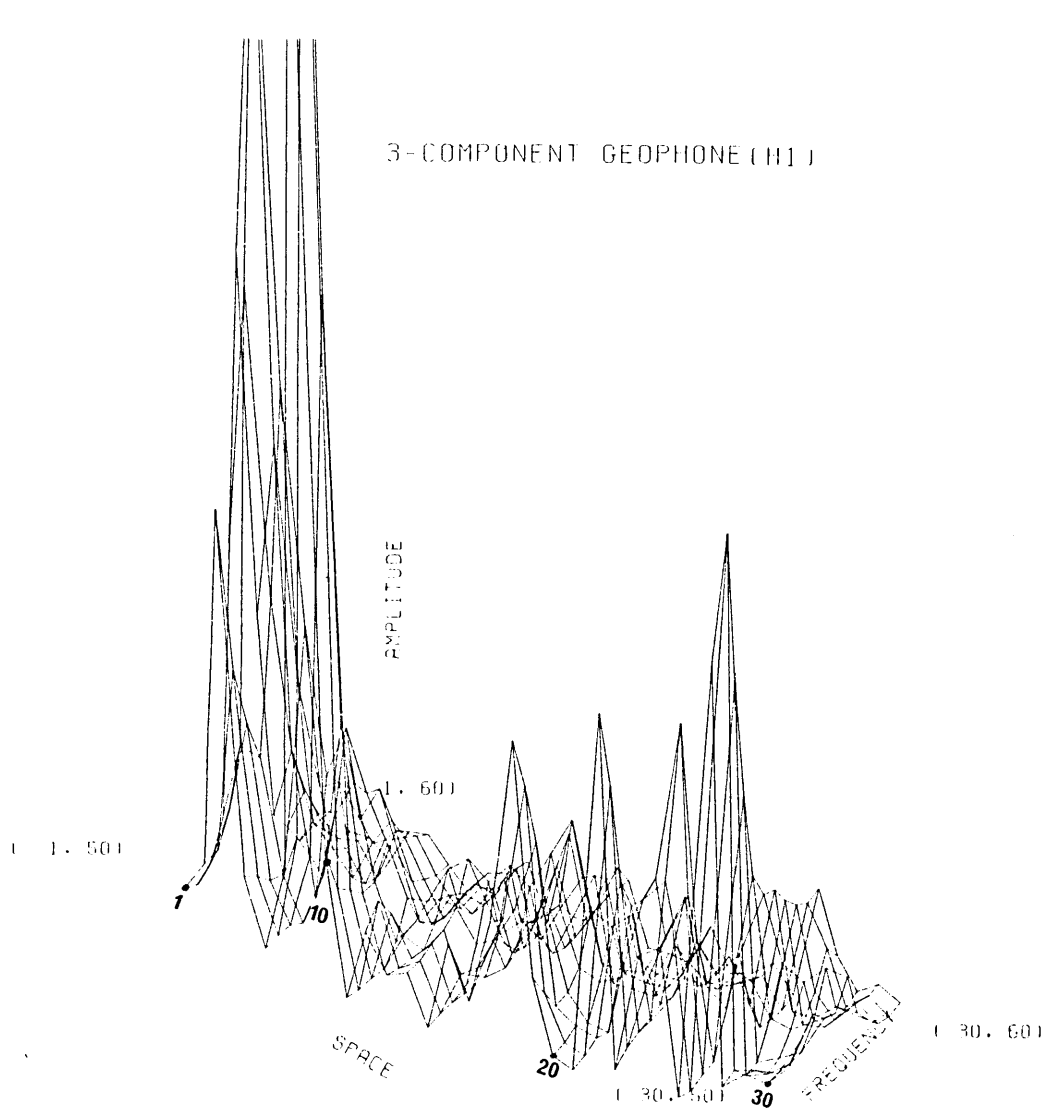

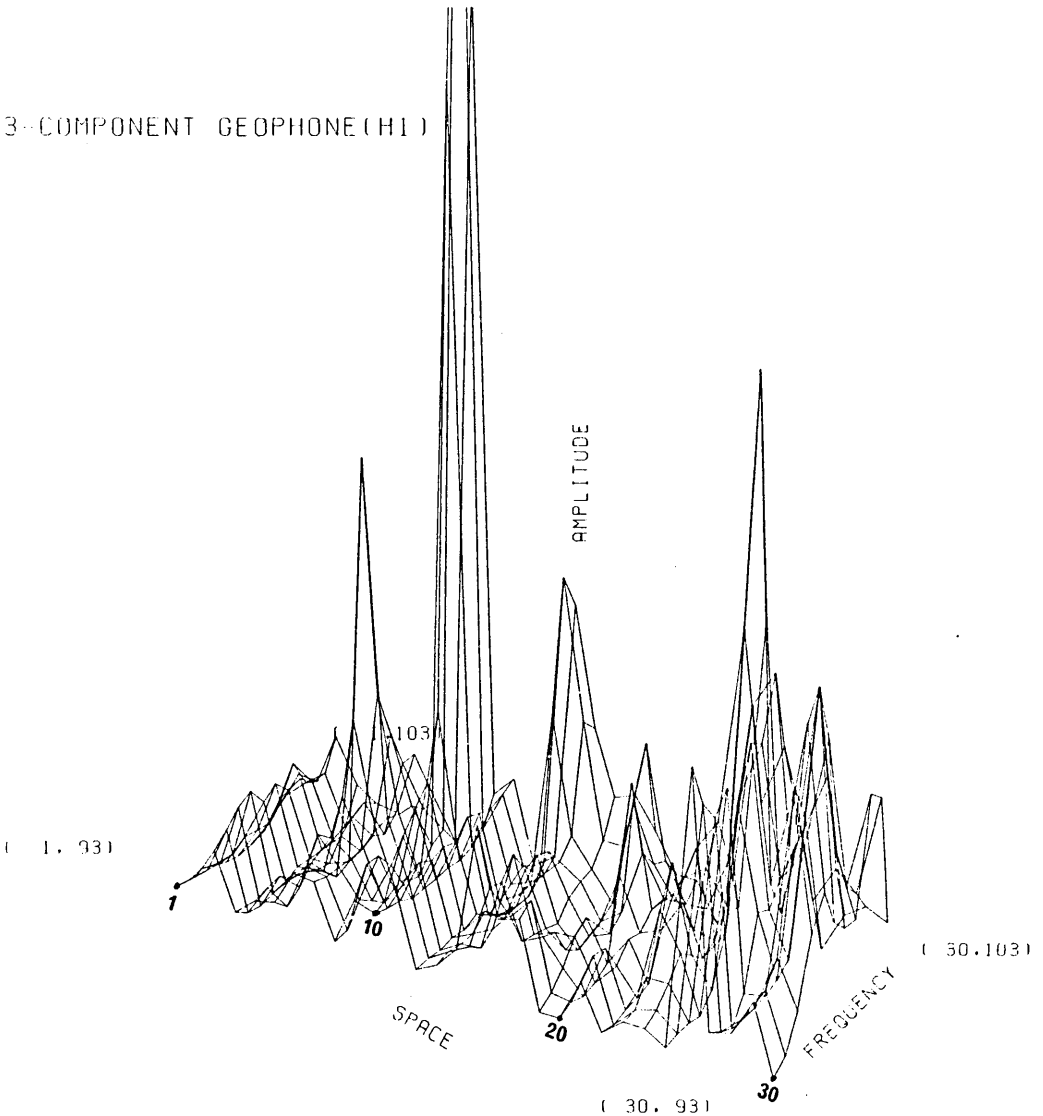

Figure A2.10 Frequencies 50-60 Hz and 93-103 Hz for the complete grid (radial)

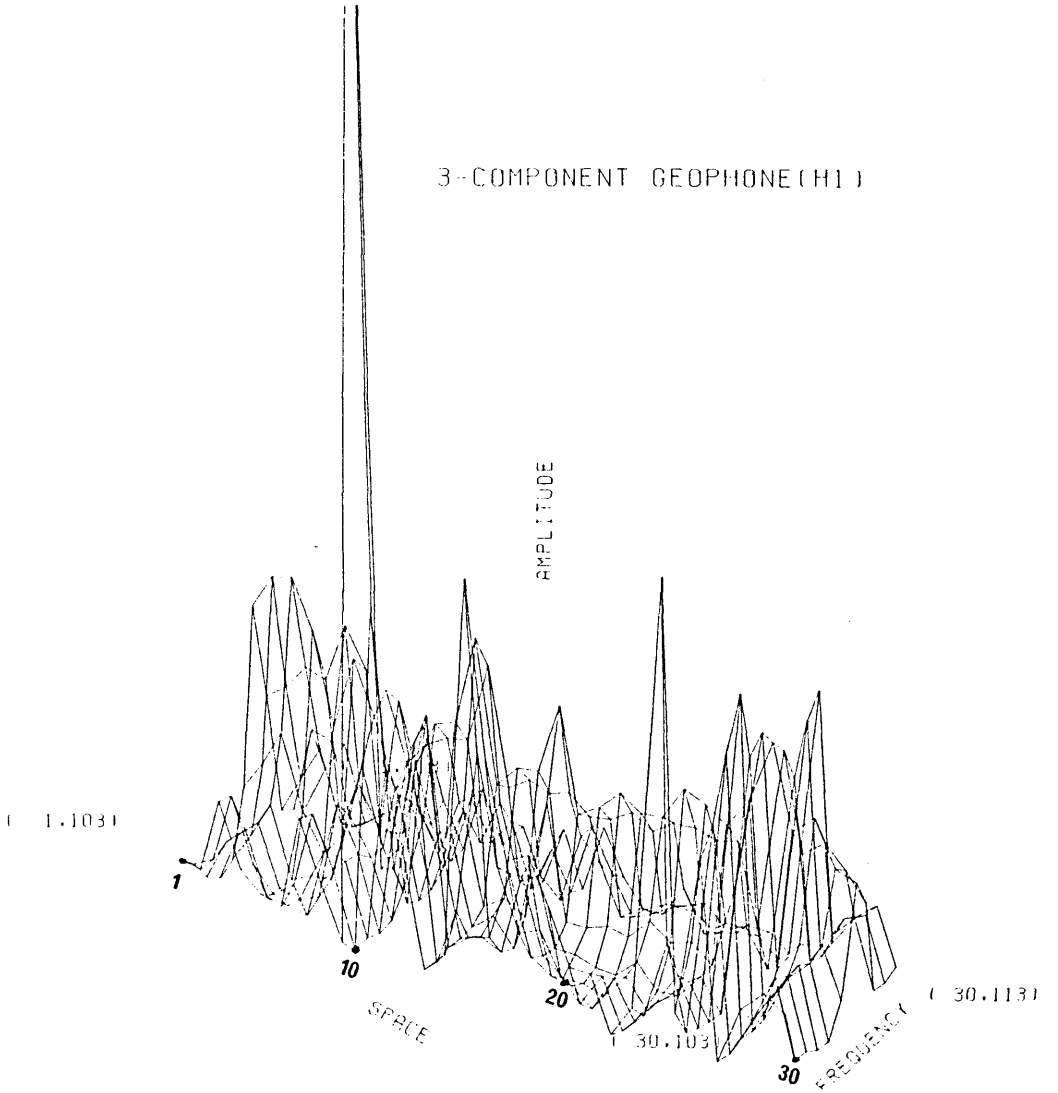

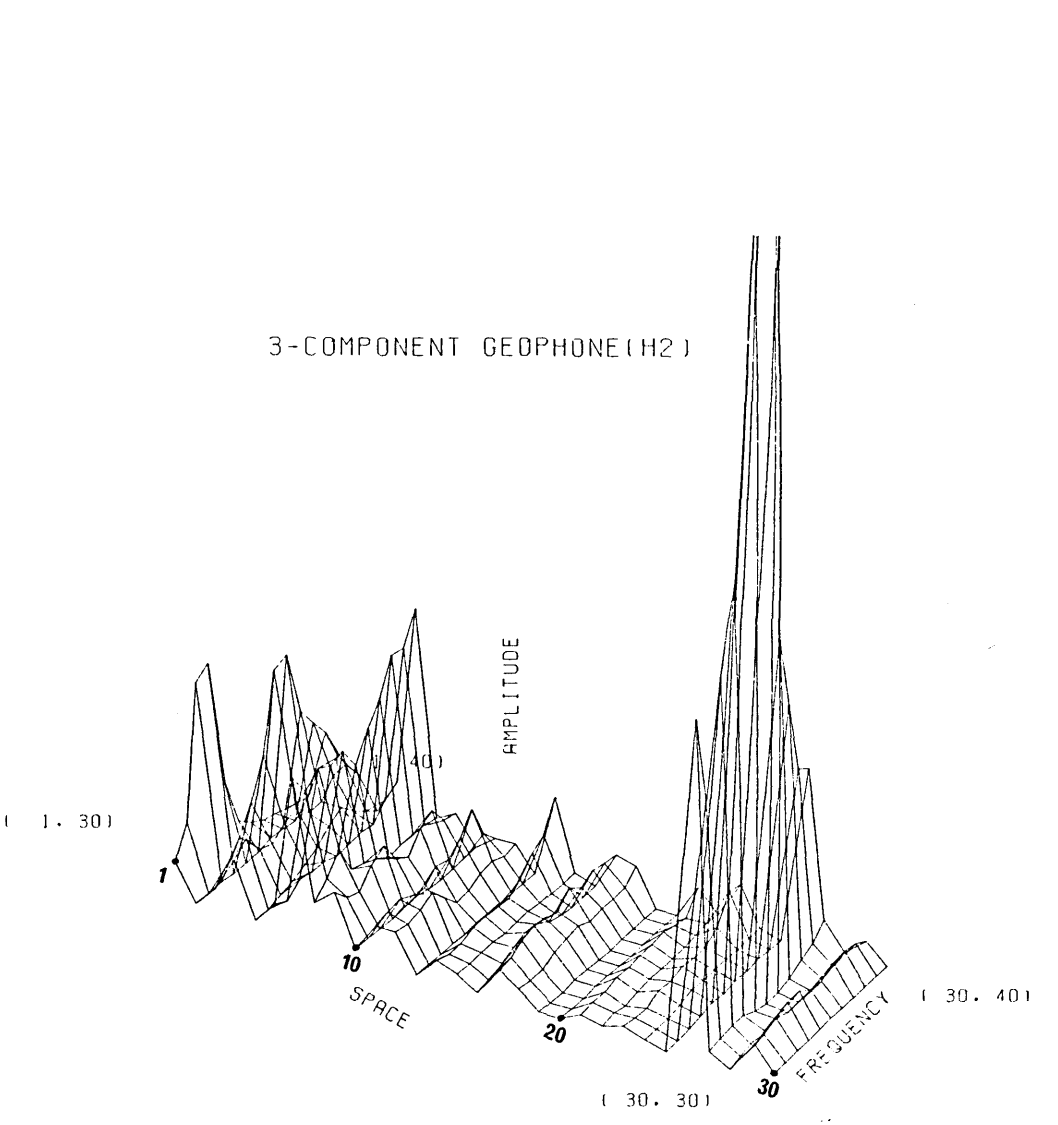

Figure A2.11 Frequencies 103-113 Hz (radial) and 30-40 Hz (tangential) for the complete grid

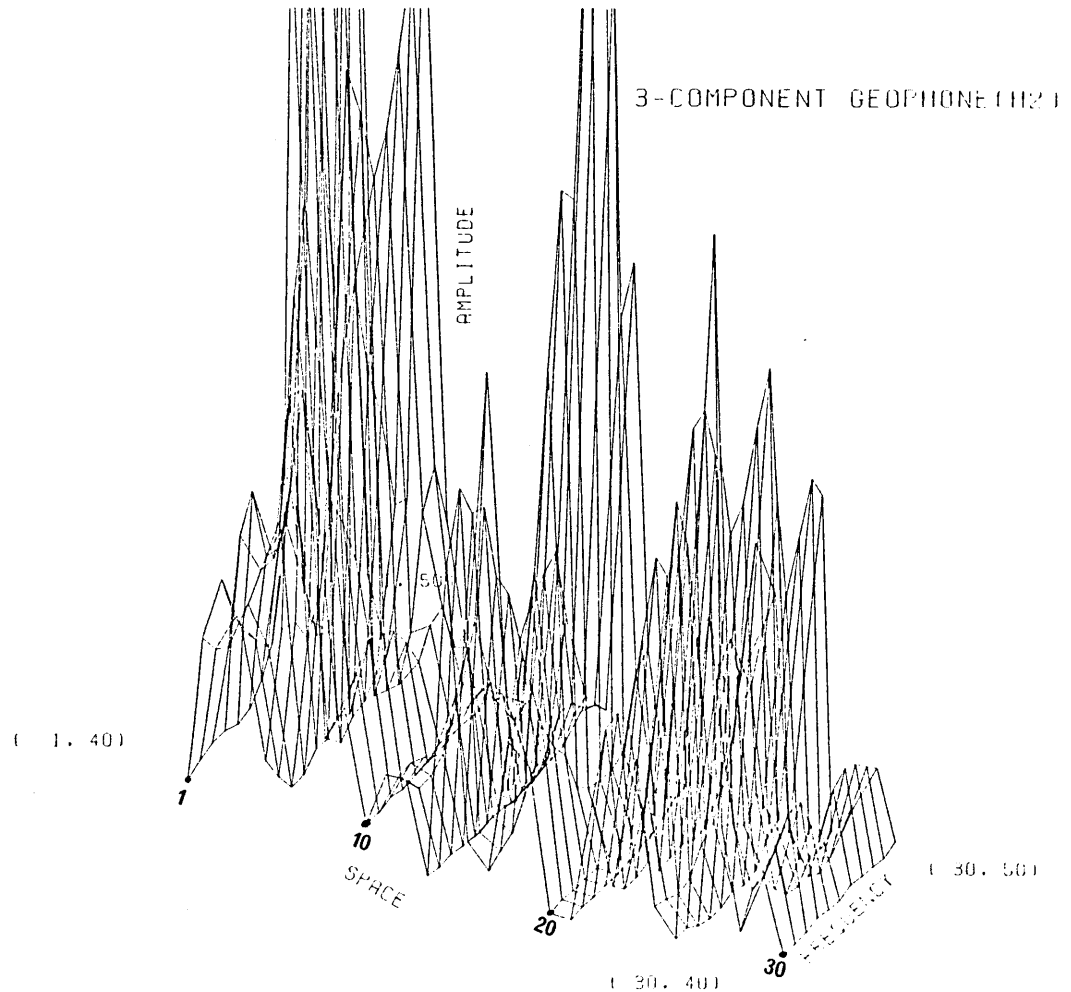

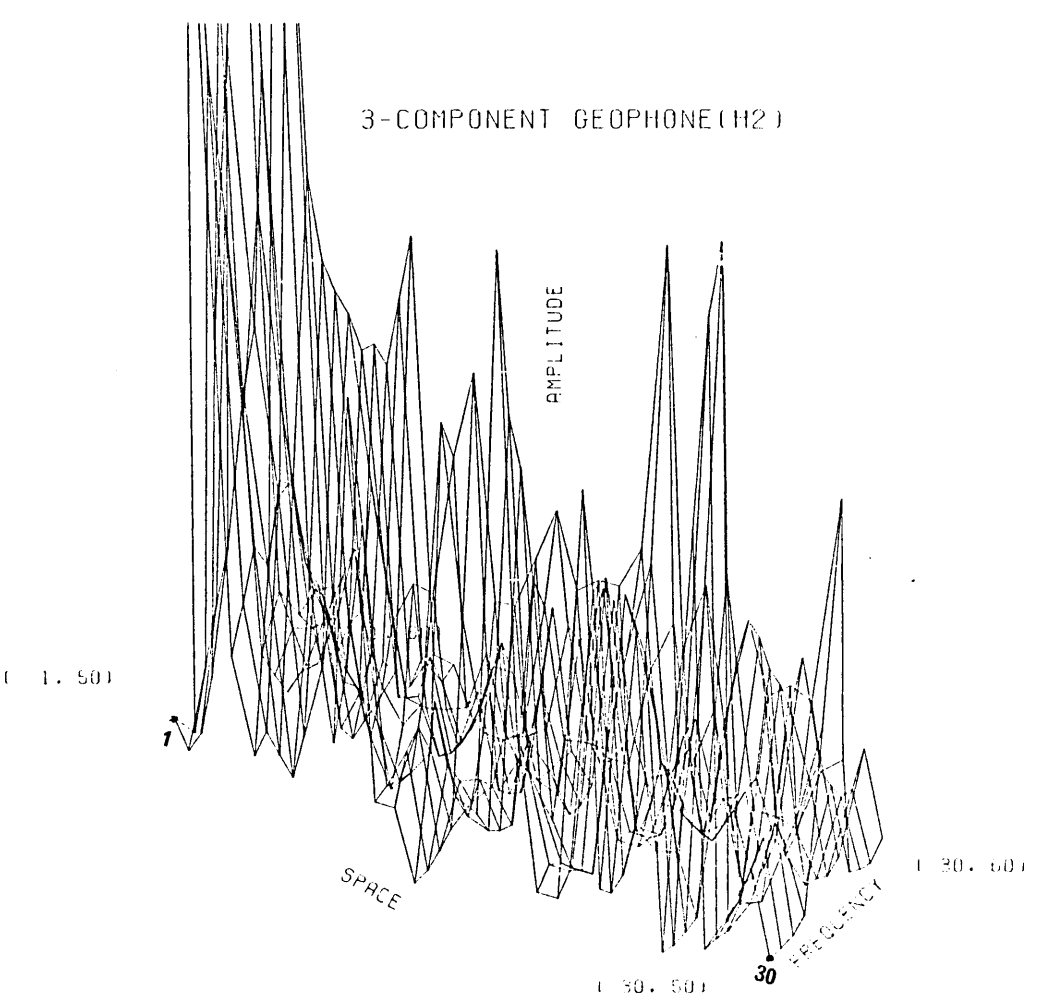

Figure A2.12 Frequencies 40-50 Hz and 50-60 Hz for the complete grid (tangential)

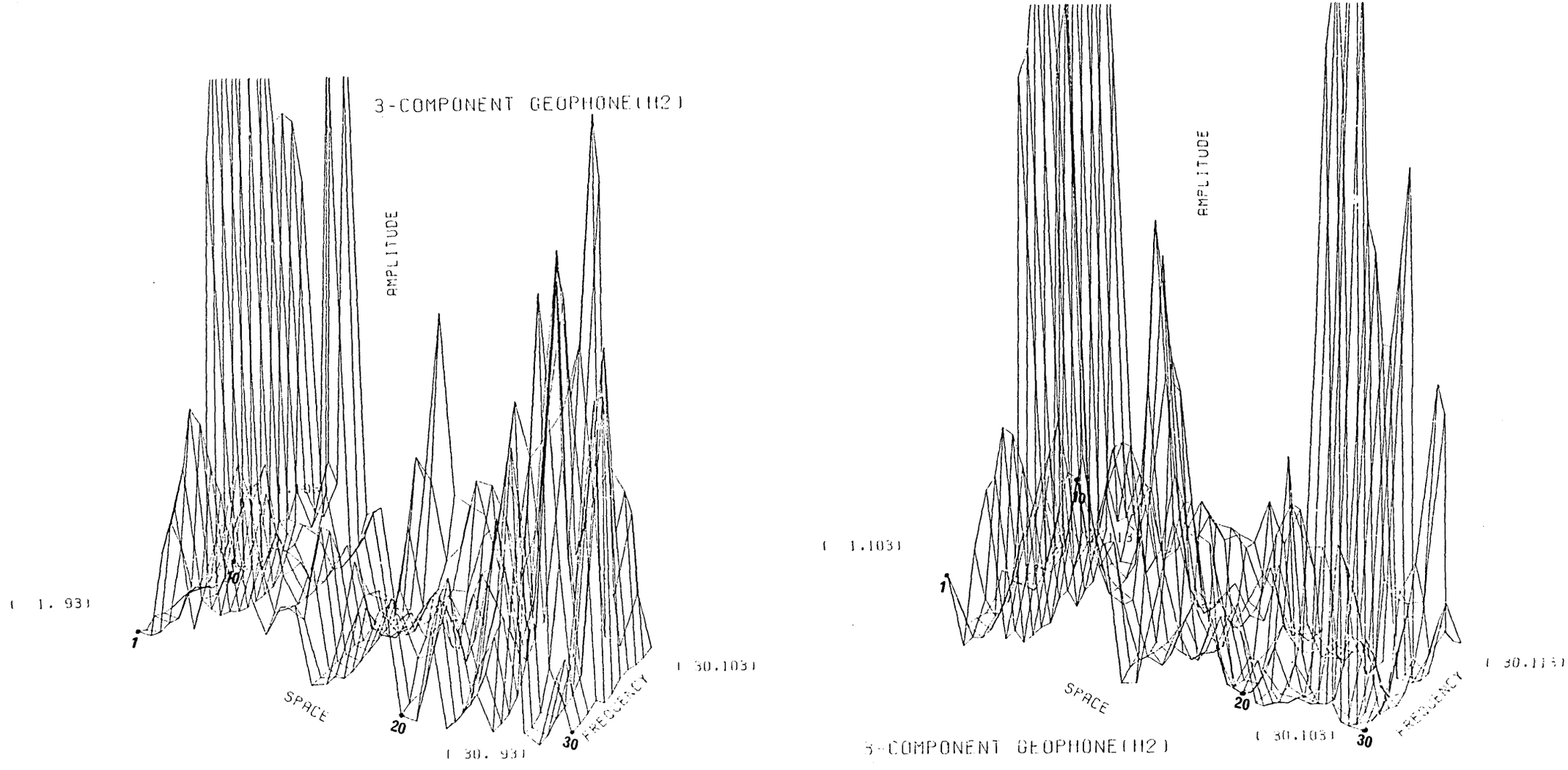

Figure A2.13 Frequencies 93-103 Hz and 103-113 Hz for the complete grid (tangential)

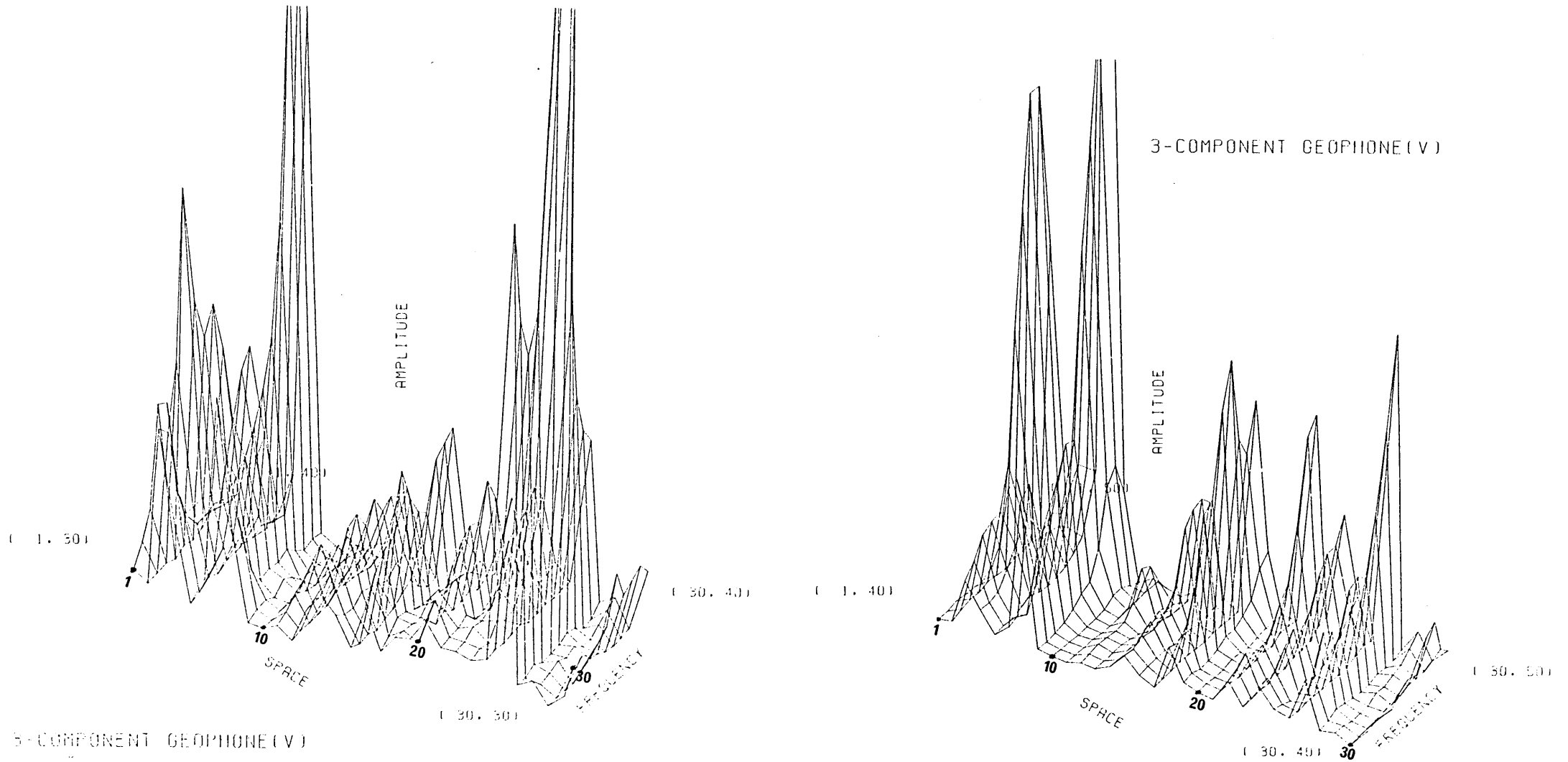

Figure A2.14 Frequencies 30-40 Hz and 40-50 Hz for the complete grid (vertical)

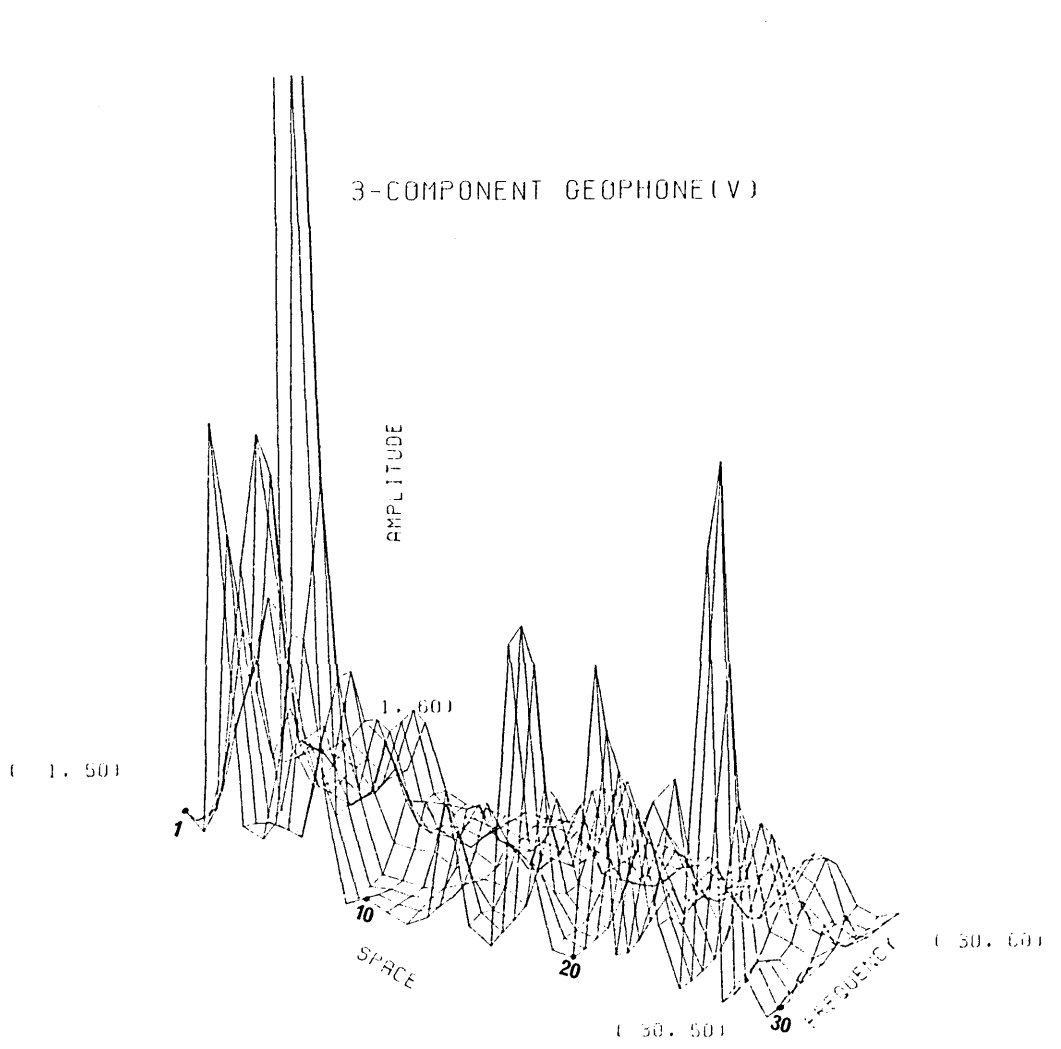

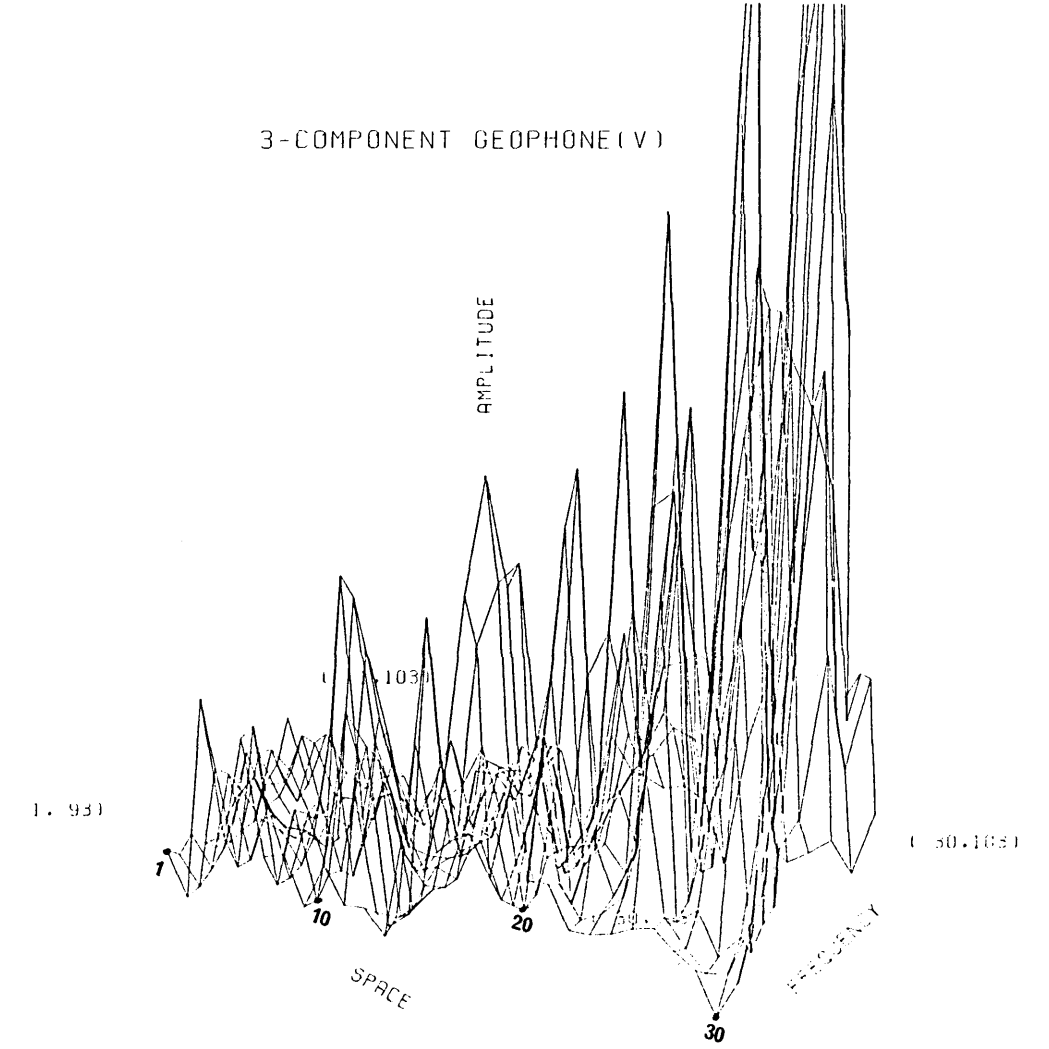

Figure A2.15 Frequencies 50-60 Hz and 93-103 Hz for the complete grid (vertical)

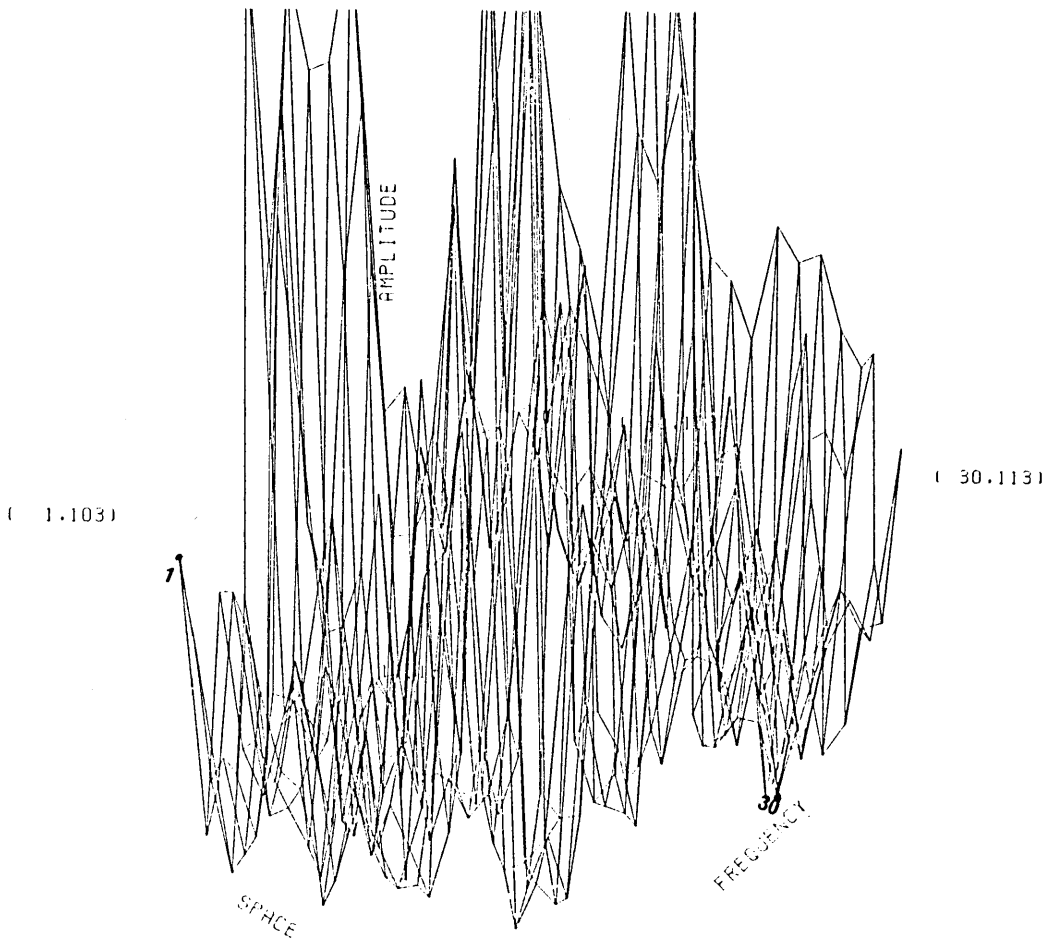

Figure A2.16 Frequencies 103-113 Hz for the complete grid (vertical)

REFERENCES

REFERENCES

Arnold, R. N. et. al. (1955)
Forced vibrations of a body on an infinite elastic solid.
J. Appl. Mechanics, 22, 391-400.

Baria, R. and McCann, D.M. (1977)
A study of borehole techniques for the detection of cavities in a rock mass.
Inst. Geol. Sci., Report 77/18.

Baria, R. et. al. (1978)
A study of tunnelling machine noise at Warrington for probing ahead of the tunnel.
Inst. Geol. Sci., Report 77/66.

Baria, R. et. al. (1978)
Assessment of rock mass conditions using geophysical techniques.
Inst. Geol. Sci., Report 78/8.

Bartlett, M. S. (1953)
An introduction to stochastic processes with special reference to methods and applications.
Cambridge Univ. Press, Cambridge.

Bartlett, M. S. and Mehdi, J. (1955)
On the efficiency of procedures for smoothing periodograms from time series with continuous spectra.
Biometrika, 42, 143-150.

Bates, E. R. (1973)
Detection of subsurface cavities.
Misc. paper S-73-40, U.S. Army Engineer Waterways Experimental Station, Vicksbury, Miss., U.S.A.

Bath, M. (1974)
Spectral analysis in geophysics.
Elsevier, Amsterdam.

Beauchamp, K. G. (1975)
Walsh functions and their applications.
Academic Press, London.

Bendat, J. S. and Piersol, A. G. (1971)
Random data: analysis and measurement procedures.
Wiley-Interscience, New York.

Beranek, L. L. (1954)
Acoustics.
McGraw-Hill, New York.

Bingham, C. et. al. (1967)
Modern techniques of power spectrum estimation.
I.E.E.E. Trans. Audio and Electroacoustics, AU-15, 56-66.

Biot, M. A. (1952)
Propagation of elastic waves in a cylindrical bore containing a fluid.
J. Appl. Phys., 23, 997-1005.

Bishop, C. (1977)
New civil engineer.
1st December, 16.

Blackman, R. B. and Tukey, J. W. (1958)
The measurement of power spectra from the point of view of communications engineering.
Dover, New York.

Bloxham, R. D. et. al. (1972)
Computer control for Imperial College engines development.
C.M.E., 19, 58-61.

Bolt, B. A. and Marussi, A. (1962)
Eigenvibrations of the earth observed at Trieste.
Geophys. J. Roy. Astron. Soc., 6, 299-311.

Booer, A. K. et. al. (1976)
Fault location by underground seismic survey.
Dept. of Electronic and Electrical Engng., Univ. College, London.

Borrodale, I. and Erickson, R. E. (1980)
Algorithms for least-squares linear prediction and maximum entropy spectral analysis -
Part I: Theory. Geophysics, 45, 420-432.
Part II: Fortran Program. Geophysics, 45, 433-446.

Bracewell, R. (1965)
The Fourier transform and its applications.
McGraw-Hill, New York.

Brekke, T. L. and Howard, T. R. (1972)
Stability problems caused by seams and faults.
Proc. First N. American rapid excavation and tunnelling conference, Chicago, 1, 25-41.

Bristow, C. (1966)
A new graphical resistivity technique for detecting air-filled cavities.
Studies in Speleology, 1, 204-226.

Buchanan, D. J. (1978)
The propagation of attenuated SH channel waves.
Geophys. Pros., 26, 16-28.

Burg, J. (1967)
Maximum entropy spectral analysis.
37th Annual Int. Meeting, Soc. of Explor. Geophys., Oklahoma City, Okla., Oct. 1967, presented paper.

Bycroft, G. N. (1956)
Forced vibrations of a rigid circular plate on a semi-infinite elastic space and on an elastic stratum.
Phil. Trans. Roy. Soc. Lond. A, 248, 327-368.

Champeney, D. C. (1973)
Fourier transforms and their physical applications.
Academic Press, London.

Chatfield, C. (1975)
The analysis of time series: theory and practice.
Chapman and Hall, London.

Clewell, D. H. and Simon, R. F. (1950)
Seismic wave propagation.
Geophysics, 15, 50-60.

Cochran, W. T. et. al. (1967)
What is the FFT?
I.E.E.E. Trans. Audio and Electroacoustics, AR-15, 45-55.

Colley, G. C. (1963)
The detection of caves by gravity measurements.
Geophys. Pros., 11, 1-9.

Collins, F. and Lee, C. C. (1956)
Seismic wave attenuation characterisitcs from pulse experiments.
Geophysics, 21, 16-40.

Cook, J. C. (1960)
Proposed monocycle-pulse VHF radar for airborne ice and snow measurement.
A.I.E.E. Comm. and Electronics, 51, 588-594.

Cook, J. C. (1964)
Progress in mapping underground solution cavities with seismic shear waves.
A.I.M.E. (mining), 229, 26-32.

Cook. J. C. (1965)
Seismic mapping of underground cavities using reflection amplitudes.
Geophysics, 30, 527-588.

Cook, J. C. (1970)
R. F. electrical properties of bituminous coal samples.
Geophysics, 35, 1079-1085.

Cook, J. C. (1972)
Seeing through rock with radar.
Proc. First N. American rapid excavation and tunnelling conference, Chicago, 1, 89-101.

Cook, J. C. (1974)
Status of ground-probing radar and some recent experience.
Proc. Eng. Found. Cont., Henniker, N. H., Am. Soc. Civil Engnrs., New York.

Cook, J. C. (1975)
Radar transparencies of mine and tunnel rocks.
Geophysics, 40, 865-885.

Cooper, D. W. et. al. (1974)
Remote profiling of lake ice thickness using a short pulse radar system aboard a C-47 aircraft.
Proc. I.E.E.E. Sympos. on Earth Environ. and Resources.

Cundall, P. (1971)
Measurement and analysis of acceleration in rock slopes.
Ph.D. Thesis, Imperial College, Univ. of London.

Dean, W. C. (1964)
Seismological applications of Laguerre expansions.
Bull. Seismol. Soc. Am., 54, 395-407.

Dieterich, J. H. and Decker, R. W. (1975)
Finite element modelling association with volcanism.
J.G.R., 80, 4094-4103.

Dix, C. H. (1955)
Seismic velocities from surface measurements.
Geophysics, 20, 68-86.

Dolphin, L. T. et. al. (1978)
Radar probing of Victoria Peak, New Mexico.
Geophysics, 43, 1441-1448.

Dowding, C. H. (1976)
Comparison of predicted and encountered geology for seven Colorado tunnels.
Proc. Third rapid excavation and tunnelling conference, Las Vegas, U.S.A.

Edelmann, H. (1966)
New filtering methods with vibroseis.
Geophys. Pros., 14, 456-469.

Erickson, E. L. et. al. (1968)
Shear-wave recording using continuous signal methods part 2 - later experimentation.
Geophysics, 33, 240-254.

Evison, F. F. (1952)
The inadequacy of the standard seismic techniques for shallow surveying.
Geophysics, 17, 867-875.

Evison, F. F. (1956)
Seismic waves from a transducer at the surface of stratified ground.
Geophysics, 21, 939-959.

Evison, F. F. (1957)
The pulsed vibrator as a seismic source.
Geophys. Pros., 5, 381-391.

Farr, J. B. (1968)
Earth holography, a potential new seismic method.
38th meeting S.E.G., Denver, Colorado. Presented paper.

Fitzpatrick, G. L. (1977)
Subsurface cavity detection using acoustic holography and related techniques.
Symp. on detection of subsurface cavities, Vicksburg, Miss. Presented paper.

Freystatter, S. and Dresen, L. (1978)
The influence of obliquely dipping discontinuities on the use of Rayleigh channel waves for the in-seam seismic reflection method.
Geophys. Pros., 26, 1-15.

Godson, R. H. and Watkins, J. S. (1968)
Seismic resonance investigation of a near-surface cavity in Anchor reservoir, Wyoming.
Bull. Assoc. Engng. Geol., 5, 27-36.

Goelen, P. (1973)
Sinkholes and subsidence, engineering geological problems related to soluble rock.
Symp. Int. Assoc. Engng. Geol., Hanover, Germany.

Goupillaud, P. L. (1976)
Signal design in the vibroseis technique.
Geophysics, 41, 1291-1304.

Green, A. S. P. (1976)
Geophysical properties of selected rock samples from a borehole in Cocking, W. Sussex.
Inst. Geol. Sci., Report No. 96.

Gubbins, D. et. al. (1971)
Two-dimensional digital filtering with Haar and Walsh transforms.
Ann. Geophys., 27, 85-104.

Harding, J. C. et. al. (1975)
Drilling and preparation of reusable long range horizontal boreholes in rock and gouge.
FHWA-RD-75-95, 96, 97.

Hermont, A. J. (1969)
Is seismic energy of diagnostic value?
Geophysics, 34, 196-212.

Hoover, G. M. (1972)
Acoustical holography using digital processing.
Geophysics, 37, 1-19.

Horton, C. W. (1959)
A loss mechanism for the Pierre shale.
Geophysics, 24, 667-680.

Howell Jr., B. F. and Budenstein, D. (1955)
Energy distribution in explosion-generated seismic pulses.
Geophysics, 20, 33-52.

Howell Jr., B. F. and Kaukonen, E. K. (1954)
Attenuation of seismic waves near an explosion.
Bull. Seismol. Soc. Am., 44, 481-491.

Howell, L. G. et. al. (1953)
Gulf coast surface waves.
Geophysics, 18, 41-53.

Howell, L. G. et. al. (1940)
Propagation of elastic waves in the earth.
Geophysics, 5, 1-14.

I.E.E.E.
I.E.E.E. Trans. Audio and Electroacoustics, AU-15, June 1967; Au-17 June 1969.

Jardetsky, W. S. and Press, F. (1952)
Rayleigh wave coupling to atmospheric compressional waves.
Bull. Seismol. Soc. Am., 42, 135-144.

Jenkins, G. M. (1961)
General considerations in the analysis of spectra.
Technometrics, 3, 133-166.

Jenkins, G. M. and Watts, D. G. (1969)
Spectral analysis and its applications.
Holden-Day, San Francisco.

Jones, R. H. (1965)
A reappraisal of the periodogram in spectral analysis.
Technometrics, 7, 531-542

Kalra, A. K. (1976)
Wavefront reconstruction method for geophysical exploration.
Geoexploration, 14, 107-123.

Karus, E. V. (1958)
The absorption of elastic vibrations in rocks during stationary excitation.
Bull. Acad. Sci. USSR, Geophys. Ser. (English Transl.), 249-254.

Kennedy, J. M. (1968)
A microwave radiometric study of buried Karst topography.
Geol. Soc. Am. Bull., 79, 735-742.

Knopoff, L. (1964)
Q
Reviews Geophys., 2, 625-660.

Krey, Th. (1969)
Remarks on the signal to noise ratio in the Vibroseis system.
Geophys. Pros., 17, 206-218.

Labreche, D. A. et. al. (1976)
Decision analysis applied to rock tunnel exploration.
Proc. 17th U.S. Symp. Rock. Mech., Snowbird, U.S.A. 5A2-1 - 5A2-8.

Lange, A. L. (1965)
Cave detection by magnetic surveys.
Cave Notes, 7, 41-54.

Levin, F. K. and Robinson, D. J. (1969)
Scattering by a random field of surface scatterers.
Geophysics, 34, 170-179.

Lighthill, M. J. (1959)
An introduction to Fourier analysis and generalized functions.
Cambridge Univ. Press, Cambridge.

Lidner, E. et. al. (1975)
Exploration: its evaluation in hard rock tunnelling.
Proc. 16th Symp. Rock Mech., Minneapolis, U.S.A., 205-216.

Lyons, T. R. (1976)
Remote sensing experiments in cultural resource studies.
Reports of Chaco Centre, No. 1, National Park Serv., U.S. Dept. Interior, and Univ. New Mexico, Alburquerque.

Lytle, R. J. et. al. (1979)
Cross-borehole electromagnetic probing to locate high contrast anomalies.
Geophysics, 44, 1667-1676.

Majtenyi, S. I. (1976)
Horizontal site investigation systems.
Proc. Rapid Excavation and Tunnelling Conf., Las Vegas, U.S.A., 3, 64-80.

Matthew, R. B. (1974)
E.L.F. magnetotelluric studies in S.W. England.
Ph.D. Thesis, Imperial College, Univ. of London.

Maxwell, G. M. (1976)
Old mine shafts and their location by geophysical surveying.
Quart. J. Engng. Geol., 9, 283-290.

Meissner, R. (1961)
Wave-front diagrams from uphole shooting.
Geophys. Pros., 9, 553-543.

Merritt, A. H. (1972)
Geologic predictions for underground excavations.
Proc. 1st N. American Rapid Excavation and Tunnelling Conf., Chicago, 1, 115-132.

Miles, J. W. (1960)
Scattering of elastic waves by small inhomogeneities.
Geophysics, 25, 642-648.

Miller, G. F. and Pursey, H. (1954)
The field and radiation impedance of mechanical radiators on the free surface of a semi-infinite isotropic solid.
Proc. Roy. Soc. Lond. A, 223, 521-541.

Miller, G. F. and Pursey, H. (1955)
On the partition of energy between elastic waves in a semi-infinite solid.
Proc. Roy. Soc. Lond. A, 223, 55-69.

Moffat, D. L. and Peters Jr., L. (1972)
An electromagnetic pulse hazard detection system.
Proc. 1st N. American Rapid Excavation and Tunnelling Conf., Chicago, 1, 235-255.

Moffat, D. L. and Puskar, R. J. (1976)
A subsurface electromagnetic pulse radar.
Geophysics, 41, 506-518.

Mooney, H. M. (1976)
Shallow reflection seismology.
Dept. Geology, Univ. Minnesota, Minneapolis, U.S.A.

Mooney, H. M. and Kaasa, R. A. (1962)
Air waves in engineering seismology.
Geophys. Pros., 10, 84-92.

Munk, W. H. et. al. (1959)
Spectra of low-frequency ocean waves.
Bull. Scripts. Inst. Oceanogr., Univ. Calif., 7, 283-362.

McCann, D. M. et. al. (1975)
Inter-borehole acoustic measurements and their use in engineering geology.
Geophys. Pros., 23, 83-95.

McDonal, F. J. et. al. (1958)
Attenuation of shear and compressional waves in Pierre shale.
Geophysics, 23, 421-439.

Neumann, R. (1967)
Le gravimetric de haute precision application aux recherches de cavities.
Geophys. Prosp., 15, 116-134.

Neumann, R. (1973)
Sinkholes and subsidence engineering geological problems related to soluble rock.
Symp. Int. Assoc. Eng. Geol., Hanover, Germany.

New, B. M. (1978)
The effects of ground vibration during bentonite shield tunnelling at Warrington.
TRRL, Laboratory Report 860.

Newbury, J. and Davenport, C. A. (1975)
Geotechnical aspects of shallow sewer tunnels in urban areas.
Quart. J. Engng. Geol., 8, 271-289.

O'Brien, P. N. S. (1957)
The variation with distance of the amplitude of critically refracted waves.
Geophys. Prosp., 5, 300-314.

Olhovich, V. A. (1964)
The causes of noise in seismic reflection and refraction work.
Geophysics, 29, 1015-1030.

Palmer, L. S. (1954)
Location of subterranean cavities by geoelectrical methods.
Mining Mag., 91, 137-141.

Peck, R. B. et. al. (1972)
State of the art of soft-ground tunnelling.
Proc. 1st N. American Rapid Excavation and Tunnelling Conf., Chicago, 1, 259-286.

Peters, L. (1976)
Proc. ARPA tunnel detection technology conf., Stanford Research Inst., Menlo Park, U.S.A.

Press, F. and Ewing, M. (1951)
Ground roll coupling to atmospheric compressional waves.
Geophysics, 16, 416-430.

Rayleigh, Lord (1871)
On the light from the sky.
Phil. Mag., 41, 107-127.

Rechtien, R. D. and Stewart, D. M. (1975)
A seismic investigation over a near-surface cavern.
Geoexploration, 13, 235-246.

Reed, J. W. (1971)
Low-frequency periodicities in Panama rainfall run-off.
J. Appl. Meteorol., 10, 666-673.

Richer, K. A. (1970)
Comments on, "A microwave radiometric study of buried karst topography".
Geol. Soc. Am. Bull., 81, 585-587.

Rietsch, E. (1977)
Vibroseis signals with prescribed power spectrum.
Geophys. Pros., 25, 613-620.

Riggs, E. D. (1955)
Seismic wave types in a borehole.
Geophysics, 20, 53-67.

Robinson, E. A. (1967)
Multichannel time series analysis with digital computer programs.
Holden-Day, San Francisco.

Rockwell, D. W. (1967)
A general wavefront method.
Seismic Refr. Pros., Musgrave, ed., Tulsa, S.E.G., 363-415.

Samson, C. (1979)
The location of subterranean cavities by geophysical prospection.
M. A. Dissertation, Univ. of Sheffield.

Sato, R. (1967)
Attenuation of seismic waves.
J. Phys. of the Earth, 15, 32-61.

Sedov, B. M. (1977)
Experimental data on the mutual conversion of longitudinal and surface waves.
Izvestiya, Earth Physics, 12, 540-543.

Snowdowne, J. B. (1968)
A gravity survey for the detection of incipient sinkholes beneath a proposed building site.
M.Sc. Thesis, Imperial College, Univ. of London.

Solodovnikov, V. V. (1960)
Introduction to the statistical dynamics of automatic control systems.
Dover, New York.

Speed, R. C. (1973)
Third Symp. on Salt., 2, 367-378.

Sturgeon, L. J. (1975)
The location of subsurface cavities by geophysical methods.
M.Sc. Thesis, Imperial College, Univ. of London.

Symposium - on detection of subsurface cavities. 12-15 July, 1977.
U.S. Army Engineer Waterways Experimental Station, Vicksburg, Mississippi, U.S.A.

Tarantolo Jr., P. J. and Unterberger, R. R. (1978)
Radar detection of boreholes in advance of mining.
Geophys. Pros., 26, 359-382.

Telford, et. al. (1976)
Applied Geophysics.
Cambridge Univ. Press, Cambridge.

Terzaghi, K. (1943)
Theoretical soil mechanics.
Wiley-Interscience, New York.

Thapar, M. R. (1972)
Laboratory measurements of spatial Q, wave velocities, attenuation of Rayleigh waves with distance and depth.
Pure Appl. Geophys., 94, 5-14.

Transport and Road Research Laboratory (1975)
Probing ahead for tunnels: a review of present methods and recommendations for research.
Supplementary Report 171UC.

Tratman, E. K. et. al. (1974)
Geoelectrical survey and excavation, Pen Park Hole, Bristol.
Cave Research Group, No. 12, 1-54.

Ulrych, T. J. and Bishop, T. N. (1975)
Maximum entropy spectral analysis and autoregressive decomposition.
Rev. Geophys., 13, 183-200.

Unterberger, R. R. (1978)
Radar propagation in rock salt.
Geophys. Pros., 26, 312-328.

Wahlstrom, E. E. (1974)
Tunnelling in rock
Elsevier, Amsterdam.

Waller, D. R. (1972)
Geophysical report on the DHSS rehabilitation centre, Stormy Down, Glamorgan.
Geophys. Div., George Wimpey and Co. Ltd.

Walsh, T. and Briggart, A. R. (1976)
The bentonite tunnelling machine at Warrington.
Tunnelling '76, Int. Symp. on Tunnelling, Inst. of Min. and Metall., M. J. Jones (ed.).

Warburton, G. B. (1957)
Forced vibration of a body on an elastic stratum.
J. Appl. Mechanics, 24, 55-58.

Ward, R. W. and Hewitt, M. R. (1977)
Monofrequency borehole traveltime survey.
Geophysics, 42,. 1137-1145.

Wardell, J. (1970)
A comparison of land seismic sources.
Geoexploration, 8, 205-229.

Watkins, J. S. et. al. (1967)
Seismic detection of near-surface cavities.
U.S. Geol. Surv., Prof. Pap. 599-A.

Watts, R. et. al. (1974)
Radio echo sounding of temperate glaciers at frequencies of 1 MHz and 5MHz.
Proc. Symp. on Remote Sensing in Glaciology, Scott Polar Inst., Cambridge, England.

Williamson, T. N. and Schmidt, R. L. (1972)
Probe drilling for rapid tunnelling.
Proc., 1st N. American Rapid Excavation and Tunnelling Conf., Chicago, 1, 65-87.

Willmore, P. L. et al. (1960)
The time term approach to refraction seismology.
Canadian Sed. Obs., Report.